Design, Synthesis and Characterization of Molecular Tools for the Histamine H₃ and H₄ Receptors – In Particular Radio- and Fluorescent Ligands

DISSERTATION

ZUR ERLANGUNG DES DOKTORGRADES DER NATURWISSENSCHAFTEN (DR. RER. NAT.)

AN DER FAKULTÄT FÜR CHEMIE UND PHARMAZIE

DER UNIVERSITÄT REGENSBURG

Vorgelegt von Edith Bartole

aus Grabatz / Rumänien

im Jahr 2020

Diese Arbeit entstand von Januar 2015 bis Juni 2020 unter der Anleitung von Prof. Dr. Armin Buschauer und Prof. Dr. Günther Bernhardt an der Fakultät für Chemie und Pharmazie der Universität Regensburg.

Promotionsgesuch eingereicht am: 09.07.2020

Tag der mündlichen Prüfung: 09.09.2020

Vorsitzender des Prüfungsausschusses: Prof. Dr. Dominik Horinek

Erstgutachter: Prof. Dr. Günther Bernhardt

Zweitgutachter: Prof. Dr. Joachim Wegener

Drittprüferin: PD Dr. Andrea Straßer

Acknowledgements

Publications, presentations and professional training

Peer-reviewed journal articles

(published prior to the submission of this thesis)

Bartole, E.; Grätz, L.; Littmann, T.; Wifling, D.; Seibel, U.; Buschauer, A.; Bernhardt, G. UR-DEBa242: a Py-5-labeled fluorescent multipurpose probe for investigations on the histamine H_3 and H_4 receptors. *J. Med. Chem.* **2020**, 63, 5297-5311.

Bartole, E.; Littmann, T.; Tanaka, M.; Ozawa, T.; Buschauer, A.; Bernhardt, G. [^{3}H]UR-DEBa176: a 2,4-diaminopyrimidine-type radioligand enabling binding studies at the human, mouse, and rat histamine H_4 receptors. *J. Med. Chem.* **2019**, 62, 8338-8356.

Oral presentations

Bartole, E.; Littmann, T.; Bernhardt, G.; Buschauer, A. "2,4-Diaminopyrimidines: towards molecular tools for investigations on human and rodent histamine H_4 receptors." Mid-term evaluation event of the GRK 1910 by the "Deutsche Forschungsgemeinschaft" (Regensburg, 2017)

Bartole, E.; Littmann, T.; Bernhardt, G.; Buschauer, A. "2,4-Diaminopyrimidines: towards molecular tools for investigations on human and rodent histamine H_4 receptors." 1st Joint meeting of the European and Japanese Histamine Research Societies (Amsterdam, 2017)

Bartole, E.; Bernhardt, G.; Buschauer, A. "Molecular tools for the investigation of GPCR orthologues: the histamine H_4 receptor as an example." Christmas Colloquium 2016 of the Department of Organic Chemistry of the University of Regensburg (Regensburg, 2016)

Bartole, E.; Tropmann K., Bernhardt, G.; Buschauer, A. "2,4-Diaminopyrimidines: towards new subtype-selective and potent agonists for the human and rodent histamine H_4 receptors." 8th Summer School in Medicinal Chemistry (Regensburg, 2016)

Poster presentations

(only contributions as presenting author are listed)

Bartole, E.; Grätz, L.; Littmann, T.; Buschauer, A.; Bernhardt, G. "Molecular tools for the human and rodent histamine H_4 receptors." 9th Summer School in Medicinal Chemistry (Regensburg, 2018)

Bartole, E.; Tropmann, K.; Baumeister, P.; Littmann, T.; Bernhardt, G.; Buschauer, A.; Strasser A. "The histamine H_4 receptor: towards molecular tools for investigations on subtype, orthologue and functional selectivity." Mid-term evaluation event of the GRK 1910 by the "Deutsche Forschungsgemeinschaft" (Regensburg, 2017)

Bartole, E.; Tropmann, K., Bernhardt, G.; Buschauer, A. "2,4-Diaminopyrimidines: towards new subtype-selective and potent agonists for the human and rodent histamine H_4 receptors." 8th Summer School in Medicinal Chemistry (Regensburg, 2016)

Bartole, E.; Bernhardt, G.; Buschauer, A. "Synthesis and pharmacological characterization of 2,4-diaminopyrimidine-type histamine H_4 receptor ligands." GLISTEN Meeting (Erlangen, 2016)

Professional training

Since 10/2016	Associated member of the research training group GRK 1910 "Medicinal Chemistry of Selective GPCR Ligands" funded by the "Deutsche Forschungsgemeinschaft"
Since 10/2016	Member of the Emil Fischer Graduate School of Pharmaceutical Sciences and Molecular Medicine, Regensburg and Erlangen
09/2017 – 07/2018	Laboratory animal training (FELASA Category B), Regensburg
03/2018	Fortbildung für Projektleiter und Beauftragte für Biologische Sicherheit (§§ 15 und 17 Gentechniksicherheitsverordnung), Regensburg

Index

1. General introduction

1.1 G-protein-coupled receptors: classification, signal transduction and ligand characterization

With over 800 identified G-protein-coupled receptors (GPCRs)[1], the GPCR superfamily represents the largest human membrane protein family and its members are among the most popular targets for marketed drugs and in drug discovery/development.[2,3] Vertebrate GPCRs can be categorized into five major classes [rhodopsin (largest class), glutamate, secretin, adhesion and frizzled/taste2], which are further divided into subfamilies based on their sequence similarity.[1,4] GPCRs are proteins with an extracellular amino (N)-terminus, an intracellular carboxyl (C)-terminus and seven hydrophobic membrane-spanning helices (TM1 – TM7).[5] The intracellular parts of GPCRs are involved in signaling mechanisms, while the extracellular region and the transmembrane domain are important for ligand binding.[6] GPCRs can recognize a variety of extracellular stimuli (e.g. biogenic amines, peptides, proteins, lipids and ions) and transduce the resulting signals by coupling to intracellular proteins (besides heterotrimeric G-proteins, e.g. arrestin[7] and kinases[8]), which subsequently activate effectors and trigger cellular responses.[3]

In Figure 1.1 the G-protein- and β-arrestin mediated signaling cascades of GPCRs are schematically illustrated. The active state of a GPCR binds to the heterotrimeric G-protein, consisting of the subunits α, β and γ, and subsequently causes a guanosine nucleotide exchange [guanosine diphosphate (GDP)/guanosine triphosphate (GTP)] in the α subunit.[9] Afterwards, the ternary complex (GPCR/Gαβγ) dissociates into the GPCR, the Gα-GTP subunit and the Gβγ complex.[9] The α subunit can be divided into four major isoforms, namely the $G\alpha_s$-, $G\alpha_i$-, $G\alpha_{q/11}$- and $G\alpha_{12/13}$ proteins[10,11] comprising GTPase activity, which converts GTP to GDP.[9] The subsequent influence on effector proteins depends on the type of the α subunit, to which the GPCR is predominantly coupled to.[9] The $G\alpha_s$ protein translocates the adenylyl cyclase (AC) and activates its enzymatic activity, which leads to the formation of cyclic adenosine monophosphate (cAMP) from adenosine triphosphate (ATP). By contrast, the coupling to $G\alpha_i$ causes a decrease in AC activity. The interaction with $G\alpha_{q/11}$ activates effectors from the phospholipase C (PLC)-β class, which catalyze the formation of inositol triphosphate (IP_3) and diacylglycerol (DAG) from phosphatidylinositol bisphosphate. The increase in IP_3 subsequently

triggers the release of Ca^{2+} into the cytosol. $G\alpha_{12/13}$ activates e.g. Rho. The $G\beta\gamma$ complex acts as a signal transducer as well, modulating e.g. PLCs and ion channels. The G-protein-mediated signaling is halted by the hydrolysis of GTP and the reformation of the heterotrimeric G-protein.[12]
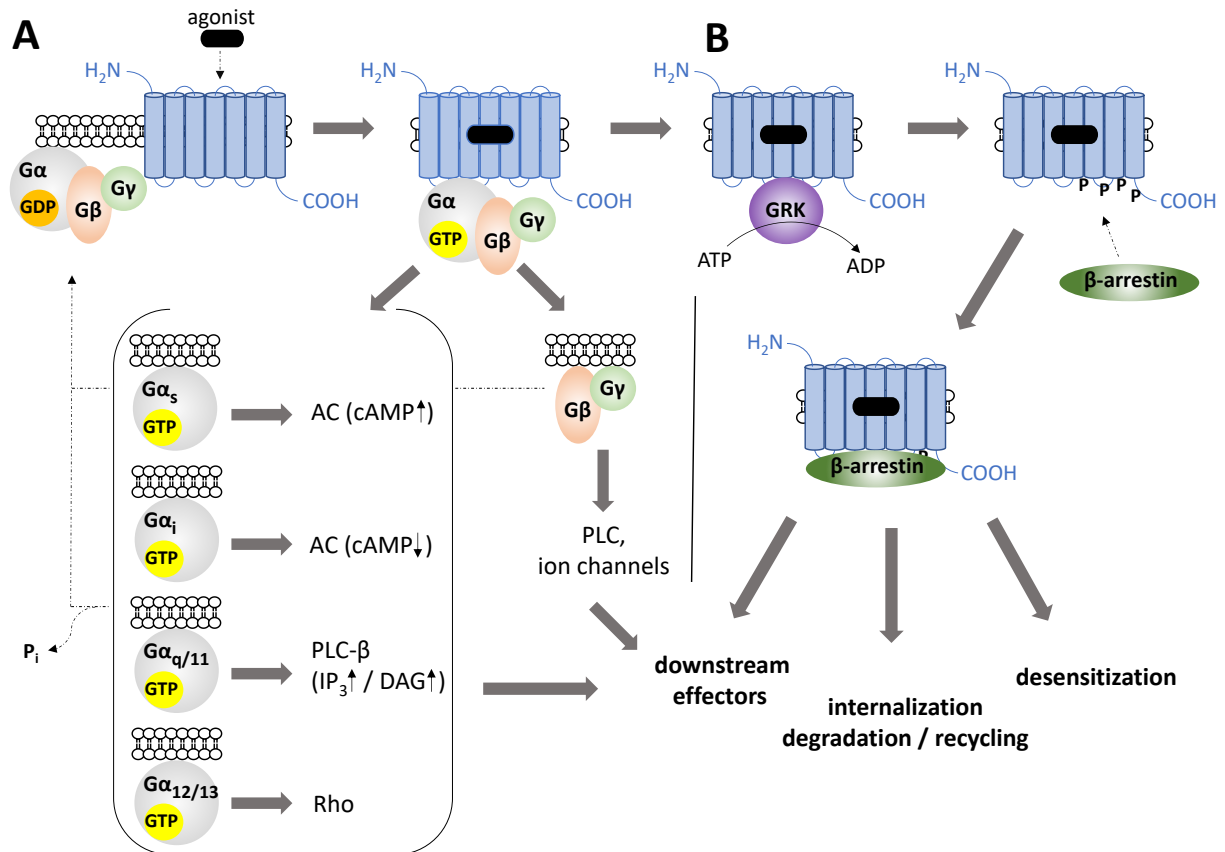
Figure 1.1. Schematic illustration of the G-protein-(A) and β-arrestin (B) mediated signaling cascades of GPCRs. Modified from Iliopoulos-Tsoutsouvas et al.[13] (**A**) Agonist binding to GPCRs promotes a conformational change of the receptor (active state), which initiates coupling to the heterotrimeric G-protein (Gαβγ) and a guanosine nucleotide (GDP/GTP) exchange occurs. Subsequently, the ternary complex (GPCR/Gαβγ) dissociates and the dissociated subunits (Gα$_x$-GTP and Gβγ) regulate their respective effector proteins such as adenylyl cyclase (AC), phospholipase C (PLC) , Rho and ion channels, which themselves regulate further downstream effectors. The hydrolysis of GTP to GPD and the reassembly of the heterotrimeric G-protein stop G-protein-mediated signaling. For a more detailed description see text. (**B**) The G-protein-coupled receptor kinase (GRK) mediates phosphorylation of the active state of a GPCR under consumption of ATP, which induces binding of β-arrestin. A conformational change in β-arrestin causes interactions with downstream effectors to initiate signaling and triggers desensitization or internalization of the GPCR followed by degradation or recycling to plasma. For a more detailed description see text.

Besides the signaling mediated by G-proteins, GPCRs are also known to be involved in G-protein-independent signaling pathways.[12] Intensively studied is the coupling of arrestin, induced by G-protein-coupled receptor kinase (GRK)-mediated phosphorylation of the active conformation of a GPCR under consumption of ATP.[14] Of the four arrestin isoforms only arrestin-2 and arrestin-3, also known as β-arrestin1 and β-arrestin2, are distributed

ubiquitously.[14] The coupling of β-arrestin to the cytosolic surface of the GPCR initially terminates G-protein signaling by steric hindrance.[14,15] A subsequent conformational change in β-arrestin allows interactions with further downstream proteins, triggering the desensitization[15] of a GPCR or its internalization[16] (via clathrin-coated pits) into endosomes followed by degradation or recycling of the GPCR to the plasma membrane[17]. Additionally, β-arrestin is involved in the activation of downstream effectors e.g. mitogen-activated protein kinase (MAPK).[18,19]

To describe the pharmacological effect of ligands interacting with GPCRs, several receptor models have been proposed, e.g. the ternary complex model[20] and the extended ternary complex model[21]. These are classic "two state" models in which the GPCR adopts two conformations, the active and the inactive. In the latter model, both states are at equilibrium and able to spontaneously isomerize without agonist binding.[22] Agonists predominantly bind to the active state of the receptor, stabilize it and induce G-protein activation. The activation of a GPCR in the absence of an agonist is called constitutive (basal) activity and is described for numerous GPCRs.[23] Inverse agonists bind preferably to the inactive state and decrease the constitutive activity of the receptor. Antagonists bind, without affecting the equilibrium, to both states and therefore inhibit the binding of (inverse) agonists. Indeed, the "two state" model helps to fundamentally understand the basic concept of GPCR pharmacology. Nonetheless, there is strong evidence that a GPCR can adopt a variety of active and inactive conformations upon ligand binding, which lead to different physiological responses.[24,25] This reflects the complexity of GPCRs, which is based on e.g. orthosteric ligand binding[26], allosterism[27], G-protein selectivity[28], G-protein independent signaling[14], receptor desensitization[15] and internalization[16], as well as receptor oligomerization[29].

1.2 Molecular tools for GPCRs: an overview

GPCRs constitute a long-standing therapeutic target as they are involved in a plethora of biological and (patho)physiological processes and interact i. a. with relatively small endogenous ligands, the action of which can be mimicked by synthetic molecules.[3,30] Over the years, the strategical development of GPCR ligands, such as biomolecules (e.g. peptides, proteins and biogenic amines) but also synthetically derived small molecules, on one hand led to the discovery of new drug candidates[2] and on the other hand built a set of so called "molecular tools" (or "pharmacological tools"). Such tools support the basic research of molecular pharmacology of GPCRs[31], with respect to e.g. receptor-ligand-interactions, subtype selectivity, (biased) signaling, allosterism and receptor oligomerization, and therefore contribute to a better understanding of their (patho)physiological roles.

In principle, the most basic molecular tools for GPCRs are ligands, which bind to the endogenous ligand (orthosteric) binding site of a particular receptor and act as full agonists, partial agonists, inverse agonists or neutral antagonists. An overview of more specialized molecular tools is given in the following. In Figure 1.2, the underlying concepts of the herein described molecular tools to study GPCRs are illustrated schematically.

1.2.1 Biased ligands

The finding that a GPCR adopts numerous conformations, thereby activating different signaling pathways induced by ligand binding, point to the complexity of GPCR signaling.[32-35] Such selective stimulation of intracellular effectors (e.g. different G-proteins or β-arrestins) is termed e.g. functional selectivity[36] or biased agonism[37]. Biased agonism of GPCRs depends on ligand binding and the specific activation of distinct effector proteins (ligand bias), but also on the stoichiometric ratio of G-proteins, arrestins or other signaling partners (system bias) in different cell types and/or tissues (dynamic bias).[38] In terms of drug development, biased agonists are considered promising drug candidates, because adverse effects are hypothesized to correlate with the activation of unfavorable signaling pathways for several receptors.[39,40] For example, an induction of β-arrestin at the μ-opioid receptor is postulated to be involved in severe side-effects.[41,42] In that regard, a G-protein-biased agonist (*PZM21*[43]) was reported. However, G-protein bias of *PZM21* and lacking respiratory depression could not be confirmed

in an independent study[44]. These contradictory results point out that the pharmacology and the (patho)physiological relevance of biased agonism at GPCRs are still barely understood. Therefore, not only robust experimental techniques and mathematical models which allow reliable quantification of signaling bias, but also rationally designed biased ligands as molecular tools are highly needed.[38]

1.2.2 Allosteric ligands

Another class of molecular tools, the quality of action of which can be explained by the principle of functional selectivity, are allosteric ligands. These ligands do not bind to the orthosteric binding site, but to distinct – allosteric – regions of GPCRs and stabilize a distinct receptor conformation.[27,45] Therefore, the compounds can have a modulatory effect (allosteric modulator) on binding and activity of orthosteric ligands.[27,45] Moreover, allosteric (inverse) agonists themselves affect binding of intracellular effector proteins (e.g. G-proteins).[27,45] The muscarinic acetylcholine M_2 receptor constitutes the first GPCR assigned to allosteric modulation[46-48] and several allosteric modulators[46,47,49,50] have been described. As molecular tools, allosteric modulators can contribute to investigations on subtype selectivity, allosteric cooperativity and GPCR signaling.[27,45] Moreover, allosteric modulators were co-crystallized with their GPCRs, e.g. as in case for the M_2 receptor[51], the chemokine receptors[52-54] and the β_2-adrenoceptor[55]. These structures contribute not least to a better understanding of allosterism at GPCRs but also to a rational design of optimized allosteric ligands.[45]

1.2.3 Bivalent ligands

There is growing evidence that GPCRs can form homo- or hetero-oligomeric complexes, which are suggested to have biological or even therapeutic relevance.[29,56-58] The bivalent ligand approach has been applied at GPCRs to study receptor dimerization[59-61] and to develop ligands with improved receptor affinities/potencies and/or subtype selectivity[62-67]. Homo- and heterobivalent ligands basically consist of two pharmacophoric units (monomeric orthosteric ligands) connected by a spacer of appropriate length and chemical composition.[68] For bridging two orthosteric sites of neighboring receptors, the length of the spacer is crucial (rule of thumb, derived from opioid receptors: 22-32 Å[66,69]). Besides the bridging of protomers, additional binding modes are possible for bivalent ligands, especially if the spacer is not

sufficient in length: e.g. monovalent binding to the orthosteric site of the receptor but also binding to another region at the same receptor.[70] The improvements in affinities/potencies of bivalent ligands compared with those of the corresponding monomeric ligands, which have been achieved for some GPCRs (see above), can be explained by a significantly lower entropy of the ligand-receptor complex by having one pharmacophore closely localized to its binding site upon binding of the other pharmacophore.[67,68]

An alternative idea of cooperative binding is the concept of bitopic (dualsteric) ligands – hybrid molecules that concomitantly occupy an orthosteric and an allosteric site on a receptor via two distinct pharmacophores.[27,68,70] Within a GPCR family, allosteric binding sites are less conserved than orthosteric binding sites, e.g. as for the muscarinic acetylcholine receptors[71-74]. Hence, they can be exploited by applying the bitopic ligand approach to improve receptor affinity and subtype selectivity.[27,75-79] Moreover, bitopic ligands can contribute to the assessment of allosteric cooperativity and GPCR signaling.[27,76,79,80]

1.2.4 Covalent ligands

Another interesting class of molecular tools for GPCRs are covalently binding ligands. These ligands, initially termed as affinity labels, are defined as high affinity compounds bearing reactive substructures, which bind irreversibly to specific amino acid residues in the binding site of a GPRC of interest.[81,82] The cross-linking moiety is either intrinsically reactive and mostly of electrophilic nature (e.g. isothiocyanates, disulfides, Michael acceptors or nitrogen mustards) or it requires an activation step that leads to a reactive chemical species.[81,82] An example of the latter is the photoconversion of so-called photoaffinity labels. Irradiation produces a highly reactive chemical substructure, e.g. a carbene or a nitrene, which subsequently leads to covalent binding of the ligand to the receptor.[81] Although photoaffinity labels have already been developed for GPCRs (e.g. for opioid receptors), their application is associated with drawbacks (e.g. photoactivation often requires tissue/cell-damaging UV-light and can cause unwanted side-reactions).[81] Therefore, intrinsically electrophilic covalent ligands gained attraction in the field of GPCRs and were described for e.g. opioid receptors[81,83,84], β_1- and β_2-adreneroceptors[85-87], the histamine H_3 receptor[88], the dopamine D_2 receptor[89] and the muscarinic acetylcholine M_2 receptor[90]. They have already been involved in the early identification of GPCR binding sites and in investigations on the function

of GPCRs and receptor reserve.[86] Moreover, covalent ligands gained recent interest as tools for structural studies of GPCRs in distinct functional receptor states.[83,85,87,90]

1.2.5 Photochromic ligands

As an intersection between medicinal chemistry and photochemistry, photopharmacology rapidly has emerged in the field of GPCR research over the last six years.[91] Here, light-sensitive photochromic compounds are used, which are expected to provide beneficial spatiotemporal precision in investigations on receptor signaling.[92,93] Such molecular tools contain a photo-switchable moiety (e.g spiropyrans[94], diarylethenes[95-97], fulgides/fulgimides[96,97] or azobenzenes[95,97-99]), which can isomerize (cis/trans isomers), induced by illumination with distinct wavelengths. Thereby the chemical/optical properties and ideally appreciably the biological effect (e.g. binding affinity, functional activity) of a photochromic ligand at its GPCRs can be altered.[91] Up to date, photochromic ligands have been described for e.g. μ-opioid receptors[100], histamine receptors[99,101,102], dopamine receptors[96,103], the chemokine receptor CXR3[98], the neuropeptide Y Y_4 receptor[97] and the muscarinic acetylcholine M_1 receptor[104,105]. Azobenzenes are mainly used as photoswitches, due to benefits with respect to facile synthesis, relatively high quantum yields, appreciable change in the end-to-end distance of the cis/trans isomers, relatively high yields of the isomers and low photobleaching.[91,95] However, there are several limitations of azobenzenes as photoswitches worth considering in the context of data interpretation and application in cell/tissue-based or *in vivo* experimental settings, which include: the scarcely quantitative light-induced isomerization, the frequent necessity for tissue-damaging UV light to initiate switching, the liability to reduction by glutathione and the toxicity of the photoswitch and its potential metabolites.[95]

1.2.6 Labeled ligands

Among molecular tools for GPCRs, labeled compounds, namely radio- and fluorescent ligands, are of central importance for investigations on receptor-ligand-interactions.

1.2.6.1 Radiolabeled ligands

Radioligands constitute the first labeled molecular tools and their application in GPCR binding studies started to gain attraction in the late 1960s.[106,107] A crucial factor in the design of a radioligand is the choice of a suitable radioisotope with a sufficient specific activity that allows

the detection of low-level receptor binding.[108] The commonly used radioisotopes for labeling endogenous ligands, but also synthetically derived (inverse) agonists / antagonists for GPCRs are tritium (^{3}H) and ^{125}I.[109] Tritium has a long half-life (12.4 years) in comparison to ^{125}I (59.6 days).[110] Therefore, once synthesized, tritiated ligands can be used longer in pharmacological studies (up to years) than ^{125}iodided compounds (up to 4 weeks).[110,111] Additionally, the handling of tritiated ligands is more convenient because shielding is not necessary due to its low emission energy (β_{max}: 0.018 MeV).[110] In contrast, ^{125}I-labeled ligands have higher specific activities[108,110], thus being useful probes for binding studies if the receptor density is very low or the amount of tissue is small.[111] Moreover, the high γ energy of ^{125}iodided ligands enables a direct detection of radiation rather than by scintillation counting.[112]

Besides the selection of an appropriate radioisotope, additional criteria must be taken into consideration for the design of radioligands: First of all, it should be evaluated whether an agonist or antagonist should be radiolabeled, since agonists bind to the active conformation of a GPCR, but antagonists target the active and the inactive state.[111] Furthermore, the labeling strategy and the purification should be simple and lead to high radiochemical yield and purity of the radioligand to avoid an unreasonable environmental burden. The radioligand should be soluble in the used buffers/media and chemically stable under experimental conditions.[108] Most importantly, the radioligand should bind selectively and with high affinity at the GPCRs of interest (at least in the one- to two-digit-nM range), while showing low nonspecific binding.[111]

Radioligands have been developed for e.g. the histamine[113,114]-, the neuropeptide[115-120]-, and the muscarinic acetylcholine M$_2$[76,79] receptors and applied in radioligand binding assays, such as saturation binding-, kinetic binding- and competition binding experiments. Radioligands are frequently used to determine affinities of unlabeled ligands at the GPCRs of interest in moderate to high throughput and allow investigations on different receptor binding modes (e.g. allosteric binding).[109]

In autoradiography, tritiated or ^{125}iodided GPCR ligands can be applied as well.[117,118,121-125] A radioligand can be detected in a sample (e.g. tissue section areas) by apposition to a photographic emulsion in the dark and by subsequent silver grain revelation.[126]

Autoradiography allows the localization of a radioligand bound to its receptors, but also its quantification, because the density of an autoradiography image is quasi-linear to the radioactive content.[126]

Over the years, an increased level of safety and legal requirements and high costs for laboratory equipment, maintenance and waste disposal have caused a decline in the use of radioligands in pharmacological studies. Nevertheless, radioligand binding experiments are still unparalleled with respect to sensitivity and robustness.

By contrast, a class of radiolabeled probes emerging in the field of GPCRs are positron emission tomography (PET) tracers.[127-133] PET is a powerful imaging technique – based on annihilation of a positron and an electron – that can be used for diagnostics in e.g. oncology, neurology and cardiology.[134] Radionuclides used in PET imaging are positron emitting isotopes with short half-lives (e.g. ^{18}F, ^{11}C, ^{124}I or ^{68}Ga), which are incorporated in a ligand that binds to the target of interest (e.g. GPCR).[134]

1.2.6.2 Fluorescently labeled ligands

Over the last decades, fluorescent ligands have increasingly become valuable complementary tools to radioligands for investigations on ligand-receptor-interactions at GPCRs.[115,135-140] In general, fluorescent probes are not affected by the above-mentioned disadvantages of radioligands (see section 1.2.6.1).[13]

A fluorescent ligand basically consists of a pharmacophore, a linker and a fluorophore, whereas the precursors of the fluorophore (e.g. pyrylium-, cyanine- and bodipy dyes) can be either readily synthesized or purchased.[13] As described above for radioligands, fluorescent ligands should fulfill the following requirements for good performance: high receptor selectivity/-affinity, low non-specific binding, high solubility in media and chemical stability under assay conditions and suitable spectral properties as well as appreciable quantum yields.[13] Nonetheless, the development of fluorescent probes can be challenging, because labeling of small GPCR ligands with comparably bulky fluorophores is often accompanied by a decrease in affinity at the target receptor.[13]

Compared to radioligands, fluorescent ligands are superior molecular tools in imaging studies on receptor localization and trafficking in tissue or distinct cells by applying e.g. confocal

microscopy[136] or high content imaging[139]. Moreover, fluorescent ligands can be applied in receptor binding experiments, such as saturation-, kinetic- and competition binding assays. Various techniques were employed, for instance flow cytometry[115,136,139] or fluorescence polarization[141], but also Förster/bioluminescence resonance energy transfer (FRET/BRET)[142,143].

The FRET/BRET-techniques are based on the radiationless energy transfer from a donor (e.g. tagged GPCR) to an acceptor (e.g. fluorescent molecular tool), which subsequently emits light. A sufficient overlap of the donor emission spectrum and the acceptor excitation spectrum, but also close proximity (1 – 10 nm[144]) and an optimal orientation of the dipole moments of the acceptor and donor are requirements for FRET/BRET.[143] For FRET assays, the GPCR has to be N-terminally tagged, either covalently [e.g. with enhanced green-fluorescent protein (eGFP)] or non-covalently (e.g. with fluorescent antibodies).[143] In contrast, luciferase enzymes [e.g. NanoLuc (NLuc)[145]], which oxidize their substrates (e.g. furimazine) to generate bioluminescence, are used as donors in BRET assays. Since no external light source is needed for BRET, lower signal-to-noise ratios can be achieved. By contrast to e.g. radioligand binding assays, the FRET/BRET-techniques enable real-time binding experiments using live cells by making washing and filtration steps dispensable (i.e. also no influence on the thermodynamic equilibrium of the receptor-ligand complex). This is especially useful when performing kinetic binding experiments with fluorescent probes, since a high temporal resolution (ms-scale) can be achieved.[143]
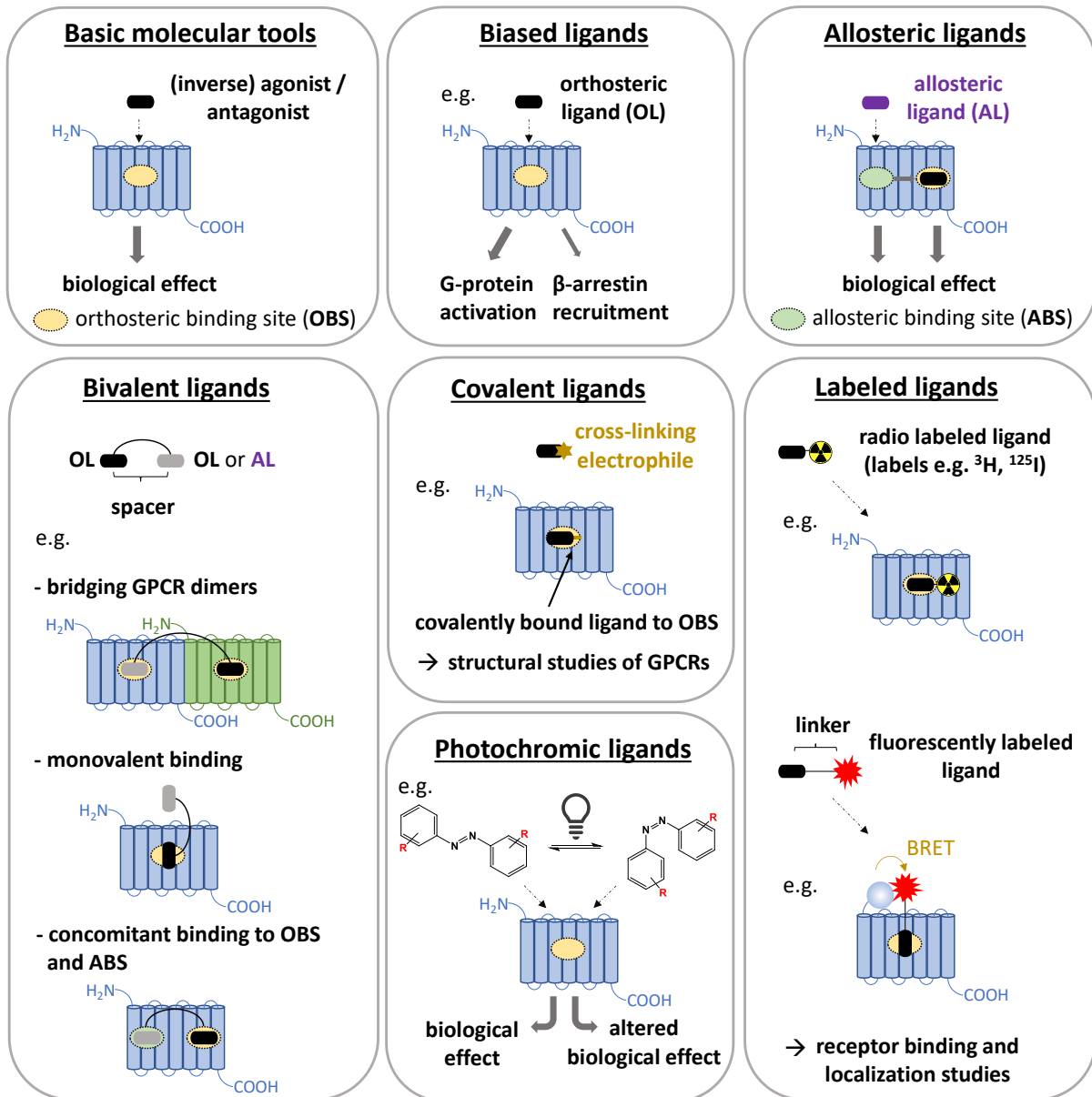
Figure 1.2. Schematic illustration of the concepts of the herein described molecular tools to study GPCRs. Basic molecular tools: a ligand binds to the orthosteric binding site of a GPCR and acts as an agonist, inverse agonist, or antagonist. **Biased ligands:** for instance, a ligand binds to the orthosteric binding site of a GPCR and causes the activation of G-proteins over the recruitment of β-arrestins. **Allosteric ligands:** a ligand binds to the allosteric binding site of a GPCR and modulates the binding and/or the biological effect of an orthosteric ligand and/or induces a biological effect itself. **Bivalent ligands:** ligands, which consist of two pharmacophoric units and a spacer of appropriate length and chemical composition. For these ligands, several binding modes at GPCRs are possible. **Covalent ligands:** a ligand, which contains an electrophilic cross-linking moiety. A covalently bound ligand, for instance to the orthosteric site of a GPCR, stabilizes a distinct receptor conformation, which allows investigations on receptor structure**. Photochromic ligands:** for instance, azobenzenes can isomerize (trans/cis) by illumination with a distinct wavelength. The cis/trans isomers may reveal e.g. different binding affinities and/or functional activities by binding to e.g. the orthosteric binding site of a GPCR. **Labeled ligands:** a radioligand constitutes e.g. an orthosteric ligand, which is labeled with a radioisotope. A fluorescent ligand consists of e.g. an orthosteric ligand, a linker and a fluorescent label. The labeling allows the quantification and the localization of the receptor-bound ligand. Furthermore, fluorescent ligands can be applied in BRET-based binding assays.

1.3 The histamine H_3 and H_4 receptors: characteristics and clinical candidates

The biological effects of the biogenic amine *histamine* (Figure 1.4) are mediated by its interaction with four histamine receptor subtypes, namely the histamine H_{1-4} receptors, which all belong to the rhodopsin-like family of GPCRs.[4] Initially, the H_1R and H_2R were pharmacologically characterized[146,147] and subsequently cloned[148,149]. In 1983, the pharmacological identification[150] of the H_3R followed, but it took 16 years for the human ortholog to be cloned[151].[152] Furthermore, cloning of the H_3R from other species (rat[151,153], guinea pig[154], mouse[155] and Rhesus monkey[156]) revealed a high conservation between these receptor orthologs of approx. 92%.[157]

In 2000/01, the histamine H_4 receptor was cloned and deorphanized[158-164], and revealed a rather high sequence homology with the H_3R (approx. 40% overall and approx. 58% within the TM domains). The identification of the H_4R subsequently led to the cloning of several species orthologs, which comprise a substantially different receptor sequence compared to the human H_4R sequence (approx. 70% homology).[165,166] Only the *Cynomolgus* monkey ortholog displays a higher homology of 92%.[167] In comparison to the H_1R and H_2R, the endogenous agonist histamine binds with higher affinity to the H_3R and H_4R.[168] While the activated H_1R and H_2R couple to $G\alpha_{q/11}$ and $G\alpha_s$ proteins, respectively, the H_3R and H_4R activate predominantly $G\alpha_{i/o}$ proteins.[5]

1.3.1 The (patho)physiological role of the H_3R and clinical candidates

The H_3R is mainly expressed in the central nervous system (CNS) and subsidiary in periphery (e.g. gastrointestinal- and respiratory tract and cardiovascular system).[152,169] The human and rodent H_3Rs are known to signal in an agonist-independent, constitutive manner.[152] Constitutive activity was not only found for the recombinant human and rat H_3Rs, but also for native rodent H_3Rs.[170-172] In the CNS, the H_3R acts as an autoreceptor and inhibits the synthesis and the release of *histamine*.[169] As a pre-synaptic heteroreceptor, the H_3R regulates the release of several neurotransmitters, e.g. acetylcholine and glutamate.[169]

The role of the H_3R, predominantly in numerous CNS functions (e.g. sleep-wake regulation and locomotor activity)[169,173], renders it a promising therapeutic target for the treatment of e.g.

narcolepsy[174,175], Parkinson's disease[176,177], schizophrenia[178], epilepsy[179,180], pain[181,182] and multiple sclerosis[183,184]. Recently, the H$_3$R antagonist *pitolisant*[185] (Figure 1.3), developed by Bioprojet, was approved in the EU and the US for the treatment of narcolepsy.[175] Currently, there are numerous clinic trials on a variety of additional indications, e.g. excessive day-time sleepiness in narcolepsy or Parkinson's disease, obstructive sleep apnea, schizophrenia and drug abuse.[169] Besides *pitolisant*, inverse agonists/antagonists, like *GSK-189254* and *GSK-239512*[186] (Figure 1.3), completed clinical trials in e.g. hyperalgesia, Alzheimer's disease[187], schizophrenia[188] or multiple sclerosis[184].[169] Additionally, Johnson & Johnson (JNJ) completed several clinical studies for Attention Deficit Hyperactivity Disorder (ADHD) with the benzamide *JNJ-31001074*[189] (Figure 1.3).[169] With the results of a trial with e.g. *PF-03654746*[190] (Figure 1.3), the role of the H$_3$R in the treatment of allergic rhinitis could be confirmed.[169]

1.3.2 The (patho)physiological role of the H$_4$R and clinical candidates

Although the H$_3$R and H$_4$R display similarities with respect to receptor structure, substantial differences are worth mentioning:

While the H$_3$R is mainly expressed in the CNS, the expression of H$_4$R in the central and peripheral nervous system is still controversially discussed and needs further research.[191,192] The H$_4$R is known to be mainly expressed in hematopoietic cells (e.g. dendritic cells, mast cells, eosinophils and T-lymphocytes)[193-195], and also in colonic epithelial cells[196] and epidermal tissue (i.e. in keratinocytes in the prickle cell layer and granular layer of the epidermis[197]). Based on its expression profile and experimental evidence, the H$_4$R is suggested to play a (patho)physiological role in autoimmune and allergic disorders (e.g. pruritus[198,199], atopic dermatitis[200], bronchial asthma[201], ulcerative colitis[202] and rheumatoid arthritis[203]) and in cancer[204,205]. As a consequence of the above-mentioned low sequence homology between the human H$_4$R and its rodent orthologs, high constitutive activity was predominantly observed for the human H$_4$R in recombinant and overexpressing systems.[168,206,207] Moreover, for the endogenous agonist *histamine* (Figure 1.4) substantial differences in affinities and potencies across the orthologs were observed.[208-210]

Up to date, only three clinical candidates for the H$_4$R are known worth mentioning.[204] One of them is *JNJ-39758979*[211] (Figure 1.3), which revealed promising results in preclinical and phase 1 studies[198,212] with healthy volunteers.[204] A phase 2a trial[213] in adults suggests its potential in

eosinophilic asthma.[204] In adults with atopic dermatitis[214] it reduced pruritus, but caused drug-induced agranulocytosis, hampering its clinical use.[204] To overcome such drug-induced side effects, a structurally different H$_4$R antagonist, namely *toreforant* (Figure 1.3), was developed and safely applied in clinical trials[215] with patients with rheumatoid arthritis, asthma and psoriasis.[204] In a phase 2 study, *toreforant* reduced symptoms of rheumatoid arthritis, but failed to reveal significant improvements in a follow up trial[216].[204] Moreover, *toreforant* showed no beneficial effect on eosinophilc asthma[217].[204] The selective H$_4$R antagonist *ZPL-3893787*[218] (Figure 1.3) was investigated in a phase 2a trial[200,219] with patients with moderate to severe atopic dermatitis and supports the antipruritic and anti-inflammatory effect of H$_4$R antagonists.[204] In summary, the data of the clinical studies implicate that clinical candidates with less side effects are needed, and that further research has to be conducted to deepen the understanding of the (patho)physiological role of the H$_4$R. The application of translational animal models constitutes a critical aspect of this research. However, the low sequence homology between the human and e.g. the rodent H$_4$R impedes the development of ligands with comparable pharmacological properties.
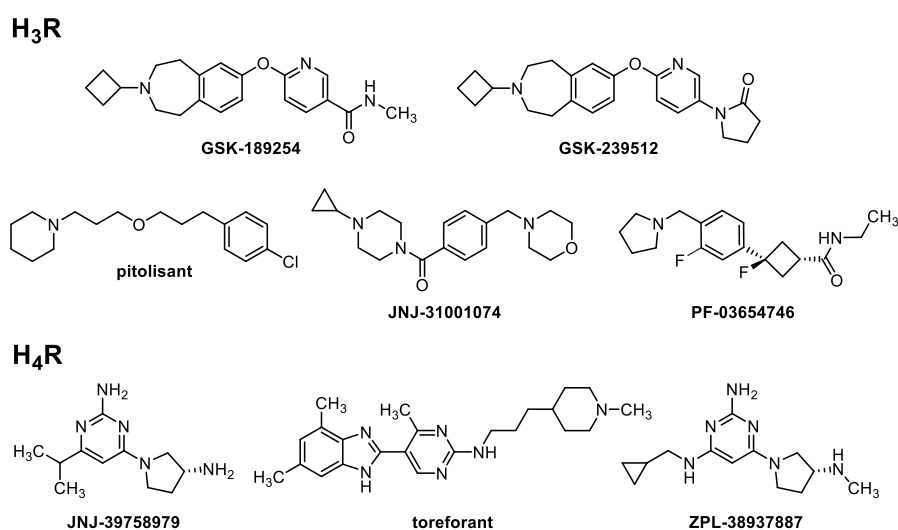
Figure 1.3. Structures of selected clinical candidates for the histamine H$_3$ and H$_4$ receptors.

1.4 Molecular tools for the histamine H_3 and H_4 receptors

Over the years a plethora of (inverse) agonists/antagonists, partly radio- and/or fluorescently labeled, were described for the H_3R and H_4R as molecular tools. Not surprisingly, due to the high sequence homology several imidazole containing ligands, initially developed for the H_3R, revealed comparable high affinities and potencies at the H_4R ($\leq$ three-digit-nM range). Apart from the endogenous ligand *histamine* (Figure 1.4), comparable affinities and potencies were reported for several H_3R agonists [e.g. *homohistamine*,

Agonists

n = 1, **histamine**
n = 2, **homohistamine**
n = 3, **imbutamine**
n = 4, **impentamine**

N^α-**methylhistamine**

R-α-**methylhistamine**

imetit

R = H, **immepip**
R = CH$_3$, **methimepip**

Inverse agonists / antagonists

thioperamide

bodilisant

iodophenpropit

clobenpropit

Figure 1.4. Structures of the endogenous histamine receptor agonist histamine and selected molecular tools for the histamine H_3 receptor.

*imbutamin*e, *impentamine*, N^α-*methylhistamine*[150], *(R)-α-methylhistamine*[220], *imetit*[221] and *immepip*[222] (Figure 1.4)], but also for H_3R inverse agonists/antagonists [e.g. *thioperamide*[223], *clobenpropit*[221] and *iodophenpropit*[224] (Figure 1.4)].[168,225,226] With respect to the quality of action, only *impentamine* and *clobenpropit* revealed substantial differences at the H_4R: *Impentamine* acts as an antagonist and *clobenpropit* revealed partial agonistic activity at the H_4R.[168] As an inverse agonist at the H_4R[168], *thioperamide* is frequently used as reference compound.

First improvements with respect to subtype selectivity for the H_3R over H_4R were achieved by methylation of *immepip*, which led to *methimepip*[227] (Figure 1.4), a highly potent and selective H_3R agonist.[168,226] The first described highly potent H_4R agonists with moderate to pronounced subtype selectivity were *VUF-8430*[228] and *4(5)-methylhistamine*[147,168] (Figure 1.5), respectively. *VUF-8430* derived from the H_2R agonist *dimaprit*, whereas *4(5)-methylhistamine* was initially described as an agonist for the H_2R.

Other H_2R agonists, for instance *impromidine* and their N^G-acylated derivatives, showed higher potencies at the H_4R as well, whereas no subtype selectivity over the H_3R was observed.[226]

Structural modifications led to e.g. *UR-PI294*[114] (Figure 1.5), a highly potent $H_{3,4}Rs$ agonist with substantial selectivity over the H_1R and H_2R. To further improve subtype selectivity towards the H_4R, the acylguanidine motif was replaced by a less basic cyanoguanidine. In combination with further structural variations highly potent H_4R agonists [e.g. *UR-PI376*[229] and *trans-(+)-(1S,3S)-UR-RG98*[230] (Figure 1.5)] with improved selectivity over the H_3R ($\approx$ 30-fold and > 100-fold, respectively) and negligible activities at the $H_{1,2}R$ were achieved.

In 2006, Johnson & Johnson introduced the *2-arylbenzimi-dazoles*[231] as new compound class. Its *histamine* and *spinaceamine derivatives* (Figure 1.5) constitute highly potent H_4R agonists with pronounced selectivity over the H_3R (up to 2700-fold[232]) and almost no affinity at the $H_{1,2}Rs$.[232,233]

Agonists

4 (5)-methylhistamine

VUF-8430

UR-PI294

trans-(+)-(1S,3S)-UR-RG98

UR-PI376

2-arylbenzimidazole-type H_4R agonists, developed by Johnson & Johnson

diaminopyrimidine-type H_4R agonists, developed by Johnson & Johnson

Inverse agonists / antagonists

JNJ-7777120

BODIPY-FL-histamine

Py-5 labeled 2-arylbenzimidazol-type H_4R ligand, designed by Dr. Roland Geyer

Figure 1.5. Structures of selected molecular tools for the histamine H_4 receptor.

Besides the search for H_4R selective ligands, there is also an interest in finding ligands comprising comparable functional profiles at the H_4R and H_1R to investigate their interlinked role in inflammatory processes, suggested in literature[234-238].

For many imidazole containing ligands class-related issues were observed, e.g. cytochrome P450 inhibition and off-target activity.[239] Therefore, the design of new H_3R and H_4R agonists and most importantly antagonists focused on non-imidazoles, aiming at improved drug-like properties for further applications *in vivo* and in the clinic. Examples of non-imidazole inverse

agonists/antagonists for the H_3R are the aforementioned clinical candidates *GSK-189254*, *GSK-239512*, *JNJ-3100104* and *pitolisant* (Figure 1.3) as well as the recently published covalent[88] and photochromic[99] ligands.

In the search for highly potent and subtype selective non-imidazole inverse agonists/antagonists for the H_4R, a high-throughput campaign led to the indole carboxamide *JNJ-7777120*[240] (Figure 1.5). Since then, *JNJ-7777120* has widely been used as a standard antagonists in animal models to investigate the (patho)physiology of the H_4R.[152] However, *in vitro* agonism at species orthologs (e.g. mouse and rat H_4Rs)[207,209,210], β-arrestin recruitment[241,242] and off-target effects at higher concentrations[209] were observed for *JNJ-7777120*, which should be taken into account when interpreting *in vivo* data.

The finding of extreme bias for *JNJ-7777120* subsequently led to extensive screening of H_4R ligands for functional selectivity[243,244], which uncovered $G\alpha_i$ protein or β-arrestin2 preferred signaling within and between different chemical classes. Nonetheless, biased H_4R signaling is still an unexplored area and screening for functional selectivity constitutes a promising approach in the development of new H_4R ligands. The identification of biased ligands as molecular tools might help to unravel the contribution of these distinct pathways in H_4R (patho)physiology.[243]

For the H_4R, species-dependent discrepancies with respect to potencies and even in the quality of action were not only found for *histamine* (Figure 1.4) or *JNJ-7777120* (Figure 1.5), but also for several H_4R ligands in recombinant systems.[207-210,245] To improve the translational value of animal models, new molecular tools for the H_4R are needed, comprising balanced functional profiles across the species with a special emphasis on the most important laboratory animals like mice and rats. With *2,4-diaminopyrimidine-type* agonists[246-248] (example see Figure 1.5) and antagonists [e.g. *JNJ-39758979*, (Figure 1.3)] this aim was achieved. While the antagonist *JNJ-39758979* has already been probed in clinical studies (see section 1.3.2), the agonists constitute promising molecular tools for studying the (patho)physiological role of the H_4R, which is still far away from being completely understood.[226]

1.4.1 Radiolabeled molecular tools for the H_3R and H_4R

With respect to radiolabeled molecular tools, several PET tracers have been described for the H_3R so far.[152,169] Among them is the ^{11}C-labeled *GSK-189254* (structure of "cold" ligand see Figure 1.3), which has been used to quantify the expression of the H_3R in human brain *in vivo*.[249] Additionally, [125]iodided and tritiated ligands were applied in radioligand binding studies at the H_3R, namely the agonists *[^{3}H]histamine*[150], *[^{3}H]N^α-methylhistamine*[250], *[^{3}H](R)-α-methylhistamine*[251] and *[^{3}H]UR-PI294*[114], but also the inverse agonists/antagonists *[^{3}H]thioperamide*[252] and *[^{125}I]iodophenpropit*[224,253] (structures of "cold" ligands see Figure 1.4 and Figure 1.5). Moreover, *[^{125}I]iodoproxyfan*[254,255] has proven useful as a high affinity H_3R radioligand, revealing binding affinities in the two-digit picomolar range.[254]

For binding studies at the human H_4R, the radioligands *[^{3}H]histamine*[160,164,165,207,208], *[^{3}H]UR-PI294*[114], *[^{125}I]iodophenpropit*[168] and *[^{3}H]JNJ-7777120*[168,256] (structures of "cold" ligands see Figure 1.4 and Figure 1.5) found application in recombinant systems, but have several drawbacks that are discussed in detail in chapter 3. In our laboratory, *[^{3}H]UR-DEBa176*[257] was developed, which constitutes the first highly affinic radioligand enabling comparative and robust binding studies at the H_4R species orthologs, namely the human, mouse and rat H_4 receptors (for details see chapter 3).

1.4.2 Fluorescently labeled molecular tools for the H_3R and H_4R

Besides radiolabeled molecular tools, also numerous fluorescent probes[140,258-260] for the H_3R have been developed. Among them, the highly affinic and subtype selective fluorescent H_3R antagonist *bodisilant*[140] (Figure 1.4), which proved useful for receptor imaging in human H_3R overexpressing cells and human brain tissue. Nonetheless, its rather unfavorable spectral properties (λ_{abs} = 468 nm; λ_{em} = 493 and 563 nm[140]) can cause interference with cellular autofluorescence and preclude a potential application as a molecular tool in BRET-based binding studies.

Despite some efforts to develop fluorescent ligands for the H_4R, only a few compounds [e.g. *Bodipy-FL-histamine*[261] and *Py-5 labeled 2-arylbenzimidazole*[262] (Figure 1.5)] with weak affinities at the human H_4R were described.[142,261,262] By contrast, the commercially available *clobenpropit-BODIPY-630/650* was successfully applied in BRET-based binding studies[142] at the

human $H_{3,4}Rs$. However, its versatile application is associated with drawbacks, which are discussed in chapter 4.

Just recently, the first highly affinic, comprehensively characterized and versatile fluorescent probe for the human H_3R and the H_4R species orthologs was described.[263] On one hand, *UR-DEBa242*[263] proved suitable for comparative BRET-based binding studies at the human H_3R and the human and mouse H_4Rs. On the other hand, it can support investigations on the expression of the H_4R by enabling the localization of the human H_4R in live cells. For further details see chapter 4.

1.5 References

1. Fredriksson, R.; Lagerstrom, M. C.; Lundin, L.-G.; Schiöth, H. B. The G-protein-coupled receptors in the human genome form five main families. Phylogenetic analysis, paralogon groups, and fingerprints. *Mol. Pharmacol.* **2003**, 63, 1256-1272.

2. Hauser, A. S.; Attwood, M. M.; Rask-Andersen, M.; Schiöth, H. B.; Gloriam, D. E. Trends in GPCR drug discovery: new agents, targets and indications. *Nat. Rev. Drug Discovery* **2017**, 16, 829-842.

3. Wacker, D.; Stevens, R. C.; Roth, B. L. How ligands illuminate GPCR molecular pharmacology. *Cell* **2017**, 170, 414-427.

4. Alexander, S. P. H.; Christopoulos, A.; Davenport, A. P.; Kelly, E.; Mathie, A.; Peters, J. A.; Veale, E. L.; Armstrong, J. F.; Faccenda, E.; Harding, S. D.; Pawson, A. J.; Sharman, J. L.; Southan, C.; Davies, J. A.; Collaborators, C. The concise guide to pharmacology 2019/2020: G protein-coupled receptors. *Br. J. Pharmacol.* **2019**, 176, S21-S141.

5. Alexander, S. P. H.; Benson, H. E.; Faccenda, E.; Pawson, A. J.; Sharman, J. L.; Spedding, M.; Peters, J. A.; Harmar, A. J.; Collaborators, C. The concise guide to pharmacology: 2013/14: G protein-coupled receptors. *Br. J. Pharmacol.* **2013**, 170, 1459-1581.

6. Luttrell, L. M. Reviews in molecular biology and biotechnology: transmembrane signaling by G protein-coupled receptors. *Mol. Biotechnol.* **2008**, 39, 239-264.

7. Luttrell, L. M.; Ferguson, S. S. G.; Daaka, Y.; Miller, W. E.; Maudsley, S.; Della Rocca, G. J.; Lin, F.-T.; Kawakatsu, H.; Owada, K.; Luttrell, D. K.; Caron, M. G.; Lefkowitz, R. J. β-Arrestin-dependent formation of β$_2$ adrenergic receptor-Src protein kinase complexes. *Science* **1999**, 283, 655-661.

8. Benovic, J. L.; DeBlasi, A.; Stone, W. C.; Caron, M. G.; Lefkowitz, R. J. β-Adrenergic receptor kinase: primary structure delineates a multigene family. *Science* **1989**, 246, 235-240.

9. Pierce, K. L.; Premont, R. T.; Lefkowitz, R. J. Seven-transmembrane receptors. *Nat. Rev. Mol. Cell Bio.* **2002**, 3, 639-650.

10. Downes, G. B.; Gautam, N. The G protein subunit gene families. *Genomics* **1999**, 62, 544-552.

11. Simon, M. I.; Strathmann, M. P.; Gautam, N. Diversity of G proteins in signal transduction. *Science* **1991**, 252, 802-808.

12. Hilger, D.; Masureel, M.; Kobilka, B. K. Structure and dynamics of GPCR signaling complexes. *Nat. Struct. Mol. Biol.* **2018**, 25, 4-12.

13. Iliopoulos-Tsoutsouvas, C.; Kulkarni, R. N.; Makriyannis, A.; Nikas, S. P. Fluorescent probes for G-protein-coupled receptor drug discovery. *Expert Opin. Drug Discovery* **2018**, 13, 933-947.

14. Lohse, M. J.; Hoffmann, C. Arrestin interactions with G protein-coupled receptors. *Handb. Exp. Pharmacol.* **2014**, 219, 15-56.

15. Lohse, M. J.; Benovic, J. L.; Codina, J.; Caron, M. G.; Lefkowitz, R. J. β-Arrestin: a protein that regulates β-adrenergic receptor function. *Science* **1990**, 248, 1547-1550.

16. Goodman, O. B., Jr.; Krupnick, J. G.; Santini, F.; Gurevich, V. V.; Penn, R. B.; Gagnon, A. W.; Keen, J. H.; Benovic, J. L. β-arrestin acts as a clathrin adaptor in endocytosis of the β$_2$-adrenergic receptor. *Nature* **1996**, 383, 447-450.

17. Kendall, R. T.; Luttrell, L. M. Diversity in arrestin function. *Cell. Mol. Life Sci.* **2009**, 66, 2953-2973.

18. Gurevich, V. V.; Gurevich, E. V. Overview of different mechanisms of arrestin-mediated signaling. *Curr. Protoc. Pharmacol.* **2014**, 67, 02.10.01 - 02.10.09.

19. Shenoy, S. K.; Lefkowitz, R. J. β-Arrestin-mediated receptor trafficking and signal transduction. *Trends Pharmacol. Sci.* **2011**, 32, 521-533.

20. De Lean, A.; Stadel, J. M.; Lefkowitz, R. J. A ternary complex model explains the agonist-specific binding properties of the adenylate cyclase-coupled β-adrenergic receptor. *J. Biol. Chem.* **1980**, 255, 7108-7117.

21. Samama, P.; Cotecchia, S.; Costa, T.; Lefkowitz, R. J. A mutation-induced activated state of the β_2-adrenergic receptor. Extending the ternary complex model. *J. Biol. Chem.* **1993**, 268, 4625-4636.

22. Kenakin, T. Efficacy at G-protein-coupled receptors. *Nat. Rev. Drug Discov.* **2002**, 1, 103-110.

23. Zhao, P.; Furness, S. G. B. The nature of efficacy at G protein-coupled receptors. *Biochem. Pharmacol.* **2019**, 170, 113647.

24. Manglik, A.; Kim, T. H.; Masureel, M.; Altenbach, C.; Yang, Z.; Hilger, D.; Lerch, M. T.; Kobilka, T. S.; Thian, F. S.; Hubbell, W. L.; Prosser, R. S.; Kobilka, B. K. Structural insights into the dynamic process of β_2-adrenergic receptor signaling. *Cell* **2015**, 161, 1101-1111.

25. Perez, D. M.; Karnik, S. S. Multiple signaling states of G-protein-coupled receptors. *Pharmacol. Rev.* **2005**, 57, 147-161.

26. Kenakin, T. Agonist-receptor efficacy. II: agonist trafficking of receptor signals. *Trends Pharmacol. Sci.* **1995**, 16, 232-238.

27. Christopoulos, A.; Changeux, J. P.; Catterall, W. A.; Fabbro, D.; Burris, T. P.; Cidlowski, J. A.; Olsen, R. W.; Peters, J. A.; Neubig, R. R.; Pin, J. P.; Sexton, P. M.; Kenakin, T. P.; Ehlert, F. J.; Spedding, M.; Langmead, C. J. International union of basic and clinical pharmacology. XC. Multisite pharmacology: recommendations for the nomenclature of receptor allosterism and allosteric ligands. *Pharmacol. Rev.* **2014**, 66, 918-947.

28. Watson, C.; Chen, G.; Irving, P.; Way, J.; Chen, W.-J.; Kenakin, T. The use of stimulus-biased assay systems to detect agonist-specific receptor active states: implications for the trafficking of receptor stimulus by agonists. *Mol. Pharmacol.* **2000**, 58, 1230-1238.

29. Bouvier, M. Oligomerization of G-protein-coupled transmitter receptors. *Nat. Rev. Neurosci.* **2001**, 2, 274-286.

30. Bradley, S. J.; Tobin, A. B. Design of next-generation G protein-coupled receptor drugs: linking novel pharmacology and in vivo animal models. *Annu. Rev. Pharmacol. Toxicol.* **2016**, 56, 535-559.

31. Florey, E. Comparative Pharmacology. In *Fundamentals of Biochemical Pharmacology*; Bacq, Z. M.,Capec, R.,Paoletti, R.; Renson, J., Eds.; Pergamon Press: Oxford, 1971; p 621.

32. Kenakin, T. P.; Morgan, P. H. Theoretical effects of single and multiple transducer receptor coupling proteins on estimates of the relative potency of agonists. *Mol. Pharmacol.* **1989**, 35, 214-222.

33. Kenakin, T.; Miller, L. J. Seven transmembrane receptors as shapeshifting proteins: the impact of allosteric modulation and functional selectivity on new drug discovery. *Pharmacol. Rev.* **2010**, 62, 265-304.

34. Pupo, A. S.; Duarte, D. A.; Lima, V.; Teixeira, L. B.; Parreiras-e-Silva, L. T.; Costa-Neto, C. M. Recent updates on GPCR biased agonism. *Pharmacol. Res.* **2016**, 112, 49-57.

35. Seifert, R.; Dove, S. Functional selectivity of GPCR ligand stereoisomers: new pharmacological opportunities. *Mol. Pharmacol.* **2009**, 75, 13-18.

36. Urban, J. D.; Clarke, W. P.; von Zastrow, M.; Nichols, D. E.; Kobilka, B.; Weinstein, H.; Javitch, J. A.; Roth, B. L.; Christopoulos, A.; Sexton, P. M.; Miller, K. J.; Spedding, M.; Mailman, R. B. Functional selectivity and classical concepts of quantitative pharmacology. *J. Pharmacol. Exp. Ther.* **2007**, 320, 1-13.

37. Jarpe, M. B.; Knall, C.; Mitchell, F. M.; Buhl, A. M.; Duzic, E.; Johnson, G. L. [D-Arg[1],D-Phe[5],D-Trp[7,9],Leu[11]]Substance P acts as a biased agonist toward neuropeptide and chemokine receptors. *J. Biol. Chem.* **1998**, 273, 3097-3104.

38. Michel, M. C.; Charlton, S. J. Biased Agonism in Drug Discovery-Is It Too Soon to Choose a Path? *Mol. Pharmacol.* **2018**, 93, 259-265.

39. Violin, J. D.; DeWire, S. M.; Yamashita, D.; Rominger, D. H.; Nguyen, L.; Schiller, K.; Whalen, E. J.; Gowen, M.; Lark, M. W. Selectively engaging β-arrestins at the angiotensin II type 1 receptor reduces blood pressure and increases cardiac performance. *J. Pharmacol. Exp. Ther.* **2010**, 335, 572-579.

40. Walker, J. K. L.; Penn, R. B.; Hanania, N. A.; Dickey, B. F.; Bond, R. A. New perspectives regarding β_2-adrenoceptor ligands in the treatment of asthma. *Br. J. Pharmacol.* **2011**, 163, 18-28.

41. DeWire, S. M.; Yamashita, D. S.; Rominger, D. H.; Liu, G.; Cowan, C. L.; Graczyk, T. M.; Chen, X. T.; Pitis, P. M.; Gotchev, D.; Yuan, C.; Koblish, M.; Lark, M. W.; Violin, J. D. A G protein-biased ligand at the μ-opioid receptor is potently analgesic with reduced gastrointestinal and respiratory dysfunction compared with morphine. *J. Pharmacol. Exp. Ther.* **2013**, 344, 708-717.

42. Raehal, K. M.; Walker, J. K. L.; Bohn, L. M. Morphine side effects in β-arrestin 2 knockout mice. *J. Pharmacol. Exp. Ther.* **2005**, 314, 1195-1201.

43. Manglik, A.; Lin, H.; Aryal, D. K.; McCorvy, J. D.; Dengler, D.; Corder, G.; Levit, A.; Kling, R. C.; Bernat, V.; Hübner, H.; Huang, X.-P.; Sassano, M. F.; Giguere, P. M.; Löber, S.; Duan, D.; Scherrer, G.; Kobilka, B. K.; Gmeiner, P.; Roth, B. L.; Shoichet, B. K. Structure-based discovery of opioid analgesics with reduced side effects. *Nature* **2016**, 537, 185-190.

44. Hill, R.; Disney, A.; Conibear, A.; Sutcliffe, K.; Dewey, W.; Husbands, S.; Bailey, C.; Kelly, E.; Henderson, G. The novel μ-opioid receptor agonist PZM21 depresses respiration and induces tolerance to antinociception. *Br. J. Pharmacol.* **2018**, 175, 2653-2661.

45. Wold, E. A.; Chen, J.; Cunningham, K. A.; Zhou, J. Allosteric modulation of class A GPCRs: targets, agents, and emerging concepts. *J. Med. Chem.* **2019**, 62, 88-127.

46. Clark, A. L.; Mitchelson, F. Inhibitory effect of gallamine on muscarinic receptors. *Br. J. Pharmacol.* **1976**, 58, 323-331.

47. Lüllmann, H.; Ohnesorge, F. K.; Schauwecker, G.-C.; Wassermann, O. Inhibition of actions of carbachol and DFP on guinea pig isolated atria by alkane-bis-ammonium compounds. *Eur. J. Pharmacol.* **1969**, 6, 241-247.

48. Mohr, K.; Tränkle, C.; Kostenis, E.; Barocelli, E.; De Amici, M.; Holzgrabe, U. Rational design of dualsteric GPCR ligands: quests and promise. *Br. J. Pharmacol.* **2010**, 159, 997-1008.

49. Croy, C. H.; Schober, D. A.; Xiao, H.; Quets, A.; Christopoulos, A.; Felder, C. C. Characterization of the novel positive allosteric modulator, LY2119620, at the muscarinic M_2 and M_4 receptors. *Mol. Pharmacol.* **2014**, 86, 106-115.

50. Schober, D. A.; Croy, C. H.; Xiao, H.; Christopoulos, A.; Felder, C. C. Development of a radioligand, [^{3}H]LY2119620, to probe the human M_2 and M_4 muscarinic receptor allosteric binding sites. *Mol. Pharmacol.* **2014**, 86, 116-123.

51. Kruse, A. C.; Ring, A. M.; Manglik, A.; Hu, J.; Hu, K.; Eitel, K.; Hübner, H.; Pardon, E.; Valant, C.; Sexton, P. M.; Christopoulos, A.; Felder, C. C.; Gmeiner, P.; Steyaert, J.; Weis, W. I.; Garcia, K. C.; Wess, J.; Kobilka, B. K. Activation and allosteric modulation of a muscarinic acetylcholine receptor. *Nature* **2013**, 504, 101-106.

52. Oswald, C.; Rappas, M.; Kean, J.; Dore, A. S.; Errey, J. C.; Bennett, K.; Deflorian, F.; Christopher, J. A.; Jazayeri, A.; Mason, J. S.; Congreve, M.; Cooke, R. M.; Marshall, F. H. Intracellular allosteric antagonism of the CCR9 receptor. *Nature* **2016**, 540, 462-465.

53. Tan, Q.; Zhu, Y.; Li, J.; Chen, Z.; Han, G. W.; Kufareva, I.; Li, T.; Ma, L.; Fenalti, G.; Li, J.; Zhang, W.; Xie, X.; Yang, H.; Jiang, H.; Cherezov, V.; Liu, H.; Stevens, R. C.; Zhao, Q.; Wu, B. Structure of the CCR5 chemokine receptor-HIV entry inhibitor maraviroc complex. *Science* **2013**, 341, 1387-1390.

54. Zheng, Y.; Qin, L.; Ortiz Zacarias, N. V.; de Vries, H.; Han, G.-W.; Gustavsson, M.; Dabros, M.; Zhao, C.; Cherney, R. J.; Carter, P.; Stamos, D.; Abagyan, R.; Cherezov, V.; Stevens, R. C.; IJzerman, A. P.; Heitman, L. H.; Tebben, A.; Kufareva, I.; Handel, T. M. Structure of CC chemokine receptor 2 with orthosteric and allosteric antagonists. *Nature* **2016**, 540, 458-461.

55. Liu, X.; Ahn, S.; Kahsai, A. W.; Meng, K.-C.; Latorraca, N. R.; Pani, B.; Venkatakrishnan, A. J.; Masoudi, A.; Weis, W. I.; Dror, R. O.; Chen, X.; Lefkowitz, R. J.; Kobilka, B. K. Mechanism of intracellular allosteric $β_2$AR antagonist revealed by X-ray crystal structure. *Nature* **2017**, 548, 480-484.

56. George, S. R.; O'Dowd, B. F.; Lee, S. P. G-protein-coupled receptor oligomerization and its potential for drug discovery. *Nat. Rev. Drug Discovery* **2002**, 1, 808-820.

57. Milligan, G. G protein-coupled receptor hetero-dimerization: contribution to pharmacology and function. *Br. J. Pharmacol.* **2009**, 158, 5-14.

58. Prinster, S. C.; Hague, C.; Hall, R. A. Heterodimerization of G protein-coupled receptors: specificity and functional significance. *Pharmacol. Rev.* **2005**, 57, 289-298.

59. Bhushan, R. G.; Sharma, S. K.; Xie, Z.; Daniels, D. J.; Portoghese, P. S. A bivalent ligand (KDN-21) reveals spinal δ and κ opioid receptors are organized as heterodimers that give rise to $δ_1$ and $κ_2$ phenotypes. Selective targeting of δ – κ heterodimers. *J. Med. Chem.* **2004**, 47, 2969-2972.

60. Hübner, H.; Schellhorn, T.; Gienger, M.; Schaab, C.; Kaindl, J.; Leeb, L.; Clark, T.; Möller, D.; Gmeiner, P. Structure-guided development of heterodimer-selective GPCR ligands. *Nat. Commun.* **2016**, 7, 12298.

61. Xie, Z.; Bhushan, R. G.; Daniels, D. J.; Portoghese, P. S. Interaction of bivalent ligand KDN21 with heterodimeric δ-κ opioid receptors in human embryonic kidney 293 cells. *Mol. Pharmacol.* **2005**, 68, 1079-1086.

62. Birnkammer, T.; Spickenreither, A.; Brunskole, I.; Lopuch, M.; Kagermeier, N.; Bernhardt, G.; Dove, S.; Seifert, R.; Elz, S.; Buschauer, A. The bivalent ligand approach leads to highly potent and selective acylguanidine-type histamine H_2 receptor agonists. *J. Med. Chem.* **2012**, 55, 1147-1160.

63. Kagermeier, N.; Werner, K.; Keller, M.; Baumeister, P.; Bernhardt, G.; Seifert, R.; Buschauer, A. Dimeric carbamoylguanidine-type histamine H_2 receptor ligands: a new class of potent and selective agonists. *Bioorg. Med. Chem.* **2015**, 23, 3957-3969.

64. Keller, M.; Kaske, M.; Holzammer, T.; Bernhardt, G.; Buschauer, A. Dimeric argininamide-type neuropeptide Y receptor antagonists: chiral discrimination between Y_1 and Y_4 receptors. *Bioorg. Med. Chem.* **2013**, 21, 6303-6322.

65. Pockes, S.; Wifling, D.; Keller, M.; Buschauer, A.; Elz, S. Highly potent, stable, and selective dimeric hetarylpropylguanidine-type Histamine H_2 receptor agonists. *ACS Omega* **2018**, 3, 2865-2882.

66. Portoghese, P. S.; Larson, D. L.; Sayre, L. M.; Yim, C. B.; Ronsisvalle, G.; Tam, S. W.; Takemori, A. E. Opioid agonist and antagonist bivalent ligands. The relationship between spacer length and selectivity at multiple opioid receptors. *J. Med. Chem.* **1986**, 29, 1855-1861.

67. Portoghese, P. S. Bivalent ligands and the message-address concept in the design of selective opioid receptor antagonists. *Trends Pharmacol. Sci.* **1989**, 10, 230-235.

68. Shonberg, J.; Scammells, P. J.; Capuano, B. Design strategies for bivalent ligands targeting GPCRs. *ChemMedChem* **2011**, 6, 963-974.

69. Portoghese, P. S. From models to molecules: Opioid receptor dimers, bivalent ligands, and selective opioid receptor probes. *J. Med. Chem.* **2001**, 44, 2259-2269.

70. Newman, A. H.; Battiti, F. O.; Bonifazi, A. 2016 Philip S. Portoghese Medicinal Chemistry Lectureship: designing bivalent or bitopic molecules for G-protein coupled receptors. The whole is greater than the sum of its parts. *J. Med. Chem.* **2019**, 63, 1779-1797.

71. Conn, P. J.; Christopoulos, A.; Lindsley, C. W. Allosteric modulators of GPCRs: a novel approach for the treatment of CNS disorders. *Nat. Rev. Drug Discov.* **2009**, 8, 41-54.

72. Conn, P. J.; Jones, C. K.; Lindsley, C. W. Subtype-selective allosteric modulators of muscarinic receptors for the treatment of CNS disorders. *Trends Pharmacol. Sci.* **2009**, 30, 148-155.

73. Voigtländer, U.; Jöhren, K.; Mohr, M.; Raasch, A.; Tränkle, C.; Buller, S.; Ellis, J.; Höltje, H. D.; Mohr, K. Allosteric site on muscarinic acetylcholine receptors: Identification of two amino acids in the muscarinic M_2 receptor that account entirely for the M_2/M_5 subtype selectivities of some structurally diverse allosteric ligands in *N*-methylscopolamine-occupied receptors. *Mol. Pharmacol.* **2003**, 64, 21-31.

74. Wess, J. Allosteric binding sites on muscarinic acetylcholine receptors. *Mol. Pharmacol.* **2005**, 68, 1506-1509.

75. Keller, M.; Tränkle, C.; She, X.; Pegoli, A.; Bernhardt, G.; Buschauer, A.; Read, R. W. M_2 Subtype preferring dibenzodiazepinone-type muscarinic receptor ligands: effect of chemical homo-dimerization on orthosteric (and allosteric?) binding. *Bioorg. Med. Chem.* **2015**, 23, 3970-3990.

76. Pegoli, A.; She, X. K.; Wifling, D.; Hübner, H.; Bernhardt, G.; Gmeiner, P.; Keller, M. Radiolabeled dibenzodiazepinone-type antagonists give evidence of dualsteric binding at the M_2 muscarinic acetylcholine receptor. *J. Med. Chem.* **2017**, 60, 3314-3334.

77. Pegoli, A.; Wifling, D.; Gruber, C. G.; She, X.; Hübner, H.; Bernhardt, G.; Gmeiner, P.; Keller, M. Conjugation of short peptides to dibenzodiazepinone-type muscarinic acetylcholine receptor ligands determines M_2R selectivity. *J. Med. Chem.* **2019**, 62, 5358-5369.

78. Schmitz, J.; van der Mey, D.; Bermudez, M.; Klöckner, J.; Schrage, R.; Kostenis, E.; Tränkle, C.; Wolber, G.; Mohr, K.; Holzgrabe, U. Dualsteric muscarinic antagonists – orthosteric binding pose controls allosteric subtype selectivity. *J. Med. Chem.* **2014**, 57, 6739-6750.

79. She, X.; Pegoli, A.; Mayr, J.; Hübner, H.; Bernhardt, G.; Gmeiner, P.; Keller, M. Heterodimerization of dibenzodiazepinone-type muscarinic acetylcholine receptor ligands leads to increased M_2R affinity and selectivity. *ACS Omega* **2017**, 2, 6741-6754.

80. Bock, A.; Mohr, K. Dualsteric GPCR targeting and functional selectivity: the paradigmatic M_2 muscarinic acetylcholine receptor. *Drug Discov. Today Technol.* **2013**, 10, e245-252.

81. Takemori, A. E.; Portoghese, P. S. Affinity labels for opioid receptors. *Annu. Rev. Pharmacol. Toxicol.* **1985**, 25, 193-223.

82. Weichert, D.; Gmeiner, P. Covalent molecular probes for class A G protein-coupled receptors: advances and applications. *ACS Chem. Biol.* **2015**, 10, 1376-1386.

83. Manglik, A.; Kruse, A. C.; Kobilka, T. S.; Thian, F. S.; Mathiesen, J. M.; Sunahara, R. K.; Pardo, L.; Weis, W. I.; Kobilka, B. K.; Granier, S. Crystal structure of the μ-opioid receptor bound to a morphinan antagonist. *Nature* **2012**, 485, 321-326.

84. Portoghese, P. S.; Larson, D. L.; Sayre, L. M.; Fries, D. S.; Takemori, A. E. A novel opioid receptor site directed alkylating agent with irreversible narcotic antagonistic and reversible agonistic activities. *J. Med. Chem.* **1980**, 23, 233-234.

85. Rosenbaum, D. M.; Zhang, C.; Lyons, J. A.; Holl, R.; Aragao, D.; Arlow, D. H.; Rasmussen, S. G. F.; Choi, H.-J.; Devree, B. T.; Sunahara, R. K.; Chae, P. S.; Gellman, S. H.; Dror, R. O.; Shaw, D. E.; Weis, W. I.; Caffrey, M.; Gmeiner, P.; Kobilka, B. K. Structure and function of an irreversible agonist-β_2 adrenoceptor complex. *Nature* **2011**, 469, 236-240.

86. Schwalbe, T.; Hübner, H.; Gmeiner, P. Development of covalent antagonists for β1-and β2-adrenergic receptors. *Bioorg. Med. Chem.* **2019**, 27, 2959-2971.

87. Weichert, D.; Kruse, A. C.; Manglik, A.; Hiller, C.; Zhang, C.; Hübner, H.; Kobilka, B. K.; Gmeiner, P. Covalent agonists for studying G protein-coupled receptor activation. *Proc. Natl. Acad. Sci. USA* **2014**, 111, 10744-10748.

88. Wagner, G.; Mocking, T. A. M.; Kooistra, A. J.; Slynko, I.; Abranyi-Balogh, P.; Keserü, G. M.; Wijtmans, M.; Vischer, H. F.; de Esch, I. J. P.; Leurs, R. Covalent inhibition of the histamine H_3 receptor. *Molecules* **2019**, 24, 4541.

89. Schwalbe, T.; Kaindl, J.; Hübner, H.; Gmeiner, P. Potent haloperidol derivatives covalently binding to the dopamine D_2 receptor. *Bioorg. Med. Chem.* **2017**, 25, 5084-5094.

90. Kruse, A. C.; Ring, A. M.; Manglik, A.; Hu, J.; Hu, K.; Eitel, K.; Hubner, H.; Pardon, E.; Valant, C.; Sexton, P. M.; Christopoulos, A.; Felder, C. C.; Gmeiner, P.; Steyaert, J.; Weis, W. I.; Garcia, K. C.; Wess, J.; Kobilka, B. K. Activation and allosteric modulation of a muscarinic acetylcholine receptor. *Nature* **2013**, 504, 101-106.

91. Gomez-Santacana, X.; de Munnik, S. M.; Mocking, T. A. M.; Hauwert, N. J.; Sun, S.; Vijayachandran, P.; de Esch, I. J. P.; Vischer, H. F.; Wijtmans, M.; Leurs, R. A toolbox of molecular photoswitches to modulate the CXCR3 chemokine receptor with light. *Beilstein J. Org. Chem.* **2019**, 15, 2509-2523.

92. Hoorens, M. W. H.; Szymanski, W. Reversible, spatial and temporal control over protein activity using light. *Trends Biochem. Sci.* **2018**, 43, 567-575.

93. Hüll, K.; Morstein, J.; Trauner, D. In Vivo Photopharmacology. *Chem. Rev.* **2018**, 118, 10710-10747.

94. Özcoban, C.; Halbritter, T.; Steinwand, S.; Herzig, L.-M.; Kohl-Landgraf, J.; Askari, N.; Groher, F.; Fürtig, B.; Richter, C.; Schwalbe, H.; Suess, B.; Wachtveitl, J.; Heckel, A. Water-soluble Py-BIPS spiropyrans as photoswitches for biological applications. *Org. Lett.* **2015**, 17, 1517-1520.

95. Harris, J. D.; Moran, M. J.; Aprahamian, I. New molecular switch architectures. *Proc. Natl. Acad. Sci. USA* **2018**, 115, 9414-9422.

96. Lachmann, D.; Studte, C.; Männel, B.; Hübner, H.; Gmeiner, P.; König, B. Photochromic dopamine receptor ligands based on dithienylethenes and fulgides. *Chem. Eur. J.* **2017**, 23, 13423-13434.

97. Lachmann, D.; Konieczny, A.; Keller, M.; König, B. Photochromic peptidic NPY Y_4 receptor ligands. *Org. Biomol. Chem.* **2019**, 17, 2467-2478.

98. Gomez-Santacana, X.; de Munnik, S. M.; Vijayachandran, P.; Da Costa Pereira, D.; Bebelman, J. P. M.; de Esch, I. J. P.; Vischer, H. F.; Wijtmans, M.; Leurs, R. Photoswitching the efficacy of a small-molecule ligand for a peptidergic GPCR: from antagonism to agonism. *Angew. Chem. Int. Ed.* **2018**, 57, 11608-11612.

99. Hauwert, N. J.; Mocking, T. A. M.; Da Costa Pereira, D.; Kooistra, A. J.; Wijnen, L. M.; Vreeker, G. C. M.; Verweij, E. W. E.; De Boer, A. H.; Smit, M. J.; De Graaf, C.; Vischer, H. F.; de Esch, I. J. P.; Wijtmans, M.; Leurs, R. Synthesis and characterization of a bidirectional photoswitchable antagonist toolbox for real-time GPCR photopharmacology. *J. Am. Chem. Soc.* **2018**, 140, 4232-4243.

100. Schönberger, M.; Trauner, D. A photochromic agonist for μ-opioid receptors. *Angew. Chem. Int. Ed.* **2014**, 53, 3264-3267.

101. Hauwert, N. J.; Mocking, T. A. M.; Da Costa Pereira, D.; Lion, K.; Huppelschoten, Y.; Vischer, H. F.; de Esch, I. J. P.; Wijtmans, M.; Leurs, R. A photoswitchable agonist for the histamine H_3 receptor, a prototypic family A G-protein-coupled receptor. *Angew. Chem. Int. Ed.* **2019**, 58, 4531-4535.

102. Rustler, K.; Pockes, S.; König, B. Light-switchable antagonists for the histamine H_1 receptor at the isolated guinea pig ileum. *ChemMedChem* **2019**, 14, 636-644.

103. Donthamsetti, P. C.; Winter, N.; Schönberger, M.; Levitz, J.; Stanley, C.; Javitch, J. A.; Isacoff, E. Y.; Trauner, D. Optical control of dopamine receptors using a photoswitchable tethered inverse agonist. *J. Am. Chem. Soc.* **2017**, 139, 18522-18535.

104. Agnetta, L.; Kauk, M.; Canizal, M. C. A.; Messerer, R.; Holzgrabe, U.; Hoffmann, C.; Decker, M. A photoswitchable dualsteric ligand controlling receptor efficacy. *Angew. Chem. Int. Ed.* **2017**, 56, 7282-7287.

105. Agnetta, L.; Bermudez, M.; Riefolo, F.; Matera, C.; Claro, E.; Messerer, R.; Littmann, T.; Wolber, G.; Holzgrabe, U.; Decker, M. Fluorination of photoswitchable muscarinic agonists tunes receptor pharmacology and photochromic properties. *J. Med. Chem.* **2019**, 62, 3009-3020.

106. Lefkowitz, R. J.; Roth, J.; Pastan, I. Radioreceptor assay of adrenocorticotropic hormone: new approach to assay of polypeptide hormones in plasma. *Science* **1970**, 170, 633-635.

107. Paton, W. D.; Rang, H. P. The uptake of atropine and related drugs by intestinal smooth muscle of the guinea-pig in relation to acetylcholine receptors. *Proc. R. Soc. Lond. B. Biol. Sci.* **1965**, 163, 1-44.

108. Qume, M. Overview of Ligand-Receptor Binding Techniques. In *Receptor Binding Techniques*; Keen, M., Ed. Human Press Inc.: Totowa, New Jersey, 1999; pp 3-23 / p 10.

109. Zhang, R.; Xie, X. Tools for GPCR drug discovery. *Acta Pharmacol. Sin.* **2012**, 33, 372-384.

110. Moyse, E.; Krantic, S. M. Visualization of Receptors In Situ: Applications of Radioligand Binding. In *Methods in Visualization*; Morel, G., Ed. CRC Press LLC: Boca Raton, Florida, 2000; pp 9-12.

111. Bylund, D. B.; Toews, M. L. Radioligand Binding Methods for Membrane Preparations and Intact Cells. In *Receptor Signal Transduction Protocols*; 3rd ed.; Willars, G. B.; Challiss, R. A. J., Eds.; Humana Press: New York, 2011; pp 135-164 /pp 157-158.

112. Xu, B.; Varasteh, Z.; Orlova, A.; Andersson, K.; Larhammar, D.; Bjorkelund, H. Detecting ligand interactions with G protein-coupled receptors in real-time on living cells. *Biochem. Biophys. Res. Commun.* **2013**, 441, 820-824.

113. Baumeister, P.; Erdmann, D.; Biselli, S.; Kagermeier, N.; Elz, S.; Bernhardt, G.; Buschauer, A. [^{3}H]UR-DE257: development of a tritium-labeled squaramide-type selective histamine H_2 receptor antagonist. *ChemMedChem* **2015**, 10, 83-93.

114. Igel, P.; Schnell, D.; Bernhardt, G.; Seifert, R.; Buschauer, A. Tritium-labeled N^1-[3-(1H-imidazol-4-yl)propyl]-N^2-propionylguanidine ([^{3}H]UR-PI294), a high-affinity histamine H_3 and H_4 receptor radioligand. *ChemMedChem* **2009**, 4, 225-231.

115. Dukorn, S.; Littmann, T.; Keller, M.; Kuhn, K.; Cabrele, C.; Baumeister, P.; Bernhardt, G.; Buschauer, A. Fluorescence- and radiolabeling of [Lys^4,Nle^{17,30}]hPP yields molecular tools for the NPY Y_4 receptor. *Bioconj. Chem.* **2017**, 28, 1291-1304.

116. Keller, M.; Pop, N.; Hutzler, C.; Beck-Sickinger, A. G.; Bernhardt, G.; Buschauer, A. Guanidine-acylguanidine bioisosteric approach in the design of radioligands: synthesis of a tritium-labeled N^G-propionylargininamide ([^{3}H]-UR-MK114) as a highly potent and selective neuropeptide Y Y_1 receptor antagonist. *J. Med. Chem.* **2008**, 51, 8168-8172.

117. Keller, M.; Bernhardt, G.; Buschauer, A. [^{3}H]UR-MK136: a highly potent and selective radioligand for neuropeptide Y Y_1 receptors. *ChemMedChem* **2011**, 6, 1566-1571.

118. Keller, M.; Kuhn, K. K.; Einsiedel, J.; Hübner, H.; Biselli, S.; Mollereau, C.; Wifling, D.; Svobodova, J.; Bernhardt, G.; Cabrele, C.; Vanderheyden, P. M.; Gmeiner, P.; Buschauer, A. Mimicking of arginine by functionalized N(ω)-carbamoylated arginine as a new broadly applicable approach to labeled bioactive peptides: high affinity angiotensin, neuropeptide Y, neuropeptide FF, and neurotensin receptor ligands as examples. *J. Med. Chem.* **2016**, 59, 1925-1945.

119. Kuhn, K. K.; Ertl, T.; Dukorn, S.; Keller, M.; Bernhardt, G.; Reiser, O.; Buschauer, A. High affinity agonists of the neuropeptide Y (NPY) Y_4 receptor derived from the C-Terminal pentapeptide of human pancreatic polypeptide (hPP): synthesis, stereochemical discrimination, and radiolabeling. *J. Med. Chem.* **2016**, 59, 6045-6058.

120. Pluym, N.; Baumeister, P.; Keller, M.; Bernhardt, G.; Buschauer, A. [^{3}H]UR-PLN196: a selective nonpeptide radioligand and insurmountable antagonist for the neuropeptide Y Y_2 receptor. *ChemMedChem* **2013**, 8, 587-593.

121. Dumont, Y.; Fournier, A.; St-Pierre, S.; Quirion, R. Autoradiographic distribution of [^{125}I]Leu^{31},Pro^{34}]PYY and [^{125}I]PYY$_{3-36}$ binding sites in the rat brain evaluated with two newly developed Y_1 and Y_2 receptor radioligands. *Synapse* **1996**, 22, 139-158.

122. Martel, J. C.; Fournier, A.; St Pierre, S.; Quirion, R. Quantitative autoradiographic distribution of [^{125}I]bolton-hunter neuropeptide Y receptor binding sites in rat brain. Comparison with [^{125}I]peptide YY receptor sites. *Neuroscience* **1990**, 36, 255-283.

123. Memminger, M.; Keller, M.; Lopuch, M.; Pop, N.; Bernhardt, G.; von Angerer, E.; Buschauer, A. The neuropeptide Y Y_1 receptor: a diagnostic marker? Expression in MCF-7 breast cancer cells is down-regulated by antiestrogens *in vitro* and in xenografts. *PLoS One* **2012**, 7, e51032.

124. Ruat, M.; Traiffort, E.; Bouthenet, M. L.; Schwartz, J. C.; Hirschfeld, J.; Buschauer, A.; Schunack, W. Reversible and irreversible labeling and autoradiographic localization of the cerebral histamine H_2 receptor using [^{125}I] iodinated probes. *Proc. Natl. Acad. Sci. USA* **1990**, 87, 1658-1662.

125. Traiffort, E.; Pollard, H.; Moreau, J.; Ruat, M.; Schwartz, J. C.; Martinez-Mir, M. I.; Palacios, J. M. Pharmacological characterization and autoradiographic localization of histamine H_2 receptors in human brain identified with [^{125}I]iodoaminopotentidine. *J. Neurochem.* **1992**, 59, 290-299.

126. Moyse, E.; Krantic, S. M. Visualization of Receptors In Situ: Applications of Radioligand Binding. In *Methods in Visualization*; Morel, G., Ed. CRC Press LLC: Boca Raton, Florida, 2000; pp 59-63.

127. Lang, C.; Maschauer, S.; Hübner, H.; Gmeiner, P.; Prante, O. Synthesis and evaluation of a ^{18}F-labeled diarylpyrazole glycoconjugate for the imaging of NTS1-positive tumors. *J. Med. Chem.* **2013**, 56, 9361-9365.

128. Maschauer, S.; Ruckdeschel, T.; Tripal, P.; Haubner, R.; Einsiedel, J.; Hübner, H.; Gmeiner, P.; Kuwert, T.; Prante, O. *In vivo* monitoring of the antiangiogenic effect of neurotensin receptor-mediated radiotherapy by small-animal positron emission tomography: a pilot study. *Pharmaceuticals* **2014**, 7, 464-481.

129. Maschauer, S.; Einsiedel, J.; Reich, D.; Hübner, H.; Gmeiner, P.; Wester, H. J.; Prante, O.; Notni, J. Theranostic value of multimers: lessons learned from trimerization of neurotensin receptor ligands and other targeting vectors. *Pharmaceuticals* **2017**, 10, 29.

130. Maschauer, S.; Prante, O. Radiopharmaceuticals for imaging and endoradiotherapy of neurotensin receptor-positive tumors. *J. Label. Compd. Radiopharma.* **2018**, 61, 309-325.

131. Maschauer, S.; Ott, J. J.; Bernhardt, G.; Kuwert, T.; Keller, M.; Prante, O. ^{18}F-labelled triazolyl-linked argininamides targeting the neuropeptide Y Y_1R for PET imaging of mammary carcinoma. *Sci. Rep.* **2019**, 9, 12990.

132. Nebel, N.; Maschauer, S.; Kuwert, T.; Hocke, C.; Prante, O. In vitro and In vivo characterization of selected fluorine-18 labeled radioligands for PET imaging of the dopamine D_3 receptor. *Molecules* **2016**, 21, 1144.

133. Stößel, A.; Brox, R.; Purkayastha, N.; Hübner, H.; Hocke, C.; Prante, O.; Gmeiner, P. Development of molecular tools based on the dopamine D_3 receptor ligand FAUC 329 showing inhibiting effects on drug and food maintained behavior. *Bioorg. Med. Chem.* **2017**, 25, 3491-3499.

134. Salvadori, P. A.; Filidei, E.; Giorgetti, A. Positron-Emitting Radiopharmaceuticals. In *Nuclear Medicine Textbook*; Volterrani, D.,Erba, P.,Carrió, I.,Strauss, H.; Mariani, G., Eds.; Springer: Cham, Switzerland, 2019; pp 57-98.

135. Erdmann, D. Histamine H_2- and H_3-Receptor Antagonists: Synthesis and Characterization of Radiolabelled and Fluorescent Pharmacological Tools. Ph.D. Dissertation, University of Regensburg, Regensburg, 2011.

136. Keller, M.; Mahuroof, S. A.; Hong Yee, V.; Carpenter, J.; Schindler, L.; Littmann, T.; Pegoli, A.; Hübner, H.; Bernhardt, G.; Gmeiner, P.; Holliday, N. D. Fluorescence labeling of neurotensin(8-13) via arginine residues gives molecular tools with high receptor affinity. *ACS Med. Chem. Lett.* **2020**, 11, 16-22.

137. Li, L.; Kracht, J.; Peng, S.; Bernhardt, G.; Elz, S.; Buschauer, A. Synthesis and pharmacological activity of fluorescent histamine H_2 receptor antagonists related to potentidine. *Bioorg. Med. Chem. Lett.* **2003**, 13, 1717-1720.

138. Rose, R. H.; Briddon, S. J.; Hill, S. J. A novel fluorescent histamine H_1 receptor antagonist demonstrates the advantage of using fluorescence correlation spectroscopy to study the binding of lipophilic ligands. *Br. J. Pharmacol.* **2012**, 165, 1789-1800.

139. She, X.; Pegoli, A.; Gruber, C. G.; Wifling, D.; Carpenter, J.; Hübner, H.; Chen, M.; Wan, J.; Bernhardt, G.; Gmeiner, P.; Holliday, N. D.; Keller, M. Red-emitting dibenzodiazepinone derivatives as fluorescent dualsteric probes for the muscarinic acetylcholine M_2 receptor. *J. Med. Chem.* **2020**, 63, 4133-4154.

140. Tomasch, M.; Schwed, J. S.; Paulke, A.; Stark, H. Bodilisant - a novel fluorescent, highly affine histamine H_3 receptor ligand. *ACS Med. Chem. Lett.* **2013**, 4, 269-273.

141. Rinken, A.; Lavogina, D.; Kopanchuk, S. Assays with detection of fluorescence anisotropy: challenges and possibilities for characterizing ligand binding to GPCRs. *Trends Pharmacol. Sci.* **2018**, 39, 187-199.

142. Mocking, T. A. M.; Verweij, E. W. E.; Vischer, H. F.; Leurs, R. Homogeneous, real-time NanoBRET binding assays for the histamine H_3 and H_4 receptors on living cells. *Mol. Pharmacol.* **2018**, 94, 1371-1381.

143. Stoddart, L. A.; White, C. W.; Nguyen, K.; Hill, S. J.; Pfleger, K. D. Fluorescence- and bioluminescence-based approaches to study GPCR ligand binding. *Br. J. Pharmacol.* **2016**, 173, 3028-3037.

144. Wu, P.; Brand, L. Resonance energy transfer: methods and applications. *Anal. Biochem.* **1994**, 218, 1-13.

145. Stoddart, L. A.; Johnstone, E. K. M.; Wheal, A. J.; Goulding, J.; Robers, M. B.; Machleidt, T.; Wood, K. V.; Hill, S. J.; Pfleger, K. D. G. Application of BRET to monitor ligand binding to GPCRs. *Nat. Methods* **2015**, 12, 661-663.

146. Ash, A. S. F.; Schild, H. O. Receptors mediating some actions of histamine. *Br. J. Pharmacol. Chemother.* **1966**, 27, 427-429.

147. Black, J. W.; Duncan, W. A. M.; Durant, C. J.; Ganellin, C. R.; Parsons, E. M. Definition and antagonism of histamine H_2-receptors. *Nature* **1972**, 236, 385-390.

148. De Backer, M. D.; Gommeren, W.; Moereels, H.; Nobels, G.; Van Gompel, P.; Leysen, J. E.; Luyten, W. H. Genomic cloning, heterologous expression and pharmacological characterization of a human histamine H_1 receptor. *Biochem. Biophys. Res. Commun.* **1993**, 197, 1601-1608.

149. Gantz, I.; Schäffer, M.; DelValle, J.; Logsdon, C.; Campbell, V.; Uhler, M.; Yamada, T. Molecular cloning of a gene encoding the histamine H_2 receptor. *Proc. Natl. Acad. Sci. USA* **1991**, 88, 429-433.

150. Arrang, J.-M.; Garbarg, M.; Schwartz, J.-C. Auto-inhibition of brain bistamine release mediated by a novel class (H_3) of histamine receptor. *Nature* **1983**, 302, 832-837.

151. Lovenberg, T. W.; Roland, B. L.; Wilson, S. J.; Jiang, X.; Pyati, J.; Huvar, A.; Jackson, M. R.; Erlander, M. G. Cloning and functional expression of the human histamine H_3 receptor. *Mol. Pharmacol.* **1999**, 55, 1101-1107.

152. Panula, P.; Chazot, P. L.; Cowart, M.; Gutzmer, R.; Leurs, R.; Liu, W. L. S.; Stark, H.; Thurmond, R. L.; Haas, H. L. International union of basic and clinical pharmacology. XCVIII. Histamine receptors. *Pharmacol. Rev.* **2015**, 67, 601-655.

153. Liu, C.; Ma, X.-J.; Lovenberg, T. W. Alternative splicing of the histamine H_3 receptor mRNA at the third cytoplasmic loop is not detectable in humans. *Mol. Brain Res.* **2000**, 83, 145-150.

154. Tardivel-Lacombe, J.; Rouleau, A.; Heron, A.; Morisset, S.; Pillot, C.; Cochois, V.; Schwartz, J. C.; Arrang, J. M. Cloning and cerebral expression of the guinea pig histamine H_3 receptor: evidence for two isoforms. *Neuroreport* **2000**, 11, 755-759.

155. Chen, J.; Liu, C.; Lovenberg, T. W. Molecular and pharmacological characterization of the mouse histamine H_3 receptor. *Eur. J. Pharmacol.* **2003**, 467, 57-65.

156. Yao, B. B.; Sharma, R.; Cassar, S.; Esbenshade, T. A.; Hancock, A. A. Cloning and pharmacological characterization of the monkey histamine H_3 receptor. *Eur. J. Pharmacol.* **2003**, 482, 49-60.

157. Hancock, A. A.; Esbenshade, T. A.; Krueger, K. M.; Yao, B. B. Genetic and pharmacological aspects of histamine H_3 receptor heterogeneity. *Life Sci.* **2003**, 73, 3043-3072.

158. Coge, F.; Guenin, S. P.; Rique, H.; Boutin, J. A.; Galizzi, J.-P. Structure and expression of the human histamine H_4-receptor gene. *Biochem. Biophys. Res. Commun.* **2001**, 284, 301-309.

159. Liu, C.; Ma, X.-J.; Jiang, X.; Wilson, S. J.; Hofstra, C. L.; Blevitt, J.; Pyati, J.; Li, X.; Chai, W.; Carruthers, N.; Lovenberg, T. W. Cloning and pharmacological characterization of a fourth histamine receptor (H_4) expressed in bone marrow. *Mol. Pharmacol.* **2001**, 59, 420-426.

160. Morse, K. L.; Behan, J.; Laz, T. M.; West jr., R. E.; Greenfeder, S. A.; Anthes, J. C.; Umland, S.; Wan, Y.; Hipkin, R. W.; Gonsiorek, W.; Shin, N.; Gustafson, E. L.; Qiao, X.; Wang, S.; Hedrick, J. A.; Greene, J.; Bayne, M.; Monsma jr., F. J. Cloning and characterization of a novel human histamine receptor. *J. Pharmacol. Exp. Ther.* **2001**, 296, 1058-1066.

161. Nakamura, T.; Itadani, H.; Hidaka, Y.; Ohta, M.; Tanaka, K. Molecular cloning and characterization of a new human histamine receptor, hH_4R. *Biochem. Biophys. Res. Commun.* **2000**, 279, 615-620.

162. Nguyen, T.; Shapiro, D. A.; George, S. R.; Setola, V.; Lee, D. K.; Cheng, R.; Rauser, L.; Lee, S. P.; Lynch, K. R.; Roth, B. L.; O'Dowd, B. F. Discovery of a Novel Member of the Histamine Receptor Family. *Mol. Pharmacol.* **2001**, 59, 427-433.

163. Oda, T.; Morikawa, N.; Saito, Y.; Masuho, Y.; Matsumoto, S. Molecular cloning and characterization of a novel type of histamine receptor preferentially expressed in leukocytes. *J. Biol. Chem.* **2000**, 275, 36781-36786.

164. Zhu, Y.; Michalovich, D.; Wu, H.-L.; Tan, K. B.; Dytko, G. M.; Mannan, I. J.; Boyce, R.; Alston, J.; Tierney, L. A.; Li, X.; Herrity, N. C.; Vawter, L.; Sarau, H. M.; Ames, R. S.; Davenport, C. M.; Hieble, J. P.; Wilson, S.; Bergsma, D. J.; Fitzgerald, L. R. Cloning, expression, and pharmacological characterization of a novel human histamine receptor. *Mol. Pharmacol.* **2001**, 59, 434-441.

165. Liu, C.; Wilson, S. J.; Kuei, C.; Lovenberg, T. W. Comparison of human, mouse, rat, and guinea pig histamine H_4 receptors reveals substantial pharmacological species variation. *J. Pharmacol. Exp. Ther.* **2001**, 299, 121-130.

166. Oda, T.; Matsumoto, S.; Masuho, Y.; Takasaki, J.; Matsumoto, M.; Kamohara, M.; Saito, T.; Ohishi, T.; Soga, T.; Hiyama, H.; Matsushime, H.; Furuichi, K. cDNA cloning and characterization of porcine histamine H_4 receptor. *Biochim. Biophys. Acta* **2002**, 1575, 135-138.

167. Oda, T.; Matsumoto, S.; Matsumoto, M.; Takasaki, J.; Kamohara, M.; Soga, T.; Hiyama, H.; Kobori, M.; Katoh, M. Molecular cloning of monkey histamine H_4 receptor. *J. Pharmacol. Sci.* **2005**, 98, 319-322.

168. Lim, H. D.; van Rijn, R. M.; Ling, P.; Bakker, R. A.; Thurmond, R. L.; Leurs, R. Evaluation of histamine H_1-, H_2-, and H_3-receptor ligands at the human histamine H_4 receptor: identification of 4-methylhistamine as the first potent and selective H_4 receptor agonist. *J. Pharmacol. Exp. Ther.* **2005**, 314, 1310-1321.

169. Ghamari, N.; Zarei, O.; Arias-Montano, J.-A.; Reiner, D.; Dastmalchi, S.; Stark, H.; Hamzeh-Mivehroud, M. Histamine H_3 receptor antagonists/inverse agonists: where do they go? *Pharmacol. Ther.* **2019**, 200, 69-84.

170. Morisset, S.; Rouleau, A.; Ligneau, X.; Gbahou, F.; Tardivel-Lacombe, J.; Stark, H.; Schunack, W.; Ganellin, C. R.; Schwartz, J.-C.; Arrang, J.-M. High constitutive activity of native H_3 receptors regulates histamine neurons in brain. *Nature* **2000**, 408, 860-864.

171. Rouleau, A.; Ligneau, X.; Tardivel-Lacombe, J.; Morisset, S.; Gbahou, F.; Schwartz, J.-C.; Arrang, J.-M. Histamine H_3-receptor-mediated [^{35}S]GTPγ[S] binding: evidence for constitutive activity of the recombinant and native rat and human H_3 receptors. *Br. J. Pharmacol.* **2002**, 135, 383-392.

172. Wieland, K.; Bongers, G.; Yamamoto, Y.; Hashimoto, T.; Yamatodani, A.; Menge, W. M. B. P.; Timmerman, H.; Lovenberg, T. W.; Leurs, R. Constitutive activity of histamine H_3 receptors stably expressed in SK-N-MC cells: display of agonism and inverse agonism by H_3 antagonists. *J. Pharmacol. Exp. Ther.* **2001**, 299, 908-914.

173. Panula, P. Histamine, histamine H_3 receptor, and alcohol use disorder. *Br. J. Pharmacol.* **2019**, 177, 634-641.

174. Gondard, E.; Anaclet, C.; Akaoka, H.; Guo, R.-X.; Zhang, M.; Buda, C.; Franco, P.; Kotani, H.; Lin, J.-S. Enhanced histaminergic neurotransmission and sleep-wake alterations, a study in histamine H_3-receptor knock-out mice. *Neuropsychopharmacology* **2013**, 38, 1015-1031.

175. Thorpy, M. J. Recently approved and upcoming treatments for narcolepsy. *CNS Drugs* **2020**, 34, 9-27.

176. Ellenbroek, B. A.; Ghiabi, B. The other side of the histamine H_3 receptor. *Trends Neurosci.* **2014**, 37, 191-199.

177. Nieto-Alamilla, G.; Marquez-Gomez, R.; Garcia-Galvez, A.-M.; Morales-Figueroa, G.-E.; Arias-Montano, J.-A. The histamine H_3 receptor: structure, pharmacology, and function. *Mol. Pharmacol.* **2016**, 90, 649-673.

178. Rapanelli, M.; Pittenger, C. Histamine and histamine receptors in tourette syndrome and other neuropsychiatric conditions. *Neuropharmacology* **2016**, 106, 85-90.

179. Lazewska, D.; Kaleta, M.; Hagenow, S.; Mogilski, S.; Latacz, G.; Karcz, T.; Lubelska, A.; Honkisz, E.; Handzlik, J.; Reiner, D.; Satala, G.; Filipek, B.; Stark, H.; Kiec-Kononowicz, K. Novel naphthyloxy derivatives - potent histamine H_3 receptor ligands. Synthesis and pharmacological evaluation. *Bioorg. Med. Chem.* **2018**, 26, 2573-2585.

180. Sadek, B.; Saad, A.; Subramanian, D.; Shafiullah, M.; Lazewska, D.; Kiec-Kononowiczc, K. Anticonvulsant and procognitive properties of the non-imidazole histamine H_3 receptor antagonist DL77 in male adult rats. *Neuropharmacology* **2016**, 106, 46-55.

181. Obara, I.; Telezhkin, V.; Alrashdi, I.; Chazot, P. L. Histamine, histamine receptors, and neuropathic pain relief. *Br. J. Pharmacol.* **2020**, 177, 580-599.

182. Riddy, D. M.; Cook, A. E.; Shackleford, D. M.; Pierce, T. L.; Mocaer, E.; Mannoury la Cour, C.; Sors, A.; Charman, W. N.; Summers, R. J.; Sexton, P. M.; Christopoulos, A.; Langmead, C. J. Drug-receptor kinetics and sigma-1 receptor affinity differentiate clinically evaluated histamine H3 receptor antagonists. *Neuropharmacology* **2019**, 144, 244-255.

183. Kremer, D.; Küry, P.; Dutta, R. Promoting remyelination in multiple sclerosis: current drugs and future prospects. *Mult. Scler. J.* **2015**, 21, 541-549.

184. Schwartzbach, C. J.; Grove, R. A.; Brown, R.; Tompson, D.; Then Bergh, F.; Arnold, D. L. Lesion remyelinating activity of GSK239512 versus placebo in patients with relapsing-remitting multiple sclerosis: a randomised, single-blind, phase II study. *J. Neurol.* **2017**, 264, 304-315.

185. Meier, G.; Apelt, J.; Reichert, U.; Graßmann, S.; Ligneau, X.; Elz, S.; Leurquin, F.; Ganellin, C. R.; Schwartz, J.-C.; Schunack, W.; Stark, H. Influence of imidazole replacement in different structural classes of histamine H_3-receptor antagonists. *Eur. J. Pharm. Sci.* **2001**, 13, 249-259.

186. Wilson, D. M.; Apps, J.; Bailey, N.; Bamford, M. J.; Beresford, I. J.; Brackenborough, K.; Briggs, M. A.; Brough, S.; Calver, A. R.; Crook, B.; Davis, R. K.; Davis, R. P.; Davis, S.; Dean, D. K.; Harris, L.; Heslop, T.; Holland, V.; Jeffrey, P.; Panchal, T. A.; Parr, C. A.; Quashie, N.; Schogger, J.; Sehmi, S. S.; Stean, T. O.; Steadman, J. G. A.; Trail, B.; Wald, J.; Worby, A.; Takle, A. K.; Witherington, J.; Medhurst, A. D. Identification of clinical candidates from the benzazepine class of histamine H_3 receptor antagonists. *Bioorg. Med. Chem. Lett.* **2013**, 23, 6890-6896.

187. Grove, R. A.; Harrington, C. M.; Mahler, A.; Beresford, I.; Maruff, P.; Lowy, M. T.; Nicholls, A. P.; Boardley, R. L.; Berges, A. C.; Nathan, P. J.; Horrigan, J. P. A randomized, double-blind, placebo-controlled, 16-week study of the H_3 receptor antagonist, GSK239512 as a monotherapy in subjects with mild-to-moderate alzheimer's disease. *Curr. Alzheimer Res.* **2014**, 11, 47-58.

188. Jarskog, L. F.; Lowy, M. T.; Grove, R. A.; Keefe, R. S. E.; Horrigan, J. P.; Ball, M. P.; Breier, A.; Buchanan, R. W.; Carter, C. S.; Csernansky, J. G.; Goff, D. C.; Green, M. F.; Kantrowitz, J. T.; Keshavan, M. S.; Laurelle, M.; Lieberman, J. A.; Marder, S. R.; Maruff, P.; McMahon, R. P.; Seidman, L. J.; Peykamian, M. A. A Phase II study of a histamine H_3 receptor antagonist GSK239512 for cognitive impairment in stable schizophrenia subjects on antipsychotic therapy. *Schizophr. Res.* **2015**, 164, 136-142.

189. Letavic, M. A.; Aluisio, L.; Apodaca, R.; Bajpai, M.; Barbier, A. J.; Bonneville, A.; Bonaventure, P.; Carruthers, N. I.; Dugovic, C.; Fraser, I. C.; Kramer, M. L.; Lord, B.; Lovenberg, T. W.; Li, L. Y.; Ly, K. S.; McAllister, H.; Mani, N. S.; Morton, K. L.; Ndifor, A.; Nepomuceno, S. D.; Pandit, C. R.; Sands, S. B.; Shah, C. R.; Shelton, J. E.; Snook, S. S.; Swanson, D. M.; Xiao, W. Novel benzamide-based histamine H_3 receptor antagonists: the identification of two candidates for clinical development. *ACS Med. Chem. Lett.* **2015**, 6, 450-454.

190. Stokes, J. R.; Romero Jr., F. A.; Allan, R. J.; Phillips, P. G.; Hackman, F.; Misfeldt, J.; Casale, T. B. The effects of an H_3 receptor antagonist (PF-03654746) with fexofenadine on reducing allergic rhinitis symptoms. *J. Allergy Clin. Immunol.* **2012**, 129, 409-412, 412e401-402.

191. Schneider, E. H.; Neumann, D.; Seifert, R. Histamine H_4-receptor expression in the brain? *Naunyn-Schmiedeberg's Arch. Pharmacol.* **2015**, 388, 5-9.

192. Schneider, E. H.; Seifert, R. The histamine H_4-receptor and the central and peripheral nervous system: a critical analysis of the literature. *Neuropharmacology* **2016**, 106, 116-128.

193. Gutzmer, R.; Diestel, C.; Mommert, S.; Köther, B.; Stark, H.; Wittmann, M.; Werfel, T. Histamine H_4 receptor stimulation suppresses IL-12p70 production and mediates chemotaxis in human monocyte-derived dendritic cells. *J. Immunol.* **2005**, 174, 5224-5232.

194. Hofstra, C. L.; Desai, P. J.; Thurmond, R. L.; Fung-Leung, W.-P. Histamine H_4 receptor mediates chemotaxis and calcium mobilization of mast cells. *J. Pharmacol. Exp. Ther.* **2003**, 305, 1212-1221.

195. Schirmer, B.; Bringmann, L.; Seifert, R.; Neumann, D. *In vivo* evidence for partial activation of eosinophils via the histamine H_4-receptor: adoptive transfer experiments using eosinophils from $H_4R^{-/-}$ and $H_4R^{+/+}$ Mice. *Front. Immunol.* **2018**, 9, 2119.

196. Schirmer, B.; Lindemann, L.; Bittkau, K. S.; Isaev, R.; Bösche, D.; Juchem, M.; Seifert, R.; Neumann, D. Mouse colonic epithelial cells functionally express the histamine H_4 receptor. *J. Pharmacol. Exp. Ther.* **2020**, 373, 167-174.

197. Yamaura, K.; Oda, M.; Suwa, E.; Suzuki, M.; Sato, H.; Ueno, K. Expression of histamine H_4 receptor in human epidermal tissues and attenuation of experimental pruritus using H_4 receptor antagonist. *J. Toxicol. Sci.* **2009**, 34, 427-431.

198. Kollmeier, A.; Francke, K.; Chen, B.; Dunford, P. J.; Greenspan, A. J.; Xia, Y.; Xu, X. L.; Zhou, B.; Thurmond, R. L. The histamine H_4 receptor antagonist, JNJ 39758979, is effective in reducing histamine-induced pruritus in a randomized clinical study in healthy subjects. *J. Pharmacol. Exp. Ther.* **2014**, 350, 181-187.

199. Thurmond, R. L.; Kazerouni, K.; Chaplan, S. R.; Greenspan, A. J. Antihistamines and itch. *Handb. Exp. Pharmacol.* **2015**, 226, 257-290.

200. Schaper-Gerhardt, K.; Rossbach, K.; Nikolouli, E.; Werfel, T.; Gutzmer, R.; Mommert, S. The role of the Histamine H_4 receptor in atopic dermatitis and psoriasis. *Br. J. Pharmacol.* **2020**, 177, 490-502.

201. Neumann, D. Role of the histamine H_4-receptor in bronchial asthma. *Handb. Exp. Pharmacol.* **2016**, 241, 347-359.

202. Deiteren, A.; De Man, J. G.; Pelckmans, P. A.; De Winter, B. Y. Histamine H_4 receptors in the gastrointestinal tract. *Br. J. Pharmacol.* **2015**, 172, 1165-1178.

203. Cowden, J. M.; Yu, F.; Banie, H.; Farahani, M.; Ling, P.; Nguyen, S.; Riley, J. P.; Zhang, M.; Zhu, J.; Dunford, P. J.; Thurmond, R. L. The histamine H_4 receptor mediates inflammation and Th17 responses in preclinical models of arthritis. *Ann. Rheum. Dis.* **2014**, 73, 600-608.

204. Nicoud, M. B.; Formoso, K.; Medina, V. A. Pathophysiological role of histamine H_4 receptor in cancer: therapeutic implications. *Front. Pharmacol.* **2019**, 10, 556.

205. Sterle, H. A.; Nicoud, M. B.; Massari, N. A.; Taquez Delgado, M. A.; Herrero Ducloux, M. V.; Cremaschi, G. A.; Medina, V. A. Immunomodulatory role of histamine H_4 receptor in breast cancer. *Br. J. Cancer* **2019**, 120, 128-138.

206. Schneider, E. H.; Schnell, D.; Papa, D.; Seifert, R. High constitutive activity and a G-protein-independent high-affinity state of the human histamine H_4-receptor. *Biochemistry* **2009**, 48, 1424-1438.

207. Schnell, D.; Brunskole, I.; Ladova, K.; Schneider, E. H.; Igel, P.; Dove, S.; Buschauer, A.; Seifert, R. Expression and functional properties of canine, rat, and murine histamine H_4 receptors in *Sf*9 insect cells. *Naunyn-Schmiedeberg's Arch. Pharmacol.* **2011**, 383, 457-470.

208. Lim, H. D.; de Graaf, C.; Jiang, W.; Sadek, P.; McGovern, P. M.; Istyastono, E. P.; Bakker, R. A.; de Esch, I. J. P.; Thurmond, R. L.; Leurs, R. Molecular determinants of ligand binding to H_4R species variants. *Mol. Pharmacol.* **2010**, 77, 734-743.

209. Nordemann, U.; Wifling, D.; Schnell, D.; Bernhardt, G.; Stark, H.; Seifert, R.; Buschauer, A. Luciferase reporter gene assay on human, murine and rat histamine H_4 receptor orthologs: correlations and discrepancies between distal and proximal readouts. *PLoS One* **2013**, 8, e73961.

210. Wifling, D.; Löffel, K.; Nordemann, U.; Strasser, A.; Bernhardt, G.; Dove, S.; Seifert, R.; Buschauer, A. Molecular determinants for the high constitutive activity of the human histamine H_4 receptor: functional studies on orthologues and mutants. *Br. J. Pharmacol.* **2015**, 172, 785-798.

211. Savall, B. M.; Chavez, F.; Tays, K.; Dunford, P. J.; Cowden, J. M.; Hack, M. D.; Wolin, R. L.; Thurmond, R. L.; Edwards, J. P. Discovery and SAR of 6-alkyl-2,4-diaminopyrimidines as histamine H_4 receptor antagonists. *J. Med. Chem.* **2014**, 57, 2429-2439.

212. Thurmond, R. L.; Chen, B.; Dunford, P. J.; Greenspan, A. J.; Karlsson, L.; La, D.; Ward, P.; Xu, X. L. Clinical and preclinical characterization of the histamine H_4 receptor antagonist JNJ-39758979. *J. Pharmacol. Exp. Ther.* **2014**, 349, 176-184.

213. Kollmeier, A. P.; Greenspan, A.; Xu, X. L.; Silkoff, P. E.; Barnathan, E. S.; Loza, M. J.; Jiang, J.; Zhou, B.; Chen, B.; Thurmond, R. L. Phase 2a, randomized, double-blind, placebo-controlled, multicentre, parallel-group study of an H_4R-antagonist (JNJ-39758979) in adults with uncontrolled asthma. *Clin. Exp. Allergy* **2018**, 48, 957-969.

214. Murata, Y.; Song, M.; Kikuchi, H.; Hisamichi, K.; Xu, X. L.; Greenspan, A.; Kato, M.; Chiou, C.-F.; Kato, T.; Guzzo, C.; Thurmond, R. L.; Ohtsuki, M.; Furue, M. Phase 2a, randomized, double-blind, placebo-controlled, multicenter, parallel-group study of a H_4R-antagonist (JNJ-39758979) in Japanese adults with moderate atopic dermatitis. *J. Dermatol.* **2015**, 42, 129-139.

215. Thurmond, R. L.; Venable, J.; Savall, B.; La, D.; Snook, S.; Dunford, P. J.; Edwards, J. P. Clinical development of histamine H_4 receptor antagonists. *Handb. Exp. Pharmacol.* **2017**, 241, 301-320.

216. Thurmond, R. L.; Greenspan, A.; Radziszewski, W.; Xu, X. L.; Miao, Y.; Chen, B.; Ge, T.; Zhou, B.; Baker, D. G.; Pavlova, D.; Ritchlin, C. T.; Tanaka, Y.; Takeuchi, T.; Smolen, J. S. Toreforant, a histamine H_4 receptor antagonist, in patients with active rheumatoid arthritis despite methotrexate therapy: results of 2 phase II studies. *J. Rheumatol.* **2016**, 43, 1637-1642.

217. Kollmeier, A. P.; Barnathan, E. S.; O'Brien, C.; Xia, Y. K.; Zhou, B.; Loza, M. J.; Chen, B.; Silkoff, P. E.; Ge, M.; Thurmond, R. L. A phase 2a study of toreforant, a histamine H_4 receptor antagonist, in eosinophilic Asthma. *Ann. Allergy, Asthma Immunol.* **2018**, 121, 568-574.

218. Mowbray, C. E.; Bell, A. S.; Clarke, N. P.; Collins, M.; Jones, R. M.; Lane, C. A. L.; Liu, W. L.; Newman, S. D.; Paradowski, M.; Schenck, E. J.; Selby, M. D.; Swain, N. A.; Williams, D. H. Challenges of drug discovery in novel target space. The discovery and evaluation of PF-3893787: a novel histamine H_4 receptor antagonist. *Bioorg. Med. Chem. Lett.* **2011**, 21, 6596-6602.

219. Werfel, T.; Layton, G.; Yeadon, M.; Whitlock, L.; Osterloh, I.; Jimenez, P.; Liu, W.; Lynch, V.; Asher, A.; Tsianakas, A.; Purkins, L. Efficacy and safety of the histamine H_4 receptor antagonist ZPL-3893787 in patients with atopic dermatitis. *J. Allergy Clin. Immunol.* **2019**, 143, 1830-1837.

220. Arrang, J. M.; Garbarg, M.; Schwartz, J. C. Autoinhibition of histamine synthesis mediated by presynaptic H_3-receptors. *Neuroscience* **1987**, 23, 149-157.

221. van der Goot, H.; Schepers, M. J. P.; Sterk, G. J.; Timmerman, H. Isothiourea analogs of histamine as potent agonists or antagonists of the histamine H_3-receptor. *Eur. J. Med. Chem.* **1992**, 27, 511-517.

222. Kitbunnadaj, R.; Zuiderveld, O. P.; De Esch, I. J. P.; Vollinga, R. C.; Bakker, R.; Lutz, M.; Spek, A. L.; Cavoy, E.; Deltent, M.-F.; Menge, W. M. P. B.; Timmerman, H.; Leurs, R. Synthesis and structure-activity relationships of conformationally constrained histamine H_3 receptor agonists. *J. Med. Chem.* **2003**, 46, 5445-5457.

223. Arrang, J.-M.; Garbarg, M.; Lancelot, J.-C.; Lecomte, J.-M.; Pollard, H.; Robba, M.; Schunack, W.; Schwartz, J.-C. Highly potent and selective ligands for histamine H_3-receptors. *Nature* **1987**, 327, 117-123.

224. Jansen, F. P.; Rademaker, B.; Bast, A.; Timmerman, H. The first radiolabeled histamine H_3 receptor antagonist, [^{125}I]iodophenpropit: saturable and reversible binding to rat cortex membranes. *Eur. J. Pharmacol.* **1992**, 217, 203-205.

225. Geyer, R.; Kaske, M.; Baumeister, P.; Buschauer, A. Synthesis and functional characterization of imbutamine analogs as histamine H_3 and H_4 receptor ligands. *Arch. Pharm.* **2014**, 347, 77-88.

226. Igel, P.; Dove, S.; Buschauer, A. Histamine H_4 receptor agonists. *Bioorg. Med. Chem. Lett.* **2010**, 20, 7191-7199.

227. Kitbunnadaj, R.; Hashimoto, T.; Poli, E.; Zuiderveld, O. P.; Menozzi, A.; Hidaka, R.; de Esch, I. J. P.; Bakker, R. A.; Menge, W. M. P. B.; Yamatodani, A.; Coruzzi, G.; Timmerman, H.; Leurs, R. N-substituted piperidinyl alkyl imidazoles: discovery of methimepip as a potent and selective histamine H_3 receptor agonist. *J. Med. Chem.* **2005**, 48, 2100-2107.

228. Lim, H. D.; Smits, R. A.; Bakker, R. A.; van Dam, C. M. E.; de Esch, I. J. P.; Leurs, R. Discovery of *S*-(2-guanidylethyl)-isothiourea (VUF 8430) as a potent nonimidazole histamine H_4 receptor agonist. *J. Med. Chem.* **2006**, 49, 6650-6651.

229. Igel, P.; Geyer, R.; Strasser, A.; Dove, S.; Seifert, R.; Buschauer, A. Synthesis and structure-activity relationships of cyanoguanidine-type and structurally related histamine H_4 receptor agonists. *J. Med. Chem.* **2009**, 52, 6297-6313.

230. Geyer, R.; Nordemann, U.; Strasser, A.; Wittmann, H.-J.; Buschauer, A. Conformational restriction and enantioseparation increase potency and selectivity of cyanoguanidine-type histamine H_4 receptor agonists. *J. Med. Chem.* **2016**, 59, 3452-3470.

231. Lee-Dutra, A.; Arienti, K. L.; Buzard, D. J.; Hack, M. D.; Khatuya, H.; Desai, P. J.; Nguyen, S.; Thurmond, R. L.; Karlsson, L.; Edwards, J. P.; Breitenbucher, J. G. Identification of 2-arylbenzimidazoles as potent human histamine H_4 receptor ligands. *Bioorg. Med. Chem. Lett.* **2006**, 16, 6043-6048.

232. Savall, B. M.; Edwards, J. P.; Venable, J. D.; Buzard, D. J.; Thurmond, R.; Hack, M.; McGovern, P. Agonist/antagonist modulation in a series of 2-aryl benzimidazole H_4 receptor ligands. *Bioorg. Med. Chem. Lett.* **2010**, 20, 3367-3371.

233. Baumeister, P. Molecular Tools for G-Protein Coupled Receptors: Synthesis, Pharmacological Characterization and [^{3}H]-Labeling of Subtype-Selective Ligands for Histamine H_4 and NPY Y_2 Receptors. Ph. D. Dissertation, University of Regensburg, Regensburg, 2014.

234. Berrebi-Bertrand, I.; Billot, X.; Calmels, T.; Capet, M.; Krief, S.; Labeeuw, O.; Lecomte, J.-M.; Levoin, N.; Ligneau, X.; Robert, P.; Schwartz, J.-C. Preparation of Benzimidazole Derivatives as Dual Histamine H_1 and Histamine H_4 Receptor Ligands. US 20190144421 A1, 2019. Chem. Abstr. 170:605377.

235. Deiteren, A.; De Man, J. G.; Ruyssers, N. E.; Moreels, T. G.; Pelckmans, P. A.; De Winter, B. Y. Histamine H_4 and H_1 receptors contribute to postinflammatory visceral hypersensitivity. *Neurogastroenterol. Motil.* **2014**, 63, 1873-1882.

236. Hammer, S. G.; Gobleder, S.; Naporra, F.; Elz, S.; Wittmann, H.-J.; Heinrich, M. R.; Strasser, A. 2,4-Diaminopyrimidines as dual ligands at the histamine H_1 and H_4 receptor-H_1/H_4-receptor selectivity. *Bioorg. Med. Chem. Lett.* **2016**, 26, 292-300.

237. Thurmond, R. L.; Gelfand, E. W.; Dunford, P. J. The role of histamine H_1 and H_4 receptors in allergic inflammation: the search for new antihistamines. *Nat. Rev. Drug Discov.* **2008**, 7, 41-53.

238. Wagner, E.; Wittmann, H.-J.; Elz, S.; Strasser, A. Pharmacological profile of astemizole-derived compounds at the histamine H_1 and H_4 receptor--H_1/H_4 receptor selectivity. *Naunyn-Schmiedeberg's Arch. Pharmacol.* **2014**, 387, 235-250.

239. Cowart, M.; Altenbach, R.; Black, L.; Faghih, R.; Zhao, C.; Hancock, A. A. Medicinal chemistry and biological properties of non-imidazole histamine H_3 antagonists. *Mini-Rev. Med. Chem.* **2004**, 4, 979-992.

240. Jablonowski, J. A.; Grice, C. A.; Chai, W.; Dvorak, C. A.; Venable, J. D.; Kwok, A. K.; Ly, K. S.; Wei, J.; Baker, S. M.; Desai, P. J.; Jiang, W.; Wilson, S. J.; Thurmond, R. L.; Karlsson, L.; Edwards, J. P.; Lovenberg, T. W.; Carruthers, N. I. The first potent and selective non-imidazole human histamine H_4 receptor antagonists. *J. Med. Chem.* **2003**, 46, 3957-3960.

241. Rosethorne, E. M.; Charlton, S. J. Agonist-biased signaling at the histamine H_4 receptor: JNJ7777120 recruits β-arrestin without activating G proteins. *Mol. Pharmacol.* **2011**, 79, 749-757.

242. Seifert, R.; Schneider, E. H.; Dove, S.; Brunskole, I.; Neumann, D.; Strasser, A.; Buschauer, A. Paradoxical stimulatory effects of the "standard" histamine H_4 receptor antagonist JNJ7777120: the H_4 receptor joins the club of 7 transmembrane domain receptors exhibiting functional selectivity. *Mol. Pharmacol.* **2011**, 79, 631-638.

243. Nijmeijer, S.; Vischer, H. F.; Rosethorne, E. M.; Charlton, S. J.; Leurs, R. Analysis of multiple histamine H_4 receptor compound classes uncovers Gα$_i$ protein- and β-arrestin2-biased ligands. *Mol. Pharmacol.* **2012**, 82, 1174-1182.

244. Nijmeijer, S.; Vischer, H. F.; Sirci, F.; Schultes, S.; Engelhardt, H.; de Graaf, C.; Rosethorne, E. M.; Charlton, S. J.; Leurs, R. Detailed analysis of biased histamine H_4 receptor signalling by JNJ 7777120 analogues. *Br. J. Pharmacol.* **2013**, 170, 78-88.

245. Strasser, A.; Wittmann, H.-J.; Buschauer, A.; Schneider, E. H.; Seifert, R. Species-dependent activities of G-protein-coupled receptor ligands: lessons from histamine receptor orthologs. *Trends Pharmacol. Sci.* **2013**, 34, 13-32.

246. Cai, H.; Chavez, F.; Dunford, P. J.; Greenspan, A. J.; Meduna, S. P.; Quiroz, J. A.; Savall, B. M.; Tays, K. L.; Thurmond, R. L.; Wei, J.; Wolin, R. L.; Zhang, X. Diamino-Pyridine, Pyrimidine, and Pyridazine Modulators of the Histamine H_4 Receptor. WO 2009152325 A1. Chem. Abstr. 152:75050

247. Tichenor, M. S. The European Histamine Research Society 43rd Annual Meeting, May 7-10, 2014, Lyon, France. *Inflamm. Res.* **2014**, 63 Suppl 1, 1-48.

248. Tichenor, M. S.; Thurmond, R. L.; Venable, J. D.; Savall, B. M. Functional profiling of 2-aminopyrimidine histamine H_4 receptor modulators. *J. Med. Chem.* **2015**, 58, 7119-7127.

249. Ashworth, S.; Rabiner, E. A.; Gunn, R. N.; Plisson, C.; Wilson, A. A.; Comley, R. A.; Lai, R. Y. K.; Gee, A. D.; Laruelle, M.; Cunningham, V. J. Evaluation of ^{11}C-GSK189254 as a novel radioligand for the H_3 receptor in humans using PET. *J. Nucl. Med.* **2010**, 51, 1021-1029.

250. van der Goot, H.; Timmerman, H. Selective ligands as tools to study histamine receptors. *Eur. J. Med. Chem.* **2000**, 35, 5-20.

251. Arrang, J. M.; Roy, J.; Morgat, J. L.; Schunack, W.; Schwartz, J. C. Histamine H_3 receptor binding sites in rat brain membranes: modulations by guanine nucleotides and divalent cations. *Eur. J. Pharmacol. (Mol. Pharmacol. Sect.)* **1990**, 188, 219-227.

252. Alves-Rodrigues, A.; Leurs, R.; Wu, T.-S.; Prell, G. D.; Foged, C.; Timmerman, H. [^{3}H]-Thioperamide as a radioligand for the histamine H_3 receptor in rat cerebral cortex. *Br. J. Pharmacol.* **1996**, 118, 2045-2052.

253. Jansen, F. P.; Mochizuki, T.; Maeyama, K.; Leurs, R.; Timmerman, H. Characterization of histamine H_3 receptors in mouse brain using the H_3 antagonist [^{125}I]iodophenpropit. *Naunyn-Schmiedeberg's Arch. Pharmacol.* **2000**, 362, 60-67.

254. Ligneau, X.; Garbarg, M.; Vizuete, M. L.; Diaz, J.; Purand, K.; Stark, H.; Schunack, W.; Schwartz, J.-C. [^{125}I]Iodoproxyfan, a new antagonist to label and visualize cerebral histamine H_3 receptors. *J. Pharmacol. Exp. Ther.* **1994**, 271, 452-459.

255. Stark, H.; Purand, K.; Hüls, A.; Ligneau, X.; Garbarg, M.; Schwartz, J.-C.; Schunack, W. [^{125}I]iodoproxyfan and related compounds: a reversible radioligand and novel classes of antagonists with high affinity and selectivity for the histamine H_3 receptor. *J. Med. Chem.* **1996**, 39, 1220-1226.

256. Thurmond, R. L.; Desai, P. J.; Dunford, P. J.; Fung-Leung, W.-P.; Hofstra, C. L.; Jiang, W.; Nguyen, S.; Riley, J. P.; Sun, S.; Williams, K. N.; Edwards, J. P.; Karlsson, L. A potent and selective histamine H_4 receptor antagonist with anti-inflammatory properties. *J. Pharmacol. Exp. Ther.* **2004**, 309, 404-413.

257. Bartole, E.; Littmann, T.; Tanaka, M.; Ozawa, T.; Buschauer, A.; Bernhardt, G. [^{3}H]UR-DEBa176: a 2,4-diaminopyrimidine-type radioligand enabling binding studies at the human, mouse, and rat histamine H_4 receptors. *J. Med. Chem.* **2019**, 62, 8338-8356.

258. Amon, M.; Ligneau, X.; Schwartz, J.-C.; Stark, H. Fluorescent non-imidazole histamine H_3 receptor ligands with nanomolar affinities. *Bioorg. Med. Chem. Lett.* **2006**, 16, 1938-1940.

259. Amon, M.; Ligneau, X.; Camelin, J. C.; Berrebi-Bertrand, I.; Schwartz, J.-C.; Stark, H. Highly potent fluorescence-tagged nonimidazole histamine H_3 receptor ligands. *ChemMedChem* **2007**, 2, 708-716.

260. Tomasch, M.; Schwed, J. S.; Weizel, L.; Stark, H. Novel chalcone-based fluorescent human histamine H_3 receptor ligands as pharmacological tools. *Front. Syst. Neurosci.* **2012**, 6, 14.

261. Mirzahosseini, A.; Kovacs, M.; Kanai, K.; Csutora, P.; Dalmadi, B. BODIPY® FL histamine as a new modality for quantitative detection of histamine receptor upregulation upon IgE sensitization in murine bone marrow-derived mast cells. *Cytometry Part A* **2015**, 87A, 23-31.

262. Geyer, R. Hetarylalkyl(aryl)cyanoguanidines as Histamine H_4 Receptor Ligands: Synthesis, Chiral Separation, Pharmacological Characterization, Structure-Activity and -Selectivity Relationships. Ph.D. Dissertation, University of Regensburg, Regensburg, 2011.

263. Bartole, E.; Grätz, L.; Littmann, T.; Wifling, D.; Seibel, U.; Buschauer, A.; Bernhardt, G. UR-DEBa242:a Py-5-labeled fluorescent multipurpose probe for investigations on the histamine H_3 and H_4 receptors. *J. Med. Chem.* **2020**, 63, 5297-5311.

2. Background, problem and objectives

Over the years, the histamine H_3 and H_4 receptors have emerged as promising therapeutic targets within the histamine receptor family ($H_{1-4}R$). Just recently, pitolisant, an H_3R antagonist, was approved for the treatment of narcolepsy.[1] At present, several H_3R inverse agonists/antagonists attained clinical trials for various indications.[2] By contrast, for the H_4R only three worth mentioning candidates reached clinical studies on atopic dermatitis, psoriasis, asthma or rheumatoid arthritis.[3] Possible reasons for this low outcome are the not fully elucidated expression pattern[4-7] of the H_4R and the marked species [human (h), mouse (m), rat (r)]-dependent differences[8-10], regarding affinities, potencies and/or even the quality of action of several H_4R ligands. Consequently, the translational value of rodent animal models is compromised. Such models are crucial for the development of new drug candidates and for investigations on the (patho)physiological role of the H_4R.

Radio- and fluorescent ligands with a balanced affinity-/functional profile at the H_4R species orthologs can be valuable molecular tools to gain a deeper understanding of the H_4R by means of rodent animal models. Although several radioligands have been successfully applied at the hH_4R in recombinant systems[11-14], no radioligand is known to be eligible for comparative and robust binding studies at the $h/m/rH_4Rs$. Furthermore, highly affinic fluorescent ligands are strongly needed to contribute to investigations on the expression of the H_4R. In addition to their application in imaging, e.g. confocal microscopy, these molecular tools can be applied in bioluminescent resonance energy transfer (BRET)-based binding studies as well. Advantages of such studies include e.g. a medium to high-throughput performance and a high temporal resolution. For the H_3R, several well-characterized radio-[12,15-19] and fluorescent[20-22] ligands have been described. However, only two commercially available and poorly characterized fluorescent ligands were applied in BRET-based binding studies[23], which are not only expensive, but show also less than ideal spectral properties.

Therefore, this thesis aimed at the development of two complementary molecular tools: on one hand, a high affinity radioligand that can be used for comparative binding studies at the $h/m/rH_4Rs$. On the other hand, an extensively characterized fluorescent ligand, which enables localization studies of the hH_4R in live cells and comparative BRET-based binding studies at the NanoLuc (NLuc)-tagged h/mH_4Rs and hH_3R.

To achieve the first goal, the following requirements of a potential radioligand were defined: a convenient radiolabeling procedure, a high degree of (radio)chemical purity/stability and a reasonable specific activity. Moreover, apart from comparable efficacies at the h/m/rH$_4$Rs, the radioligand should reveal binding constants in the one- to two-digit-nM range and a low nonspecific binding around the K_d value. Therefore, it was aimed at the synthesis of a library of 2,4-diaminopyrimidines, based on the structure of the equipotent h/m/rH$_4$Rs agonist (*R*)-4-(3-aminopyrrolidin-1-yl)-*N*-neopentylpyrimidin-2-amine[24]. It was intended to structurally modify position 4 of the molecule by introducing (cyclic) aliphatic amines (partly methylated, propionylated or guanidinylated), histamine, and some of its homologs, while keeping the neopentylamine in position 2. The compounds had to be characterized by radioligand binding and in functional assays. The results of functional assays at the human and rodent H$_4$Rs should guide the selection of target structures for radiolabeling. Finally, the tritiated 2,4-diaminopyrimide had to be analytically and pharmacologically characterized.

In order to meet the second aim, histamine and several homologs were chosen as pharmacophores to be labeled with the fluorophore pyrylium-5[25] (Py-5, 4-{(*1E,3E*)-4-[4-(dimethylamino)phenyl]buta-1,3-dienyl}-2,6-dimethylpyrylium tetrafluoroborate), with or without the introduction of a propylene spacer. The Py-5 label, as it is well-suited for an NLuc-based BRET assay, convinced due to its spectral properties, its small size, and the convenient labeling procedure. As described for the developed radioligand, the library of fluorescent probes had to be investigated by applying radioligand binding and functional assays. The compound with highest binding affinities and/or potencies (at least in two-digit-nM range) at the hH$_3$R and the h/mH$_4$Rs was planned to be extensively characterized by using e.g. confocal microscopy, BRET-based binding assays and flow cytometry.

2.1 References

1. Thorpy, M. J. Recently approved and upcoming treatments for narcolepsy. *CNS Drugs* **2020**, 34, 9-27.

2. Ghamari, N.; Zarei, O.; Arias-Montano, J.-A.; Reiner, D.; Dastmalchi, S.; Stark, H.; Hamzeh-Mivehroud, M. Histamine H$_3$ receptor antagonists/inverse agonists: where do they go? *Pharmacol. Ther.* **2019**, 200, 69-84.

3. Nicoud, M. B.; Formoso, K.; Medina, V. A. Pathophysiological role of histamine H$_4$ receptor in cancer: therapeutic implications. *Front. Pharmacol.* **2019**, 10, 556.

4. Capelo, R.; Lehmann, C.; Ahmad, K.; Snodgrass, R.; Diehl, O.; Ringleb, J.; Flamand, N.; Weigert, A.; Stark, H.; Steinhilber, D.; Kahnt, A. S. Cellular analysis of the histamine H$_4$ receptor in human myeloid cells. *Biochem. Pharmacol.* **2016**, 103, 74-84.

5. Sanna, M. D.; Ghelardini, C.; Thurmond, R. L.; Masini, E.; Galeotti, N. Behavioural phenotype of histamine H$_4$ receptor knockout mice: focus on central neuronal functions. *Neuropharmacology* **2017**, 114, 48-57.

6. Schneider, E. H.; Neumann, D.; Seifert, R. Histamine H$_4$-receptor expression in the brain? *Naunyn-Schmiedeberg's Arch. Pharmacol.* **2015**, 388, 5-9.

7. Schneider, E. H.; Seifert, R. The histamine H$_4$-receptor and the central and peripheral nervous system: a critical analysis of the literature. *Neuropharmacology* **2016**, 106, 116-128.

8. Liu, C.; Wilson, S. J.; Kuei, C.; Lovenberg, T. W. Comparison of human, mouse, rat, and guinea pig histamine H$_4$ receptors reveals substantial pharmacological species variation. *J. Pharmacol. Exp. Ther.* **2001**, 299, 121-130.

9. Schnell, D.; Brunskole, I.; Ladova, K.; Schneider, E. H.; Igel, P.; Dove, S.; Buschauer, A.; Seifert, R. Expression and functional properties of canine, rat, and murine histamine H$_4$ receptors in *Sf*9 insect cells. *Naunyn-Schmiedeberg's Arch. Pharmacol.* **2011**, 383, 457-470.

10. Wifling, D.; Bernhardt, G.; Dove, S.; Buschauer, A. The extracellular loop 2 (ECL2) of the human histamine H$_4$ receptor substantially contributes to ligand binding and constitutive activity. *PLoS One* **2015**, 10, e0117185.

11. Zhu, Y.; Michalovich, D.; Wu, H.-L.; Tan, K. B.; Dytko, G. M.; Mannan, I. J.; Boyce, R.; Alston, J.; Tierney, L. A.; Li, X.; Herrity, N. C.; Vawter, L.; Sarau, H. M.; Ames, R. S.; Davenport, C. M.; Hieble, J. P.; Wilson, S.; Bergsma, D. J.; Fitzgerald, L. R. Cloning, expression, and pharmacological characterization of a novel human histamine receptor. *Mol. Pharmacol.* **2001**, 59, 434-441.

12. Igel, P.; Schnell, D.; Bernhardt, G.; Seifert, R.; Buschauer, A. Tritium-labeled N^1-[3-(1H-imidazol-4-yl)propyl]-N^2-propionylguanidine ([^{3}H]UR-PI294), a high-affinity histamine H$_3$ and H$_4$ receptor radioligand. *ChemMedChem* **2009**, 4, 225-231.

13. Lim, H. D.; van Rijn, R. M.; Ling, P.; Bakker, R. A.; Thurmond, R. L.; Leurs, R. Evaluation of histamine H$_1$-, H$_2$-, and H$_3$-receptor ligands at the human histamine H$_4$ receptor: identification of 4-methylhistamine as the first potent and selective H$_4$ receptor agonist. *J. Pharmacol. Exp. Ther.* **2005**, 314, 1310-1321.

14. Thurmond, R. L.; Desai, P. J.; Dunford, P. J.; Fung-Leung, W.-P.; Hofstra, C. L.; Jiang, W.; Nguyen, S.; Riley, J. P.; Sun, S.; Williams, K. N.; Edwards, J. P.; Karlsson, L. A potent and selective histamine H$_4$ receptor antagonist with anti-inflammatory properties. *J. Pharmacol. Exp. Ther.* **2004**, 309, 404-413.

15. Arrang, J. M.; Garbarg, M.; Schwartz, J. C. Autoinhibition of histamine synthesis mediated by presynaptic H$_3$-receptors. *Neuroscience* **1987**, 23, 149-157.

16. Arrang, J. M.; Roy, J.; Morgat, J. L.; Schunack, W.; Schwartz, J. C. Histamine H$_3$ receptor binding sites in rat brain membranes: modulations by guanine nucleotides and divalent cations. *Eur. J. Pharmacol. (Mol. Pharmacol. Sect.)* **1990**, 188, 219-227.

17. Alves-Rodrigues, A.; Leurs, R.; Wu, T.-S.; Prell, G. D.; Foged, C.; Timmerman, H. [^{3}H]-Thioperamide as a radioligand for the histamine H$_3$ receptor in rat cerebral cortex. *Br. J. Pharmacol.* **1996**, 118, 2045-2052.

18. Jansen, F. P.; Mochizuki, T.; Maeyama, K.; Leurs, R.; Timmerman, H. Characterization of histamine H$_3$ receptors in mouse brain using the H$_3$ antagonist [^{125}I]iodophenpropit. *Naunyn-Schmiedeberg's Arch. Pharmacol.* **2000**, 362, 60-67.

19. Stark, H.; Purand, K.; Hüls, A.; Ligneau, X.; Garbarg, M.; Schwartz, J.-C.; Schunack, W. [^{125}I]iodoproxyfan and related compounds: a reversible radioligand and novel classes of antagonists with high affinity and selectivity for the histamine H$_3$ receptor. *J. Med. Chem.* **1996**, 39, 1220-1226.

20. Tomasch, M.; Schwed, J. S.; Paulke, A.; Stark, H. Bodilisant - a novel fluorescent, highly affine histamine H$_3$ receptor ligand. *ACS Med. Chem. Lett.* **2013**, 4, 269-273.

21. Tomasch, M.; Schwed, J. S.; Weizel, L.; Stark, H. Novel chalcone-based fluorescent human histamine H$_3$ receptor ligands as pharmacological tools. *Front. Syst. Neurosci.* **2012**, 6, 14.

22. Amon, M.; Ligneau, X.; Camelin, J. C.; Berrebi-Bertrand, I.; Schwartz, J.-C.; Stark, H. Highly potent fluorescence-tagged nonimidazole histamine H$_3$ receptor ligands. *ChemMedChem* **2007**, 2, 708-716.

23. Mocking, T. A. M.; Verweij, E. W. E.; Vischer, H. F.; Leurs, R. Homogeneous, real-time NanoBRET binding assays for the histamine H$_3$ and H$_4$ receptors on living cells. *Mol. Pharmacol.* **2018**, 94, 1371-1381.

24. Tichenor, M. S. The European Histamine Research Society 43rd Annual Meeting, May 7-10, 2014, Lyon, France. *Inflamm. Res.* **2014**, 63 Suppl 1, 1-48.

25. Wetzl, B. K.; Yarmoluk, S. M.; Craig, D. B.; Wolfbeis, O. S. Chameleon labels for staining and quantifying proteins. *Angew. Chem. Int. Ed.* **2004**, 43, 5400-5402.

3. [³H]UR-DEBa176: a 2,4-diaminopyrimidine-type radioligand enabling binding studies at the human, mouse and rat histamine H_4 receptors

Prior to the submission of this thesis, parts of this chapter were published in cooperation with partners:

Author contributions:
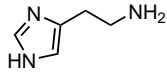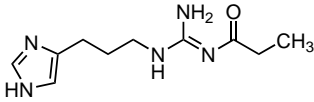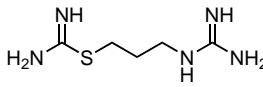
E.B. conceived the project with input from A.B and G.B. E.B. synthesized compounds, performed experiments and data analysis with supervision from A.B. and G.B. M.T. cloned the vector hH$_4$R-ELucC/ELucN-β-arrestin2 under supervision of T.O. T.L. cloned the vectors mH$_4$R-ELucC/ELucN-β-arrestin2 and rH$_4$R-ELucC/ELucN-β-arrestin2 and generated the respective HEK293T cell lines under supervision of G.B. and A.B. E.B. and G.B. wrote the manuscript with input from all co-authors.

3.1 Introduction

The human histamine H_4 receptor (hH_4R) was discovered at the turn of the millennium as the latest member of the histamine receptor family ($H_{1-4}Rs$)[1-7] and is expected to be a promising target for the treatment of disorders of the immune system (e.g. rheumatoid arthritis, bronchial asthma).[8,9] The expression and a potential physiological role of the H_4R in the brain was controversially discussed in the literature.[10] For investigations on the (patho)physiology of the H_4R, mouse and rat became the most important laboratory animals.[11] However, the pharmacological evaluation of the rodent histamine H_4 receptors (mH_4R, rH_4R) is compromised by species-dependent discrepancies regarding the potencies (e.g. **3.01**, **3.02**[12], and **3.03**[13]) and/or the quality of action (e.g. **3.04**[14], **3.05**[15] and **3.06**[14]) of standard ligands for the hH_4R (Figure 3.1).[16-18] These differences are probably caused by the substantially different constitutive activities of the H_4R species orthologs[4,17,19,20] and the low sequence homology ($68 - 69\%$[21]) of the mH_4R and the rH_4R with the hH_4R.

For radioligand binding studies at the H_4R, only four radioligands [[³H]**3.01**[4,5,16,21,22], [³H]**3.02**[12], [³H]**3.05**[14,23] and [125I]iodophenpropit[14] (not shown)] were reported, but their use is limited: due to the low potencies at the rodent receptors (Figure 3.1) in combination with the specific activity of $10 - 25$ Ci/mmol of the commercially available labeled histamine [³H]**3.01**, relatively high amounts of radioligand and the receptor protein are required for binding studies.[12] Additionally, binding experiments with [³H]**3.01** revealed either significantly different binding constants [K_d (nM): $5 - 9$ (hH_4R); $42 - 78$ (mH_4R); $134 - 178$ (rH_4R)][21-24] at the receptor orthologs or failed[16] at the mouse and rat H_4Rs. Iodophenpropit is a high-affinity hH_4R ligand (pK_i: 7.9[14]). Nonetheless, the use of [125I]iodophenpropit as a radioligand is limited due to the poor chemical stability, short half-life of the 125I-label (59.4 days) in comparison to ³H-labeled ligands (12.4 years) and the need to follow special safety precautions (e.g. shielding) during preparation and handling.[12] The radiolabeled agonist [³H]**3.02**[12] (Figure 3.1) was developed for the hH_3R and hH_4R with comparably high affinities at both receptor subtypes. By contrast, the potency of **3.02** at the mH_4R and rH_4R was in the three-to four-digit-nM range (Figure 3.1) in a functional assay with a proximal readout ([35S]-GTPγS assay[17]). Therefore, [³H]**3.02** is inappropriate for radioligand binding experiments at the mH_4R or rH_4R. Binding studies with [³H]**3.05** revealed comparably high affinities at the h/m/rH_4Rs.[23] By contrast, saturation

binding experiments with [³H]**3.05** in our laboratory[25] were only feasible at the hH₄R expressed in *Sf*9 membranes, accompanied by a high level of nonspecific binding (30 – 40% of total binding around the K_d)[25]. Additionally, the substantial species-dependent differences in the quality of action of **3.05** in several functional assays (e. g. [³⁵S]-GTPγS[17] and luciferase reporter gene[18] assays) may compromise H₄R radioligand binding studies across species. Moreover, [³H]**3.05** is not commercially available and a customer commissioned synthesis would be expensive.[25]

histamine
3.01

xH₄R	pEC$_{50}$	α
h	8.13	1.00
m	5.17	1.00
r	4.28	1.00

UR-PI294
3.02

xH₄R	pEC$_{50}$	α
h	8.35	1.02
m	6.10	0.95
r	5.48	1.09

VUF8430
3.03

xH₄R	pEC$_{50}$	α
h	7.42	0.84
m	5.06	0.68
r	4.47	0.43
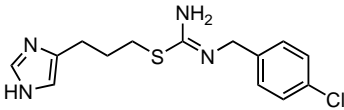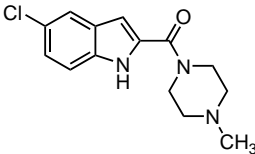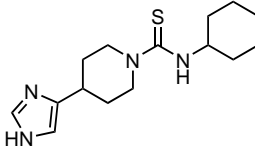
clobenpropit
3.04

xH₄R	pEC$_{50}$/(pK_b)	α
h	7.65	0.45
m	6.07	0.20
r	(6.28)	0

JNJ7777120
3.05

xH₄R	pEC$_{50}$/(pK_b)	α
h	(7.60)	-0.39
m	6.10	0.44
r	6.13	0.24

thioperamide
3.06

xH₄R	pK_b	α
h	6.83	-1.39
m	7.12	0
r	6.44	0

Figure 3.1. Structures and functional data of known hH₄R ligands obtained from [³⁵S]-GTPγS-binding assays[17] on the human (h), mouse (m) and rat (r) H₄R receptors.

Due to the aforementioned drawbacks of the reported radioligands for the H₄R, we were aiming at a new radioligand as a molecular tool, allowing comparative and robust binding studies at the h/m/rH₄Rs with the following characteristics: convenient synthesis (e.g. by methylation[26] or propionylation[27] in the last synthetic step), high degree of chemical/radiochemical purity and stability, high specific activity, low nonspecific binding (< 20% of total binding), binding constants (K_d values) in the one- to two-digit-nM range and comparable intrinsic activities at the h/m/rH₄Rs. Therefore, a set of 2,4-diaminopyrimidines

was prepared, based on the structure of **3.33**[28,29] (Scheme 3.1), which was reported as an equipotent agonist at the human and rodent H$_4$Rs[29]. For structural modification (cyclic) aliphatic amines, histamine **3.01,** and some of its homologs were introduced in position 4 of the 2,4-diaminopyrimidine scaffold, whereas in position 2, a neopentylamine moiety was kept constant (Scheme 3.1). Some cyclic aliphatic amines were methylated, propionylated or guanidinylated (Scheme 3.1). Initially, the structure-affinity relationships of the small library were explored at the hH$_4$R. The selection of target structures for radiolabeling was based on the results of various functional assays at the human and the rodent H$_4$R species variants.

3.2 Results and discussion

3.2.1 Chemistry

Heating the amine precursors **3.07** – **3.18** (structures see Scheme A 3.1 – Scheme A 3.3 and Figure A 3.1, source or synthesis see in section 3.5.1) with the 2,4-dichloropyrimidine **3.19** (Scheme 3.1) in a microwave reactor or in a round-bottom flask[28] under basic conditions in isopropyl alcohol (*i*-PrOH), the intermediates **3.20** – **3.31** (Scheme 3.1) were prepared (synthesis see in section 3.5.2). Subsequently, a second nucleophilic substitution reaction of **3.20** with an excess of 2,2-dimethylpropan-1-amine was performed in a protic solvent (*i*-PrOH) and in the presence of *N,N*-diisopropylethylamine (DIPEA) using a microwave reactor over 6 hours to get the Boc-protected 2,4-diaminopyrimidine **3.32** (Scheme 3.1). After removal of the protection group under acidic conditions [trifluoroacetic acid (TFA)], the desired 2,4-diaminopyrimidine **3.33** was obtained in good yield (78.4%). Basically, target compounds **3.34** – **3.44** were prepared under comparable conditions, starting with intermediates **3.21** – **3.31**. For the preparation of **3.44**, deprotection was unnecessary.

Treating the Boc-protected intermediate **3.32** with an excess of $LiAlH_4$ (5 equiv) in anhydrous tetrahydrofuran (THF)[30], the monomethylated 2,4-diaminopyrimidine **3.45** was obtained in moderate yield (43.1%) after refluxing for 7 h (Scheme 3.1).

Target compounds **3.33** – **3.35** were methylated under Eschweiler-Clarke conditions using formaldehyde and formic acid to give the mono- or dimethylated 2,4-diaminopyrimidines **3.46** – **3.48** (Scheme 3.1).

The guanidinylations of **3.33** – **3.35** using 1,3-bis(*tert*-butoxycarbonyl)-2-methyl-2-thiopseudourea[25] and $HgCl_2$ under basic conditions were performed as previously described[31]. Subsequent deprotection under acidic conditions led to **3.49** – **3.51** (Scheme 3.1).

Compound **3.33** was propionylated under basic conditions using 1-propionylpyrrolidine-2,5-dione, based on a previously described procedure[27] to give **3.52** (Scheme 3.1).

All target compounds (Scheme 3.1) were purified by preparative high-performance liquid chromatography (HPLC) to obtain the respective TFA salts in high chemical purity (> 96%) (for details see in section 3.4).

Scheme 3.1. Synthesis of the 2,4-diaminopyrimidines 3.33 – 3.52.
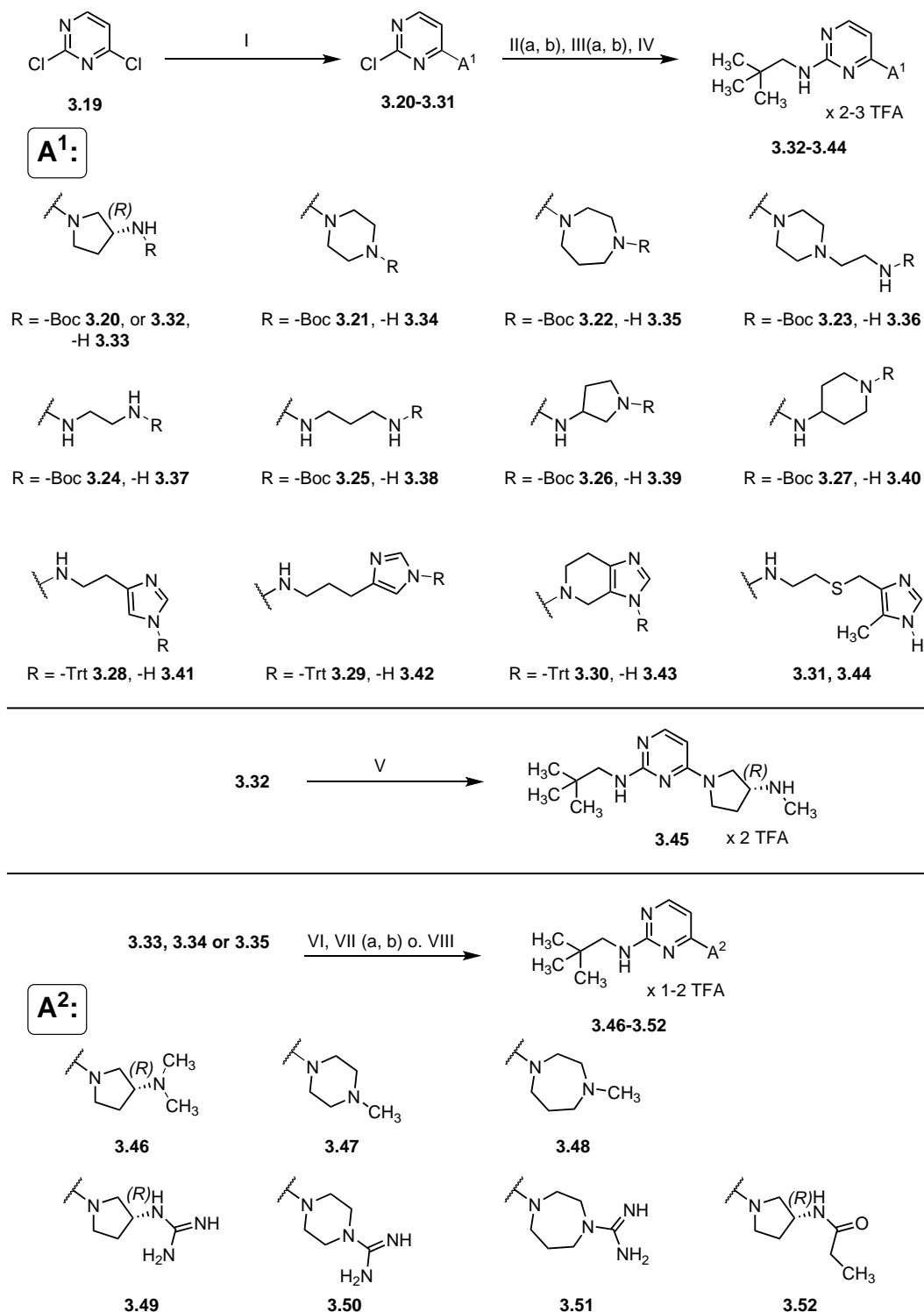
Reagents and conditions: (I) **3.07 – 3.18** (see in section 3.5.1), DIPEA, *i*-PrOH, 120 °C (microwave), 1 h, 72.5% (**3.20**), or 55 – 85 °C, 4 – 20 h, 64 – 95% (**3.21 – 3.31**) (see in section 3.5.2); (IIa) **3.20**, 2,2-dimethylpropan-1-amine, DIPEA, *i*-PrOH, 130 °C (microwave), 6 h, 96.1% (**3.32**), (IIb) **3.32**, TFA, DCM, rt, 8 h, 78.4% (**3.33**); (IIIa) **3.21 – 3.30**, 2,2-dimethylpropan-1-amine, DIPEA, *i*-PrOH, 120 – 130 °C (microwave), 5 – 11 h, (IIIb) TFA, DCM, rt, 7 – 18 h, 14 – 65% (**3.34 – 3.43**); (IV) **3.31**, 2,2-dimethylpropan-1-amine, DIPEA, *i*-PrOH, 120 °C (microwave), 4 h, 17.4% (**3.44**); (V) LiAlH₄, anhydrous THF, 70 °C, 7 h, 43.1% (**3.45**). (VI) **3.33 – 3.35**, formic acid/formamide 1/1 (*v/v*), 95 °C, 3 – 5 h, 49 – 73% (**3.46 – 3.48**); (VIIa) **3.33 – 3.35**, 1,3-bis(*tert*-butoxycarbonyl)-2-methyl-2-thiopseudourea, HgCl₂, TEA, DCM, rt, 6 h, (VIIb) TFA, DCM, rt, 5 – 7 h, 25 – 40% (**3.49 – 3.51**); (VIII) **3.33**, 1-propionylpyrrolidine-2,5-dione, DIPEA, DCM, rt, 24 h, 57.0% (**3.52**).

3.2.2 Investigations on chemical stability

The chemical stability of **3.43** (UR-DEBa148), **3.46** (UR-DEBa176), **3.48** and **3.49** was investigated in phosphate-buffered saline (PBS, pH 7.4) at 23 °C and over a time period of 24 h. Under these conditions, the investigated 2,4-diaminopyrimidines proved stable (for graphs see Figure A 3.33 – Figure A 3.36 in section 3.5.5.3, for details see section 3.4.4).

3.2.3 Structure affinity and subtype selectivity relationships of the target compounds (3.33 – 3.52) at the human histamine receptors

With the 2,4-diaminopyrimdines, radioligand competition binding experiments were performed to investigate their structure-affinity relationships at the hH₄R and their subtype selectivity over the hH₁₋₃Rs. The binding constants (pK_i values) at the hH₁₋₄R, expressed in membrane preparations of *Sf*9 insect cells, are presented in Table 3.1. The structures of the synthesized 2,4-diaminopyrimidines are depicted in Table 3.1.

The (*R*)-3-aminopyrrolidine **3.33**[28,29] and the homopiperazine **3.35**[28] revealed comparable high affinities at the hH₄R (pK_i = 8.07 and 7.88, respectively). Selectivity over the hH₃R was improved for **3.35** (≈ 30-fold compared to **3.33**), whereas **3.33** was almost equi-affinic. In comparison to **3.35**, the hH₄R affinity of the piperazine **3.34**[28] was reduced (≈ 14-fold), which is remarkable because the difference is only one methylene group in the aliphatic ring. The selectivity over hH₃R was comparable. By introducing an ethylenediamine moiety into **3.34**, and thereby adding an additional basic primary amine to the eastern part of the molecule and increasing flexibility, the decrease in hH₄R affinity was striking (**3.36**: pK_i < 5). The coupling of ethylenediamine, 3-aminopyrrolidine or 4-aminopiperidine to the 4-position of the pyrimidine core (**3.37**, **3.39** and **3.40**) via the primary amine function was not successful in gaining affinity for the hH₄R and hH₃R (pK_i < 7.0). An additional H-bond donor and/or an increased flexibility in the aliphatic amine motif seemed not to be tolerated by the hH₄R and hH₃R. By contrast, an elongation of the alkine chain, as for the propylenediamine **3.38**, improved affinity for the hH₄R (≈ 6-fold compared to **3.37**) and the selectivity over the hH₃R (≈ 105-fold) was striking.

Despite the fact that imidazole-containing compounds lack subtype selectivity[32], in **3.41 – 3.44** the endogenous ligand histamine **3.01** and some of its homologs, previously used as precursors in the development of hH₄R ligands[12,33-36], were merged with the

2,4-diaminopyrimidine chemotype. Interestingly, the histamine derivative **3.41** and homohistamine derivative **3.42** showed comparably weak hH_4R affinities (pK_i = 6.69 and 6.35, respectively), while selectivity for the hH_3R increased with the elongation of the alkine chain of the histamine analog (**3.41**: ≈ 20-fold; **3.42**: ≈ 50-fold). Spinaceamine, the rigid congener of histamine **3.01**, was merged with the 2-arylbenzimidazole chemotype by Johnson & Johnson in 2010 to gain subtype selectivity for the hH_4R (≈ 2700-fold[36]). With the introduction of spinaceamine in the 4-position of the 2,4-diaminopyrimidines high affinity for the hH_4R (**3.43**, UR-DEBa148: pK_i = 8.29) was obtained. Unfortunately, with respect to subtype selectivity, **3.43** was almost equi-affinic at the hH_3R. Compound **3.44** revealed weak affinities (pK_i ≤ 6.22) for all receptor subtypes with a tendency for the hH_2R.

Mono (**3.45**[28])- and dimethylation (**3.46**, UR-DEBa176) of the pyrrolidine derivative **3.33** revealed comparably high affinities at the hH_4R (pK_i = 8.42 and 7.93, respectively). Interestingly, the selectivity over the hH_3R increased with the number of introduced methyl groups (**3.45**: ≈ 4-fold compared to **3.33**; **3.46**: ≈ 8-fold compared to **3.33**). Nonetheless, the introduction of methyl groups did not increase the bulkiness very much, which might explain this finding. It is more likely that the H-bond donor group in the pyrrolidine derivatives **3.33** and **3.45** is more relevant for hH_3R binding than for binding to the hH_4R. Methylation of **3.34** and **3.35** did not effect hH_4R affinity (**3.47**: pK_i = 6.94; **3.48**: pK_i = 7.20) or subtype selectivity over the hH_3R (**3.47**: ≈ 1.1-fold compared to **3.34**; **3.48**: ≈ 1.7-fold compared to **3.35**).
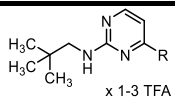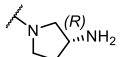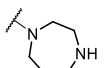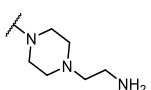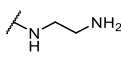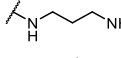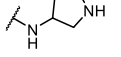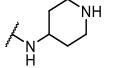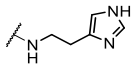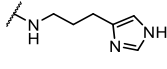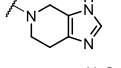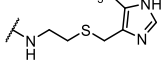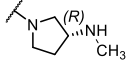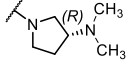
The bioisosteric replacement of primary and secondary amines by a guanidine was previously proven effective in case of several selective hH_3R and hH_4R agonists (e.g. **3.02**[12], **3.03**[13], see Figure 3.1). This concept was transferred to the 2,4-diaminopyrimidine scaffold. Guanidinylation of **3.33**, **3.34** and **3.35** led to a decrease in affinity for the hH_4R (**3.49**: ≈ 8-fold compared to **3.33**; **3.50**: ≈ 3-fold compared to **3.34**; **3.51**: ≈ 204-fold compared to **3.35**) and affinities at the hH_3R were weak as well (pK_i < 6.0). This illustrates that the introduction of a bulky but polar H-bond donor group was not well tolerated by the hH_4R and the hH_3R.

Strikingly, structural modification by introducing a propionyl moiety into **3.33**, and thereby reducing the basicity of the molecule, resulted in a marked decrease in affinity for the hH_4R (**3.52**: ≈ 390-fold compared to **3.33**) and the hH_3R (**3.52:** ≈ 219-fold compared to **3.33**).
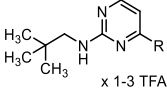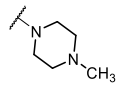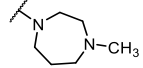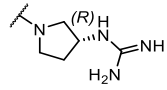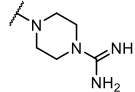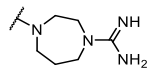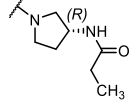
The 2,4-diaminopyrimidines with pK_i values > 6.0 at the hH_4R showed distinct subtype selectivity over the hH_1R and the hH_2R (Table 3.1).

Aiming at a new radioligand for comparative binding studies at hH_4R orthologs, selected 2,4-diaminopyrimidines with pK_i values > 7.0 at the hH_4R (**3.33**, **3.35**, **3.38**, **3.43**, **3.45, 3.46**, **3.48** and **3.49**) were further assessed in a luciferase reporter gene- and β-arrestin2 recruitment assay at the $h/m/rH_4Rs$. Their ortholog selectivity was studied to identify compounds with comparable potencies and efficacies across the H_4R species variants.

Table 3.1. Affinities at the $hH_{1-4}Rs$ and subtype selectivity profile of the 2,4-diaminopyrimidines.

No.	R	pK_i				fold selectivity	
		hH_4R	**hH_3R**	**hH_2R**	**hH_1R**	**H_3R/H_4R**	**H_2R/H_4R**
3.33		8.07 ± 0.10^a	7.86 ± 0.14^c	< 5.0	< 5.0	1.62	> 1175
3.34		6.73 ± 0.02^a	$< 5.0^c$	< 5.0	< 5.0	> 53.7	> 53.7
3.35		7.88 ± 0.06^b	6.20 ± 0.06^d	< 5.0	< 5.0	47.9	> 759
3.36		$< 5.0^a$	$< 5.0^c$	< 5.0	< 5.0	1.00	1.00
3.37		6.69 ± 0.14^a	6.16 ± 0.04^c	< 5.0	< 5.3	3.39	> 49.0
3.38		7.44 ± 0.05^b	$5.42 \pm 0.17^{c,d}$	< 6.0	< 5.0	105	> 27.5
3.39		6.51 ± 0.02^b	$6.69 \pm 0.21^{c,d}$	< 6.0	< 5.0	0.66	> 3.42
3.40		5.72 ± 0.16^b	$5.46 \pm 0.01^{c,d}$	< 6.0	< 5.0	1.82	> 0.52
3.41		6.69 ± 0.07^b	8.02 ± 0.07^d	n.d.	n.d.	0.05	n.a.
3.42		6.35 ± 0.04^b	8.03 ± 0.04^d	n.d.	n.d.	0.02	n.a.
3.43		8.29 ± 0.13^a	8.48 ± 0.04^c	< 5.0	< 5.0	0.65	> 1950
3.44		$< 5.0^a$	$< 5.0^c$	6.22 ± 0.03	< 5.3	1.00	< 0.06
3.45		8.42 ± 0.07^b	$7.56 \pm 0.11^{c,d}$	< 5.0	< 5.0	7.24	> 2630
3.46		7.93 ± 0.04^a	6.84 ± 0.07^c	< 6.0	< 5.0	12.3	> 85.1

[^{3}H]UR-DEBa176: a 2,4-diaminopyrimidine-type radioligand enabling binding studies at the human, mouse and rat histamine H_4 receptors

No.	R	pK_i				fold selectivity	
		hH_4R	**hH_3R**	**hH_2R**	**hH_1R**	**H_3R/H_4R**	**H_2R/H_4R**
3.47	*(structure)*	6.94 ± 0.08^a	5.26 ± 0.04^c	< 5.0	< 5.0	47.9	> 87.1
3.48	*(structure)*	7.20 ± 0.05^a	5.75 ± 0.14^c	< 6.0	< 5.0	28.2	> 15.9
3.49	*(structure)*	$7.16 \pm 0.06^{a,b}$	5.95 ± 0.07^c	< 6.0	< 5.0	16.2	> 14.5
3.50	*(structure)*	6.20 ± 0.01^a	5.22 ± 0.04^c	< 5.0	< 5.3	9.55	> 15.9
3.51	*(structure)*	5.57 ± 0.13^b	$< 5.0^c$	< 5.0	< 5.0	> 3.72	> 3.72
3.52	*(structure)*	5.48 ± 0.08^b	$5.52 \pm 0.15^{c,d}$	< 5.0	< 5.0	0.91	> 3.02

Competition binding determined at cell membranes of *Sf9* insect cells expressing the hH_4R + G$i_{\alpha2}$ + $\beta_1\gamma_2$, hH_3R + G$i_{\alpha2}$ + $\beta_1\gamma_2$, hH_2R-Gs$_{\alpha s}$ or hH_1R + RGS4. Radioligands for hH_4R: [^{3}H]**3.01** (c$_{final}$ = 10 nM^a or 40 nM^b); hH_3R: [^{3}H]N$^\alpha$-methylhistamine (c$_{final}$ = 3 nM)^c or [^{3}H]**3.02**[12] (c$_{final}$ = 2 nM)^d; hH_2R: [^{3}H]UR-DE257[27] (c$_{final}$ = 20 nM); hH_1R: [^{3}H]pyrilamine (c$_{final}$ = 5 nM). The pK_i values represent means ± SEM. Data represent 2 – 3 (for pK_i values ≤ 6.22) or 3 – 4 (for pK_i values > 6.22) independent experiments, each performed in triplicates. Fold selectivity was calculated based on the ratio of the K_i values of the respective compound at the hH_4R, hH_3R and hH_2R. n.d.: not determined. n.a.: not applicable.

3.2.4 Functional characterization of selected target compounds at the h/m/rH_4Rs

The potencies (pEC$_{50}$ values) and the efficacies (α values) of the selected 2,4-diaminopyrimidines, which were obtained in the luciferase reporter gene assay and the β-arrestin2 recruitment assay at the H_4R orthologs, are presented in Table 3.2. Functional assays with distal (reporter gene) and proximal (β-arrestin2) readouts allow a comprehensive investigation on the ortholog selectivity of **3.33**, **3.35**, **3.38**, **3.43**, **3.45**, **3.46**, **3.48** and **3.49**. Of note, due to the distal readout, the luciferase reporter gene assay implies signal amplification.[18] In this study, this was reflected by the discrepancies in the functional profiles of the 2,4-diaminopyrimidines obtained from the different functional assays at all H_4R orthologs. In the luciferase reporter gene assay, all investigated 2,4-diaminopyrimidines (**3.33**, **3.35**, **3.38**, **3.43**, **3.45**, **3.46**, **3.48** and **3.49)** appeared as partial to full agonists with high pEC$_{50}$ values (> 7.0) at the h/m/rH_4Rs (Table 3.2). While **3.33, 3.35** and **3.38** revealed potencies and efficacies comparable between species (balanced functional profiles) in the reporter gene

assays, **3.48** and **3.49** showed unbalanced functional profiles among the H_4R orthologs (Table 3.2). In the β-arrestin2 recruitment assays, **3.33**, **3.35**, **3.38**, **3.48** and **3.49** appeared as partial agonists at the receptor orthologs, but potencies, especially at the mouse and/or rat H_4Rs were weak ($pEC_{50} < 7.0$) (Table 3.2). By contrast, the spinaceamine **3.43** (UR-DEBa148) showed (partial) agonistic activities in the sub-nM range in the luciferase reporter gene assays and in the one- to two-digit-nM range in the β-arrestin2 recruitment assays at the h/m/rH_4Rs.

Using the potencies and the efficacies obtained from luciferase reporter gene- and the β-arrestin2 recruitment assays at the h/m/rH_4Rs, a bias analysis for **3.33**, **3.35**, **3.38**, **3.43**, **3.45,** **3.46**, **3.48** and **3.49** (Figure A 3.2 in section 3.5.3) was performed as described by van der Westhuizen et al.[37] based on the operational model of agonism[38-42], using histamine **3.01** as reference agonist. The bias analysis accounts for several assay specific effects, such as the aforementioned signal amplification. Other effects, including cross-talks between different signaling, influence the determined bias profile, too. Nevertheless, it can be taken as a hint at functionally selective signaling profiles of the investigated 2,4-diaminopyrimdines. Based on this analysis, **3.33**, **3.43**, **3.45**, **3.46**, **3.48** and **3.49** showed a preference for the G-protein mediated pathway [$\Delta\Delta\log (\tau/K_A) > 0$] for at least one of the investigated receptor orthologs, whereas **3.35** and **3.38** were found to have a balanced bias profile [$\Delta\Delta\log (\tau/K_A) \approx 0$] (Figure A 3.2 in section 3.5.3).

Additionally, the 2,4-diaminopyrimidines with pK_i values < 7.0 at the hH_4R (**3.34**, **3.36**, **3.37**, **3.39 – 3.42**, **3.44**, **3.47** and **3.50 – 3.52**) were screened for activity at the mH_4R and the rH_4R in the β-arrestin2 recruitment- and luciferase reporter gene assays applying three distinct concentrations (c_{final} = 100 nM, 1 μM, 10 μM) for each compound in the agonist mode and/or the antagonist mode ($\alpha < 0.1$) (Table A 3.1 in section 3.5.4). For all investigated compounds, no indication for ortholog selectivity for the mH_4R or rH_4R was found.

[³H]UR-DEBa176: a 2,4-diaminopyrimidine-type radioligand enabling binding studies at the human, mouse and rat histamine H₄ receptors

Table 3.2 Potencies and efficacies of the 2,4-diaminopyrimidines at the h/m/rH₄Rs in luciferase reporter gene- and β-arrestin2 recruitment assays.

No.	R	pEC_{50} / (α)					
		hH₄R		**mH₄R**		**rH₄R**	
		reporter gene	β-arr2	reporter gene	β-arr2	reporter gene	β-arr2
3.01	–	7.77^{18} (1.00)	7.47 ± 0.12 (1.00)	7.06^{18} (1.00)	5.63 ± 0.07 (1.00)	6.53^{18} (1.00)	5.43 ± 0.06 (1.00)
3.33		8.48 ± 0.10 (0.83 ± 0.03)	7.84 ± 0.03 (0.38 ± 0.03)	8.38 ± 0.07 (0.99 ± 0.09)	6.87 ± 0.11 (0.83 ± 0.03)	8.75 ± 0.12 (0.98 ± 0.01)	7.47 ± 0.11 (0.31 ± 0.04)
3.35		7.74 ± 0.09 (0.91 ± 0.05)	7.37 ± 0.09 (0.43 ± 0.02)	7.29 ± 0.06 (0.96 ± 0.05)	6.45 ± 0.04 (0.68 ± 0.01)	7.03 ± 0.08 (1.01 ± 0.01)	6.19 ± 0.07 (0.67 ± 0.03)
3.38		7.53 ± 0.10 (0.94 ± 0.06)	7.40 ± 0.14 (0.67 ± 0.02)	7.29 ± 0.10 (1.06 ± 0.07)	5.97 ± 0.06 (0.65 ± 0.02)	7.64 ± 0.07 (0.94 ± 0.07)	6.72 ± 0.03 (0.71 ± 0.05)
3.43		9.91 ± 0.11 (0.58 ± 0.02)	8.38 ± 0.09 (0.19 ± 0.02)	9.60 ± 0.06 (0.77 ± 0.06)	7.94 ± 0.10 (0.58 ± 0.04)	10.30 ± 0.09 (0.98 ± 0.03)	7.78 ± 0.05 (0.36 ± 0.01)
3.45		9.22 ± 0.01 (0.54 ± 0.06)	8.16 ± 0.09 (0.12 ± 0.02)	8.96 ± 0.05 (0.96 ± 0.01)	7.59 ± 0.03 (0.62 ± 0.04)	9.21 ± 0.05 (0.84 ± 0.08)	7.53 ± 0.10 (0.11 ± 0.01)
3.46		8.72 ± 0.09 (0.64 ± 0.01)	7.73 ± 0.12 (0.25 ± 0.01)	8.99 ± 0.05 (0.93 ± 0.03)	7.29 ± 0.06 (0.74 ± 0.05)	9.19 ± 0.10 (1.05 ± 0.02)	7.59 ± 0.07 (0.68 ± 0.05)
3.48		7.71 ± 0.07 (0.87 ± 0.02)	6.86 ± 0.01 (0.34 ± 0.03)	7.45 ± 0.05 (0.90 ± 0.04)	6.08 ± 0.01 (0.72 ± 0.05)	8.93 ± 0.10 (0.98 ± 0.02)	6.48 ± 0.11 (0.75 ± 0.03)
3.49		7.45 ± 0.04 (0.91 ± 0.04)	7.05 ± 0.09 (0.44 ± 0.02)	8.21 ± 0.19 (0.92 ± 0.03)	6.64 ± 0.13 (0.72 ± 0.05)	8.86 ± 0.13 (0.99 ± 0.02)	6.84 ± 0.14 (0.92 ± 0.07)

Data of luciferase reporter gene assay, using HEK293-SF-hH₄R-His6-CRE-Luc, HEK293T-SF-mH₄R-His6-CRE-Luc or HEK293T-SF-rH₄R-His6-CRE-Luc cells and β-arrestin2 recruitment assay, using HEK293T-β-arr2-xH₄R cells (x = h, m, r). The intrinsic activity (α) of histamine **3.01** was set to 1.0 and α values of other compounds were referred to this value. Data (mean values ± SEM) were determined in 3 – 6 independent experiments, each performed in duplicates or triplicates.

In view of a radioligand for comparative binding studies at the h/m/rH$_4$Rs, three 2,4-diaminopyrimidines **3.43**, **3.45** and **3.46** qualified as potential candidates, having high potencies (pEC$_{50}$ > 7.0) and comparable efficacies across all analyzed H$_4$R orthologs in both functional assays. As a number of important requirements should be fulfilled for radiosynthesis, **3.43** and **3.45** were not considered for tritium labeling. First of all, the labeled moiety should be introduced in the last synthetic step under as mild and controllable reaction conditions as possible. The labeling reagent should be easy to handle and should not be too reactive. Moreover, according to the ALARA principle ("As Low As Reasonable Achievable"; see Recommendation of the International Commission on Radiological Protection, e.g IRCP Publication 26[43] and 103[44]), the reaction should lead to a high radiochemical yield and as little radioactive side-products and waste as possible. Finally, the "hot" compound should be easy to purify without the need for complex work-up procedures and too specialized equipment. Therefore, **3.46** (UR-DEBa176) was favored due to its convenient synthesis by controlled mono-methylation of an excess of **3.45** with a tritium labeled reagent (e.g. methyl nosylate [methyl-^{3}H] or methyl iodide [methyl-^{3}H]) (Figure 3.2).

3.2.5 Synthesis, analytical characterization, and long-term stability of [^{3}H]3.46

The tritium-labeled 2,4-diaminopyrimidine [^{3}H]**3.46** ([^{3}H]UR-DEBa176) was prepared by treating an excess of the methylamine precursor **3.45** with commercially available methyl nosylate [methyl-^{3}H] ([^{3}H]**3.53**) in the presence of K$_2$CO$_3$ at room temperature (Figure 3.2). Methyl nosylate [methyl-^{3}H] was favored over the commonly used volatile methyl iodine [methyl-^{3}H] due to technical reasons (handling, safety precautions). The desired radioligand [^{3}H]**3.46** ([^{3}H]UR-DEBa176) was isolated by reverse phase (RP)-HPLC in a radiochemical yield of 29% (108.5 MBq) and of a high radiochemical purity of 99%. The specific activity amounted to 1.59 TBq/mmol (43.08 Ci/mmol) and the final activity concentration was adjusted to 58.1 MBq/mL (1.6 mCi/mL). Radioligand [^{3}H]**3.46** revealed a high chemical stability over a storage period of 11 months at -20 °C in EtOH/H$_2$O (70/30) (Figure 3.2).

A
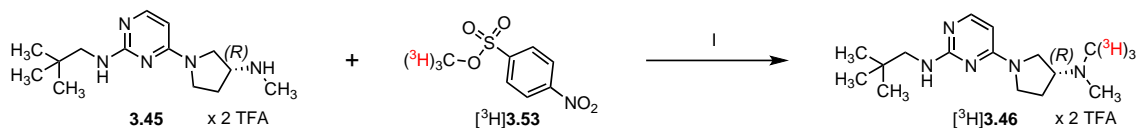
B
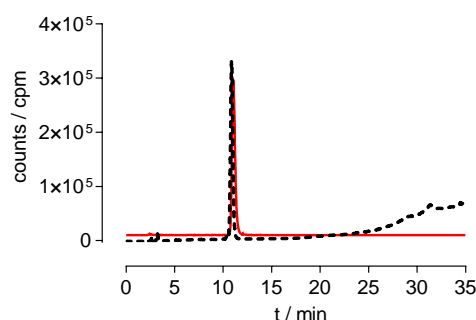
C
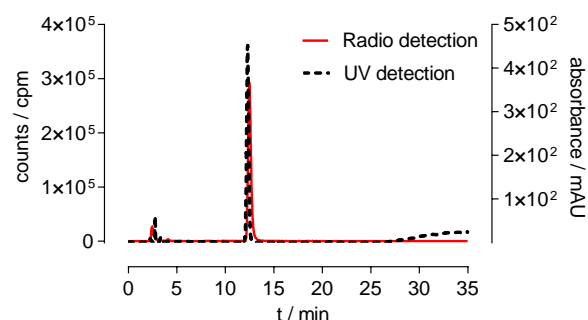
Figure 3.2. Synthesis (A), analytical characterization (B) and long-term stability (C) of [³H]3.46. (A) Synthesis of [³H]**3.46** by a monomethylation reaction of the amine precursor **3.45** with the radiolabeled precursor [³H]**3.53**. Reagents and conditions: (I) K_2CO_3, MeCN, rt, 22 h, 29% (radiochemical yield of [³H]**3.46**). (B) Chromatograms of [³H]**3.46**, spiked with the "cold" **3.46**, recorded 4 days after synthesis and (C) after 11 months of storage at -20 °C in EtOH/H_2O (70/30) using radiometric and UV detection (for details see section 3.4.5).

3.2.6 Saturation binding experiments with [³H]3.46 at the h/m/rH₄Rs

Saturation binding experiments with [³H]**3.46** were performed with homogenates of HEK293T-SF-His6-CRE-Luc cells co-expressing the hH₄R, mH₄R or rH₄R. Representative saturation binding curves and the corresponding Scatchard plots are depicted in Figure 3.3. [³H]**3.46** bound to all H₄R orthologs in a saturable manner, revealing comparable pK_d values at the h/m/rH₄Rs of 7.39 ± 0.02, 7.77 ± 0.02 and 7.66 ± 0.01, respectively (Figure 3.3, Table 3.3). The pK_d values for [³H]**3.46** were in agreement with the pK_i or pEC_{50} values obtained in the competition binding assay (hH₄R) or in the β-arrestin2 recruitment assays (h/m/rH₄Rs) for the unlabeled **3.46** (Table 3.1, Table 3.2, Table 3.3). The nonspecific binding is low, amounting 11 – 17% of total binding at concentrations around the K_d (Figure 3.3). The maximal number of binding sites (B_{max}) resulted in approx. 3.9 (hH₄R), 2.0 (mH₄R) and 2.9 (rH₄R) pmol · mg^{-1} soluble homogenate protein.
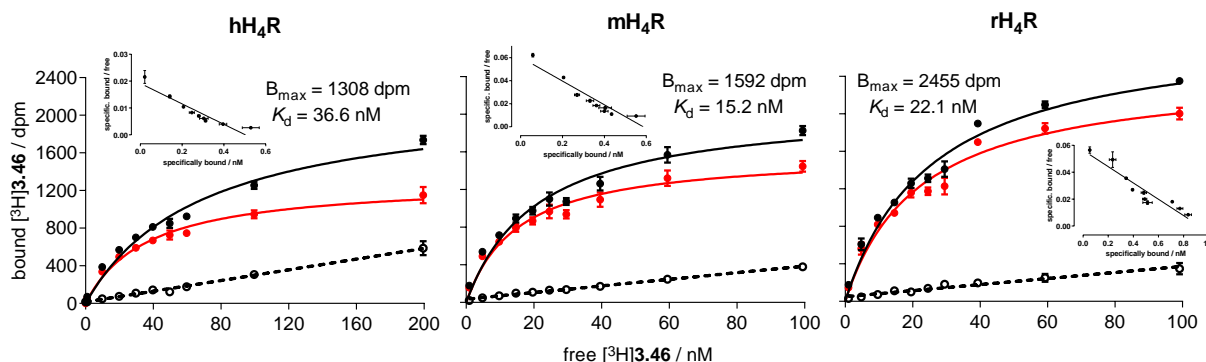
Figure 3.3. Representative data from saturation binding experiments at the hH₄R, mH₄R or rH₄R, co-expressed in homogenates of HEK293T-SF-His6-CRE-Luc cells. Total binding (black curve), specific binding (red curve) and nonspecific binding [dashed line, determined in the presence of **3.06** (1000-fold excess)] of [³H]**3.46** are depicted. Insets: Scatchard transformations of shown specific binding curves. The experiments were performed in triplicate. Error bars of specific binding and in the Scatchard plots were calculated according to the Gaussian law of error propagation. Error bars of total and nonspecific binding represent SEMs.

3.2.7 Kinetic binding experiments with [³H]3.46 at the h/m/rH₄Rs

Kinetic binding experiments with [³H]**3.46** were performed with homogenates of HEK293T-SF-His6-CRE-Luc cells co-expressing the hH₄R, mH₄R or rH₄R. Representative nonlinear and linear plots for the association and dissociation of [³H]**3.46** are shown in Figure 3.4. Association was complete after 25 minutes for all three H₄R orthologs. After 30 minutes, the residual specific binding of [³H]**3.46** reached approx. 30% at the h/m/rH₄Rs, which might be partly explained by (pseudo)irreversible binding. This phenomenon was observed before, with respect to radioligands for several GPCRs.[27,45-47] Nonetheless, the kinetically derived dissociation constants [K_d (nM) = k_{off}/k_{on} = 59 ± 18 (hH₄R), 34 ± 12 (mH₄R) and 34 ± 6 (rH₄R)] were in a good agreement with the pK_d values obtained from saturation binding experiments (Table 3.3).
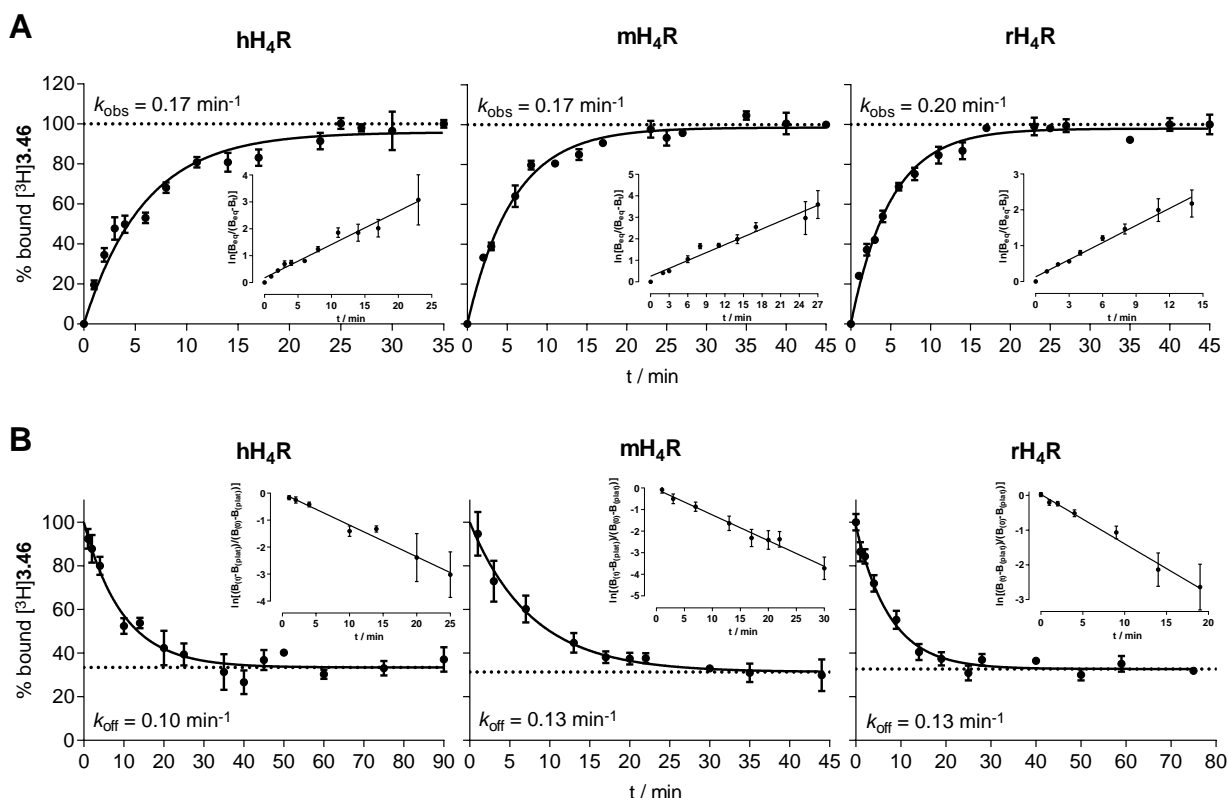
Figure 3.4. Comparison of the kinetic binding experiments with [³H]3.46 at the hH₄R, mH₄R or rH₄R, co-expressed in homogenates of HEK293T-SF-His6-CRE-Luc cells. (A) Representative associations of [³H]**3.46** (c_{final} = 40 nM, hH₄R; c_{final} = 20 nM, mH₄R; c_{final} = 30 nM, rH₄R) as a function of time (k_{obs}, observed association rate constant). Insets: transformation of the depicted association kinetics using ln $[B_{(eq)}/(B_{(eq)} - B_{(t)})]$ versus time. (B) Representative dissociation of [³H]**3.46** (preincubation: 30 − 45 min, c_{final} = 40 nM, hH₄R; c_{final} = 20 nM, mH₄R; c_{final} = 30 nM, rH₄R) in the presence of **3.06** (1000-fold excess) as a function of time (k_{off}, dissociation rate constant), showing an incomplete monophasic exponential decline [plateau: 33.4% (hH₄R), 31.3% (mH₄R), 33.5% (rH₄R)]. Insets: transformation of the depicted dissociation kinetics using ln $[(B_{(t)} - B_{(plateau)})/(B_{(0)} - B_{(plateau)})]$ versus time. Each experiment was performed in triplicates. Error bars represent propagated errors according to the Gaussian law of error.

Table 3.3. Comparison of kinetic and thermodynamic binding constants of [³H]3.46 at the h/m/rH₄Rs.

H₄R	K_d (sat)[a] / nM	pK_d (sat)[a]	K_d (kin)[b] / nM	k_{obs}[c] / min⁻¹	k_{on}[d] / min⁻¹ · nM⁻¹	k_{off}[e] / min⁻¹ $t_{1/2}$[e] / min
h	44.4; 39.3 44.9; 36.6	7.39 ± 0.02	59 ± 18	0.19 ± 0.02	0.0019 ± 0.0005	0.113 ± 0.010 6.2 ± 0.6
m	15.2; 17.8; 16.4; 18.8	7.77 ± 0.02	34 ± 12	0.19 ± 0.02	0.0035 ± 0.0013	0.1204 ± 0.0093 5.8 ± 0.4
r	22.1; 21.8; 21.5	7.66 ± 0.01	34 ± 6	0.205 ± 0.006	0.0032 ± 0.0005	0.11 ± 0.01 6.6 ± 0.7

[a]Equilibrium dissociation constant determined by saturation binding on homogenates of HEK293T-SF-His6-CRE-Luc cells co-expressing the respective receptor; K_d values were transformed into pK_d values for each experiment and indicated pK_d values represent means ± SEM from 3 − 4 independent experiments each performed in triplicate. [b]Kinetically derived dissociation constant [K_d (kin) = k_{off}/k_{on}] (means ± propagated error). [c]Observed association rate constant represents means ± SEM from 2 − 3 independent experiments each performed in triplicate at homogenates of HEK293T-SF-His6-CRE-Luc cells co-expressing the respective receptor. [d]Association rate constant [k_{on} = (k_{obs} − k_{off})/[RL]] (means ± propagated error). [e]Dissociation rate constant and derived half-life represent means ± SEM from 2 − 3 independent experiments each performed in triplicate at homogenates of HEK293T-SF-His6-CRE-Luc cells co-expressing the respective receptor.

3.2.8 Competition binding experiments with [³H]3.46 at the h/m/rH₄Rs

Competition binding experiments with [³H]**3.46** and with several standard ligands (**3.01** and **3.04** – **3.06**) for the hH_4R were performed with homogenates of HEK293T-SF-His6-CRE-Luc cells co-expressing the hH_4R, mH_4R or rH_4R (Table 3.4, Figure 3.5). At the hH_4R, the pK_i values of the inverse agonists/antagonists (**3.05** and **3.06**) were in good agreement with the published data. In contrast, for the investigated agonists (**3.01** and **3.04**) slightly lower affinities were observed for the hH_4R in comparison to the literature, most distinctive for histamine **3.01**, with 0.8 orders of magnitude. These discrepancies might reflect the different efficacies of the radioligands used. While [³H]**3.46** appeared as a partial agonist, the standard hH_4R radioligands [³H]**3.01** or [³H]**3.02** reveal full agonistic activities[18]. In this context, the unknown and varying G-protein expression levels in the different assay systems can carry weight as well. A report on competition binding studies at the 5-HT$_{2A}$ receptor[48] supports this hypothesis, showing that the affinities of agonists depend on the intrinsic efficacy of the used radioligand. Nonetheless, the affinities of all analyzed standard ligands at the mH_4R and rH_4R fit in the ranges defined by their pEC_{50} and/or pK_b values, derived from different functional assays with different signal readouts (Table 3.4). Therefore, [³H]**3.46** allows comparative binding studies at the h/m/rH_4Rs.
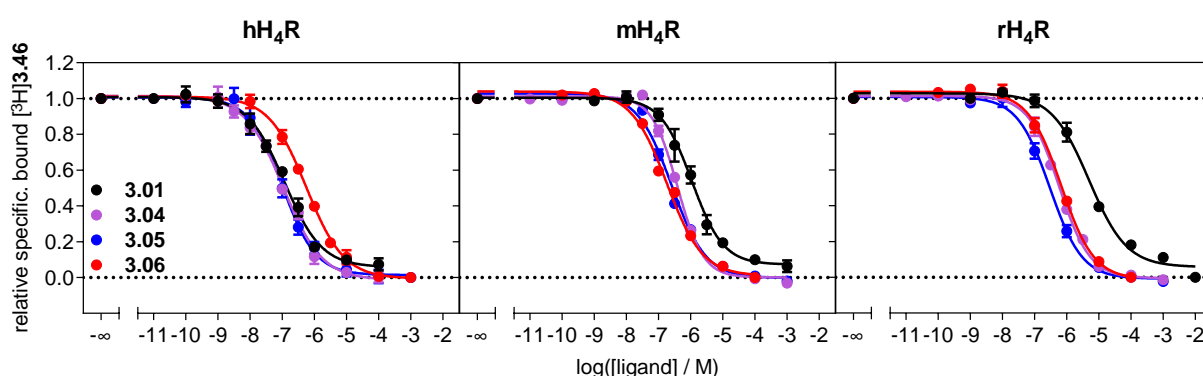
Figure 3.5. Radioligand displacement curves for 3.01 and 3.04 – 3.06 from competition binding experiments performed with [³H]3.46 at the hH₄R (c$_{final}$ = 40 nM), mH₄R (c$_{final}$ = 20 nM) or rH₄R (c$_{final}$ = 30 nM), co-expressed in homogenates of HEK293T-SF-His6-CRE-Luc cells. Data represent mean values ± SEM of independent experiments (3 – 4, hH₄R; 5 – 6, mH₄Rs; 4 – 5, rH₄R), each performed in triplicate.

Table 3.4: Comparison of the determined binding data (pK_i) of unlabeled hH$_4$R ligands (3.01, 3.04 – 3.06), using [³H]3.46 as radioligand at the H$_4$R orthologs, to reference data.

No.	pK_i / pEC$_{50}$ or pK_b / (α)					
	hH$_4$R		mH$_4$R		rH$_4$R	
	[³H]3.46[a]	reference[b]	[³H]3.46[a]	reference[c-f]	[³H]3.46[a]	reference[c-f]
3.01	**7.22 ± 0.07**	**7.8 – 8.2**[1, 3-6]	**6.31 ± 0.06**	5.2 – 7.1 (1.0)	**5.71 ± 0.06**	4.3 – 6.5 (1.0)
3.04	**7.25 ± 0.07**	**7.6 – 8.4**[1, 3-6]	**6.79 ± 0.05**	6.1 (0.2)[c] 6.7 (0.6)[f]	**6.57 ± 0.04**	*6.3* (0.0)[c] 6.8 (0.4)[f]
3.05	**7.30 ± 0.09**	**7.2 – 8.4**[1-6]	**6.94 ± 0.05**	6.1 – 6.9, *7.6* (-0.2 – 0.6)	**6.91 ± 0.10**	6.1 – 8.2 (0.2 – 0.5)
3.06	**6.45 ± 0.07**	**6.3 – 7.3**[1-6]	**7.13 ± 0.05**	6.5, *7.1 – 7.6* (-0.4 – 0.0)	**6.56 ± 0.03**	*5.9 – 6.9* (-0.2 – 0.0)

[a]Data from competition binding experiments (pK_i) with [³H]3.46 (c$_{final}$ = 40 nM, hH$_4$R; c$_{final}$ = 20 nM, mH$_4$R; c$_{final}$ = 30 nM, rH$_4$R) for hH$_4$R standard ligands (3.01, 3.04 – 3.06), determined at the human, mouse or rat H$_4$Rs, co-expressed in homogenates of HEK293T-SF-His6-CRE-Luc cells. The pK_i values represent means ± SEM and were determined in independent experiments (3 – 4, hH$_4$R; 5 – 6, mH$_4$Rs; 4 – 5, rH$_4$R), each performed in triplicate. [b]Data from radioligand competition binding experiments with [1] [³H]3.02 or [2-6] [³H]3.01, performed on: [1] membrane preparations of *Sf*9 insect cells, stably expressing the hH$_4$R-RGS19 fusion protein + Gα$_{i2}$ + Gβ$_1$γ$_2$[12], [2] membrane preparations of *Sf*9 insect cells, stably expressing the hH$_4$R-RGS19 fusion protein + Gα$_i$ + Gβ$_1$γ$_2$[16], [3] membrane preparations of *Sf*9 insect cells, stably expressing the hH$_4$R + Gα$_{i2}$ + Gβ$_1$γ$_2$[17,33,49], [4] homogenates of SK-N-MC-cells, stably expressing the hH$_4$R[14], [5] membranes from SK-N-MC cells, stably expressing the hH$_4$R[3,23,50], or [6] homogenates of HEK293T cells, stably expressing the hH$_4$R[22,24]. [c]Data from [³⁵S]GTPγS assays[17], performed on *Sf*9 cell membranes expressing the mH$_4$R or rH$_4$R + Gα$_{i2}$ + Gβ$_1$γ$_2$. [d]Data from steady-state [³²P]GTPase assays[16], performed on *Sf*9 cell membranes expressing the mH$_4$R or rH$_4$R + Gα$_{i2}$ + Gβ$_1$γ$_2$ + GAIP. [e]Data from β-arr2 recruitment assays in HEK293T cells, stably expressing the mH$_4$ or rH$_4$R-ELucC/ELucN-β-arrestin2 construct. [f]Data from CRE-controlled luciferase reporter gene assays[18] in HEK293T cells, stably expressing the mH$_4$R or rH$_4$R.

3.3 Conclusion

Here we report on the development of the 2,4 diaminopyrimidine-type radioligand [³H]UR-DEBa176 ([³H]**3.46**) enabling robust comparative binding studies at the h/m/rH₄Rs [pK_d = 7.4, 7.8, 7.7, respectively; low nonspecific binding (11 – 17%, ~ K_d); fast association/dissociation kinetics (25 – 30 min)]. Therefore, extensive investigations on the prepared 2,4-diaminopyrimidines with respect to their affinities at the hH₄R and their functional profiles at the h/m/rH₄Rs in different assays (luciferase reporter gene-, β-arrestin2 recruitment assays) were conducted. On one hand, **3.43** (UR-DEBa148) was found to exhibit subnanomolar potencies at the h/m/rH₄Rs in luciferase reporter gene assays (pEC$_{50}$ = 9.9, 9.6, 10.3, respectively) and was slightly G-protein biased. On the other hand, (partial) agonist **3.46** (UR-DEBa176), with comparable potencies at the h/m/rH₄Rs (pEC$_{50}$ (reporter gene) = 8.7, 9.0, 9.2, respectively), was found to constitute the "cold" form of a potential radioligand. Subsequently, by employing commercially available methyl nosylate [methyl-³H] ([³H]**3.53**), [³H]UR-DEBa176 ([³H]**3.46**) was obtained in a radiochemical yield of 29% and of a high radiochemical purity of 99%. As a molecular tool [³H]UR-DEBa176 ([³H]**3.46**) allows pharmacological investigations on the H₄R with respect to translational animal models (e.g. early stage characterization of novel molecular tools or potential drug candidates in radioligand binding assays at the h/m/rH₄Rs). To conclude, the herein presented SAR results and especially [³H]UR-DEBa176 ([³H]**3.46**) should support the future development of h/m/rH₄Rs ligands and can help to further unravel the (patho)physiological role of the H₄R.

3.4 Experimental section

3.4.1 General experimental conditions

Chemicals and solvents were purchased from Acros Organics B. V. B. A. (Geel, Belgium), Alfa Aesar & Co. KG (Karlsruhe, Germany), Sigma-Aldrich Chemie GmbH (Taufkirchen, Germany), TCI Deutschland GmbH (Eschborn, Germany), Tocris Bioscience (Bristol, UK) and Merck KGaA (Darmstadt, Germany) and were used without further purification. All solvents were purchased in analytical grade or distilled prior to use and stored over molecular sieves (4 Å). Acetonitrile (gradient grade) for HPLC was obtained from Merck KGaA (Darmstadt, Germany). Millipore water was used for the preparation of HPLC eluents. Deuterated solvents for nuclear magnetic resonance (NMR) spectroscopy were from Deutero GmbH (Kastellaun, Germany). For column chromatography Merck silica gel 60 (0.040 – 0.063 mm) was used. Flash chromatography was performed on an Intelli Flash-310 Flash-Chromatography Workstation from Varian Deutschland GmbH (Darmstadt, Germany). Reaction controls were performed using thin layer chromatography (TLC) on Merck silica gel 60 F_{254} thin layer chromatography (TLC) aluminium sheets (visualization either by UV radiation (λ = 254 or 310 nm) or staining with ninhydrine or vanillin, respectively). For microwave-driven reactions a Biotage Initiator microwave synthesizer (Biotage AB, Uppsala, Sweden) was used. NMR spectra were recorded on a Bruker Avance 300 (7.05 T, ^{1}H 300 MHz; ^{13}C 75 MHz), Bruker Avance III HD 400 (9.40 T, ^{1}H 400 MHz; ^{13}C 101 MHz) or Bruker Avance III HD 600, equipped with a cryogenic probe (14.1 T, ^{1}H 600 MHz; ^{13}C 151 MHz) (Bruker BioSpin GmbH, Karlsruhe, Germany) with tetramethylsilane (TMS) as an external standard. Multiplicities are specified with the following abbreviations: s (singlet), d (doublet), t (triplet), q (quartet), m (multiplet), br (broad signal) and quat. (quaternary carbon atom). The coupling constants (J values) are given in hertz (Hz). High-resolution mass spectrometry (HRMS) analysis was performed on an Agilent 6540 UHD Accurate-Mass Q-TOF LC/MS system (Agilent Technologies, Santa Clara, CA, USA) using an electrospray ionization (ESI) source. Melting points (mp) were determined (if applicable) on a Büchi 530 (Büchi GmbH, Essen, Germany) and were uncorrected. Preparative HPLC was performed on a Knauer device (Berlin, Germany), comprising two K-1800 pumps and a K-2001 detector. An Interchim puriFlash C18 HQ 15 UM (120G Flash COLUMN 15 µm) with a flow rate of 50 mL/min or a Phenomenex Kinetex 5u XB-C18 (250 × 21.2 mm) with a flow rate of 15 or

20 mL/min were used as stationary phases. Mixtures of 0.1% TFA (A) and MeCN (B) served as the mobile phase. The detection wavelength was set to 220 nm. All compound solutions were filtered through polytetrafluoroethylene (PTFE) filters (25 mm, 0.2 μm, Phenomenex Ltd., Aschaffenburg, Germany) prior to injection. The solvent of the collected fractions was removed under reduced pressure followed by lyophilization using an Alpha 2-4 LD apparatus (Martin Christ GmbH, Osterode am Harz, Germany) equipped with a RZ 6 rotary vane vacuum pump (Vacuubrand GmbH & Co. KG, Wertheim, Germany). For all target compounds, 10 mM stock solutions in dimethyl sulfoxide (DMSO) and 20 mM HCl (1/1) were prepared in polypropylene reaction vessels (1.5 mL) with a screw cap (Süd-Laborbedarf GmbH, Gauting, Germany). Analytical HPLC analysis (purity control and determination of the chemical stability of compounds) was performed with a system from Agilent Technologies (Series 1100) composed of a binary pump equipped with a degasser (G1312A), autosampler (ALS, G1329A), thermostated column compartment (COLCOM, G1316A) and diode array detector (DAD, G1315B). A Phenomenex Kinetex-XB C18 (2.6 μm, 100 mm × 3 mm) was used as a stationary phase at a flow rate of 0.8 mL/min. Mixtures of 0.5% TFA (A) and MeCN + 0.5% TFA (B) served as the mobile phase. The following linear gradient was applied throughout: A/B (*v/v*) 0 – 30 min, 90/10 – 10/90; 30 – 33 min, 10/90 – 5/95; 33 – 40 min, 5/95. For all analytical runs, the oven temperature was set to 30 °C and detection was performed at 220 nm. The injection volume for purity controls was 60 μL of a 100 μM solution (10 mM stock solution diluted with starting eluent, A/B 90/10). Retention (capacity) factor (k) was calculated based on the determined retention time (t_R) according to $k = (t_R - t_0)/t_0$ (t_0 = dead time = 3.21 min).

3.4.2 Compound characterization

The synthesized compounds **3.08**, **3.09**, **3.11 – 3.15**, **3.20 – 3.52**, **3.61** and **3.63 – 3.67** were characterized by ¹H- and ¹³C-NMR spectroscopy, HRMS and melting point (if applicable) (¹H-, ¹³C-NMR spectra for selected target structures see Figure A 3.3 – Figure A 3.22 in section 3.5.5.1). Additionally, compounds **3.08**, **3.09**, **3.11 – 3.13, 3.15**, **3.20 – 3.52**, **3.61**, **3.63** and **3.65 – 3.67** were characterized by 2D-NMR spectroscopy (¹H-COSY, HSQC, HMBC). The intermediate compounds **3.07** and **3.10** were characterized by ¹H-NMR spectroscopy, HRMS and melting point (if applicable). The purity of the target compounds (**3.33 – 3.52**) was

> 96% throughout, determined by RP-HPLC (220 nm) (conditions see in section 3.4.1; chromatograms see Figure A 3.23 – Figure A 3.32 in section 3.5.5.2).

The comment regarding the NMR spectra (^{1}H, ^{13}C) of the target 2,4-diaminpyrimidines, substituted with unsymmetrical cyclic aliphatic amines in the 4-position (**3.33**, **3.35**, **3.43**, **3.45**, **3.46, 3.48, 3.49**, **3.51** and **3.52**) is the following: the slow rotation around the amine bond on the NMR time scale resulted in two isomers (ratios are given in the experimental protocols), which were evident in the ^{1}H- and ^{13}C-NMR spectra.

3.4.3 Synthesis of the target compounds (3.33 – 3.52)

General procedure for **3.33 – 3.43**

The respective 4-amino-2-chloropyrimidine (1 equiv), DIPEA (1.5 – 6 equiv) and 2,2-dimethylpropan-1-amine (2 – 6 equiv) were dissolved in *i*-PrOH. The reaction mixture was stirred in the microwave reactor for 5 – 11 h at 120 – 130 °C. After removing the solvent under reduced pressure the product was purified by chromatography or automated flash-chromatography. The residue was dissolved in dichloromethane (DCM), TFA was added and the mixture was stirred at rt until the removal of the protection group was complete (7 – 18 h). The crude product was purified by preparative HPLC.

(R)-4-(3-Aminopyrrolidin-1-yl)-*N*-neopentylpyrimidin-2-amine   bis(2,2,2-trifluoroacetate) (3.33)[28]. According to the general procedure, the title compound was prepared in the microwave reactor (6 h, 130 °C, 4 bar, 3 min prestirring) from **3.20** (400 mg, 1.34 mmol), DIPEA (456 μL, 2.68 mmol) and 2,2-dimethylpropan-1-amine (475 μL, 4.06 mmol) in *i*-PrOH (4 mL). The crude product was purified by chromatography [eluent: DCM/MeOH (*v/v*) 100/0 – 95/5, SiO$_2$ 50 g] to give **3.32** as pale, yellow sticky foam (450 mg, 96.1%). R$_f$ = 0.45 (DCM/MeOH 92.5/7.5). ^{1}H-NMR (400 MHz, DMSO-d_6): δ (ppm) 7.72 (d, *J* = 5.8 Hz, 1H), 7.18 (br, 1H), 6.43 (br, 1H), 5.67 (d, *J* = 5.8 Hz, 1H), 4.22 – 3.07 (m, 7H), 2.20 – 1.73 (m, 2H), 1.39 (s, 9H), 0.87 (s, 9H). ^{13}C-NMR (101 MHz, DMSO-d_6, HSQC, HMBC): δ (ppm) 162.56 (quat., 1C), 160.61 (quat., 1C), 155.71, 155.44 (quat., 1C), 93.77, 78.31 (quat., 1C), 52.00, 51.84, 50.17, 44.53, 32.85, 30.76, 28.68 (3C), 27.99 (3C). HRMS (ESI): *m/z* [*M*+H]$^+$ calcd for [C$_{18}$H$_{32}$N$_5$O$_2$]$^+$ 350.2551, found 350.2564. C$_{18}$H$_{31}$N$_5$O$_2$ (349.48). Deprotection of 3.32 (140 mg, 0.401 mmol) in DCM (4 mL) and TFA (0.6 mL) followed by preparative HPLC (Interchim puriFlash C18 HQ 15 UM 120G Flash

COLUMN 15 µm; gradient 0 – 30 min: A/B (*v/v*) 95/5 – 38/62, t_R = 9.5 min) afforded **3.33** as colorless hygroscopic foam (150 mg, 78.4%). R_f = 0.3 (DCM/1.75 M NH$_3$ in MeOH 90/10). RP-HPLC (220 nm): 99.9% (*k* = 1.81). Ratio of configurational isomers evident in NMR: ca. 1:1.4. ^{1}H-NMR (600 MHz, DMSO-*d$_6$*): δ (ppm) 12.47 (br, 1H), 8.43 (m, 1H), 8.22 (m, 3H), 7.88 (m, 1H), 6.21 (d, *J* = 7.0 Hz, 1H), 4.10 – 3.49 (m, 5H), 3.22 (m, 2H), 2.41 – 2.01 (m, 2H), 0.90 (s, 9H). ^{13}C-NMR (151 MHz, DMSO-*d$_6$*, HSQC, HMBC): δ (ppm) 159.54 (quat., 1C), 159.43 (quat., 1C), 158.55(q, *J* = 33.0 Hz, TFA), 153.43, 142.51, 116.64 (q, *J* = 296.9 Hz, TFA), 95.44, 51.29, 50.51, 50.48, 49.45, 48.62, 45.02, 44.84, 32.26 (quat., 1C), 28.90, 28.18, 27.14 (3C). HRMS (ESI): *m/z* [*M* + H]$^+$ calcd for [C$_{13}$H$_{24}$N$_5$]$^+$ 250.2026, found 250.2033. C$_{13}$H$_{23}$N$_5$ · C$_4$H$_2$F$_6$O$_4$ (249.36 + 228.05).

***N*-Neopentyl-4-(piperazin-1-yl)pyrimidin-2-amine bis(2,2,2-trifluoroacetate) (3.34)[28].** According to the general procedure, the title compound was prepared in the microwave reactor (7 h, 120 °C, 4 bar, 3 min prestirring) from **3.21** (800 mg, 2.68 mmol), DIPEA (917 µL, 5.39 mmol) and 2,2-dimethylpropan-1-amine (953 µL, 8.14 mmol) in *i*-PrOH (10 mL). The crude product was purified by chromatography [DCM/MeOH (*v/v*) 100/0 – 95/5, SiO$_2$ 80 g] to give a colorless sticky foam (470 mg, 50.2%). R_f = 0.3 (DCM/MeOH 95/5). Deprotection (90 mg, 0.26 mmol) in DCM (2 mL) and TFA (0.5 mL) followed by preparative HPLC [column: Phenomenex Kinetex 5u XB-C18 250 × 21.2 mm; gradient: 0 – 30 min: A/B (*v/v*) 95/5 – 43/57, flow 15 mL/min, t_R = 14 min] afforded **3.34** as colorless hygroscopic foam (112 mg, 90.2%). R_f = 0.4 (DCM/1.75 M NH$_3$ in MeOH 90/10). RP-HPLC (220 nm): 98.4% (*k* = 1.65). ^{1}H-NMR (300 MHz, MeOH-*d$_4$*): δ (ppm) 7.80 (d, *J* = 7.5 Hz, 1H), 6.50 (d, *J* = 7.5 Hz, 1H), 4.16 (m, 4H), 3.40 (m, 6H), 0.98 (s, 9H). ^{1}H-NMR (600 MHz, DMSO-*d$_6$*): δ (ppm) 12.92 (br, 1H), 9.26 (br, 2H), 8.56 (s, 1H), 7.97 (d, *J* = 7.4 Hz, 1H), 6.52 (d, *J* = 7.4 Hz, 1H), 3.96 (m, 4H), 3.23 (m, 6H), 0.90 (s, 9H). ^{13}C-NMR (151 MHz, DMSO-*d$_6$*, HSQC, HMBC): δ (ppm) 161.17 (quat., 1C), 158.89 (q, *J* = 32.4 Hz, TFA), 153.73 (quat., 1C), 143.67, 116.83 (q, *J* = 297.5 Hz, TFA), 94.28, 51.36, 42.21 (2C), 40.04 (2C), 32.26 (quat., 1C), 27.10 (3C). HRMS (ESI): *m/z* [*M* + H]$^+$ calcd for [C$_{13}$H$_{24}$N$_5$]$^+$ 250.2026, found 250.2029. C$_{13}$H$_{23}$N$_5$ · C$_4$H$_2$F$_6$O$_4$ (249.36 + 228.05).

4-(1,4-Diazepan-1-yl)-*N*-neopentylpyrimidin-2-amine bis(2,2,2-trifluoroacetate) (3.35)[28]. According to the general procedure the title compound was prepared in the microwave

reactor (5.5 h, 130 °C, 3 bar, 3 min prestirring) from **3.22** (110 mg, 0.352 mmol), DIPEA (120 µL, 0.689 mmol) and 2,2-dimethylpropan-1-amine (83 µL, 0.70 mmol) in *i*-PrOH (2 mL). The crude product was purified by automated flash chromatography [gradient 0 – 20 min: DCM/MeOH (*v/v*) 100/0 – 95/5, SF 10 – 4 g] to give a colorless sticky foam (50 mg, 39.1%). R$_f$ = 0.3 (DCM/MeOH 95/5). Deprotection (50 mg, 0.14 mmol) in DCM (2 mL) and TFA (0.3 mL) followed by preparative HPLC [column: Phenomenex Kinetex 5u XB-C18 250 × 21.2 mm; gradient: 0 – 30 min: A/B (*v/v*) 95/5 – 33/67, flow 20 mL/min, t$_R$ = 11 min] afforded **3.35** as colorless hygroscopic foam (34 mg, 50.1%). R$_f$ = 0.5 (DCM/1.75 M NH$_3$ in MeOH 80/20). RP-HPLC (220 nm): 97.5% (*k* = 1.86). Ratio of configurational isomers evident in NMR performed in DMSO-*d$_6$*: ca 1:1.5. ^{1}H-NMR (400 MHz, MeOH-*d$_4$*): δ (ppm) 7.78 (d, *J* = 7.4 Hz, 1H), 6.46 (d, *J* = 6.9 Hz, 1H), 4.21 (t, *J* = 5.3 Hz, 1.3H), 4.04 (m, 1.4H), 3.81 (t, *J* = 6.1 Hz, 1.3 H), 3.50 – 3.31 (m, 6H), 2.20 (m, 2H), 0.99 (s, 9H). ^{1}H-NMR (600 MHz, DMSO-*d$_6$*): δ (ppm) 12.84 (br, 1H), 9.08 (m, 2H), 8.49 (m, 1H), 7.92 (m, 1H), 6.45 (m, 1H), 4.13 – 3.62 (m, 4H), 3.41 – 3.11 (m, 6H), 2.04 (m, 2H), 0.91 (s, 9H). ^{13}C-NMR (151 MHz, DMSO-*d$_6$*, HSQC, HMBC): δ (ppm) 161.68 (quat., 1C), 158.84 (q, *J* = 32.2 Hz, TFA), 153.58 (quat., 1C), 153.49 (quat., 1C), 143.11, 143.01, 116.87 (q, *J* = 298.2 Hz, TFA), 94.61, 51.31, 46.85, 45.64, 44.35, 44.27, 44.23, 44.13, 43.10, 32.20, 32.14, 27.12 (3C), 24.42, 24.13. HRMS (ESI): *m/z* [*M* + H]$^+$ calcd for [C$_{14}$H$_{26}$N$_5$]$^+$ 264.2183, found 264.2183. C$_{14}$H$_{25}$N$_5$ · C$_4$H$_2$F$_6$O$_4$ (263.39 + 228.05).

4-[4-(2-Aminoethyl)piperazin-1-yl]-*N*-neopentylpyrimidin-2-amine tris(2,2,2-trifluoroacetate) (3.36). According to the general procedure, the title compound was prepared in the microwave reactor (9 h, 120 °C, 1 bar, 3 min prestirring) from **3.23** (110 mg, 0.322 mmol), DIPEA (110 µL, 0.632 mmol) and 2,2-dimethylpropan-1-amine (114 µL, 0.974 mmol) in *i*-PrOH (2 mL). The crude product was purified by chromatography [DCM/MeOH (*v/v*) 100/0 – 90/10, SiO$_2$] to give a pale, yellow sticky foam (80 mg, 63.4%). R$_f$ = 0.4 (DCM/MeOH 90/10). Deprotection (80 mg, 0.20 mmol) in DCM (4 mL) and TFA (0.7 mL), followed by preparative HPLC [column: Phenomenex Kinetex 5u XB-C18 250 × 21.2 mm; gradient: 0 – 30 min: A/B (*v/v*) 90/10 – 24/76, flow 15 mL/min, t$_R$ = 10 min] afforded **3.36** as colorless hygroscopic foam (56 mg, 44.0%). RP-HPLC (220 nm): 99.9% (*k* = 1.55). ^{1}H-NMR (300 MHz, MeOH-*d$_4$*): δ (ppm) 7.71 (d, *J* = 7.6 , 1H), 6.44 (d, *J* = 7.6 Hz, 1H), 4.07 (m, 2H), 3.79 (m, 2H), 3.30 – 3.09 (m, 4H), 2.87 – 2.65 (m, 6H), 0.97 (s, 9H). ^{1}H-NMR

(600 MHz, DMSO-d_6): δ (ppm) 12.60 (br, 1H), 8.42 (br. 1H), 7.90 (m, 4.5H), 6.53 (d, J = 7.3 Hz, 1H), 3.86 (m, 4H), 3.24 – 2.63 (m, 10H), 0.90 (s, 9H). ^{13}C-NMR (151 MHz, DMSO-d_6, HSQC, HMBC): δ (ppm) 160.69 (quat., 1C), 158.65 (q, J = 33.0 Hz, TFA), 153.62 (quat., 1C), 143.27, 116.64 (q, J = 296.2 Hz, TFA), 94.19, 53.32, 51.47, 51.32, 44.29, 42.19, 34.90 (2C), 32.28 (quat., 1C), 27.10 (3C). HRMS (ESI): m/z [M + H]$^+$ calcd for [C$_{15}$H$_{29}$N$_6$]$^+$ 293.2448, found 293.2451. C$_{15}$H$_{28}$N$_6$ · C$_6$H$_3$F$_9$O$_6$ (292.43 + 342.07).

N^4-(2-Aminoethyl)-N^2-neopentylpyrimidine-2,4-diamine bis(2,2,2-trifluoroacetate) (3.37). According to the general procedure, the title compound was prepared in the microwave reactor (6 h, 120 °C, 1 bar, 3min prestirring) from **3.24** (150 mg, 0.550 mmol), DIPEA (140 µL, 0.82 mmol) and 2,2-dimethylpropan-1-amine (194 µL, 1.65 mmol) in i-PrOH (2 mL). The crude product was purified by automated flash chromatography [gradient 0 – 20 min: DCM/MeOH (v/v) 100/0 – 90/10, SF 10-4 g] to give a colorless sticky oil (160 mg, 90.0%). R$_f$ = 0.45 (DCM/MeOH 90/10). Deprotection (120 mg, 0.371 mmol) in DCM (2.5 mL) and TFA (0.5 mL) followed by preparative HPLC [Phenomenex Kinetex 5u XB-C18 250 × 21.2 mm; gradient 0 – 30 min: A/B (v/v) 95/5 – 38/62; flow: 15 mL/min; t$_R$ = 12.5 min] afforded **3.37** as colorless hygroscopic foam (120 mg, 71.7%). RP-HPLC (220 nm): 99.9% (k = 1.61). ^{1}H-NMR (300 MHz, MeOH-d_4): δ (ppm) 7.62 (d, J = 7.3 Hz, 1H), 6.10 (d, J = 7.0 Hz, 1H), 3.77 (t, J = 6.0 Hz, 2H), 3.33 (m, 2H), 3.22 (t, J = 6.1 Hz, 2H), 0.99 (s, 9H). ^{1}H-NMR (600 MHz, DMSO-d_6): δ (ppm) 12.31 (br, 1H), 8.98 (s, 1H), 8.40 (s, 1H), 7.99 (br, 3H), 7.73 (d, J = 7.0 Hz, 1H), 6.04 (d, J = 7.0 Hz, 1H), 3.61 (m, 2H), 3.23 (m, 2H), 3.03 (m, 2H), 0.90 (s, 9H). ^{13}C-NMR (151 MHz, DMSO-d_6, HSQC, HMBC): δ (ppm) 162.84 (quat., 1C), 158.71 (q, J = 32.3 Hz, TFA), 154.32 (quat., 1C), 141.45, 116.89 (q, J = 297.4 Hz, TFA), 97.42, 51.16, 37.99, 37.62, 32.16 (quat., 1C), 27.08 (3C). HRMS (ESI): m/z [M + H]$^+$ calcd for [C$_{11}$H$_{22}$N$_5$]$^+$ 224.1870, found 224.1874. C$_{11}$H$_{21}$N$_5$ · C$_4$H$_2$F$_6$O$_4$ (223.32 + 228.05).

N^4-(3-Aminopropyl)-N^2-neopentylpyrimidine-2,4-diamine bis(2,2,2-trifluoroacetate) (3.38). According to the general procedure, the title compound was prepared in the microwave reactor (7 h, 120 °C, 2 bar, 3 min prestirring) from **3.25** (250 mg, 0.872 mmol), DIPEA (222 µL, 1.27 mmol) and 2,2-dimethylpropan-1-amine (616 µL, 5.26 mmol) in i-PrOH (2 mL). The crude product was purified by automated flash chromatography [gradient 0 – 20 min: DCM/MeOH

(*v/v*) 100/0 – 95/5, SF 10 – 4 g] to give a colorless sticky oil (200 mg, 68.0%). R_f = 0.4 (DCM/MeOH 90/10). Deprotection of (190 mg, 0.563 mmol) in DCM (2 mL) and TFA (0.5 mL) followed by preparative HPLC [column: Phenomenex Kinetex 5u XB-C18 250 × 21.2 mm; gradient: 0 – 30 min: A/B (*v/v*) 92/8 – 49/51, flow 20 mL/min, t_R = 11 min] afforded **3.38** as colorless hygroscopic foam (188 mg, 71.7%). RP-HPLC (220 nm): 99.9% (*k* = 1.80). ^{1}H-NMR (300 MHz, MeOH-d_4): δ (ppm) 7.56 (d, *J* = 7.3 Hz, 1H), 6.05 (d, *J* = 7.2 Hz, 1H), 3.58 (t, *J* = 6.7 Hz, 2H), 3.01 (m, 2H), 1.99 (m, 2H), 0.98 (s, 9H). ^{1}H-NMR (600 MHz, DMSO-d_6, HSQC, HMBC): δ (ppm) 12.05 (br, 1H), 8.90 (br, 1H), 8.28 (br, 1H), 7.82 (br, 3H), 7.69 (d, *J* = 7.0 Hz, 1H), 6.03 (d, *J* = 7.0 Hz, 1H), 3.43 (m, 2H), 3.22 (m, 2H), 2.85 (m, 2H), 1.81 (m, 2H), 0.91 (s, 9H). ^{13}C-NMR (151 MHz, DMSO-d_6): δ (ppm) 162.28 (quat., 1C), 158.48 (q, *J* = 31.4 Hz, TFA), 154.27 (quat., 1C), 141.21, 117.06 (q, *J* = 299.2 Hz, TFA), 97.16, 51.21, 37.50, 36.83, 32.14 (quat., 1C), 27.12 (3C), 26.54. HRMS (ESI): *m/z* $[M + H]^+$ calcd for $[C_{12}H_{24}N_5]^+$ 238.2026, found 238.2032. $C_{12}H_{23}N_5 \cdot C_4H_2F_6O_4$ (237.35 + 228.05).

N^2-Neopentyl-N^4-(pyrrolidin-3-yl)pyrimidine-2,4-diamine bis(2,2,2-trifluoroacetate) (3.39). According to the general procedure, the title compound was prepared in the microwave reactor (8 h, 120 °C, 2 bar, 3 min prestirring) from **3.26** (200 mg, 0.669 mmol), DIPEA (180 μL, 1.06 mmol) and 2,2-dimethylpropan-1-amine (237 μL, 2.03 mmol) in *i*-PrOH (2 mL). The crude product was purified by chromatography [DCM/MeOH (*v/v*) 100/0 – 90/10, SiO_2 30 g] to give a pale yellow sticky oil (160 mg, 68.4%). R_f = 0.4 (DCM/MeOH 90/10). Deprotection (150 mg, 0.430 mmol) in DCM (2 mL) and TFA (0.5 mL) followed by preparative HPLC [column: Phenomenex Kinetex 5u XB-C18 250 × 21.2 mm; gradient: 0 – 30 min: A/B (*v/v*) 90/10 – 52/48, flow 20 mL/min, t_R = 10.5 min] afforded **3.39** as colorless hygroscopic foam (97 mg, 47.3%). RP-HPLC (220 nm): 99.9% (*k* = 1.73). ^{1}H-NMR (300 MHz, MeOH-d_4): δ (ppm) 7.64 (d, *J* = 7.2 Hz, 1H), 6.10 (d, *J* = 7.2 Hz, 1H), 4.74 (m, 1H), 3.52 (m, 6H), 2.29 (m, 2H), 0.99 (s, 9H). ^{1}H-NMR (600 MHz, DMSO-d_6): δ (ppm) 12.42 (br, 1H), 9.15 (br, 3H), 8.50 (m, 1H), 7.76 (d, *J* = 7.1 Hz, 1H), 6.06 (d, *J* = 7.1 Hz, 1H), 4.55 (m, 1H), 3.45 (m, 1H), 3.40 – 2.98 (m, 5H), 2.27 (m, 1H), 1.95 (m, 1H), 0.91 (s, 9H). ^{13}C-NMR (151 MHz, DMSO-d_6, HSQC, HMBC): δ (ppm) 162.17 (quat., 1C), 158.76 (q, *J* = 32.0 Hz, TFA), 154.22 (quat., 1C), 141.82, 116.95 (d, *J* = 298.5 Hz, TFA), 97.10, 51.23, 49.90, 49.30, 43.80, 32.17 (quat., 1C), 29.49, 27.07 (3C). HRMS

(ESI): m/z [M + H]$^+$ calcd for [$C_{13}H_{24}N_5$]$^+$ 250.2026, found 250.2031. $C_{13}H_{23}N_5 \cdot C_4H_2F_6O_4$ (249.36 + 228.05).

N^2-Neopentyl-N^4-(piperidin-4-yl)pyrimidine-2,4-diamine bis(2,2,2-trifluoroacetate) (3.40). According to the general procedure, the title compound was prepared in the microwave reactor (7 h, 120 °C, 2 bar, 3 min prestirring) from **3.27** (250 mg, 0.799 mmol), DIPEA (204 µL, 1.17 mmol) and 2,2-dimethylpropan-1-amine (282 µL, 2.41 mmol) in i-PrOH (2 mL). The crude product was purified by automated flash chromatography [gradient 0 – 20 min: DCM/MeOH (v/v) 100/0 – 95/5, SF 10 – 4 g] to give a colorless sticky oil (120 mg, 41.3%). R$_f$ = 0.4 (DCM/MeOH 90/10). Deprotection (110 mg, 0.303 mmol) in DCM (2 mL) and TFA (0.5 mL) followed by preparative HPLC [column: Phenomenex Kinetex 5u XB-C18 250 × 21.2 mm; gradient: 0 – 30 min: A/B (v/v) 90/10 – 47/53, flow 20 mL/min, t$_R$ = 10 min] afforded **3.40** as colorless hygroscopic foam (100 mg, 67.2%). RP-HPLC (220 nm): 99.9% (k = 1.76). ^{1}H-NMR (300 MHz, MeOH-d_4): δ (ppm) 7.59 (d, J = 7.3 Hz, 1H), 6.06 (d, J = 7.3 Hz, 1H), 4.30 (m, 1H), 3.32 (m, 6H), 2.24 (m, 2H), 1.80 (m, 2H), 0.98 (s, 9H). ^{1}H-NMR (600 MHz, DMSO-d_6): δ (ppm) 12.29 (br, 1H), 9.92 (d, J = 6.4 Hz, 1H), 8.81 (br, 1H), 8.63 (br, 1H), 8.41 (m, 1H), 7.71 (d, J = 7.1 Hz, 1H), 6.03 (d, J = 7.0 Hz, 1H), 4.13 (m, 1H), 3.32 (m, 2H), 3.22 (m, 2H), 3.06 (m, 2H), 2.03 (m, 2H), 1.66 (m, 2H), 0.90 (s, 9H). ^{13}C-NMR (151 MHz, DMSO-d_6, HSQC, HMBC): δ (ppm) 161.67 (quat., 1C), 158.66 (q, J = 47.3 Hz, TFA), 154.32 (quat., 1C), 141.54, 117.06 (q, J = 298.6 Hz, TFA), 97.12, 51.15, 45.20, 41.72 (2C), 32.19 (quat., 1C), 27.52 (2C), 27.12 (3C). HRMS (ESI): m/z [M + H]$^+$ calcd for [$C_{14}H_{26}N_5$]$^+$ 264.2183, found 264.2185. $C_{14}H_{25}N_5 \cdot C_4H_2F_6O_4$ (263.39 + 228.05).

N^4-[2-(1H-Imidazol-4-yl)ethyl]-N^2-neopentylpyrimidine-2,4-diamine bis(2,2,2-trifluoroacetate) (3.41). According to the general procedure, the title compound was prepared in the microwave reactor (11 h, 130 °C, 4 bar, 3 min prestirring) from **3.28** (150 mg, 0.322 mmol), DIPEA (330 µL, 1.89 mmol) and 2,2-dimethylpropan-1-amine (230 µL, 1.97 mmol) in i-PrOH (2 mL). The crude product was purified by automated flash chromatography [gradient 0 – 20 min: DCM/MeOH (v/v) 100/0 – 90/10, SF 10-4 g] to give a colorless sticky foam (65 mg, 39.1%). R$_f$ = 0.4 (DCM/MeOH 90/10). Deprotection (60 mg, 0.12 mmol) in DCM (2 mL) and TFA (0.5 mL) followed by preparative HPLC [Phenomenex

Kinetex 5u XB-C18 250 × 21.2 mm; gradient 0 − 30 min: A/B (*v/v*) 85/15 − 28/72; flow: 20 mL/min; t_R = 8 min] afforded **3.41** as colorless hygroscopic foam (21 mg, 36.0%). RP-HPLC (220 nm): 99.0% (*k* = 2.02). ^{1}H-NMR (300 MHz, MeOH-d_4): δ (ppm) 8.84 (s, 1H), 7.56 (d, *J* = 7.2 Hz, 1H), 7.38 (s, 1H), 6.02 (d, *J* = 7.0 Hz, 1H), 3.80 (t, *J* = 6.5 Hz, 1H), 3.28 (m, 2H), 3.07 (t, *J* = 6.5 Hz, 1H), 0.97 (s, 9H). ^{1}H-NMR (600 MHz, DMSO-d_6, +10 μL TFA): δ (ppm) 11.98 (br, 3H), 9.00 (s, 1H), 8.89 (m, 1H), 8.24 (m, 1H), 7.67 (m, 1H), 7.44 (s, 1H), 6.00 (d, *J* = 6.9 Hz, 1H), 3.66 (m, 2H), 3.19 (m, 2H), 2.94 (m, 2H), 0.89 (s, 9H). ^{13}C-NMR (151 MHz, DMSO-d_6, +10 μL TFA, HSQC, HMBC): δ (ppm) 162.46 (quat., 1C), 158.49 (q, *J* = 37.4 Hz, TFA), 154.24 (quat., 1C), 141.33, 133.99, 130.64 (quat., 1C), 116.39, 115.42 (q, *J* = 291.6 Hz, TFA), 97.22, 51.24, 39.33, 32.12 (quat., 1C), 27.11 (3C), 23.60. HRMS (ESI): *m/z* [*M* + H]$^+$ calcd for [C$_{14}$H$_{23}$N$_5$]$^+$ 275.1979, found 275.1983. C$_{14}$H$_{22}$N$_5$ · C$_4$H$_2$F$_6$O$_4$ (274.37 + 228.05).

N^4-[3-(1H-Imidazol-4-yl)propyl]-N^2-neopentylpyrimidine-2,4-diamine bis(2,2,2-trifluoroacetate) (3.42). According to the general procedure the title compound was prepared in the microwave reactor (10 h, 130 °C, 3 bar, 3 min prestirring) from **3.29** (140 mg, 0.292 mmol), DIPEA (300 μL, 1.72 mmol) and 2,2-dimethylpropan-1-amine (206 μL, 1.75 mmol) in *i*-PrOH (2 mL). The crude product was purified by automated flash chromatography [gradient 0 − 20min: DCM/MeOH (*v/v*) 100/0 − 90/10, SF 10-4 g] to a colorless sticky foam (100 mg, 64.5%). R$_f$ = 0.45 (DCM/MeOH 90/10). Deprotection (70 mg, 0.13 mmol) in DCM (2 mL) and TFA (0.5 mL), followed by preparative HPLC [Phenomenex Kinetex 5u XB-C18 250 × 21.2 mm; gradient 0 − 30 min: A/B (*v/v*) 90/10 − 33/67, flow: 20 mL/min; t$_R$ = 10.5 min] afforded **3.42** as hygroscopic foam (35 mg, 51.4%). RP-HPLC (220 nm): 99.9% (*k* = 2.23). ^{1}H-NMR (300 MHz, MeOH-d_4): δ (ppm) 8.82 (m, 1H), 7.55 (d, *J* = 7.3 Hz, 1H), 7.35 (s, 1H), 6.04 (d, *J* = 7.2 Hz, 1H), 3.56 (t, *J* = 6.8 Hz, 2H), 3.27 (m, 2H), 2.82 (t, *J* = 7.7 Hz, 2H), 2.02 (m, 2H), 0.96 (s, 9H). ^{1}H-NMR (600 MHz, DMSO-d_6, +10 μL TFA): δ (ppm) 11.89 (br, 3H), 8.98 (m, 1H), 8.81 (m, 1H), 8.13 (m, 1H), 7.67 (m, 1H), 7.43 (s, 1H), 6.02 (d, *J* = 7.0 Hz, 1H), 3.40 (m, 2H), 3.15 (m, 2H), 2.69 (t, *J* = 7.5 Hz, 2H), 1.89 (m, 2H), 0.87 (s, 9H). ^{13}C-NMR (151 MHz, DMSO-d_6, +10 μL TFA, HSQC, HMBC): δ (ppm) 162.32 (quat., 1C), 158.49 (q, *J* = 37.4 Hz, TFA), 154.26 (quat., 1C), 141.15, 133.89, 132.67 (quat., 1C), 115.63, 115.46 (q, *J* = 290.2 Hz, TFA), 97.19, 51.20, 39.20, 32.16 (quat., 1C), 27.11 (3C), 27.00, 21.41. HRMS (ESI):

m/z [*M* + H]⁺ calcd for [$C_{15}H_{25}N_6$]⁺ 289.2135, found 289.2136. $C_{15}H_{24}N_6 \cdot C_4H_2F_6O_4$ (288.40 + 228.05).

_N_-Neopentyl-4-(1,4,6,7-tetrahydro-5*H*-imidazo[4,5-c]pyridin-5-yl)pyrimidin-2-amine bis(2,2,2-trifluoroacetate) (3.43). According to the general procedure, the title compound was prepared in the microwave reactor (7.5 h, 130 °C, 3 bar, 3 min prestirring) from **3.30** (200 mg, 0.418 mmol), DIPEA (220 µL, 1.26 mmol) and 2,2-dimethylpropan-1-amine (150 µL, 1.27 mmol) in *i*-PrOH (3 mL). The crude product was purified by automated flash chromatography [gradient 0 – 20 min: DCM/MeOH (*v/v*) 100/0 – 90/10, SF 10-4 g] to give a yellow sticky oil (160 mg, 72.4%). R_f = 0.3 (DCM/MeOH 90/10). Deprotection (75 mg, 0.14 mmol) in DCM (2 mL) and TFA (0.4 mL) followed by preparative HPLC [column: Phenomenex Kinetex 5u XB-C18 250 × 21.2 mm; gradient: 0-30 min: A/B (*v/v*) 95/5 – 33/67, flow 15 mL/min, t_R = 13.5 min] afforded **3.43** as colorless hygroscopic foam (30 mg, 41.1%). RP-HPLC (220 nm): 96.2% (*k* = 1.97). Ratio of configurational isomers evident in NMR performed in DMSO-*d₆*: ca. 1:1.1. ¹H-NMR (300 MHz, MeOH-*d₄*): δ (ppm) 8.79 (s, 1H), 7.81 (d, *J* = 7.5 Hz, 1H), 6.57 (m, 1H), 4.69 (m, 2H), 4.21 (m, 2H), 3.34 (m, 2H), 2.94 (m, 2H), 0.99 (s, 9H). ¹H-NMR (600 MHz, DMSO-*d₆*): δ (ppm) 13.96 (br, 2H), 8.86 (s, 1H), 8.47 (br, 1H), 7.97 (d, *J* = 7.3 Hz, 1H), 6.61 (m, 1H), 5.00 – 3.00 (1 proton (NH⁺) presumably superimposed by H_2O), 4.91 (m, 2H), 4.12 (m, 2H), 3.24 (m, 2H), 2.83 (m, 2H), 0.91 (s, 9H). ¹³C-NMR (151 MHz, DMSO-*d₆*, HSQC, HMBC): δ (ppm) 161.79 (quat., 1C) 158.72 (q, *J* = 32.3 Hz, TFA), 153.65 (quat., 1C), 143.82, 133.68, 125.76 (quat., 1C), 124.13 (quat., 1C), 116.90 (q, *J* = 297.8 Hz, TFA), 94.47, 51.42, 42.94, 42.86, 40.04, 32.26 (quat., 1C), 27.09 (3C), 20.82, 20.76. HRMS (ESI): *m/z* [*M* + H]⁺ calcd for [$C_{15}H_{23}N_6$]⁺ 287.1979, found 287.1982. $C_{15}H_{22}N_6 \cdot C_4H_2F_6O_4$ (286.38 + 228.05).

_N⁴_-(2-{[(5-Methyl-1H-imidazol-4-yl)methyl]thio}ethyl)-_N²_-neopentylpyrimidine-2,4-diamine bis(2,2,2-trifluoroacetate) (3.44). The title compound was prepared in the microwave reactor (4 h, 120 °C, 3 bar, 3 min prestirring) from **3.31** (110 mg, 0.388 mmol), DIPEA (132 µL, 0.756 mmol) and 2,2-dimethylpropan-1-amine (137 µL, 1.17 mmol) in *i*-PrOH (3 mL). After the solvent was removed under reduced pressure the residue was dissolved in DCM (5 mL). The organic phase was washed with H_2O (3 × 2 mL) and brine (5 mL) and dried over MgSO₄. The crude product was purified by chromatography [DCM/MeOH (*v/v*)

100/0 – 92.5/7.5, SiO$_2$ 13 g] and preparative HPLC [column: Phenomenex Kinetex 5u XB-C18 250 × 21.2 mm; gradient: 0-30 min: A/B (*v/v*) 85/15 – 52/48, flow 15 mL/min, t$_R$ = 14.5 min] to yield **3.44** as colorless hygroscopic foam (38 mg, 17.4%). RP-HPLC (220 nm): 98.9% (*k* = 2.55). ^{1}H-NMR (300 MHz, MeOH-*d$_4$*): δ (ppm) 8.75 (s, 1H), 7.56 (d, *J* = 7.3 Hz, 1H), 6.05 (d, *J* = 7.2 Hz, 1H), 3.88 (s, 2H), 3.68 (t, *J* = 6.8 Hz, 2H), 2.77 (t, *J* = 6.8 Hz, 2H), 2.33 (s, 3H), 0.96 (s, 9H). ^{1}H-NMR (600 MHz, DMSO-*d$_6$*): δ (ppm) 14.24 (br, 3H), 8.99 (m, 1H), 8.88 (s, 1H), 8.39 (m, 1H), 7.69 (d, J = 7.0 Hz, 1H), 6.05 (d, *J* = 7.0 Hz, 1H), 3.86 (s, 2H), 3.55 (m, 2H), 3.19 (m, 2H), 2.68 (t, *J* = 6.7 Hz, 2H), 2.24 (s, 3H), 0.98 (s, 9H). ^{13}C-NMR (151 MHz, DMSO-*d$_6$*, HSQC, HMBC): δ (ppm) 162.32 (quat., 1C), 158.59 (q, *J* = 31.4 Hz, TFA), 154.29 (quat., 1C), 141.40, 133.03, 125.94 (quat., 1C), 125.71 (quat., 1C), 117, 07 (q, *J* = 299.9 Hz, TFA), 97.10, 51.22, 39.74, 32.11 (quat., 1C), 29.81, 27.07 (3C), 23.13, 8.57. HRMS (ESI): *m/z* [*M* + H]$^+$ calcd for [C$_{16}$H$_{27}$N$_6$S]$^+$ 335.2012, found 335.2017. C$_{16}$H$_{26}$N$_6$ S · C$_4$H$_2$F$_6$O$_4$ (334.49 + 228.05).

(*R*)-4-[3-(Methylamino)pyrrolidin-1-yl]-*N*-neopentylpyrimidin-2-amine bis(2,2,2-trifluoroacetate) (3.45)[28]. In an argon-flushed Schlenk flask **3.32** (480 mg, 1.37 mmol) was dissolved in anhydrous THF (10 mL). LiAlH$_4$ (267 mg, 7.04 mmol) was added in portions and the reaction was stirred at 70 °C for 7 h. The reaction was cooled to 0 °C, quenched with H$_2$O (3 mL) and extracted with DCM (3 × 30 mL). The organic phases were combined, washed with brine (50 mL) and dried over MgSO$_4$. The crude product was purified by chromatography [DCM/1% NH$_{3 (aq)}$ in MeOH (isocratic): 90/15 (*v/v*), SiO$_2$ 30 g] and preparative HPLC [column: Phenomenex Kinetex 5u XB-C18 250 × 21.2 mm; gradient: 0 – 30 min: A/B (*v/v*) 90/10 – 38/62, flow 20 mL/min, *t$_R$* = 9 min] to yield **3.45** as colorless hygroscopic foam (290 mg, 43.1%). RP-HPLC (220 nm): 99.8% (*k* = 1.88). Ratio of configurational isomers evident in NMR performed in DMSO-*d$_6$*: ca 1:1.5. ^{1}H-NMR (300 MHz, MeOH-*d$_4$*): δ (ppm) 7.74 (d, *J* = 7.4 Hz, 1H), 6.22 (m, 1H), 3.88 (m, 5H), 3.47 – 3.20 (m, 2H), 2.80 (s, 3H), 2.41 (m, 2H), 0.98 (m, 9H). ^{1}H-NMR (600 MHz, DMSO-*d$_6$*): δ (ppm) 12.83 (br, 1H), 9.18 (m, 2H), 8.52 (m, 1H), 7.90 (m, 1H), 6.20 (d, *J* = 6.9 Hz, 1H), 3.97 – 3.56 (m, 5H), 3.23 (m, 2H), 2.64 (s, 3H), 2.42 – 2.12 (m, 2H), 0.90 (s, 9H). ^{13}C-NMR (151 MHz, DMSO-*d$_6$*, HSQC, HMBC): δ (ppm) 159.57 (quat., 1C), 159.46 (quat., 1C), 158.97 (q, *J* = 32.6 Hz, TFA), 153.55 (quat., 1C), 143.53, 116.78 (q, *J* = 297.1 Hz, TFA), 95.44, 95.33, 57.37, 56.53, 51.30, 49.11, 48.79, 45.02, 44.85, 32.27 (quat.,

1C), 31.22, 31.07, 27.13 (3C), 27.01, 26.66. HRMS (ESI): m/z [M + H]$^+$ calcd for [C$_{14}$H$_{26}$N$_5$]+ 264.2183, found 264.2182. C$_{14}$H$_{25}$N$_5$ · C$_4$H$_2$F$_6$O$_4$ (263.39 + 228.05).

General procedure for **3.46 – 3.48**

The respective 2,4-diaminopyrimidine bis(hydrotrifluoroacetate) (**3.33 – 3.35**) was dissolved in formic acid/formamide (1/1 *v/v*, 1.6 mL) and stirred at 95 °C until conversion was complete. Subsequently, the reaction mixture was quenched with saturated NaHCO$_{3\ (aq)}$ and extracted with EtOAc. The organic phases were combined, washed with brine and dried over MgSO$_4$. After the solvent was removed under reduced pressure the product was purified by preparative HPLC.

(*R*)-4-[3-(Dimethylamino)pyrrolidin-1-yl]-*N*-neopentylpyrimidin-2-amine bis(2,2,2-trifluoroacetate) (3.46). According to the general procedure, the title compound was prepared from **3.33** (150 mg, 0.314 mmol) over 5 h. The reaction mixture was quenched with saturated NaHCO$_{3\ (aq)}$ (7 mL) and extracted with EtOAc (2 × 100 mL). The organic phases were combined, washed with brine (100 mL) and dried over MgSO$_4$. After removing the solvent under reduced pressure, the product was purified by preparative HPLC [column: Phenomenex Kinetex 5u XB-C18 250 × 21.2 mm; gradient: 0 – 30 min: A/B (*v/v*) 90/10 – 43/57, flow 15 mL/min, t$_R$ = 12 min] to yield **3.46** as colorless hygroscopic foam (90 mg, 56.7%). R$_f$ = 0.4 (DCM/1.75 M NH$_3$ in MeOH 90/10). RP-HPLC (220 nm): 99.3% (*k* = 1.89). Ratio of configurational isomers evident in NMR performed in DMSO-*d₆*: ca 1:1.5. ^{1}H-NMR (300 MHz, MeOH-*d₄*): δ (ppm) 7.74 (m, 1H), 6.22 (m, 1H), 3.94 (m, 5H), 3.30 (m, 2H), 2.99 (m, 6H), 2.46 (m, 2H), 0.98 (m, 2H). ^{1}H-NMR (600 MHz, DMSO-*d₆*): δ (ppm) 12.50 (br, 1H), 10.54 (br, 1H), 8.35 (br, 1H), 7.92 (m, 1H), 6.22 (m, 1H), 4.00 (m, 2H), 3.87 (m, 0.6H), 3.74 (m, 1.6H), 3.55 (m, 1H), 3.25 (m, 1.8H), 2.85 (s, 6H), 2.29 (m, 2H), 0.90 (m, 9H). ^{13}C-NMR (151 MHz, DMSO-*d₆*, HSQC, HMBC): δ (ppm) 159.50 (quat., 1C), 159.41 (quat., 1C), 158.62 (q, *J* = 32.2 Hz, TFA), 153.47 (quat., 1C), 142.70, 116.87 (q, *J* = 298.1 Hz, TFA), 95.37, 95.18, 63.76, 63.00, 51.30, 51.24, 47.92, 47.78, 45.60, 45.52, 41.50 (2C), 32.30 (quat 1C), 32.23 (quat., 1C), 27.14 (3C), 26.02, 25.86. HRMS (ESI): *m/z* [*M* + H]$^+$ calcd for [C$_{15}$H$_{28}$N$_5$]$^+$ 278.2339, found 278.2342. C$_{15}$H$_{27}$N$_5$ · C$_4$H$_2$F$_6$O$_4$ (277.42 + 228.05).

4-(4-Methylpiperazin-1-yl)-*N*-neopentylpyrimidin-2-amine bis(2,2,2-trifluoroacetate) (3.47)[28]. According to the general procedure, the title compound was prepared from **3.34** (150 mg, 0.314 mmol) over 5 h. The reaction mixture was quenched with saturated NaHCO$_3$ (aq) (7 mL) and extracted with EtOAc (2 × 100 mL). The organic phases were combined, washed with brine (100 mL) and dried over MgSO$_4$. After removing the solvent under reduced pressure, the product was purified by preparative HPLC [column: Phenomenex Kinetex 5u XB-C18 250 × 21.2 mm; gradient: 0 – 30 min: A/B (*v/v*) 95/5 – 43/57, flow 15 mL/min, t$_R$ = 13.5 min] to yield **3.47** as colorless hygroscopic foam (75 mg, 48.6%). R$_f$ = 0.6 (DCM/1.75 M NH$_3$ in MeOH 90/10). RP-HPLC (220 nm): 98.7% (*k* = 1.67). ¹H-NMR (300 MHz, MeOH-*d*$_4$): δ (ppm) 7.82 (d, *J* = 7.5 Hz, 1H), 6.52 (d, *J* = 7.4 Hz, 1H), 4.71 – 3.31 (m, 10H), 2.96 (s, 3H), 0.98 (s, 9H). ¹H-NMR (600 MHz, DMSO-*d*$_6$): δ (ppm) 12.84 (br, 1H), 10.67 (br, 1H), 8.57 (br, 1H), 7.99 (d, *J* = 7.3 Hz, 1H), 6.54 (d, *J* = 7.4 Hz, 1H), 5.26 – 3.02 (m, 10H), 2.82 (s, 3H), 0.90 (s, 9H). ¹³C-NMR (151 MHz, DMSO-*d*$_6$, HSQC, HMBC): δ (ppm) 161.19 (quat., 1C), 158.83 (q, *J* = 32.4 Hz, TFA), 153.76 (quat., 1C), 143.92, 116.89 (q, *J* = 298.6 Hz, TFA), 94.25, 51.67, 51.33 (2C), 42.10, 39.92 (2C), 32.29 (quat., 1C), 27.09 (3C). HRMS (ESI): *m/z* [*M* + H]⁺ calcd for [C$_{14}$H$_{26}$N$_5$]⁺ 264.2183, found 264.2184. C$_{14}$H$_{25}$N$_5$ · C$_4$H$_2$F$_6$O$_4$ (263.39 + 228.05).

4-(4-Methyl-1,4-diazepan-1-yl)-*N*-neopentylpyrimidin-2-amine bis(2,2,2-trifluoroacetate) (3.48). According to the general procedure, the title compound was prepared from **3.35** (80 mg, 0.16 mmol) over 3 h. The reaction mixture was quenched with saturated NaHCO$_3$ (aq) (5 mL) and extracted with EtOAc (3 × 30 mL). The organic phases were combined, washed with brine (50 mL) and dried over MgSO$_4$. After removing the solvent under reduced pressure, the product was purified by preparative HPLC [column: Phenomenex Kinetex 5u XB-C18 250 × 21.2 mm; gradient: 0 – 30 min: A/B (*v/v*) 95/5 – 33/67, flow 15 mL/min, t$_R$ = 13 min] to yield **3.48** as colorless hygroscopic foam (60 mg, 72.8%). R$_f$ = 0.8 (DCM/1.75 M NH$_3$ in MeOH 80/20). RP-HPLC (220 nm): 99.1% (*k* = 1.84). Ratio of configurational isomers evident in NMR performed in DMSO-*d*$_6$: ca 1:1.7. ¹H-NMR (300 MHz, MeOH-*d*$_4$): δ (ppm) 7.78 (m, 1H), 6.43 (m, 1H), 3.72 (m, 10 H), 2.96 (m, 3H), 2.32 (m, 2H), 0.99 (m, 9H). ¹H-NMR (600 MHz, DMSO-*d*$_6$): δ (ppm) 12.78 (br, 1H), 10.24 (br, 1H), 8.47 (br, 1H), 7.94 (d, *J* = 7.1 Hz, 1H), 6.45 (m, 1H), 3.93 (m, 6H), 3.20 (m, 4H), 2.82 (m, 3H), 2.16 (m, 2H), 0.90 (s, 9H). ¹³C-NMR (151 MHz, DMSO-*d*$_6$, HSQC, HMBC): δ (ppm) 161.76 (quat., 1C), 161.67 (quat., 1C), 158.71 (q, *J* = 32.0 Hz, TFA),

153.55 (quat., 1C), 153.38 (quat., 1C), 143.29, 142.99, 116.88 (q, J = 298.5 Hz, TFA), 94.63, 94.56, 54.76, 54.74, 54.59, 54.52, 51.33, 46.52, 45.13, 43.46, 43.27, 42.73, 41.20, 32.17 (quat., 1C), 27.12 (3C), 23.20, 22.95. HRMS (ESI): m/z [M + H]$^+$ calcd for [C$_{15}$H$_{28}$N$_5$]$^+$ 278.2339, found 278.2340. C$_{15}$H$_{27}$N$_5 \cdot$ C$_4$H$_2$F$_6$O$_4$ (277.42 + 228.05).

<u>General procedure for **3.49 – 3.51**</u>

The respective 2,4-diaminopyrimidine bis(hydrotrifluoroacetate) (**3.33 – 3.35**) (1 equiv), 1,3-bis(tert-butoxycarbonyl)-2-methyl-2-thiopseudourea (1.2 equiv), HgCl$_2$ (1.5 equiv) and triethylamine [TEA (10 equiv)] were suspended in DCM and stirred at rt for 6 h. The suspension was filtered through a Cellite® pad and the filtrate was concentrated under reduced pressure. The crude product was purified by chromatography. After the removal of the protection group with TFA in DCM (5 – 7 h), the product was purified by preparative HPLC.

(*R*)-1-{1-[2-(Neopentylamino)pyrimidin-4-yl]pyrrolidin-3-yl}guanidine bis(2,2,2-trifluoroacetate) (3.49). According to the general procedure, the title compound was prepared from **3.33** (200 mg, 0.419 mmol), 1,3-bis(tert-butoxycarbonyl)-2-methyl-2-thiopseudourea (146 mg, 0.503 mmol), HgCl$_2$ (171 mg, 0.629 mmol) and TEA (600 µL, 4.33 mmol) in DCM (5 mL). The crude product was purified by chromatography [DCM/MeOH (*v/v*) 100/0 – 95/5, SiO$_2$ 40 g] to give a pale yellow sticky oil (120 mg, 58.3%). R$_f$ = 0.4 (DCM/MeOH 90/10). Deprotection of (100 mg, 0.203 mmol) in DCM (5 mL) and TFA (2 mL), followed by preparative HPLC [column: Phenomenex Kinetex 5u XB-C18 250 × 21.2 mm; gradient: 0 – 30 min: A/B (*v/v*) 85/15 – 28/72, flow 15 mL/min, t$_R$ = 11.5 min] afforded **3.49** as colorless hygroscopic foam (72 mg, 68.3%). R$_f$ = 0.2 (DCM/1.75 M NH$_3$ in MeOH 90/10). RP-HPLC (220 nm): 99.8% (*k* = 2.21). Ratio of configurational isomers evident in NMR performed in DMSO-*d$_6$*: ca 1:1.7. ^{1}H-NMR (300 MHz, MeOH-*d$_4$*): δ (ppm) 7.70 (m, 1H), 6.20 (m, 1H), 4.30 (m, 1H), 4.40 – 3.48 (m, 4H), 3.39 – 3.28 (m, 2H), 2.29 (m, 2H), 0.97 (s, 9H). ^{1}H-NMR (600 MHz, DMSO-*d$_6$*): δ (ppm) 12.44 (br, 1H), 8.36 (m, 2H), 7.87 (m, 1H), 7.40 (m, 4H), 6.20 (m, 1H), 4.26 (m, 1H), 3.81 (m, 1H), 3.71 – 3.41 (m, 3H), 3.22 (m, 2H), 2.27 (m, 1H), 1.98 (m, 1H), 0.90 (s, 9H). ^{13}C-NMR (151 MHz, DMSO-*d$_6$*, HSQC, HMBC): δ (ppm) 159.60 (quat., 1C), 159.47 (quat., 1C), 159.02 (q, J = 31.8 Hz, TFA), 156.46 (quat., 1C), 153.49 (quat., 1C), 153.45 (quat., 1C), 142.43, 142.32, 116.92 (q, J = 297.8 Hz, TFA), 95.52, 95.27, 52.06, 51.94, 51.29, 51.27,

50.44, 49.65, 45.24, 45.16, 32.27 (quat., 1C), 32.23 (quat., 1C), 30.63, 29.77, 27.15 (3C). HRMS (ESI): m/z $[M + H]^+$ calcd for $[C_{14}H_{26}N_7]^+$ 292.2244, found 292.2247. $C_{14}H_{25}N_7 \cdot C_4H_2F_6O_4$ (291.40 + 228.05).

4-[2-(Neopentylamino)pyrimidin-4-yl]piperazine-1-carboximidamide bis(2,2,2-trifluoroacetate) (3.50). According to the general procedure, the title compound was prepared from **3.34** (200 mg, 0.419 mmol), 1,3-bis(tert-butoxycarbonyl)-2-methyl-2-thiopseudourea (146 mg, 0.503 mmol), HgCl$_2$ (171 mg, 0.630 mmol) and TEA (600 µL, 4.33 mmol) in DCM (5 mL). The product was purified by chromatography [DCM/MeOH (v/v) 100/0 – 95/5, SiO$_2$ 25 g] to give a yellow oil (200 mg, 97.1%). R$_f$ = 0.3 (DCM/MeOH 95/5). Deprotection (180 mg, 0.366 mmol) in DCM (3 mL) and TFA (1 mL), followed by preparative HPLC [column: Phenomenex Kinetex 5u XB-C18 250 × 21.2 mm; gradient: 0 – 30 min: A/B (v/v) 90/10 – 38/62, flow 15 mL/min, t$_R$ = 12.5 min] afforded **3.50** as colorless hygroscopic foam (48 mg, 25.2%). R$_f$ = 0.05 (DCM/MeOH 90/10). RP-HPLC (220 nm): 99.9% (k = 2.02). ^{1}H-NMR (300 MHz, MeOH-d_4): δ (ppm) 7.76 (d, J = 7.6 Hz, 1H), 6.43 (d, J = 7.5 Hz, 1H), 4.23 – 3.32 (m, 9H), 0.98 (s, 9H). ^{1}H-NMR (600 MHz, DMSO-d_6): δ (ppm) 12.47 (br, 1H), 8.31 (br, 1H), 7.92 (d, J = 6.9 Hz, 1H), 7.57 (br, 4H), 6.49 (d, J = 7.4 Hz, 1H), 3.87 (br, 4H), 3.58 (m, 4H), 3.21 (br, 2H), 0.90 (s, 9H). ^{13}C-NMR (151 MHz, DMSO-d_6, HSQC, HMBC): δ (ppm) 160.97 (quat., 1C), 158.58 (q, J = 31.2 Hz, TFA), 156.22 (quat., 1C), 153.77 (quat., 1C), 143.63, 117.15 (q, J = 300.0 Hz, TFA), 94.29, 51.35, 43.86 (2C), 42.91, 42.58, 32.28 (quat., 1C), 27.13 (3C). HRMS (ESI): m/z $[M + H]^+$ calcd for $[C_{14}H_{26}N_7]^+$ 292.2244, found 292.2247. $C_{14}H_{25}N_7 \cdot C_4H_2F_6O_4$ (291.40 + 228.05).

4-[2-(Neopentylamino)pyrimidin-4-yl]-1,4-diazepane-1-carboximidamide bis(2,2,2-trifluoroacetate) (3.51). According to the general procedure, the title compound was prepared from **3.35** (250 mg, 0.509 mmol), 1,3-bis(*tert*-butoxycarbonyl)-2-methyl-2-thiopseudourea (177 mg, 0.610 mmol), HgCl$_2$ (207 mg, 0.762 mmol) and TEA (705 µL, 5.09 mmol) in DCM (5 mL). The product was purified by chromatography [DCM/MeOH (v/v) 100/0 – 95/5, SiO$_2$ 35 g] to give a pale yellow sticky foam (240 mg, 93.2%). R$_f$ = 0.3 (DCM/MeOH 95/5). Deprotection (230 mg, 0.45 mmol) in DCM (5 mL) and TFA (1 mL), followed by preparative HPLC [column: Phenomenex Kinetex 5u XB-C18 250 × 21.2 mm;

gradient: 0 – 30 min: A/B (*v/v*) 90/10 – 48/52, flow 20 mL/min, t_R = 12 min] afforded **3.51** as colorless hygroscopic foam (116 mg, 48.2%). R_f = 0.05 (DCM/MeOH 95/5). RP-HPLC (220 nm): 99.8% (*k* = 2.09). Ratio of configurational isomers evident in NMR performed in DMSO-d_6: ca 1:1.4. ^{1}H-NMR (300 MHz, MeOH-d_4): δ (ppm) 7.75 (d, *J* = 7.5 Hz, 1H), 6.43 (m, 1H), 4.15 (m, 1.2H), 3.97 (m, 1.5 H), 3.79 (m, 3H), 3.64 (m, 2H), 1.98 (m, 2H), 0.98 (m, 9H). ^{1}H-NMR (600 MHz, DMSO-d_6): δ (ppm) 12.74 (br, 1H), 8.41 (br, 1H), 7.91 (m, 1H), 7.51 (br, 4H), 6.45 (d, *J* = 7.4 Hz, 1H), 3.59 (m, 10H), 1.83 (m, 2H), 0.90 (s, 9H). ^{13}C-NMR (151 MHz, DMSO-d_6, HSQC, HMBC): δ (ppm) 161.25 (quat., 1C), 158.86 (q, *J* = 31.5 Hz, TFA), 155.93 (quat., 1C), 153.84 (quat., 1C), 153.76 (quat., 1C), 143.60, 117.07 (d, *J* = 297.8 Hz, TFA), 94.15, 51.39, 47.42, 47.30, 46.86, 46.73, 46.72, 46.67, 46.34, 46.02, 32.15 (quat., 1C), 27.13 (3C), 25.17, 24.08. HRMS (ESI): *m/z* [*M* + H]$^+$ calcd for [$C_{15}H_{28}N_7$]$^+$ 306.2401, found 306.2402. $C_{15}H_{27}N_7 \cdot C_4H_2F_6O_4$ (305.43 + 228.05).

(R)-N-{1-[2-(Neopentylamino)pyrimidin-4-yl]pyrrolidin-3-yl}propionamide 2,2,2-trifluoroacetate (3.52). 3.33 (100 mg, 0.209 mmol), DIPEA (630 μL, 3.70 mmol) and 1-propionylpyrrolidine-2,5-dione (70 mg, 0.45 mmol) were dissolved in DCM (5 mL). The reaction was stirred at rt for 24 h. The solvent was removed under reduced pressure and the crude product was purified by preparative HPLC [column: Phenomenex Kinetex 5u XB-C18 250 × 21.2 mm; gradient: 0 – 30 min: A/B (*v/v*) 81/19 – 38/62, flow 20 mL/min, t_R = 11 min] to yield **3.52** as colorless hygroscopic powder (50 mg, 57.0%). RP-HPLC (220 nm): 97.9% (*k* = 3.34). Ratio of configurational isomers evident in NMR: ca 1:1.4. ^{1}H-NMR (600 MHz, DMSO-d_6): δ (ppm) 12.30 (br, 1H), 8.24 (br, 1H), 8.10 (m, 1H), 7.83 (m, 1H), 6.17 (m, 1H), 4.36 (m, 1H), 3.67 (m, 3H), 3.46 (m, 0.5H), 3.32 (m, 0.5H); 3.21 (m, 2H), 2.07 (m, 3H), 1.89 (m, 1H), 0.98 (m, 3H), 0.90 (m, 9H). ^{13}C-NMR (151 MHz, DMSO-d_6, HSQC, HMBC): δ (ppm) 172.92 (quat., 1C), 159.36 (quat., 1C), 159.27 (quat., 1C), 158.63 (q, *J* = 32.0 Hz, TFA), 153.40 (quat., 1C), 142.07, 116.90 (q, *J* = 298.7 Hz, TFA), 95.51, 95.34, 52.32, 52.22, 51.25, 48.40, 47.55, 45.47, 45.41, 32.22 (quat., 1C), 30.48, 29.61, 28.26, 27.15 (3C), 9.73. HRMS: (ESI) *m/z* [*M* + H]$^+$, calcd for [$C_{16}H_{28}N_5O$]$^+$: 306.2288, found 306.2291. $C_{16}H_{27}N_5 \cdot C_2HF_3O_2$ (305.43 + 114.02).

3.4.4 Chemical stability

The chemical stability of **3.43**, **3.46**, **3.48** and **3.49** was investigated in PBS (pH 7.4) at 23 °C over 24 h. For this purpose, 200 µM dilutions in PBS (stock solution: 10 mM in DMSO) were prepared and incubated. After 0, 1, 5 and 24 h, 100 µL of this solution was added to 100 µL of MeCN/0.5% TFA 10/90 (*v/v*). This solution was filtered through PTFE-filters prior to analysis by RP-HPLC (conditions for analytical HPLC see section 3.4.1, graphs see Figure A 3.33 – Figure A 3.36 in section 3.5.5.3). Injection volume: 70 µL; k = 2.02 (**3.43**), k = 1.95 (**3.46**), k = 1.89 (**3.48**), k = 2.26 (**3.49**).

3.4.5 Synthesis of radioligand [³H]3.46

Compound [³H]**3.46** was essentially prepared according to a previously described radiolabeling protocol[45], using succinimidyl [³H]propionate as tritiated precursor, with the following modifications:

The amine precursor **3.45** was methylated with commercially available methyl nosylate [methyl-³H] ([³H]**3.53**), dissolved in MeCN (specific activity 60 – 80 Ci/mmol, 2.22 – 2.96 TBq/mmol, activity concentration 100 mCi/mL, Biotrend Chemikalien GmbH, Köln, Germany). Therefore, in a 2 mL reaction vessel with a screw cap, 11.5 µL of a solution of **3.45** in acetone (67.8 mM, 0.775 µmol, 6.2 equiv) and pestled K_2CO_3 (6.378 µmol, 51 equiv) were suspended in MeCN (124.3 µL) and transferred into a glass ampule containing 100 µL of [³H]**3.53** in MeCN (0.125 µmol, 1 equiv, 10 mCi). The 2 mL reaction vessel was washed with 124.3 µL of MeCN and the same volume was transferred to the reaction mixture, too. The reaction mixture was stirred at room temperature for 22.5 h, before the reaction was quenched with 40 µL of TFA $_{(aq)}$ (10%). The solvent was removed in a vacuum concentrator within 45 min. The residual material was diluted to a final volume of 800 µL with a mixture of MeOH/0.05% TFA 8/92 (*v/v*) for the purification, using an analytical HPLC system (Waters GmbH, Eschborn, Germany) consisting of two 510 pumps, a pump control module, a 486 UV/Vis detector, and a Flow-one/Beta series A-500 radio detector (Packard Instrument Company, Meriden, CT, USA). As the stationary phase, a Luna C18 (3 µm, 150 mm × 4.6 mm, Phenomenex, Aschaffenburg, Germany) column was used at a flow rate of 0.7 mL/min. The mobile phase consisted of MeOH + 0.05% TFA (A) and 0.05% TFA (B). Isolation of [³H]**3.46** was realized by performing 10 HPLC runs with injection volumes of 80 µL (only UV detection at

220 nm), applying the following conditions: 0 – 26 min, A/B 18.5/81.5; 26 – 27 min, 18.5/81.5 – 95/5; 27 – 34 min, 95/5; t_R ~ 25 min. The fractions containing the radioligand were collected in 2-mL reaction vessels with screw caps and the volumes were reduced in a vacuum concentrator to a final volume of 163.3 µL. After EtOH (381 µL) was added, the solution was transferred to a 3-mL borosilicate glass vial with conical bottom (Wheaton, NextGen 3 mL V-vials). The reaction vessels were washed twice with EtOH/H_2O 70/30 (*v/v*) and the volumes were combined to obtain the tentative stock solution (846 µL). For quantification, a four-point calibration curve with unlabeled **3.46** [0.5, 1, 2, 5 µM in MeCN/0.05% TFA (*v/v*) 8/92] was constructed. For this purpose, the above described HPLC system was used under the following modified conditions: 0 – 16 min, MeCN + 0.04% TFA/0.05% TFA 12/88; 16 – 19 min, 12/88 – 95/5; 19 – 26 min, 95/5; injection volume: 100 µL; flow rate 1 mL/min; UV detection at 220 nm; t_R = 15.0 min. An aliquot of the tentative stock (2µL) was diluted with MeCN/0.05% TFA [8/92 (*v/v*)] (128 µL), and 100 µL of this solution was analyzed by HPLC. Two µL was added to 3 mL of Rotiszint eco plus (Carl Roth, Karlsruhe, Germany) and 5 replicates were counted with a LS 6500 liquid scintillation counter (Beckmann Coulter Biomedical, München, Germany). This procedure was repeated. The molarity of the tentative stock was calculated from the mean of the peak areas and the determined calibration curve. A solution of [³H]**3.46** [c_{final} = 1 µM in MeCN/0.05% TFA (8/92 *v/v*)] was spiked with unlabeled **3.46** [c_{final} = 1 mM, in MeCN/0.05% TFA (8/92 *v/v*)] and analyzed by HPLC (0 – 15 min, MeCN + 0.04% TFA/0.05% TFA 10/90 – 32.5/67.5; 15 – 25 min, 32.5/67.5 – 90/10; 25 – 35 min, 90/10; flow rate 0.8 mL/min; injection volume 100 µL; UV detection at 220 nm) and radiometric detection [flow rate of the liquid scintillator (Rotiszint eco plus/MeCN (85/15 *v/v*): 4 mL/min)] to confirm the chemical identity (t_R = 11.1 min) and to determine the radiochemical purity (99%). After storage at -20 °C for 11 months, this experiment was repeated, giving a radiochemical purity of 94%. Calculated specific activity: 1.59 TBq/mmol (43.08 Ci/mmol). The final activity concentration was adjusted to 58.1 MBq/mL (1.6 mCi/mL) by adding EtOH/H_2O (70/30 *v/v*) to come to a molarity of 36.4 µM. Radiochemical yield: 108.54 MBq, 29%.

3.4.6 Cell culture, transfection and preparation of cell membranes and homogenates

General procedures for the generation of the recombinant baculovirus, the culture of *Sf*9 cells and the membrane preparation were described previously.[16,51] The generation and culture of HEK293T-SF-hH$_4$R-His6-CRE-Luc, HEK293T-SF-mH$_4$R-His6-CRE-Luc and HEK293T-SF-rH$_4$R-His6-CRE-Luc cells were described previously.[18] In contrast to the published procedure, HEK293T-SF-mH$_4$R-His6-CRE-Luc cells were cultured in the presence of 700 µg/mL of hygromycin B (MoBiTec GmbH, Göttingen, Germany). Cell homogenates were prepared after growing the cells in 30 culture dishes (145 cm^2) to 80% confluency in a humidified atmosphere (95% air, 5% CO$_2$, 37 °C), using Dulbecco's modified eagle's medium (DMEM) (Sigma-Aldrich Chemie GmbH, Taufkirchen, Germany) and 10% fetal calf serum (FCS) (Biochrom GmbH, Berlin, Germany). Subsequently, the cells were rinsed with PBS (10 mL/dish, 100 mM NaCl, 80 mM Na$_2$HPO$_4$, 20 mM NaH$_2$PO$_4$, pH 7.4) and scraped off the dish using a sterile cell scraper in the presence of a harvest buffer[52] [7 mL/dish, 10 mM tris(hydroxymethyl)aminomethane hydrochloride (Tris-HCl), 0.5 mM ethylenediaminetetraacetic acid (EDTA), 5.5 mM KCl, 140 mM NaCl, pH 7.4]. After centrifugation [1000 revolutions per minute (rpm), 10 min], the cells were suspended in ice-cold homogenate buffer[52] (15 mL, 50 mM Tris-HCl, 5 mM EDTA, 1.5 mM CaCl$_2$, 5 mM MgCl$_2$, 120 mM NaCl, pH 7.4) and supplemented with protease inhibitors (SigmaFAST™, Cocktail Tablets, EDTA-free, Sigma-Aldrich Chemie GmbH, Taufkirchen, Germany). Afterwards, the cells were lysed (20,000 rpm/min, 5 × 5 s, ice-cooled, Ultra-TURRAX®, Janke & Kunkel, IKA®-Werke GmbH & Co. KG, Staufen, Germany), and the lysate was centrifuged (23,000 rpm, 45 min, 4 °C, Optima™-L70-Preparative Ultracentrifuge, Beckmann Coulter, München, Germany). The remaining pellets were suspended in ice-cold binding buffer[51] (15 mL, 12.5 mM MgCl$_2$, 1 mM EDTA, 75 mM Tris-HCl, pH 7.4), homogenized with a Dounce homogenizer (10 times, ice-cooled) and stored at -80 °C in small aliquots (0.2 mL, 0.5 mL).

HEK293T cells, stably expressing xH$_4$R-ELucC/ELucN-β-arrestin2 (x = h, m, r) were generated as follows: the cDNAs, encoding the C-terminal luciferase fragment of the emerald luciferase (ELucC)[53] fused to the C-terminus of either hH$_4$R, mH$_4$R or rH$_4$R, were generated by replacing the hH$_1$R in the previously described pcDNA4 hH$_1$R-ELucC vector[54] by each xH$_4$R cDNA without

their stop codons. Then, HEK293T cells stably expressing the ELucN-β-arrestin2 construct[54] were stably transfected with each pcDNA4 xH$_4$R-ELucC vector as described.[54] The HEK293T-β-arr2-hH$_4$R, HEK293T-β-arr2-mH$_4$R and HEK293T-β-arr2-rH$_4$R cells were cultivated as previously described for HEK293T-β-arr2-hH$_1$R cells.[54]

3.4.7 Radioligand binding experiments

Competition binding experiments on membrane preparations of *Sf*9 insect cells, expressing the hH$_1$R + RGS4, hH$_2$R-Gs$_{\alpha s}$, hH$_3$R + G$_{i\alpha2}$ + β$_1$γ$_2$ or hH$_4$R + G$_{i\alpha2}$ + β$_1$γ$_2$, were essentially performed as described previously[55] with the following modifications: the experiments were performed in 96-well plates (PP microplates 96 well, Greiner Bio-One GmbH, Frickenhausen, Germany) in a total volume of 100 μL, containing 5 – 25 μg (hH$_4$R), 24 – 35 μg (hH$_3$R), 15 μg (hH$_2$R) and 23 μg (hH$_1$R) of soluble membrane protein and 0.2% bovine serum albumin (BSA). Used radioligands:

hH$_1$R: [³H]pyrilamine (c$_{final}$ = 5 nM, specific activity 20.0 Ci/mmol, K_d = 4.5 nM[55], Hartmann Analytics GmbH, Braunschweig, Germany),

hH$_2$R: [³H]UR-DE257[27] [resynthesized by Dr. Sabrina Biselli (data not published): c$_{final}$ = 20 nM, specific activity 33.0 Ci/mmol, K_d = 12.1 nM],

hH$_3$R: [³H]UR-PI294[12] ([³H]**3.02**) (c$_{final}$ = 2 nM, specific activity 93.3 Ci/mmol, K_d = 1.1 nM) or [³H]N$^\alpha$-methylhistamine (c$_{final}$ = 3 nM, specific activity 85.3 Ci/mmol, K_d = 8.6 nM[56], Hartmann Analytics GmbH, Braunschweig, Germany) and

hH$_4$R: [³H]histamine ([³H]**3.01**) [c$_{final}$ = 10 or 40 nM, (depending on the used batches), specific activity 25.0 Ci/mmol, K_d = 14.7 nM or 45 nM (depending on the batches), Biotrend Chemikalien GmbH, Köln, Germany]

For competition binding, saturation binding and kinetic binding experiments with [³H]**3.46**, the radioligand solution [36.4 μM in EtOH/H$_2$O 70/30 (*v/v*)] was mixed with a solution of "cold" **3.46** [36.4 μM in EtOH/H$_2$O 70/30 (*v/v*)] (1/3) due to economic reasons. The HEK293T-SF-hH$_4$R-His6-CRE-Luc-, HEK293T-SF-mH$_4$R-His6-CRE-Luc- or HEK293T-SF-rH$_4$R-His6-CRE-Luc cell homogenates were thawed and sedimented by centrifugation (16, 100 × g, 4 °C, 10 min) before the supernatant was discarded. The pellets were suspended in ice-cooled binding buffer to come to 1.8 μg (hH$_4$R), 2.8 μg (mH$_4$R) and 3.1 μg (rH$_4$R) protein per μL of binding

buffer. The experiments were performed in 96-well plates (PP microplates 96 well, Greiner Bio-One GmbH, Frickenhausen, Germany) in a total volume of 100 μL containing 18 μg (hH_4R), 28 μg (mH_4R), 31 μg (rH_4R) homogenate protein and 0.2% BSA. After different incubation periods at room temperature, the previously described procedure[55] for competition binding experiments using *Sf*9 cell membranes was followed.

In competition binding experiments, the final concentration of [³H]**3.46** was 40 nM (hH_4R) 30 nM (rH_4R) or 20 nM (mH_4R), while increasing concentrations of unlabeled ligands (**3.01**, **3.04**, **3.05** and **3.06**) were applied. The plates were shaken at 250 rpm for 60 min.

For the analysis of the data obtained from experiments on *Sf*9 membranes, total binding [in disintegrations per minute (dpm)] was plotted versus log (concentration competitor) and normalized [1.0 = bound radio ligand (dpm) in the absence of competitor, 0.0 = nonspecifically bound radioligand (dpm) in the presence of **3.01** (c_{final} = 10 μM, h$H_{3,4}$R), diphenhydramine (c_{final} = 10 μM, hH_1R) or famotidine (c_{final} = 100 μM, hH_2R)]. For competition binding experiments at HEK293T-CRE-Luc cell homogenates total binding (dpm) was plotted versus log (concentration competitor) and normalized [1.0 = bound radioligand (dpm) in the absence of a competitor, 0.0 = nonspecifically bound radioligand (dpm) in the presence of **3.06** (c_{final} = 100 μM, h, m, r H_4R)]. Applying a four-parameter logistic equation [log-(inhibitor) vs response-variable slope] (GraphPad Prism Software 7.1, GraphPad Software Inc., San Diego, CA, USA), pIC_{50} values were obtained. The pK_i values were calculated based on the Cheng-Prusoff equation[57].

Saturation binding experiments were conducted with various concentrations of [³H]**3.46**, while nonspecific binding was determined in the presence of **3.06** (1000-fold excess to each concentration of [³H]**3.46**). The plates were shaken at 250 rpm for 60 min. Specific binding data (dpm) were plotted against the free radioligand concentration (nM) and analyzed by a two-parameter equation describing hyperbolic binding to obtain K_d and B_{max} values (GraphPad Prism 7.1). The free radioligand concentration is the difference between the amount of specifically bound radioligand (nM) (calculation includes the amount of specifically bound [³H]**3.46** in dpm, the specific activity of [³H]**3.46** and the volume per well) and total radioligand concentration. Nonspecific binding data were fitted by linear regression (GraphPad Prism 7.1).

For association experiments, the h, m or rH_4R expressing homogenates were incubated with [³H]**3.46** (c_{final} = 40 nM hH_4R, c_{final} = 30 nM rH_4R, c_{final} = 20 nM mH_4R). Incubation was stopped after different time points (0 – 45 min) by addition of **3.06** (1000-fold excess to the [³H]**3.46** concentration). Nonspecific binding was determined in the presence of **3.06** (1000-fold excess to the concentration of [³H]**3.46**). The plates were shaken at 250 rpm throughout. In dissociation experiments, the h, m or rH_4R expressing homogenates were incubated with [³H]**3.46** (c_{final} = 40 nM hH_4R, c_{final} = 30 nM rH_4R, c_{final} = 20 nM mH_4R) for 30 min, before **3.06** (1000-fold excess to the concentration of [³H]**3.46**) was added at different time points (0 – 90 min). For the determination of the nonspecific binding, the procedure was performed identically, but **3.06** (1000-fold excess to the concentration of [³H]**3.46**) was added during the incubation step. The plates were shaken at 250 rpm throughout. The specific binding data (dpm) from association experiments were analyzed by a three-parameter equation describing exponential incline (GraphPad Prism 7.1) to a maximum to obtain k_{obs} (observed association rate constant) and $B_{(eq)}$ (maximum of specifically bound radioligand), used for the calculation of specifically bound radioligand ($B_{(t)}$) in %, which is plotted over time. In dissociation experiments, $B_{(t)}$ (%) were plotted over time and analyzed by a three-parameter equation describing exponential decline (GraphPad Prism 7.1) to obtain the dissociation rate constant k_{off} and $B_{(plateau)}$ (%, bottom of specifically bound radioligand).

3.4.8 Luciferase reporter gene assay

The luciferase reporter gene assay, using HEK293T-SF-hH_4R-His6-CRE-Luc, HEK293T-SF-mH_4R-His6-CRE-Luc or HEK293T-SF-rH_4R-His6-CRE-Luc cells, was performed as described previously[18], applying the following modifications:

After seeding 0.8×10^5 (hH_4R) and 1.6×10^5 (r,mH_4Rs) cells per well (160 µL) into colorless flat-bottomed 96-well plates (Greiner Bio-One GmbH, Frickenhausen, Germany), they were allowed to attach for 17 – 24 h in a humidified atmosphere (95% air, 5% CO_2, 37 °C), using DMEM without phenol red supplemented with 5% (*v/v*) FCS. A stock solution (10 mM) of forskolin (Sigma-Aldrich Chemie GmbH, Taufkirchen, Germany) in DMSO was used to prepare the feed solution in DMEM without phenol red [5% (*v/v*) FCS]. Forskolin solution (20 µL, c_{final} = 0.5 µM for hH_4R, c_{final} = 1.0 µM for m/rH_4Rs) and 20 µL of a 10-fold concentrated solution of the respective compound in various concentrations [10 mM stock solutions (see in

section 3.4.1) diluted with DMEM] was added. The cells were incubated for 5 h in a humidified atmosphere (95% air, 5% CO_2, 37 °C). The final DMSO concentration in the assay did not exceed 1%. Afterward, all media were discarded, followed by the addition of 80 μL of lysis buffer[18] to each well. The cells were shaken at room temperature for 30 – 45 min (180 rpm). For the luminescence measurement, 40 μL of the lysate was transferred to a white flat-bottomed 96-well plate (Greiner) and was supplemented with 80 μL of luciferase assay buffer[18] (120 μL/well). Luminescence, expressed as RLUs (relative light units), was measured for 1 s per well using the GENios Pro microplate reader (Tecan GmbH, Grödig/Salzburg, Austria) or the EnSpire multimode reader (PerkinElmer Inc., Waltham, MA,USA). Data were processed by plotting the RLUs versus log (concentration agonist) followed by a normalization (1.0 = forskolin-stimulated luciferase activity, 0.0 = induced change in forskolin-stimulated luciferase activity caused by 10 μM of the endogenous agonist histamine **3.01**) and transformation step (standard function: Y = 1.0 – Y). The analysis of the data was performed applying a four-parameter logistic equation [log(agonist) vs response – variable slope, GraphPad Prism 7.1].

3.4.9 β-Arrestin2 recruitment assay

The recruitment of the β-arrestin2 was measured via split-luciferase complementation. Agonist potencies were determined using HEK293T cells, stably expressing xH_4R-ELucC/ELucN-β-arrestin2 (x = h, m, r), using the GENios Pro microplate reader (Tecan GmbH, Grödig/Salzburg, Austria) as previously described for HEK293T-β-arr1-H_1R and HEK293T-β-arr2-H_1R cells.[54] Data were processed by plotting the RLUs versus log (concentration agonist) followed by a normalization step (agonist mode: 1.0 = maximum of β-arrestin2 recruitment caused by 100 μM of the endogenous agonist histamine **3.01**, 0.0 = basal activity). The normalized data were analyzed by applying a four-parameter logistic equation [log(agonist) vs response – variable slope,GraphPad Prism 7.1]. In antagonist mode, the solutions containing the antagonist were pre-incubated for 15 min before a solution of **3.01** in H_2O (c_{final} = 10 μM) was added. Data from antagonist mode were processed by plotting the RLUs versus log (concentration antagonist) followed by a normalization step (1.0 = β-arrestin2 recruitment caused by 10 μM of the endogenous agonist **3.01**, 0.0 = basal activity).

3.5 Appendix

3.5.1 Source or preparation of the amine precursors (3.07 – 3.18)

Some amine precursors (**3.07 – 3.15**) had to be prepared prior their use in the synthesis of the 2-chloro-4-aminopyrimidines **3.21 – 3.31**. Therefore, several procedures were applied as depicted in Scheme A 3.1 – Scheme A 3.3. Compound **3.16** was purchased from TCI Deutschland GmbH (Eschborn, Germany), **3.17**[34] and **3.18**[34,58] were provided by Dr. Patrick Igel (Figure A 3.1). Compound 1,3-Bis(tert-butoxycarbonyl)-2-methyl-2-thiopseudourea[25] was provided by Dr. Paul Baumeister.

The mono-Boc-protected diamines **3.07 – 3.12** (Scheme A 3.1) were prepared by applying the respective diamines **3.54 – 3.59** in an excess (2 – 3 equiv), while boc anhydride was slowly added at 0 °C.[59] The amine precursor **3.13** (Scheme A 3.1) was prepared via boc-protection of bromoethan-1-amine hydrobromide **3.60** to give **3.61**, followed by a Finkelstein reaction[60] in a microwave reactor with **3.54**, sodium iodide and K_2CO_3 in acetone.

Scheme A 3.1. Synthesis of the Boc-protected amines 3.07 – 3.13.
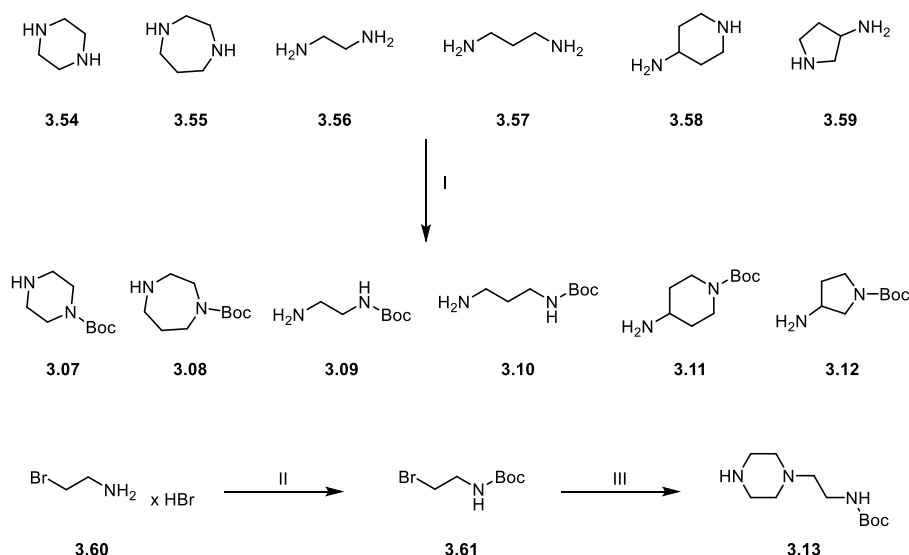
Reagents and conditions: (I) Boc anhydride, DCM, 0 °C or 0 °C → rt, 2 – 7 h, 60 – 98%; (II) Boc anhydride, DIPEA, DCM, 0 °C → rt, overnight, 80.1%; (III) **3.54**, NaI, K_2CO_3, acetone, 110 °C (microwave), 10 min, 65.1%.

To come to the trityl-protected histamine **3.14** (Scheme A 3.2), histamine dihydrochloride **3.62** and phthalic anhydride were refluxed in toluene using a *Dean-Stark* apparatus to give phthalimide **3.63**.[61] The following introduction of the trityl group was realized in the presence

of TEA. Finally, the liberation of the primary amine from the trityl- and phthaloyl-protected histamine **3.64** was performed via *Ing-Manske* hydrazinolysis as a variation of the *Gabriel* synthesis.[33]

Scheme A 3.2. Synthesis of 2-(1-Trityl-1*H*-imidazol-4-yl)ethan-1-amine 3.14
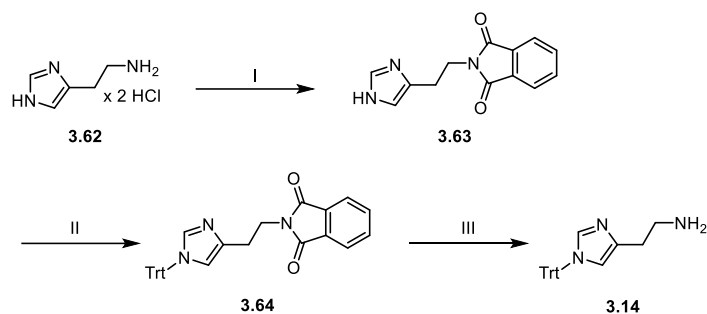
Reagents and conditions: (I) phthalic anhydride, TEA, toluene, 5 h, 110 °C, 46.1%; (II) trityl chloride, TEA, 24 h, rt, 78.8%; (III) N₂H₅OH, EtOH abs., 24 h, rt → 0 °C, 72.2%.

The spinaceamine dihydrochloride **3.65** was obtained by a modified *Pictet-Spengler* reaction[62-64] with **3.62** and dimethoxymethane in 0.01 M HCl $_{(aq)}$ (Scheme A 3.3). Cbz-protection of the secondary amine with benzyl succinimidyl carbonate gave **3.66** (Scheme A 3.3). After trityl-protection of the imidazole moiety, **3.67** was converted to the trityl-protected spinaceamine **3.15** via hydrogenolysis[25] (Scheme A 3.3).

Scheme A 3.3. Synthesis of 3-Trityl-4,5,6,7-tetrahydro-3*H*-imidazo[4,5-c]pyridine 3.15
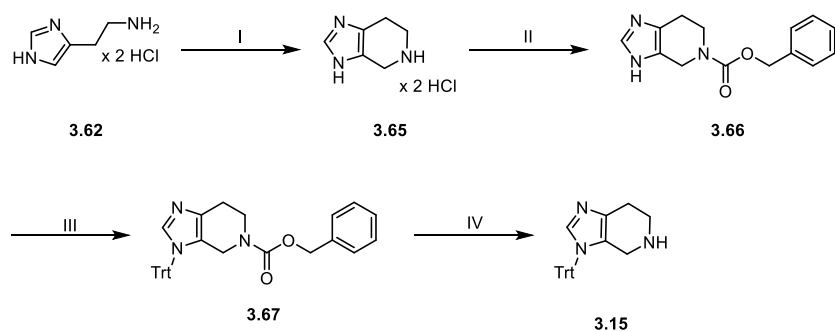
Reactions and conditions: (I) dimethoxymethane, 0.01 M HCl, overnight, reflux, 79.5%; (II) benzyl succinimidyl carbonate, TEA, DCM/DMF 4/1 (v/v), 1 h, rt, 48.1%; (III) trityl chloride, TEA, MeCN, overnight, rt, 78.4%; (IV) Pd/C, H₂, MeOH, 4 h, rt, 89.0%.

Figure A 3.1. Structures of the amine precursors 3.16 – 3.18.

3.5.1.1 Synthesis of compounds **3.07** – **3.13**

***tert*-Butyl piperazine-1-carboxylate (3.07)[65,66]. 3.54** (1.00 g, 11.6 mmol) was dissolved in DCM (10 mL) and cooled to 0 °C. A solution of boc anhydride (1.30 g, 5.96 mmol) in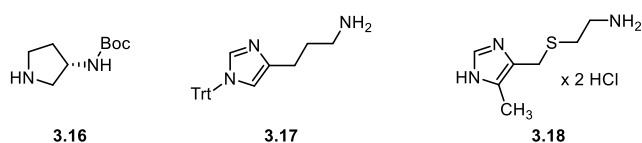 DCM (4 mL) was added slowly. The reaction could warm to rt for 5 h to turn to a colorless suspension. The colorless solid was filtered off. The filtrate was concentrated under reduced pressure and cold H_2O (20 mL) was added. After another filtration step, the aqueous phase was basified to pH 12 with saturated $K_2CO_{3\ (aq)}$ and the product was extracted with methyl tert-butyl ether (MTBE, 3 × 80 mL). After washing with brine (70 mL) and drying over $MgSO_4$ the solvent was removed under reduced pressure to give **3.07** as colorless solid (810 mg, 73.0%), mp 45 – 47 °C (lit 45 – 46 °C)[65]. R_f = 0.2 (DCM/1.7 M NH_3 in MeOH 95/5). ^{1}H-NMR (300 MHz, CDCl₃): δ (ppm) 3.33 (m, 4H), 2.75 (m, 4H), 1.68 (s, 1H), 1.45 (s, 9H). HRMS (ESI): m/z [M + H]⁺ calcd for $[C_9H_{19}N_2O_2]^+$ 187.1441, found 187.1441. $C_9H_{18}N_2O_2$ (186.26).

***tert*-Butyl 1,4-diazepane-1-carboxylate (3.08)[67,68]. 3.55** (1.8 g, 18 mmol) was dissolved in DCM (30 mL) and cooled to 0 °C. A solution of boc anhydride (1.0 g, 4.6 mmol) in DCM (13 mL) was added slowly. The reaction was stirred for 2 h to turn to a colorless suspension. After cold H_2O (50 mL) was added, the mixture was basified to pH 12 with 5% $NaHCO_{3\ (aq)}$ and the product was extracted with DCM (2 × 100 mL). After washing with brine and drying over $MgSO_4$ the solvent was removed under reduced pressure to give **3.08** as colorless oil (900 mg, 98.1%). R_f = 0.2 (DCM/2% $NH_{3\ (aq)}$ in MeOH 90/10). ^{1}H-NMR (400 MHz, CDCl₃): δ (ppm) 3.53 – 3.26 (m, 4H), 2.95 – 2.58 (m, 5H), 1.86 – 1.66 (m, 2H), 1.43 (s, 9H). ^{13}C-NMR (101 MHz, CDCl₃, HSQC, HMBC): δ (ppm) 155.58 (quat., 1C), 79.46 (quat., 1C), 49.27, 48.11, 46.03, 45.31, 30.18, 28.57 (3C). HRMS (ESI): m/z [M + H]⁺ calcd for $[C_{10}H_{21}N_2O_2]^+$ 201.1598, found 201.1602. $C_{10}H_{20}N_2O_2$ (200.28).

***tert*-Butyl (2-aminoethyl)carbamate (3.09)[69]. 3.56** (918 µL, 13.7 mmol) was dissolved in DCM (80 mL) and cooled to 0 °C. A solution of boc anhydride (1.0 g, 4.6 mmol) in DCM (40 mL) was added slowly. After stirring under ice-cooling for 5 h, the mixture turned to a colorless suspension. The colorless solid was filtered off. The filtrate was concentrated under reduced pressure and cold H_2O (100 mL) was added. After basification to pH 12 with saturated $K_2CO_{3\ (aq)}$ the product was extracted with MTBE (3 × 200 mL). After washing with brine

(100 mL) and drying over $MgSO_4$ the solvent was removed under reduced pressure to give **3.09** as colorless oil (440 mg, 59.9%). $R_f = 0.2$ (DCM/MeOH 90/10). ^{1}H-NMR (400 MHz, DMSO-d_6): δ (ppm) 6.56 (s, 1H), 2.90 (m, 2H), 2.51 (m, 2H), 1.80 (br, 2H), 1.37 (s, 9H). ^{13}C-NMR (101 MHz, DMSO-d_6, HSQC, HMBC): δ (ppm) 155.67 (quat., 1C), 77.37 (quat., 1C), 43.67, 41.61, 28.25 (3C). HRMS (ESI): m/z $[M + H]^+$ calcd for $[C_7H_{17}N_2O_2]^+$ 161.1285, found 161.1285. $C_7H_{16}N_2O_2$ (160.22).

***tert*-Butyl (3-aminopropyl)carbamate (3.10)[70,71].** **3.57** (568 μL, 6.74 mmol) was dissolved in DCM (40 mL) and cooled to 0 °C. A solution of boc anhydride (736 mg, 3.37 mmol) in DCM (20 mL) was added slowly. After stirring under ice-cooling for 7 h, the mixture turned to a colorless suspension. The colorless solid was filtered off. The filtrate was concentrated under reduced pressure and cold H_2O (30 mL) was added. After basification to pH 12 with saturated $K_2CO_{3\,(aq)}$ the product was extracted with MTBE (3 × 100 mL). After washing with brine (100 mL) and drying over $MgSO_4$ the solvent was removed under reduced pressure to give **3.10** as colorless oil (530 mg, 90.2%). $R_f = 0.1$ (DCM/1.7 M NH_3 in MeOH 90/10). ^{1}H-NMR (300 MHz, CDCl₃): δ (ppm) 4.95 (s, 1H), 3.17 (m, 2H), 2.77 (t, $J = 6.0$ Hz, 2H), 2.10 (s, 2H), 1.63 (m, 2H), 1.43 (s, 9H). HRMS (ESI): m/z $[M + H]^+$ calcd for $[C_8H_{19}N_2O_2]^+$ 175.1441, found 175.1463. $C_8H_{18}N_2O_2$ (174.24).

***tert*-Butyl 4-aminopiperidine-1-carboxylate (3.11)[72,73].** **3.58** (974 μL, 9.19 mmol) was dissolved in DCM (60 mL) and cooled to 0 °C. A solution of boc anhydride (1.0 g, 4.6 mmol) in DCM (30 mL) was added slowly to the reaction. After stirring under ice-cooling for 5 h, the mixture turned to a pale red suspension. The pale red crystals were filtered off. The filtrate was concentrated under reduced pressure and cold H_2O (30 mL) was added. After basification to pH 12 with saturated $K_2CO_{3\,(aq)}$ the product was extracted with MTBE (3 × 70 mL). After washing with brine and drying over $MgSO_4$ the solvent was removed under reduced pressure to give **3.11** as colorless powder (660 mg, 71.6%), mp 106.4 – 110.4 °C. $R_f = 0.2$ (DCM/1.7 M NH_3 in MeOH 90/10). ^{1}H-NMR (300 MHz, DMSO-d_6): δ (ppm) 3.80 (m, 2H), 2.73 (m, 3H), 1.64 (m, 4H), 1.38 (s, 9H), 1.06 (m, 2H). ^{1}H-NMR (400 MHz, CDCl₃): δ (ppm) 4.02 (m, 2H), 3.03 – 2.58 (m, 3H), 1.94 – 1.67 (m, 4H), 1.45 (s, 9H), 1.33 – 1.16 (m, 2H). ^{13}C-NMR (101 MHz, CDCl₃, HSQC, HMBC): δ (ppm) 154.96 (quat., 1C), 79.57 (quat., 1C), 48.96, 42.73 (2C), 35.48 (2C), 28.57 (3C).

HRMS (ESI): m/z $[M + H]^+$ calcd for $[C_{10}H_{21}N_2O_2]^+$ 201.1598, found 201.1601. $C_{10}H_{20}N_2O_2$ (200.28).

***tert*-Butyl 3-aminopyrrolidine-1-carboxylate (3.12)[74,75]. 3.59** (816 μL, 9.30 mmol) was dissolved in DCM (50 mL) and cooled to 0 °C. A solution of boc anhydride (1.0 g, 4.6 mmol) in DCM (20 mL) was added slowly. After stirring under ice-cooling for 7 h the mixture turned to an orange suspension. The off-white solid was filtered off. The filtrate was concentrated under reduced pressure and cold H_2O (30 mL) was added. After basification to pH 12 with saturated $K_2CO_{3 (aq)}$ the product was extracted with MTBE (3 × 150 mL). After washing with brine and drying over $MgSO_4$ the solvent was removed under reduced pressure to give **3.12** as pale yellow oil (610 mg, 71.2%). R_f = 0.3 (DCM/1.7 M NH_3 in MeOH 90/10). ^{1}H-NMR (300 MHz, DMSO-d_6): δ (ppm) 3.49 – 3.09 (m, 4H), 2.85 (m, 1H), 1.92 – 1.44 (m, 4H), 1.38 (s, 9H). ^{1}H-NMR (400 MHz, CDCl₃): δ (ppm) 4.12 (m, 2H), 2.88 – 2.60 (m, 3H), 1.75 – 1.59 (m, 4H), 1.44 (s, 9H). ^{13}C-NMR (101 MHz, CDCl₃, HSQC, HMBC): δ (ppm) 154.84 (quat., 1C), 79.66 (quat., 1C), 43.45, 43.13, 38.25, 28.55 (3C), 28.09. HRMS (ESI): m/z $[M + H]^+$ calcd for $[C_9H_{19}N_2O_2]^+$ 187.1441, found 187.1444. $C_9H_{18}N_2O_2$ (186.26).

***tert*-Butyl [2-(piperazin-1-yl)ethyl]carbamate (3.13)[47]. 3.60** (7.00 g, 24.5 mmol) and DIPEA (8.52 mL, 50.0 mmol) were dissolved in DCM (30 mL) and cooled to 0 °C. A solution of boc anhydride (6.0 g, 27 mmol) in DCM (20 mL) was added slowly. The reaction could warm to rt overnight. After H_2O (50 mL) was added, the mixture was acidified to pH 5 with 2 M HCl. The organic phase was separated, washed with 10% $NaHCO_{3 (aq)}$ (50 mL) and brine (50 mL), and dried over $MgSO_4$ followed by the removal of the solvent under reduced pressure. The product was purified by automated flash chromatography (isocratic, DCM 100%, SF 25-40 g) to give **3.61**[76,77] as pale yellow oil (4.4 g, 80.1%). R_f = 0.6 (PE/EtOAc 80/20). ^{1}H-NMR (400 MHz, CDCl₃): δ (ppm) 5.00 (s, 1H), 3.49 (m, 2H), 3.43 (m, 2H), 1.42 (s, 9H). ^{13}C-NMR (101 MHz, CDCl₃, HSQC, HMBC): δ (ppm) 155.69 (quat., 1C), 79.85 (quat., 1C), 42.44, 32.80, 28.42 (3C). HRMS (ESI): m/z $[M + Na]^+$ calcd for $[C_7H_{14}BrNaNO_2]^+$ 248.0080, found 248.0082. $C_7H_{14}BrNO_2$ (224.10).

3.61 (900 mg, 4.02 mmol), **3.54** (1.40 g, 16.3 mmol), NaI (903 mg, 6.02 mmol) and K_2CO_3 (834 mg, 6.03 mmol) were suspended in acetone (45 mL) and stirred as fractions (3 × 15 mL)

at 100 °C for 10 min in the microwave reactor (prestirring 3 min, 2 – 3 bar). The fractions were combined, and the colorless salt was filtered off. The filtrate was concentrated under reduced pressure. Cold H_2O (100 mL) was added and the product was extracted with DCM (3 × 100 mL). The organic layer was washed with brine (100 mL) and dried over $MgSO_4$. The product was purified by automated flash chromatography [gradient (I) 0 – 20 min: DCM/2% $NH_{3\,(aq)}$ in MeOH (v/v) 100/0 – 90/10; gradient (II) 20 – 35 min: DCM/2% $NH_{3\,(aq)}$ in MeOH (v/v) 90/10 – 80/20, SF 15 – 12 g] to give **3.13** as pale yellow oil (600 mg, 65.1%). $R_f = 0.1$ (DCM/2% $NH_{3\,(aq)}$ in MeOH 90/10). ¹H-NMR (400 MHz, CDCl₃): δ (ppm) 5.00 (s, 1H), 3.20 (m, 2H), 2.86 (m, 4H), 2.41 (m, 6H), 2.26 (s, 1H), 1.42 (s, 9H). ¹³C-NMR (101 MHz, CDCl₃, HSQC, HMBC): δ (ppm) 156.08 (quat., 1C), 79.23 (quat., 1C), 57.84, 54.16 (2C), 45.97 (2C), 37.01, 28.52 (3C). HRMS (ESI): m/z [M + H]⁺ calcd for [$C_{11}H_{24}N_3O_2$]⁺ 230.1863, found 230.1873. $C_{11}H_{23}N_3O_2$ (229.32).

3.5.1.2 Synthesis of **3.14**[78,79]

2-[2-(1*H*-Imidazol-4-yl)ethyl]isoindoline-1,3-dione (3.63)[79]. 3.62 (1.0 g, 5.4 mmol), phthalic anhydride (970 mg, 6.55 mmol) and TEA (2.30 mL, 16.5 mmol) were dissolved in toluene and stirred at 110 °C for 5 h using a *Dean Stark* apparatus. After adding H_2O (30 mL), the mixture was basified with alkaline brine to pH 10 and the product was extracted by EtOAc (3 × 150 mL). The organic phases were combined, dried over $MgSO_4$ and the solvent was removed under reduced pressure to give the titled compound as colorless powder (600 mg, 46.1%), mp 182 – 183 °C (lit 189 – 191 °C)[80]. $R_f = 0.6$ (DCM/MeOH/TEA 85/14/1). ¹H-NMR (400 MHz, DMSO-*d₆*): δ (ppm) 11.80 (br, 1H), 7.83 (m, 4H), 7.51 (d, *J* = 1.0 Hz, 1H), 6.81 (m, *J* = 1.0 Hz, 1H), 3.79 (t, *J* = 7.4 Hz, 2H), 2.83 (t, *J* = 7.4 Hz, 2H). ¹³C-NMR (101 MHz, DMSO-*d₆*, HSQC, HMBC): δ (ppm) 167.63 (quat., 2C), 134.80, 134.21 (2C), 133.87 (quat., 1C), 131.54 (quat., 2C), 122.86 (2C), 116.21, 37.62, 25.56. HRMS (ESI): *m/z* [*M*+H]⁺ calcd for [$C_{13}H_{12}N_3O_3$]⁺ 242.0930, found 242.0933. $C_{13}H_{11}N_3O_3$ (241.25).

2-[2-(1-Trityl-1*H*-imidazol-4-yl)ethyl]isoindoline-1,3-dione (3.64)[79]. 3.63 (570 mg, 2.36 mmol) and TEA (494 µL, 3.54 mmol) were dissolved in dimethylformamide (DMF, 10 mL) and cooled to 0 °C. Trityl chloride (988 mg, 3.54 mmol) was added slowly and the reaction could warm to rt for 24 h. After removing the solvent under reduced pressure the product was purified by automated flash chromatography [gradient 0 – 60 min: petroleum ether

(PE)/EtOAc (*v/v*) 100/0 – 30/70, SF 15-12 g] to give the titled compound as colorless crystals (900 mg, 78.8%), mp 181 – 182 °C. R_f = 0.15 (PE/EtOAc 67/33). ^{1}H-NMR (400 MHz CDCl$_3$): δ (ppm) 7.85 – 7.63 (m, 4H), 7.34 – 7.01 (m, 16 H), 6.53 (m, 1H), 3.97 (t, *J* = 7.0 Hz, 2H), 2.95 (t, *J* = 7.0 Hz, 2H). ^{13}C-NMR (101 MHz, CDCl$_3$): δ (ppm) 168.12 (2C), 142.50 (3C), 138.75, 137.75, 133.74 (2C), 132.21 (2C), 129.77 (6C), 127.96 (6C), 127.92 (3C), 123.17 (2C), 118.65, 75.06, 38.05, 27.36. HRMS (ESI): *m/z* [*M*+H]$^+$ calcd for [C$_{32}$H$_{26}$N$_3$O$_2$]$^+$ 484.2025, found 484.2020. C$_{32}$H$_{25}$N$_3$O$_2$ (483.57).

2-(1-Trityl-1*H*-imidazol-4-yl)ethan-1-amine (3.14)[78,79]. **3.64** (850 mg, 1.76 mmol) and hydrazine monohydrate (513 µL, 10.5 mmol) were suspended in EtOH abs. (10 mL). The reaction was stirred at rt overnight. Before the colorless precipitate was filtered off, the reaction mixture was stored in the fridge for 2 h. After the filtrate was concentrated under reduced pressure, the product was purified by automated flash chromatography [gradient 0 – 35min: DCM/3.5 M NH$_3$ in MeOH (*v/v*) 100/0 – 85/15, SF 15-12 g] to give the titled compound as colorless foam (450 mg, 72.2%), mp 123 – 125 °C (lit 126 – 128 °C)[81]. R_f = 0.2 (DCM/3.5 M NH$_3$ in MeOH 85/15). ^{1}H-NMR (400 MHz, CDCl$_3$): δ (ppm) 7.39 – 7.02 (m, 16H), 6.59 (s, 1H), 3.02 (t, *J* = 6.4 Hz, 2H), 2.71 (t, *J* = 6.3 Hz, 2H). ^{13}C-NMR (101 MHz, CDCl$_3$): δ (ppm) 142.55 (3C), 139.13, 138.74, 129.85 (6C), 128.14 (6C), 125.94 (3C), 118.73, 75.30, 41.56, 31.15. HRMS (ESI): *m/z* [*M*+H]$^+$ calcd for [C$_{24}$H$_{24}$N$_3$]$^+$ 354.1970, found 354.1969. C$_{24}$H$_{23}$N$_3$ (353.47).

3.5.1.3 Synthesis of **3.15**[25]

4,5,6,7-Tetrahydro-3*H*-imidazo[4,5-c]pyridine dihydrochloride (3.65)[25,62,63]. **3.62** (2.0 g, 10.9 mmol) and dimethoxymethane (965 µL, 10.9 mmol) were dissolved in 0.01 M HCl $_{(aq)}$ (90 mL). The reaction was stirred at reflux conditions overnight to turn to a yellow solution. The mixture was evaporated to dryness. The remaining solid was stirred in EtOH (30 mL) for 2 h, filtered off and dried under reduced pressure to give a colorless powder (1.7 g, 79.5%), mp 265 – 267 °C dec (lit 267 – 269 °C dec)[63]. ^{1}H-NMR (400 MHz, MeOH-d_4): δ (ppm) 8.97 (s, 1H), 4.50 (s, 2H), 3.68 (t, *J* = 6.1 Hz, 2H), 3.16 (t, *J* = 6.1 Hz, 2H). ^{13}C-NMR (101 MHz, MeOH-d_4, HSQC, HMBC): δ (ppm) 135.79, 126.38 (quat., 1C), 122.01 (quat., 1C), 42.34, 40.98, 19.21. HRMS (EI+, GC-MS): m/z [M]$^{+\bullet}$ calcd for [C$_6$H$_9$N$_3$]$^{+\bullet}$ 123.0791, found 123.0793. C$_6$H$_9$N$_3$ · Cl$_2$H$_2$ (123.16 + 72.92).

Benzyl 3,4,6,7-tetrahydro-5*H*-imidazo[4,5-c]pyridine-5-carboxylate (3.66)[25,82]. 3.65 (1.0 g, 5.1 mmol) and TEA (2.1 mL, 15 mmol) were dissolved in DCM (80 mL) and cooled to 0 °C. A solution of benzyl succinimidyl carbonate (1.3 g, 5.2 mmol) in DMF (20 mL) was slowly added and the reaction could warm to rt for 1 h. After H$_2$O (50 mL) was added, the mixture was basified to pH 10 with saturated NaHCO$_3$ (aq) and the product was extracted by DCM (2 × 50 mL). The organic phases were combined, washed with brine (50 mL) and dried over MgSO$_4$ followed by the removal of the solvent under reduced pressure to give a yellow sticky oil (620 mg, 48.1%). R$_f$ = 0.35 (DCM/MeOH 90/10). ^{1}H-NMR (400 MHz, CDCl$_3$): δ (ppm) 8.50 (br, 1H), 7.53 (s, 1H), 7.34 (m, 5H), 5.15 (s, 2H), 4.55 (s, 2H), 3.77 (m, 2H), 2.67 (t, *J* = 4.9 Hz, 2H). ^{13}C-NMR (101 MHz, CDCl$_3$, HSQC, HMBC): δ (ppm) 155.87 (quat., 1C), 136.61 (quat., 1C), 134.26, 129.68 (quat., 1C), 128.25 (2C), 128.21 (2C), 127.98, 125.26 (quat., 1C), 67.52, 42.84, 41.95, 22.16. HRMS (ESI): m/z [M+H]$^+$ calcd for [C$_{14}$H$_{16}$N$_3$O$_2$]$^+$ 258.1237, found 258.1239. C$_{14}$H$_{15}$N$_3$O$_2$ (257.29).

Benzyl 3-trityl-3,4,6,7-tetrahydro-5*H*-imidazo[4,5-c]pyridine-5-carboxylate (3.67)[25]. 3.66 (1.3 g, 5.1 mmol) and TEA (1.4 mL, 10 mmol) were dissolved in MeCN (150 mL). Trityl chloride (1.4 g, 5.1 mmol) was added slowly and the reaction was stirred at rt overnight. After removing the solvent under reduced pressure the product was purified by automated flash chromatography [gradient 0 – 25 min: DCM/MeOH (*v/v*) 100/0 – 95/5, SF 15-20 g] to give the titled compound as yellow foam-like solid (2.0 g, 78.4%), mp 84 – 86 °C. R$_f$ = 0.2 (DCM/MeOH 95/5). ^{1}H-NMR (400 MHz, CDCl$_3$): δ (ppm) 7.41 – 7.27 (m, 14H), 7.11 (m, 7H), 5.13 (br, 2H), 4.58 (br, 2H), 3.46 (m, 2H), 1.65 (br, 2H).^{13}C-NMR (101 MHz, CDCl$_3$, HSQC, HMBC): δ (ppm) 155.25 (quat., 1C), 141.63 (quat., 3C), 141.22 (quat., 1C), 138.19, 136.68 (quat., 1C), 135.02 (quat., 1C), 130.03 (6C), 128.57 (2C), 128.32 (2C), 128.22(6C), 128.18 (3C), 127.91, 74.95 (quat., 1C), 67.28, 43.73, 41.35, 24.36. HRMS (ESI): m/z [M+H]$^+$ calcd for [C$_{33}$H$_{30}$N$_3$O$_2$]$^+$ 500.2333, found 500.2337. C$_{33}$H$_{29}$N$_3$O$_2$ (499.61).

3-Trityl-4,5,6,7-tetrahydro-3*H*-imidazo[4,5-c]pyridine (3.15)[25]. 3.67 (2.0 g, 4.0 mmol) was dissolved in MeOH (80 mL), 10% Pd/C (w/w) (200 mg, 1.88 mmol) was added and a stream of hydrogen was delivered by a glass tube directly in the stirred solution. After 4 h the TLC indicated complete conversion. The reaction was filtered through Cellite® pad and the solvent was removed under reduced pressure to give **3.15** as yellow sticky foam (1.3 g, 89.0%). R$_f$ = 0.1

(DCM/MeOH 90/10). ^{1}H-NMR (400 MHz, CDCl$_3$): δ (ppm) 7.31 – 7.28 (m, 10H), 7.11 (m, 6H), 3.90 (s, 2H), 2.76 (t, J = 5.6 Hz, 2H), 2.32 (br, 1H), 1.55 (t, J = 5.5 Hz, 2H).^{13}C-NMR (101 MHz, CDCl$_3$, HSQC, HMBC): δ (ppm) 141.83 (quat., 3C), 137.33, 130.14 (6C), 128.10 (6C), 128.00 (3C), 127.38 (quat., 1C), 126.71 (quat., 1C), 74.75 (quat., 1C), 44.93, 43.61, 25.93. HRMS (ESI): m/z [M+H]$^+$ calcd for [C$_{25}$H$_{24}$N$_3$]$^+$ 366.1965, found 366.1968. C$_{25}$H$_{23}$N$_3$ (365.48).

3.5.2 Synthesis of the 4-amino-2-chloro pyrimidines (3.20 – 3.31)

<u>General procedure</u>

2,4-Dichloropyrimidine (**3.19**, 1 equiv) and DIPEA (1.5 – 3.0 equiv) were dissolved in *i*-PrOH. The respective amine **3.07 – 3.18** (1.0 – 1.2 equiv) was added and stirred in the microwave reactor at 120 °C for 1 h or in a round bottomed flask at 55 – 85 °C for 4 – 20 h. After removing the solvent under reduced pressure the product was purified by chromatography or automated flash-chromatography.

***tert*-Butyl (*R*)-[1-(2-chloropyrimidin-4-yl)pyrrolidin-3-yl]carbamate (3.20)[28].** According to the general procedure the title compound was prepared in the microwave reactor (2 bar) from **3.19** (2.0 g, 13 mmol), DIPEA (3.4 mL, 20 mmol) and **3.16** (2.8 g, 15 mmol) in *i*-PrOH (14 mL). The crude product was purified by chromatography [PE/EtOAc (*v/v*) 100/0 – 50/50, SiO$_2$ 180 g] to give **3.20** as pale yellow powder (2.9 g, 72.5%), mp 111.0 – 113.8 °C. R$_f$ = 0.3 (PE/EtOAc 50/50). ^{1}H-NMR (400 MHz, CDCl$_3$): δ (ppm) 7.97 (d, J = 6.0 Hz, 1H), 6.17 (d, J = 5.8 Hz, 1H), 4.88 (br, 1H), 4.31 (br, 1H), 3.88 – 3.23 (m, 4H), 2.01 (m, 2H), 1.42 (s, 9H). ^{13}C-NMR (101 MHz, CDCl$_3$, HSQC, HMBC): δ (ppm) 161.14 (quat., 1C), 160.38 (quat., 1C), 156.16, 155.40 (quat., 1C), 102.17, 80.13 (quat., 1C), 52.71, 50.0, 44.90, 31.31, 28.44 (3C). HRMS (ESI): *m/z* [*M*+H]$^+$ calcd for [C$_{13}$H$_{20}$ClN$_4$O$_2$]$^+$ 299.1269, found 299.1273. C$_{13}$H$_{19}$ClN$_4$O$_2$ (298.77).

***tert*-Butyl 4-(2-chloropyrimidin-4-yl)piperazine-1-carboxylate (3.21)[28,83].** According to the general procedure the title compound was prepared from **3.19** (470 mg, 3.15 mmol), DIPEA (816 μL, 4.80 mmol) and **3.07** (600 mg, 3.22 mmol) in *i*-PrOH (12 mL) at 55 °C for 16 h. The crude product was purified by chromatography [DCM/MeOH (*v/v*) 100/0 – 97.5/2.5, SiO$_2$ 90 g] to give **3.21** as colorless powder (860 mg, 91.3%), mp 169.5 – 171.6 °C. R$_f$ = 0.3

(DCM/MeOH 97.5/2.5). ^{1}H-NMR (400 MHz, CDCl$_3$): δ (ppm) 8.05 (d, J = 6.2 Hz, 1H), 6.40 (d, J = 6.2 Hz, 1H), 3.72 – 3.49 (m, 8H), 1.47 (s, 9H). ^{13}C-NMR (101 MHz, CDCl$_3$, HSQC, HMBC): δ (ppm) 162.69 (quat., 1C), 160.49 (quat., 1C), 157.10, 154.63 (quat., 1C), 101.38, 80.62 (quat., 1C), 43.90 (2C), 42.95 (2C), 28.47 (3C). HRMS (ESI): m/z [M+H]$^+$ calcd for [C$_{13}$H$_{20}$ClN$_4$O$_2$]$^+$ 299.1269, found 299.1274. C$_{13}$H$_{19}$ClN$_4$O$_2$ (298.77).

tert-Butyl 4-(2-chloropyrimidin-4-yl)-1,4-diazepane-1-carboxylate (3.22) (CAS: 1696857-87-0). According to the general procedure the title compound was prepared from **3.19** (800 mg, 5.37 mmol), DIPEA (1.4 mL, 8.2 mmol) and **3.08** (1.1 g, 5.5 mmol) in i-PrOH (20 mL) at 55 °C for 5 h. The crude product was purified by chromatography [PE/EtOAc (v/v) 75/25 – 50/50, SiO$_2$ 80 g] to give **3.22** as colorless powder (1.3 g, 77.4%), mp 100.1 – 104.0 °C. R$_f$ = 0.3 (PE/EtOAc 50/50). ^{1}H-NMR (400 MHz, CDCl$_3$): δ (ppm) 8.00 (d, J = 6.1 Hz, 1H), 6.33 (d, J = 5.9 Hz, 1H), 4.04 – 3.20 (m, 8H), 1.91 (m, 2H), 1.38 (s, 9H). ^{13}C-NMR (101 MHz, CDCl$_3$, HSQC, HMBC): δ (ppm) 162.23 (quat., 1C), 160.57 (quat., 1C), 156.88, 155.18 (quat., 1C), 101.14, 80.10 (quat., 1C), 48.70, 47.71, 46.82, 45.91, 28.39 (3C), 25.02. HRMS (ESI): m/z [M+H]$^+$ calcd for [C$_{14}$H$_{22}$ClN$_4$O$_2$]$^+$ 313.1426, found 313.1430. C$_{14}$H$_{21}$ClN$_4$O$_2$ (312.80).

tert-Butyl {2-[4-(2-chloropyrimidin-4-yl)piperazin-1-yl]ethyl}carbamate (3.23). According to the general procedure the title compound was prepared from **3.19** (100 mg, 0.671 mmol), DIPEA (228 µL, 1.34 mmol) and **3.13** (170 mg, 0.741 mmol) in i-PrOH (10 mL) at 85 °C for 5 h. The crude product was purified by automated flash-chromatography [gradient 0 – 20 min: DCM/MeOH (v/v) 100/0 – 93/7, SF 10-4 g] to give **3.23** as colorless powder (150 mg, 65.5%), mp 89.1 – 92.0 °C. R$_f$ = 0.45 (DCM/MeOH 90/10). ^{1}H-NMR (400 MHz, CDCl$_3$): δ (ppm) 8.02 (d, J = 6.2 Hz, 1H), 6.36 (d, J = 6.2 Hz, 1H), 4.96 (br, 1H), 3.65 (m, 4H), 3.25 (m, 2H), 2.51 (m, 6H), 1.44 (s, 9H). ^{13}C-NMR (101 MHz, CDCl$_3$, HSQC, HMBC): δ (ppm) 162.66 (quat., 1C), 160.91 (quat., 1C), 157.45, 156.03 (quat., 1C), 101.30, 79.47 (quat, 1C), 57.33, 52.46 (2C), 44.01 (2C), 37.18, 28.54 (3C). HRMS (ESI): m/z [M+H]$^+$ calcd for [C$_{15}$H$_{25}$ClN$_5$O$_2$]$^+$ 342.1691, found 342.1695. C$_{15}$H$_{24}$ClN$_5$O$_2$ (341.84).

tert-Butyl {2-[(2-chloropyrimidin-4-yl)amino]ethyl}carbamate (3.24)[84]. According to the general procedure the title compound was prepared **3.19** (100 mg, 0.671 mmol), DIPEA (172 µL, 1.01 mmol) and **3.09** (120 mg, 0.749 mmol) in i-PrOH (10 mL) at 85 °C for 16 h. The

crude product was purified by automated flash-chromatography [gradient 0 – 20 min: PE/EtOAc (*v/v*) 100/0 – 50/50, SF 10-4 g] to give **3.24** as colorless powder (130 mg, 71.2%), mp 128.8 – 130.7 °C. R_f = 0.25 (PE/EtOAc 50/50). ^{1}H-NMR (400 MHz, CDCl$_3$): δ (ppm) 7.95 (m, 1H), 6.26 (m, 2H), 5.08 (m, 1H), 3.65 – 3.25 (m, 4H), 1.41 (s, 9H). ^{13}C-NMR (101 MHz, CDCl$_3$, HSQC, HMBC): δ (ppm) 163.95 (quat., 1C), 160.80 (quat., 1C), 157.28, 157.01 (quat., 1C), 104.66, 80.08 (quat., 1C), 42.51, 40.01, 28.44 (3C). HRMS (ESI): *m/z* [*M*+H]$^+$ calcd for [C$_{11}$H$_{18}$ClN$_4$O$_2$]$^+$ 273.1113, found 273.1117. C$_{11}$H$_{17}$ClN$_4$O$_2$ (272.73).

tert-Butyl {3-[(2-chloropyrimidin-4-yl)amino]propyl}carbamate (3.25)[85]. According to the general procedure the title compound was prepared from **3.19** (200 mg, 1.34 mmol), DIPEA (343 µL, 2.02 mmol) and **3.10** (281 mg, 1.61 mmol) in *i*-PrOH (5 mL) at 55 °C for 4 h. The crude product was purified by chromatography [DCM/MeOH (*v/v*) 100/0 – 97.5/2.5, SiO$_2$ 40 g, height 12 cm] to give **3.25** as pale yellow crystals (280 mg, 72.8%), mp 112.6 – 120.8 °C. R_f = 0.3 (DCM/MeOH 95/5). ^{1}H-NMR (400 MHz, CDCl$_3$): δ (ppm) 7.92 (m, 1H), 6.28 (m, 2H), 4.97 (br, 1H), 3.46 (m, 2H), 3.19 (m, 2H), 1.71 (m, 2H) 1.43 (s, 9H). ^{13}C-NMR (101 MHz, CDCl$_3$, HSQC, HMBC): δ (ppm) 163.73 (quat., 1C), 160.73 (quat., 1C), 156.98, 155.55 (quat., 1C), 104.93, 79.73 (quat., 1C), 37.08, 37.21, 29.84, 28.48 (3C). HRMS (ESI): *m/z* [*M*+H]$^+$ calcd for [C$_{12}$H$_{20}$ClN$_4$O$_2$]$^+$ 287.1269, found 287.1276. C$_{12}$H$_{19}$ClN$_4$O$_{22}$ (286.76).

tert-Butyl 3-[(2-chloropyrimidin-4-yl)amino]pyrrolidine-1-carboxylate (3.26) (CAS: 945895-38-5). According to the general procedure the title compound was prepared from **3.19** (200 mg, 1.34 mmol), DIPEA (343 µL, 2.02 mmol) and **3.12** (275 mg, 1.48 mmol) in *i*-PrOH (5 mL) at 55 °C for 5 h. The crude product was purified by chromatography [DCM/MeOH (*v/v*) 100/0 – 97.5/2.5, SiO$_2$ 45 g, height 13 cm] to give **3.26** as pale yellow crystals (380 mg, 94.9%), mp 126.1 – 130.1 °C. R_f = 0.35 (DCM/MeOH) 95/5). ^{1}H-NMR (400 MHz, CDCl$_3$): δ (ppm) 7.98 (m, 1H), 6.38 (m, 2H), 3.73 – 3.08 (m, 7H), 1.44 (s, 9H). ^{13}C-NMR (101 MHz, CDCl$_3$, HSQC, HMBC): δ (ppm) 163.14 (quat., 1C), 160.19 (quat., 1C), 155.52, 154.66 (quat., 1C), 104.15, 80.00 (quat., 1C), 51.71, 51.34, 51.09, 44.00, 28.59 (3C). HRMS (ESI): *m/z* [*M*+H]$^+$ calcd for [C$_{13}$H$_{20}$ClN$_4$O$_2$]$^+$ 299.1269, found 299.1275. C$_{13}$H$_{19}$ClN$_4$O$_2$ (298.77).

tert-Butyl 4-[(2-chloropyrimidin-4-yl)amino]piperidine-1-carboxylate (3.27)[86]. According to the general procedure the title compound was prepared from **3.19** (200 mg, 1.34 mmol),

DIPEA (343 µL, 2.02 mmol) and **3.11** (323 mg, 1.61 mmol) in *i*-PrOH (5 mL) at 55 °C for 5 h. The crude product was purified by chromatography [DCM/MeOH (*v/v*) 100/0 – 97.5/2.5, SiO$_2$ 40 g, height 12 cm] to give **3.27** as pale yellow sticky oil (273 mg, 65.1%). R$_f$ = 0.35 (DCM/MeOH 95/5). ^{1}H-NMR (400 MHz, CDCl$_3$): δ (ppm) 7.94 (m, 1H), 6.29 (d, *J* = 6.00 Hz, 1H), 5.74 (br, 1H), 4.31 – 3.58 (m, 3H), 3.10 – 2.73 (m, 2H), 2.15 – 1.88 (m, 2H), 1.43 (m, 11H). ^{13}C-NMR (101 MHz, CDCl$_3$, HSQC, HMBC): δ (ppm) 162.74 (quat., 1C), 160.39 (quat., 1C), 155.61, 154.68 (quat., 1C), 103.78, 79.91 (quat., 1C), 48.28, 42.38 (2C), 31.67 (2C), 28.43 (3C). HRMS (ESI): *m/z* [*M*+H]$^+$ calcd for [C$_{14}$H$_{22}$ClN$_4$O$_2$]$^+$ 313.1426, found 313.1430. C$_{14}$H$_{21}$ClN$_4$O$_2$ (312.80).

2-Chloro-*N*-[2-(1-trityl-1*H*-imidazol-4-yl)ethyl]pyrimidin-4-amine (3.28). According to the general procedure the title compound was prepared from **3.19** (200 mg, 1.34 mmol), DIPEA (350 µL, 2.06 mmol) and **3.14** (570 mg, 1.61 mmol) in *i*-PrOH (20 mL) at 85 °C for 17 h. The crude product was purified by automated flash-chromatography [gradient 0 – 30 min: DCM/MeOH (*v/v*) 100/0 – 95/5, SF 10-8 g] to give **3.28** as pale yellow foam-like solid (400 mg, 64.0%), mp 67.7 – 73.8 °C. R$_f$ = 0.2 (DCM/MeOH 95/5). ^{1}H-NMR (400 MHz, CDCl$_3$): δ (ppm) 7.91 (m, 1H), 7.37 (d, *J* = 1.3 Hz, 1H), 7.35 – 7.27 (m, 9H), 7.16 – 7.04 (m, 6H), 6.61 (s, 1H), 6.21 (d, *J* = 5.8 Hz; 1H), 5.99 (br, 0.5H), 3.64 (m, 2H), 2.79 (t, *J* = 6.2 Hz, 2H). ^{13}C-NMR (101 MHz, CDCl$_3$, HSQC, HMBC): δ (ppm) 163.68 (quat., 1C); 160.80 (quat., 1C), 159.13, 142.41 (quat., 3C), 138.84, 129.80 (6C), 128.19 (9C), 118.98, 104.90, 75.39 (quat., 1C), 53.54 (quat., 1C), 41.29, 27.15. HRMS (ESI): *m/z* [*M*+H]$^+$ calcd for [C$_{28}$H$_{25}$ClN$_5$]$^+$ 466.1793, found 466.1800. C$_{28}$H$_{24}$ClN$_5$ (465.99).

2-Chloro-*N*-[3-(1-trityl-1*H*-imidazol-4-yl)propyl]pyrimidin-4-amine (3.29). According to the general procedure the title compound was prepared from **3.19** (100 mg, 0.671 mmol), DIPEA (340 µL, 2.00 mmol) and **3.17**[34] (296 mg, 0.81 mmol) in *i*-PrOH (10 mL) at 85 °C for 20 h. The crude product was purified by automated flash-chromatography [gradient 0 – 20 min: DCM/MeOH (*v/v*) 100/0 – 93/7, SF 10-4 g] to give **3.29** as colorless powder (287 mg, 89.1%), mp 136.7 – 138 °C. R$_f$ = 0.3 (DCM/MeOH 90/10). ^{1}H-NMR (400 MHz, CDCl$_3$): δ (ppm) 7.89 (m, 1H), 7.45 (m, 1H), 7.38 – 7.30 (m, 9H), 7.17 – 7.07 (m, 6H), 6.58 (m, 1H), 6.20 (d, *J* = 5.6 Hz, 1H), 5.87 (br, 0.5 H), 3.43 (m, 2H), 2.66 (m, 2H), 1.95 (m, 2H). ^{13}C-NMR (101 MHz, CDCl$_3$, HSQC,

HMBC): δ (ppm) 163.78 (quat., 1C), 160.93 (quat., 1C), 159.15, 142.37 (quat., 3C), 139.98, 129.81 (9C), 128.26 (6C), 118.55, 104.90, 75.75 (quat., 1C), 53.55 (quat., 1C), 41.27, 28.31, 25.41. HRMS (ESI): *m/z* [*M*+H]$^+$ calcd for [C$_{29}$H$_{27}$ClN$_5$]$^+$ 480.1950, found 480.1954. C$_{29}$H$_{26}$ClN$_5$ (480.01).

5-(2-Chloropyrimidin-4-yl)-1-trityl-4,5,6,7-tetrahydro-1*H*-imidazo[4,5-c]pyridine **(3.30).**

According to the general procedure the title compound was prepared from **3.19** (250 mg, 1.68 mmol), DIPEA (571 µL, 3.36 mmol) and **3.15** (700 mg, 1.92 mmol) in *i*-PrOH (10 mL) at 85 °C for 4 h. The crude product was purified by chromatography [DCM/MeOH (*v/v*) 100/0 – 97.5/2.5, SiO$_2$ 80 g] to give **3.30** as yellow foam-like solid (610 mg, 76.0%), mp 115.2 – 120.3 °C. R$_f$ = 0.3 (DCM/MeOH) 97.5/2.5). ^{1}H-NMR (400 MHz, CDCl$_3$): δ (ppm) 8.03 (d, *J* = 6.1 Hz, 1H), 7.42 (m, 1H), 7.36 – 7.30 (m, 9H), 7.14 – 7.09 (m, 6H), 6.37 (d, *J* = 6.2 Hz, 1H), 4.52 (s, 2H), 3.78 (m, 2H), 1.72 (m, 2H). ^{13}C-NMR (101 MHz, CDCl$_3$, HSQC, HMBC): δ (ppm) 163.05 (quat., 1C), 157.50, 157.38 (quat., 1C), 141.47 (quat., 3C), 138.42, 134.13 (quat., 1C), 129.96 (6C), 128.30 (9C), 126.95 (quat., 1C), 101.82, 75.14 (quat., 1C), 44.69, 41.11, 24.04. HRMS (ESI): *m/z* [*M*+H]$^+$ calcd for [C$_{29}$H$_{25}$ClN$_5$]$^+$ 478.1793, found 478.1791. C$_{29}$H$_{24}$ClN$_5$ (478.00).

2-Chloro-*N*-(2-{[(5-methyl-1*H*-imidazol-4-yl)methyl]thio}ethyl)pyrimidin-4-amine **(3.31).**

According to the general procedure the title compound was prepared from **3.19** (100 mg, 0.671 mmol), DIPEA (342 µL, 2.01 mmol) and **3.18** (197 mg, 0.807 mmol) in *i*-PrOH (5 mL) at 55 °C for 5 h. The crude product was purified by chromatography [DCM/1.75 M NH$_3$ in MeOH (*v/v*) 97.5/2.5 – 90/10, SiO$_2$ 20 g] to give **3.31** as clear sticky oil (160 mg, 84.0%). R$_f$ = 0.2 (DCM/1.75 M NH$_3$ in MeOH 95/5). ^{1}H-NMR (400 MHz, MeOH-*d$_4$*): δ (ppm) 7.82 (m, 1H), 7.48 (m, 1H), 6.40 (d, *J* = 6.1 Hz, 1H), 3.73 (s, 2H), 3.51 (m, 2H), 2.64 (t, *J* = 6.9 Hz, 2H), 2.20 (s, 3H). ^{13}C-NMR (101 MHz, MeOH-*d$_4$*, HSQC, HMBC): δ (ppm) 165.20 (quat., 1C), 161.52 (quat., 1C), 155.71, 134.66, 130.16 (quat., 1C), 128.02 (quat., 1C), 105.94, 40.99, 31.32, 27.22, 10.21. HRMS (ESI): *m/z* [*M*+H]$^+$ calcd for [C$_{11}$H$_{15}$ClN$_5$S]$^+$ 284.0731, found 284.0735. C$_{11}$H$_{14}$ClN$_5$S (283.78).

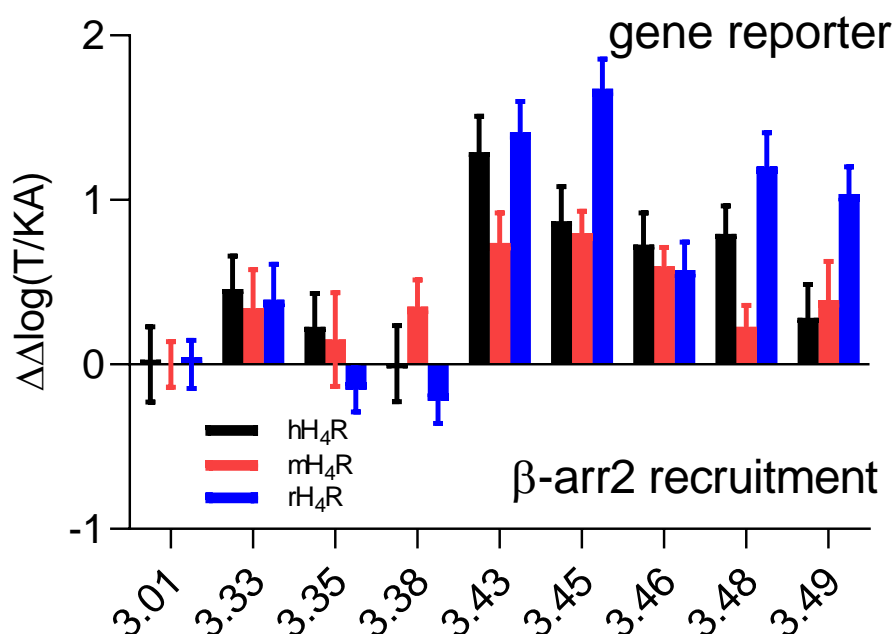### 3.5.3 Bias analysis for selected target compounds

Figure A 3.2. Bias analysis for compounds 3.33, 3.35, 3.38, 3.43, 3.45, 3.46, 3.48 and 3.49 performed on the basis of the pEC$_{50}$ and α values obtained from luciferase reporter gene- and β-arrestin2 recruitment assays at the h/m/rH₄Rs, as described by van der Westhuizen et. al.[37], using histamine (3.01) as reference agonist. A ΔΔlog (τ/K_A) ratio = 0 indicate an equal activation of the G-protein- and β-arrestin2 pathways, while a ΔΔlog (τ/K_A) ratio ≠ 0 indicates a preference for one signal pathway over the other. Error bars represent the propagated error.

3.5.4 Screening of selected target compounds for activity at the m/rH₄Rs

Three distinct concentrations (c_{final} = 100 nM, 1 μM, 10 μM) for each ligand with pK_i values < 7.00 at the hH₄R (**3.34**, **3.36**, **3.37**, **3.39 – 3.42**, **3.44**, **3.47** and **3.50 – 3.52**) were screened for activity at the m/rH₄Rs in luciferase reporter gene- and β-arrestin2 recruitment assays (see sections 3.4.8 and 3.4.9) in agonist and/or antagonist mode (performed if α < 0.1). Data were processed and normalized as described above for the respective functional assay and were plotted as bar graphs (GraphPad Prism Software 7.1). The pEC$_{50}$/pIC$_{50}$ values and the efficacies (α) were estimated (Table A 3.1).

Table A 3.1. Screening of compounds with pK_i values < 7.00 at the hH_4R for activity at the mH_4R and rH_4R in luciferase reporter gene- and β-arrestin2 recruitment assays.

No.	pEC_{50} or pIC_{50} / (α)			
	mH_4R		**rH_4R**	
	reporter gene	β-arr2	reporter gene	β-arr2
3.34	≤ 7.0 (1.06 ± 0.01)	≤ 6.0 (≥ 0.1)	≤ 7.0 (1.01 ± 0.01)	≤ 6.0 (≥ 0.3)
3.36	n.d. -	< 5.0 (< 0.1)	n.a (≤ 0.2)	< 5.0 (< 0.1)
3.37	< 7.0 (≥ 0.4)	< 5.0 (≤ 0.2)	n.a (≤ 0.2)	< 5.0 (< 0.1)
3.39	≤ 7.0 (≥ 0.8)	≤ 6.0 (≥ 0.3)	≤ 7.0 (0.93 ± 0.04)	≤ 6.0 (≤ 0.2)
3.40	≤ 6.0 (≥ 0.4)	< 5.0 (< 0.1)	≤ 6.0 (≥ 0.6)	< 5.0 (< 0.1)
3.41	≤ 8.0 (1.05 ± 0.04)	≤ 6.0 (≥ 0.1)	≤ 8.0 (1.04 ± 0.05)	≤ 7.0 (≤ 0.2)
3.42	≤ 8.0 (0.49 ± 0.01)	≤ 6.0 (0.002 ± 0.001)	≤ 7.0 (0.48 ± 0.01)	n.d. (0.021 ± 0.001)
3.44	≤ 7.0 (≥ 0.4)	< 5.0 (< 0.1)	n.a. (≤ 0.2)	< 5.0 (< 0.1)
3.47	≤ 8.0 (0.96 ± 0.03)	≤ 6.0 (≥ 0.4)	n.d. n.d.	≤ 6.0 (≥ 0.5)
3.50	≤ 7.0 (1.01 ± 0.05)	≤ 6.0 (≥ 0.3)	≤ 7.0 (1.00 ± 0.02)	≤ 6.0 (≥ 0.5)
3.51	≤ 6.0 (≥ 0.4)	< 5.0 (< 0.1)	≤ 6.0 (≥ 0.6)	< 5.0 (< 0.1)
3.52	≤ 7.0 (1.02 ± 0.01)	< 5.0 (< 0.1)	≤ 6.0 (> 0.8)	≤ 6.0 (≤ 0.2)

Data of luciferase reporter gene assay, using HEK293T-SF-mH_4R-His6-CRE-Luc or HEK293T-SF-rH_4R-His6-CRE-Luc cells and β-arrestin2 recruitment assay, using HEK293T-β-arr2-xH_4R cells (x = m, r) and applying three distinct concentrations (c_{final} = 100 nM, 1 μM, 10 μM) of the respective compound in agonist mode or antagonist mode (α < 0.1). In antagonist mode, solutions containing the antagonist were pre-incubated for 15 min before histamine **3.01** (c_{final} = 10 μM) was added. Data represent estimated values (some α values represent mean values ± SEM) of two independent experiments each performed in triplicate. The intrinsic activity (α) of histamine was set to 1.0 and α values of other compounds were referred to this value. n.d.: not determined. n.a.: not applicable.

3.5.5 ¹H-NMR, ¹³C-NMR spectra and RP-HPLC chromatograms

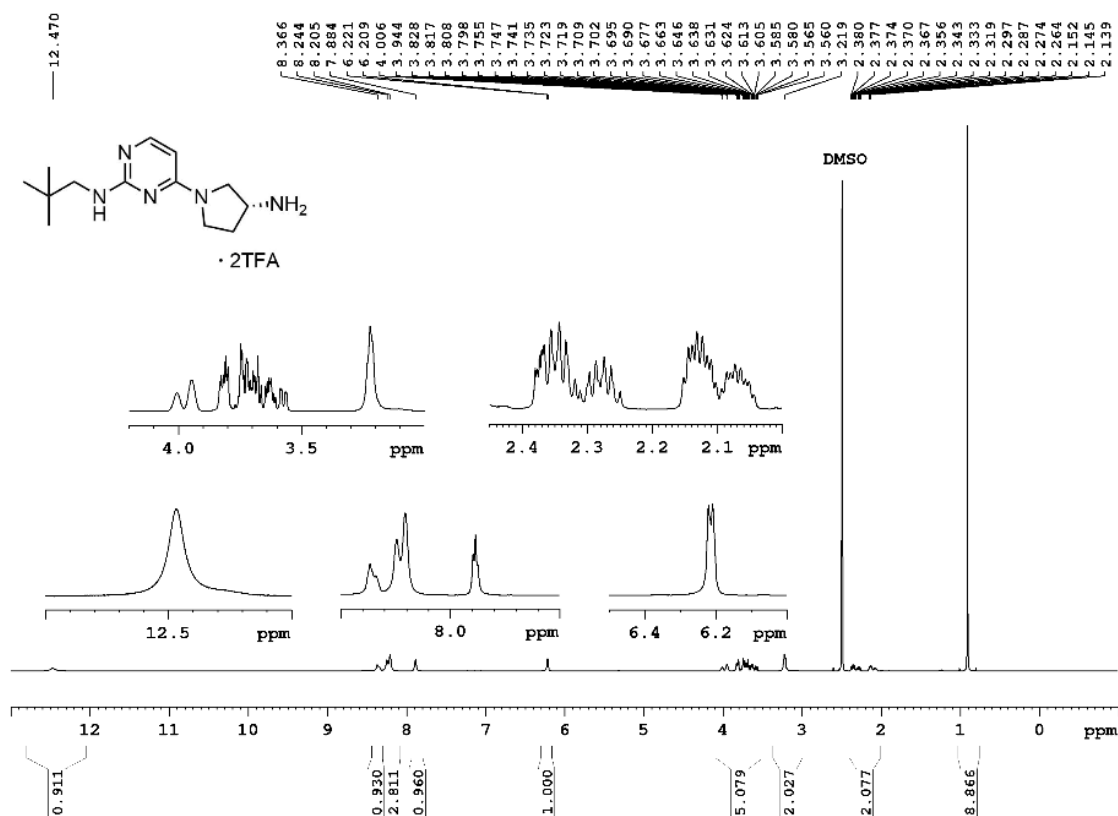### 3.5.5.1 ¹H-NMR and ¹³C-NMR spectra of selected target compounds

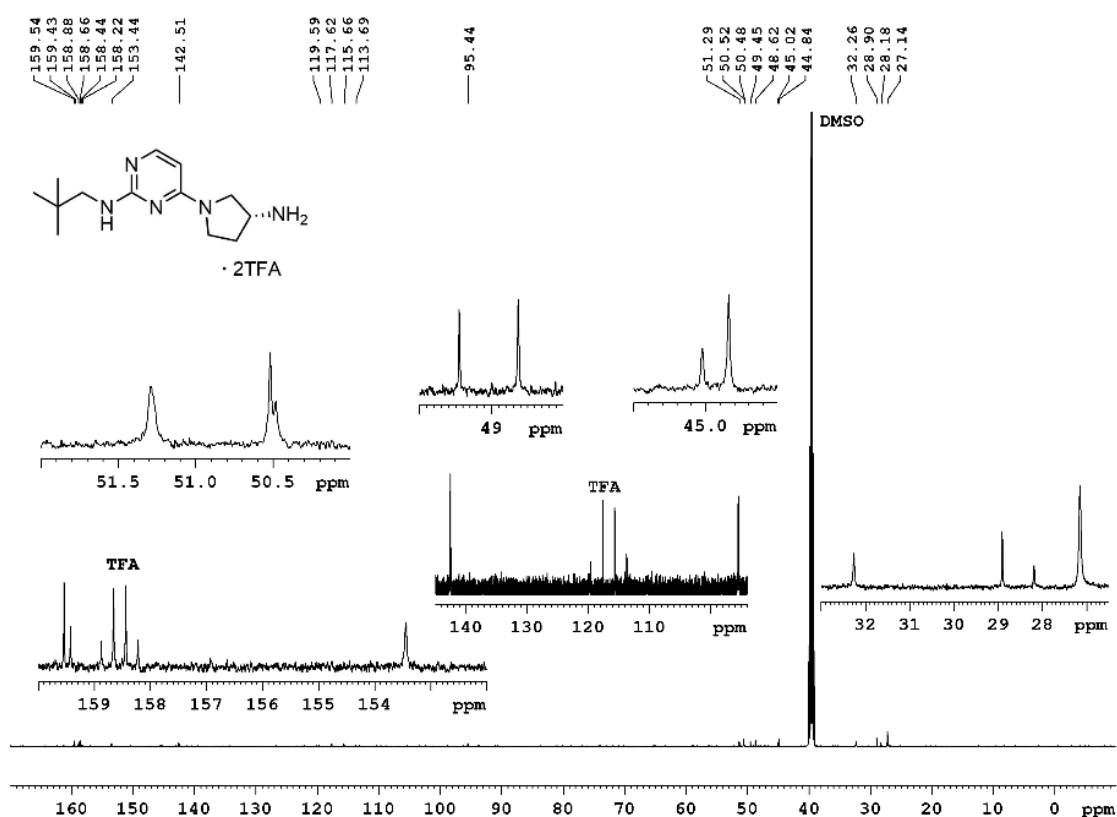**Figure A 3.3. ¹H-NMR spectrum (600 MHz, DMSO-*d₆*) of compound 3.33.**

Figure A 3.4. ^{13}C-NMR spectrum (151 MHz, DMSO-d_6) of compound 3.33.
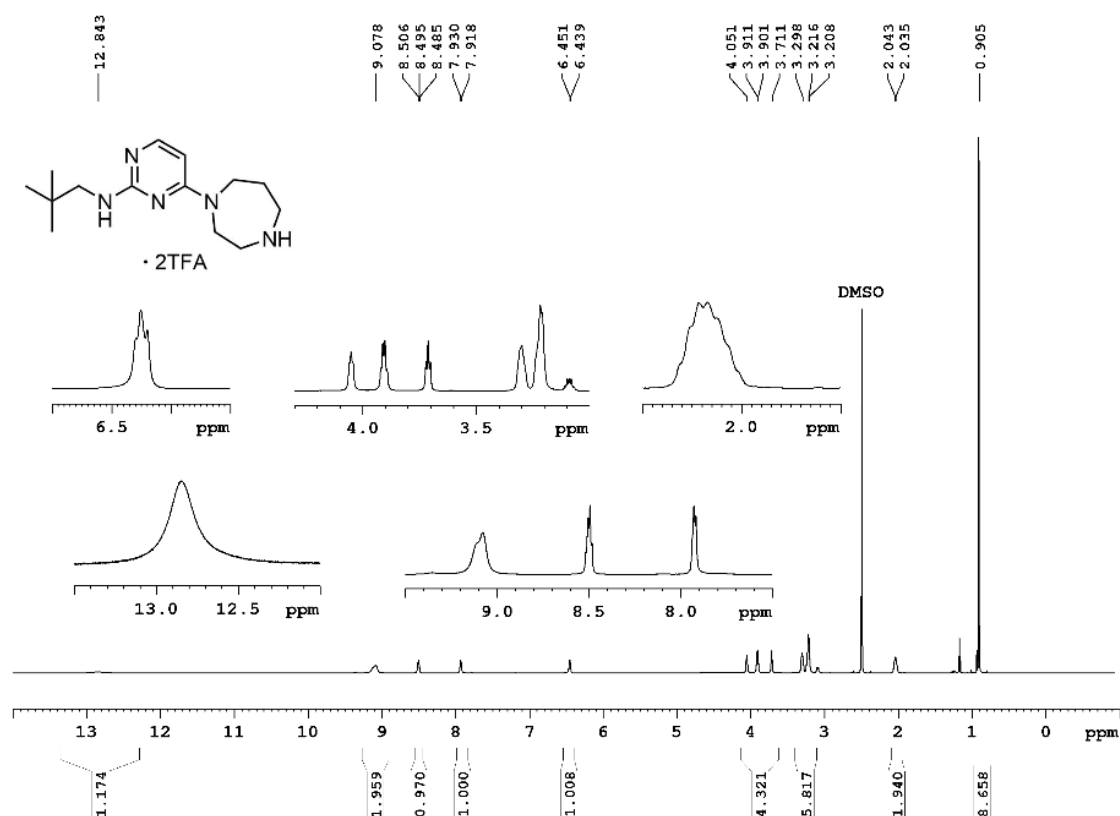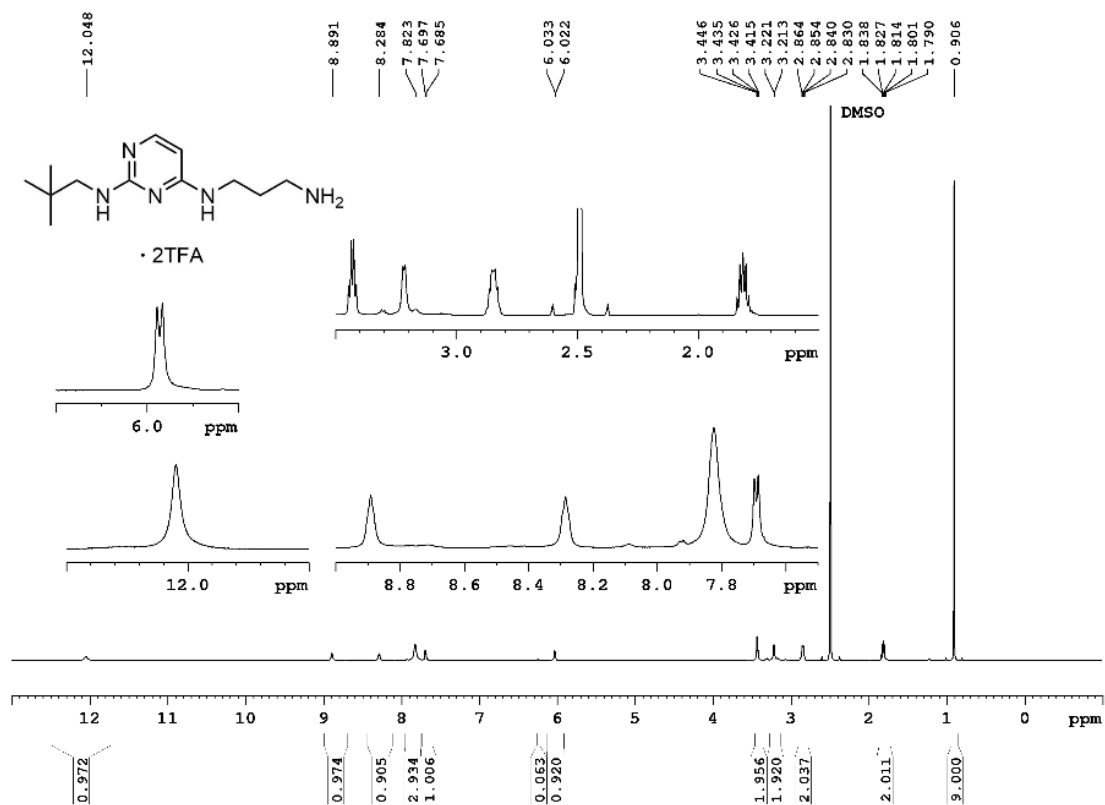
Figure A 3.5. ^{1}H-NMR spectrum (600 MHz, DMSO-d_6) of compound 3.35.
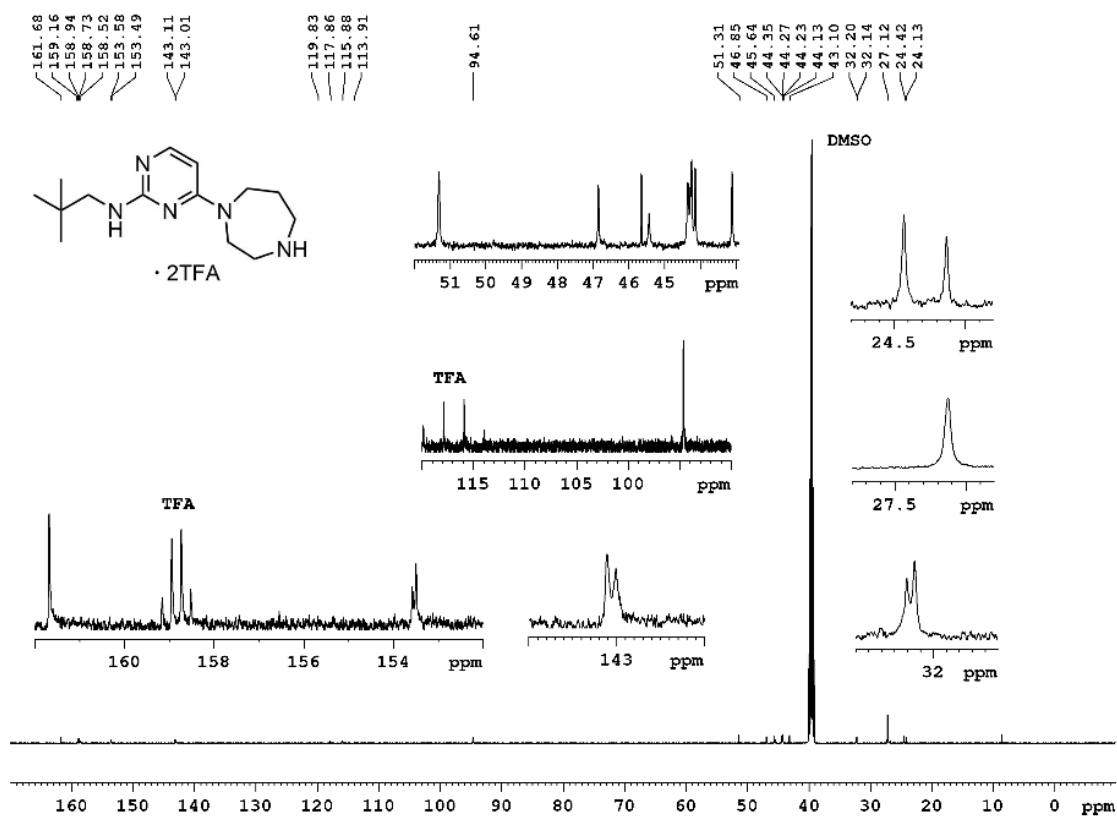
Figure A 3.6. ^{13}C-NMR spectrum (151 MHz, DMSO-d_6) of compound 3.35.

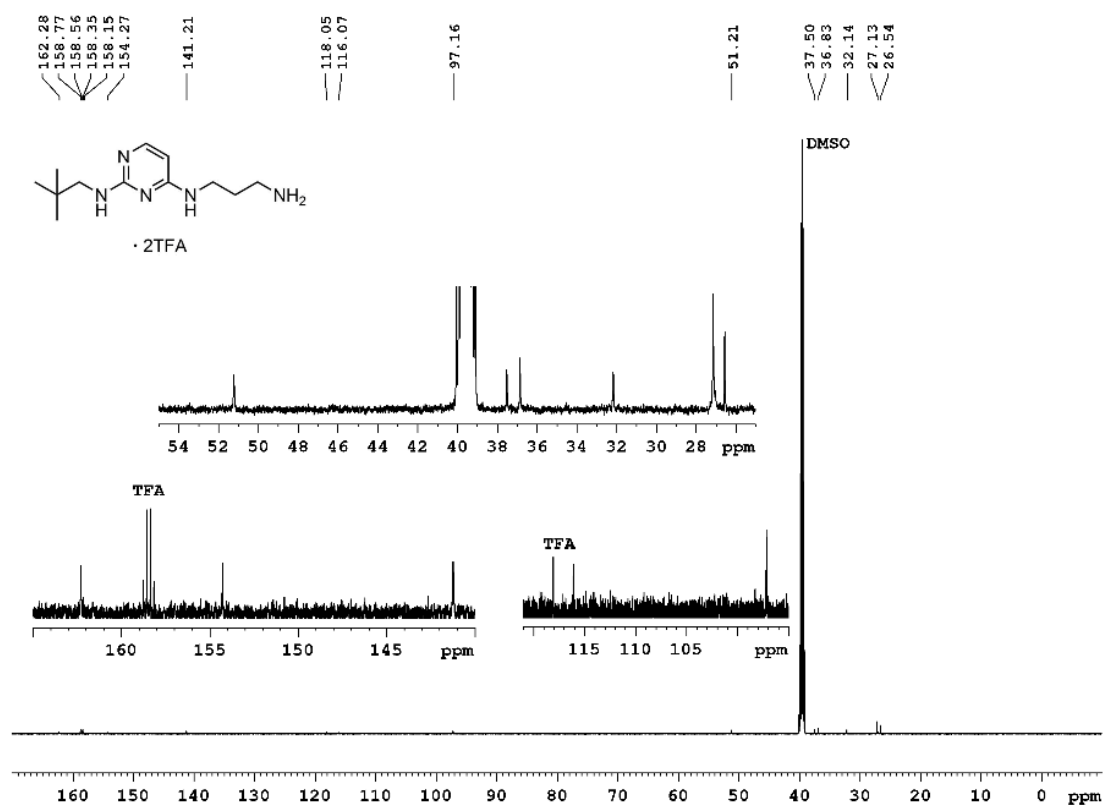**Figure A 3.7.** ^{1}H-NMR spectrum (600 MHz, DMSO-d_6) of compound 3.38.

Figure A 3.8. ^{13}C-NMR spectrum (151 MHz, DMSO-d_6) of compound 3.38.
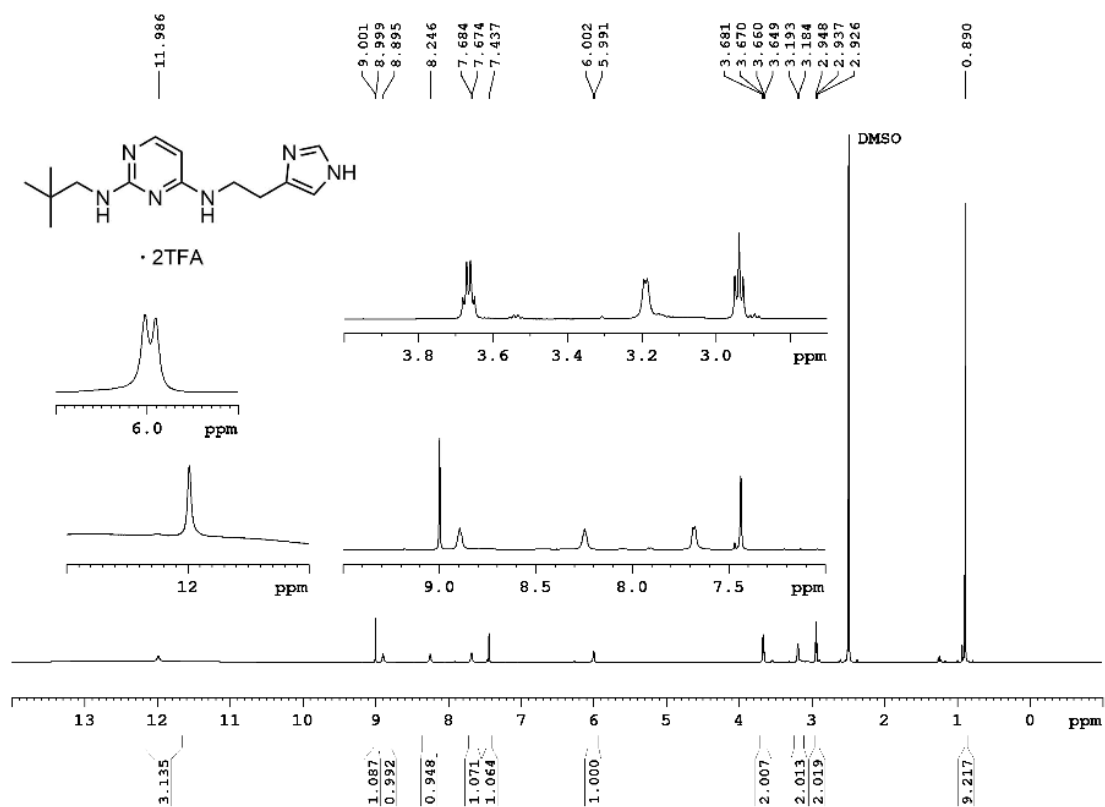
Figure A 3.9. ¹H-NMR spectrum (600 MHz, DMSO-d_6) of compound 3.41.

Figure A 3.10. ^{13}C-NMR spectrum (151 MHz, DMSO-d_6) of compound 3.41.

Figure A 3.11. ^{1}H-NMR spectrum (600 MHz, DMSO-d_6) of compound **3.43**.
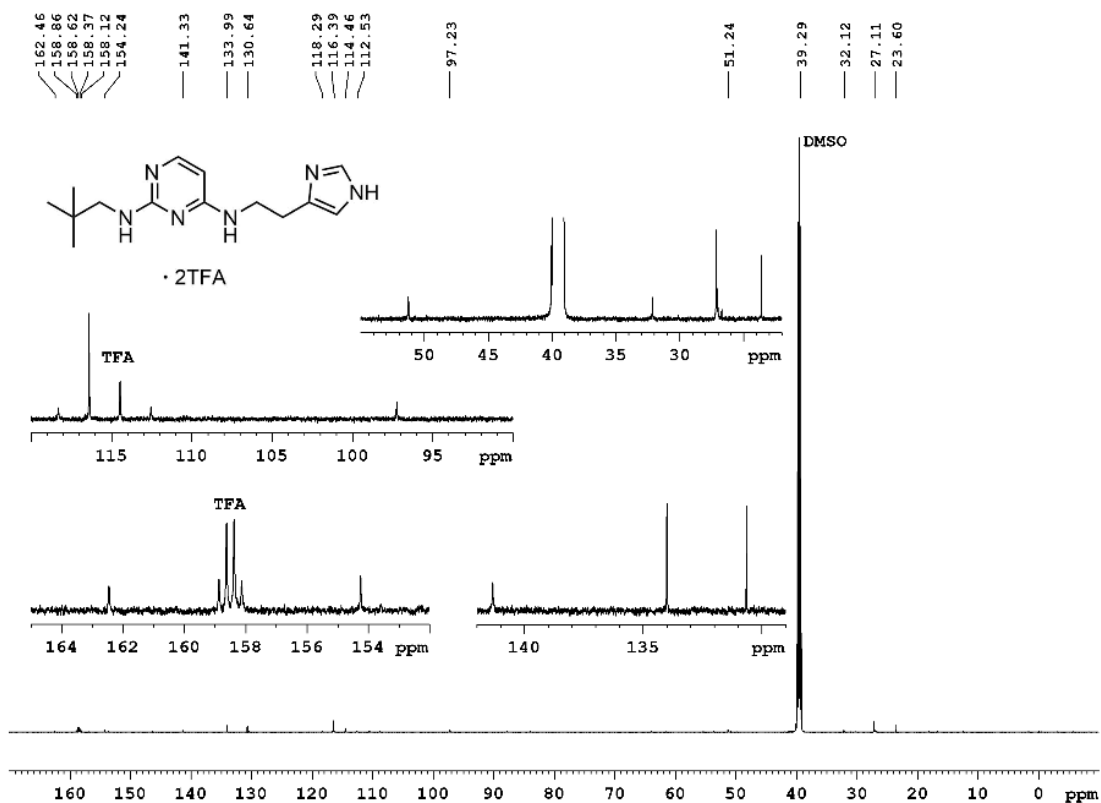
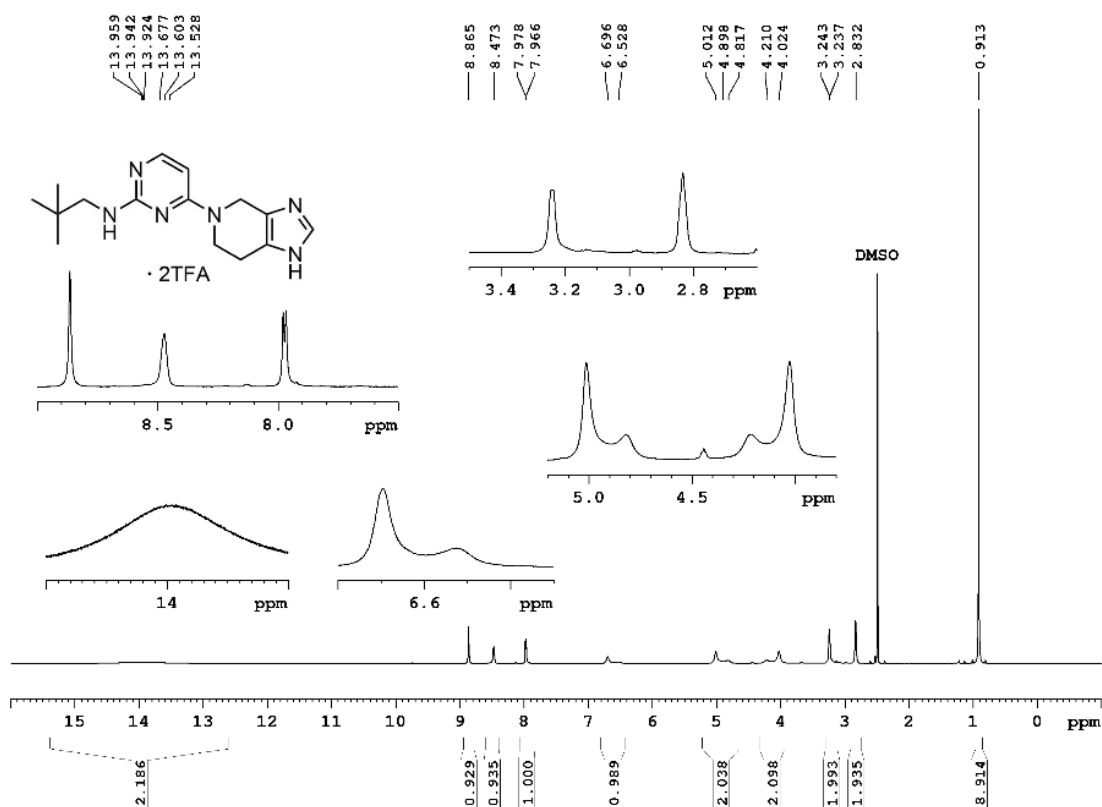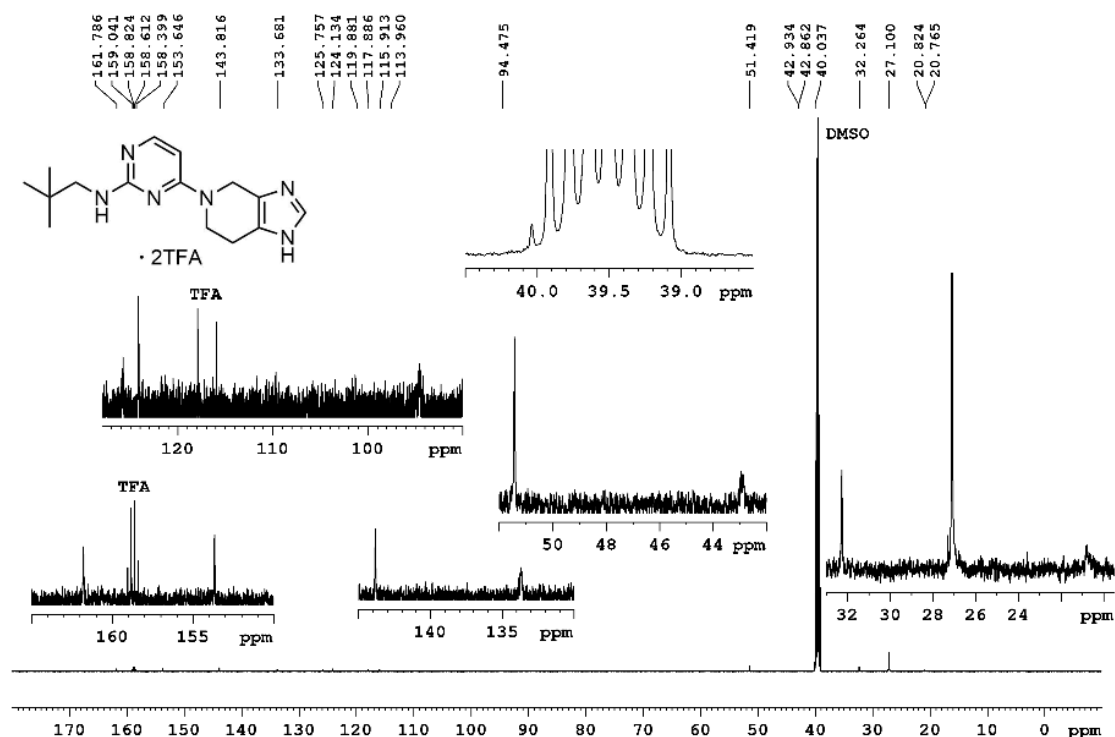**Figure A 3.12.** ^{13}C-NMR spectrum (151 MHz, DMSO-d_6) of compound 3.43.
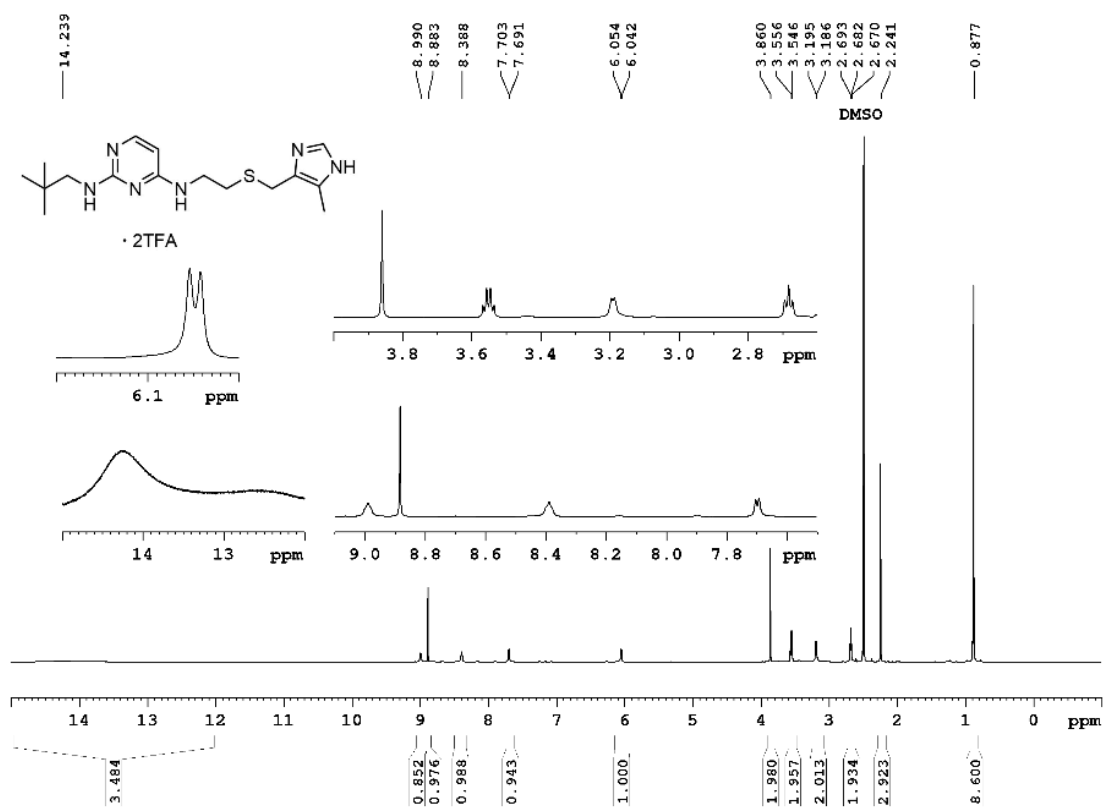
Figure A 3.13. ¹H-NMR spectrum (600 MHz, DMSO-d_6) of compound 3.44.
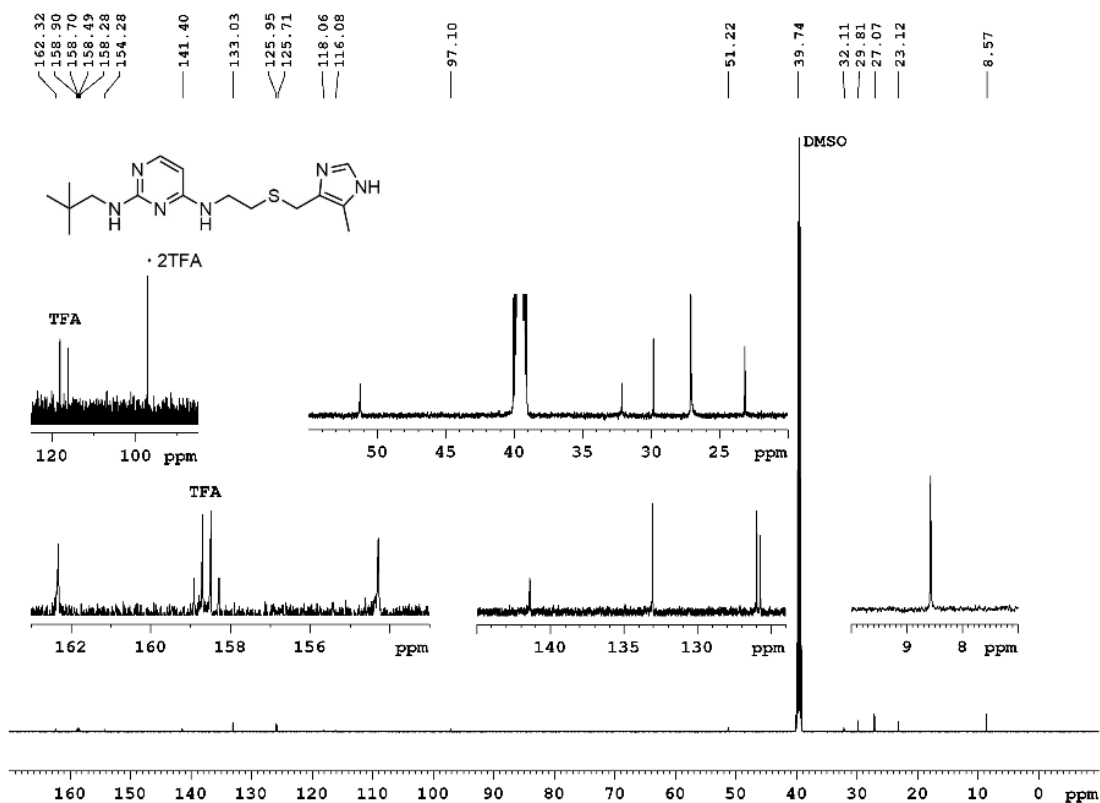
Figure A 3.14. ^{13}C-NMR spectrum (151 MHz, DMSO-d_6) of compound 3.44.
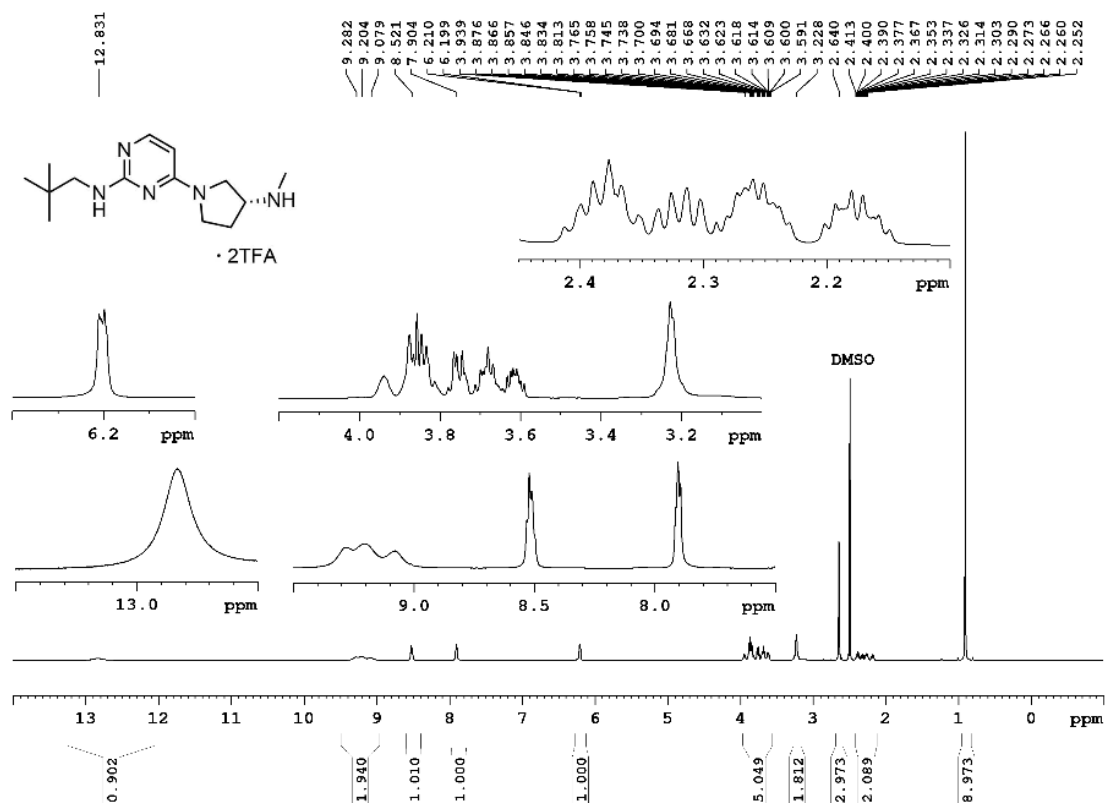
Figure A 3.15. ^{1}H-NMR spectrum (600 MHz, DMSO-d_6) of compound **3.45**.
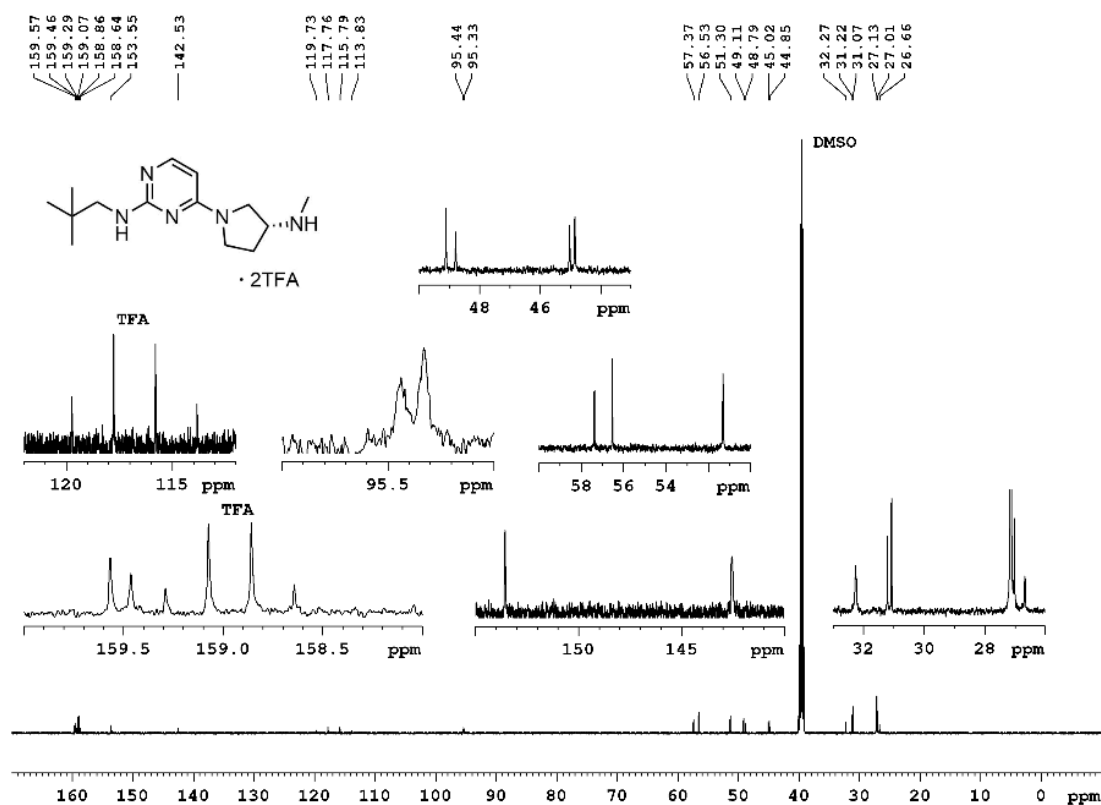
Figure A 3.16. ^{13}C-NMR spectrum (151 MHz, DMSO-d_6) of compound 3.45.
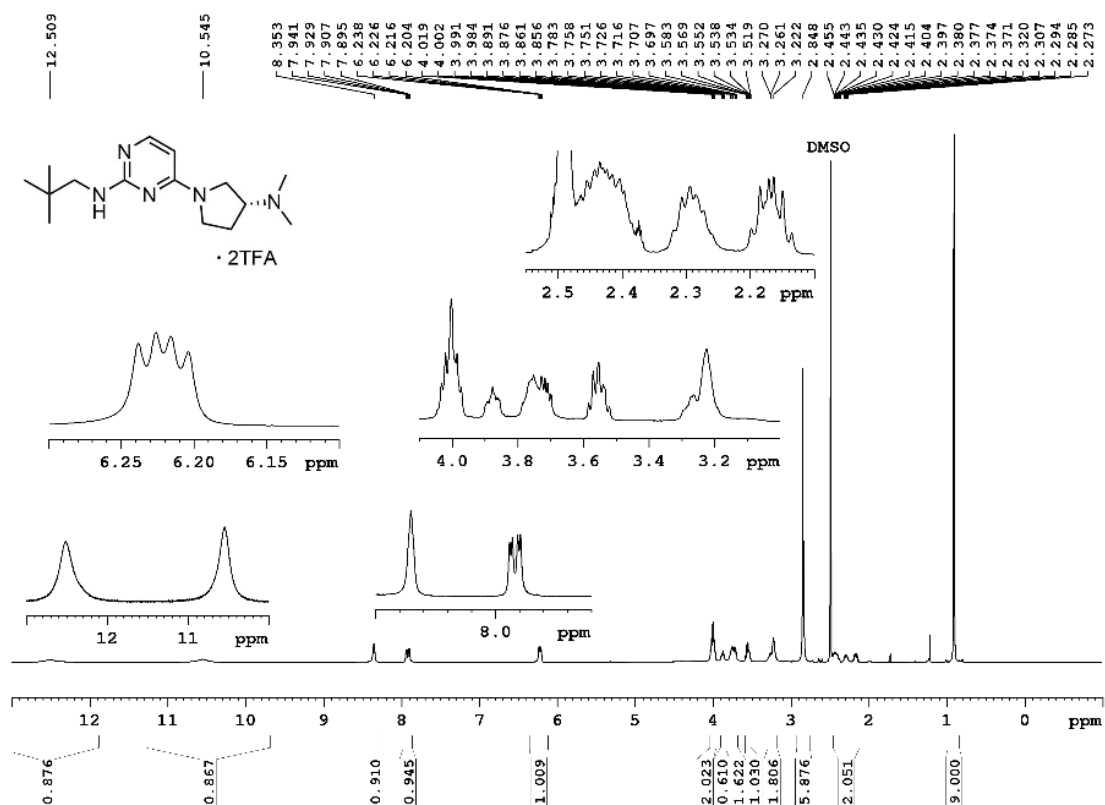
Figure A 3.17. ^{1}H-NMR spectrum (600 MHz, DMSO-d_6) of compound **3.46**.
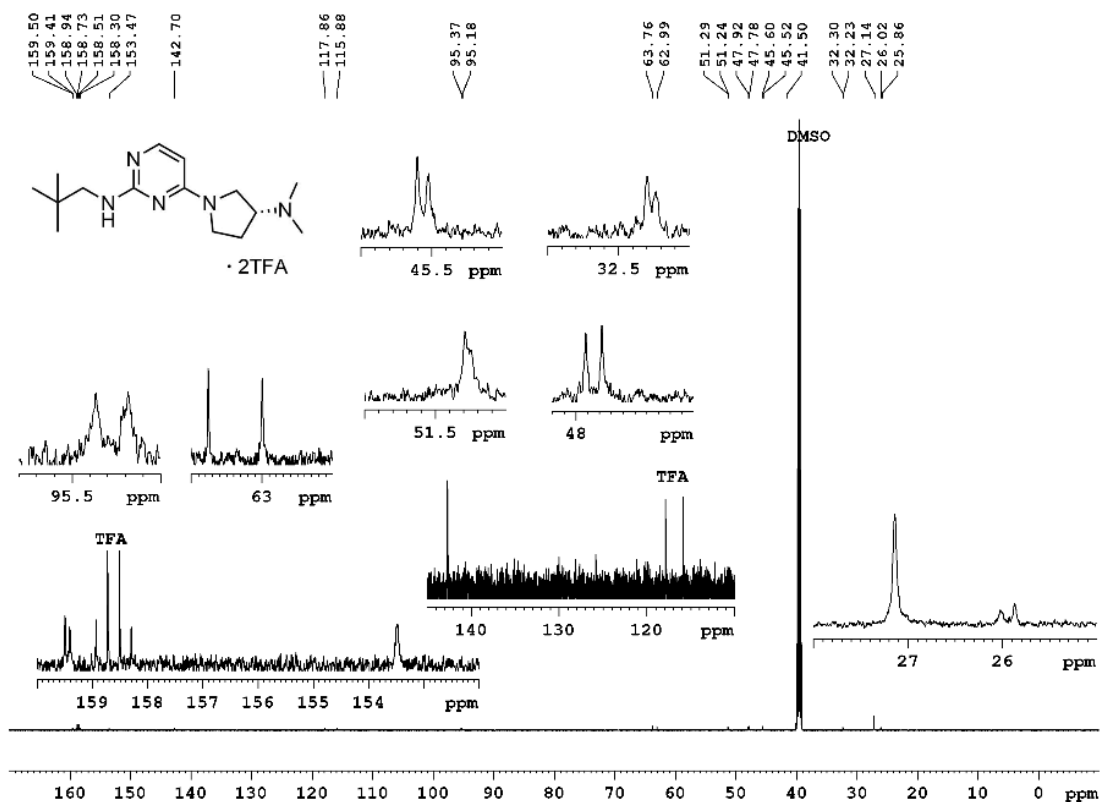
Figure A 3.18. ^{13}C-NMR spectrum (151 MHz, DMSO-d_6) of compound 3.46.
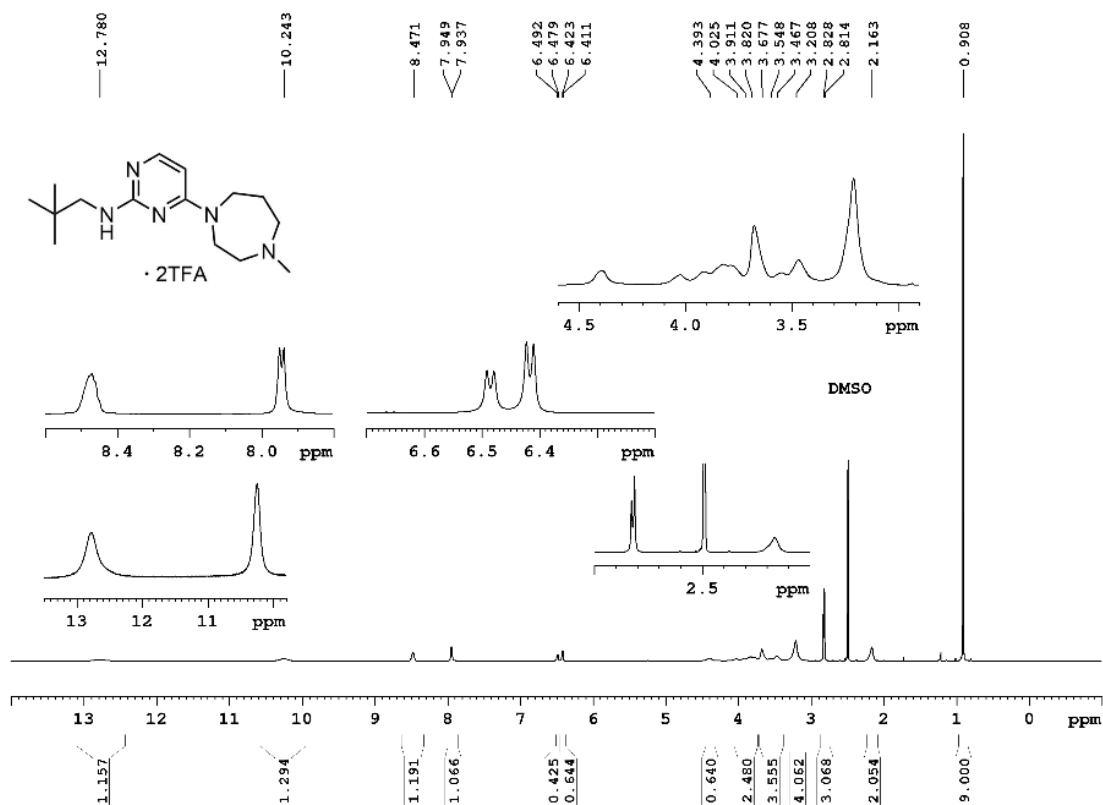
Figure A 3.19. ^{1}H-NMR spectrum (600 MHz, DMSO-d_6) of compound **3.48**.
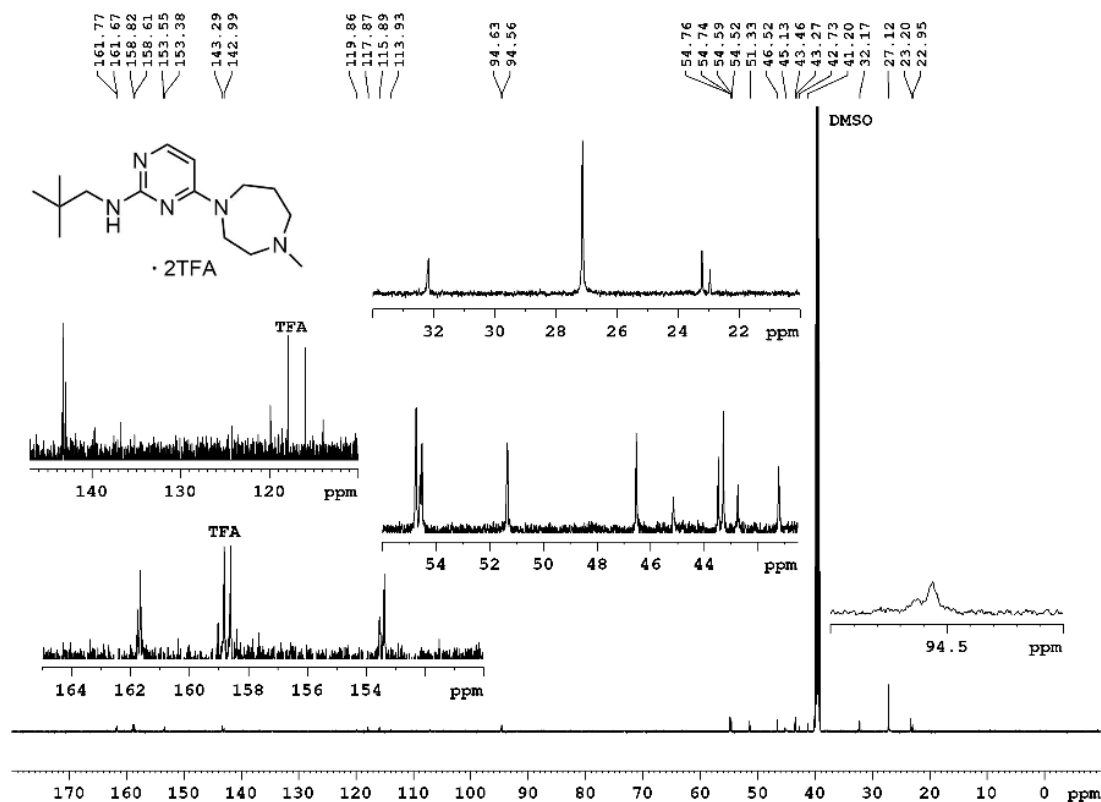
Figure A 3.20. ^{13}C-NMR spectrum (151 MHz, DMSO-d_6) of compound 3.48.
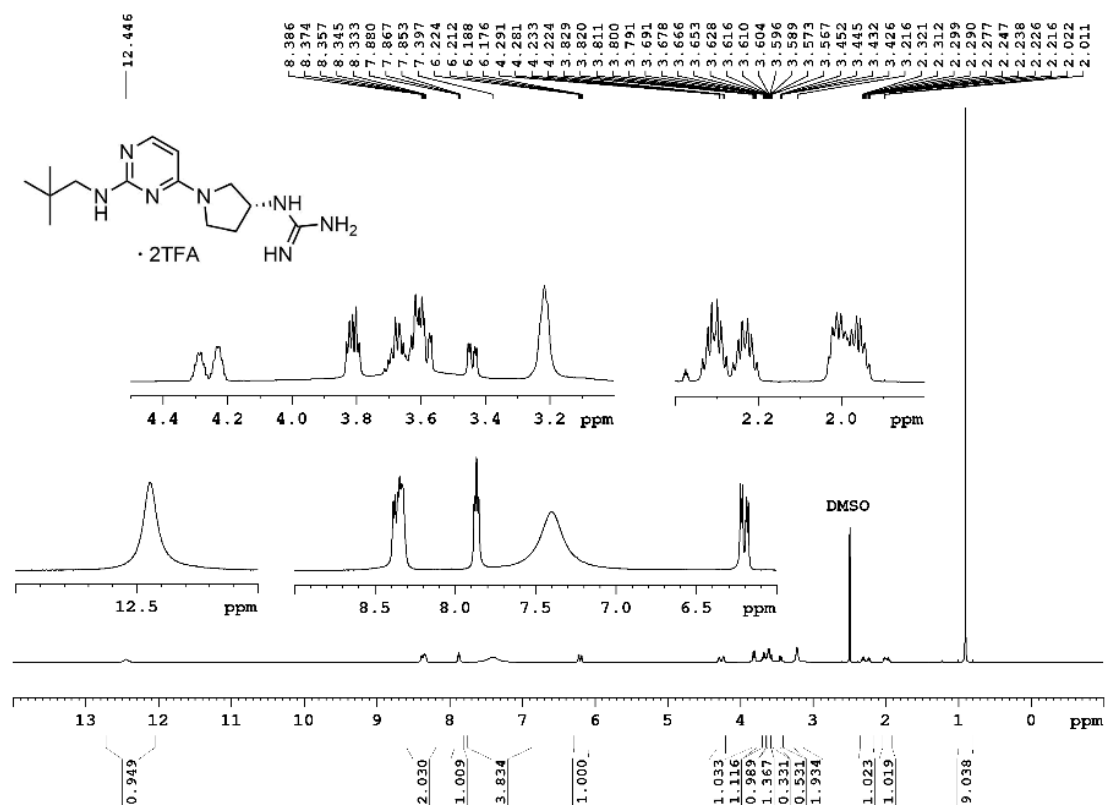
Figure A 3.21. ^{1}H-NMR spectrum (600 MHz, DMSO-d_6) of compound 3.49.
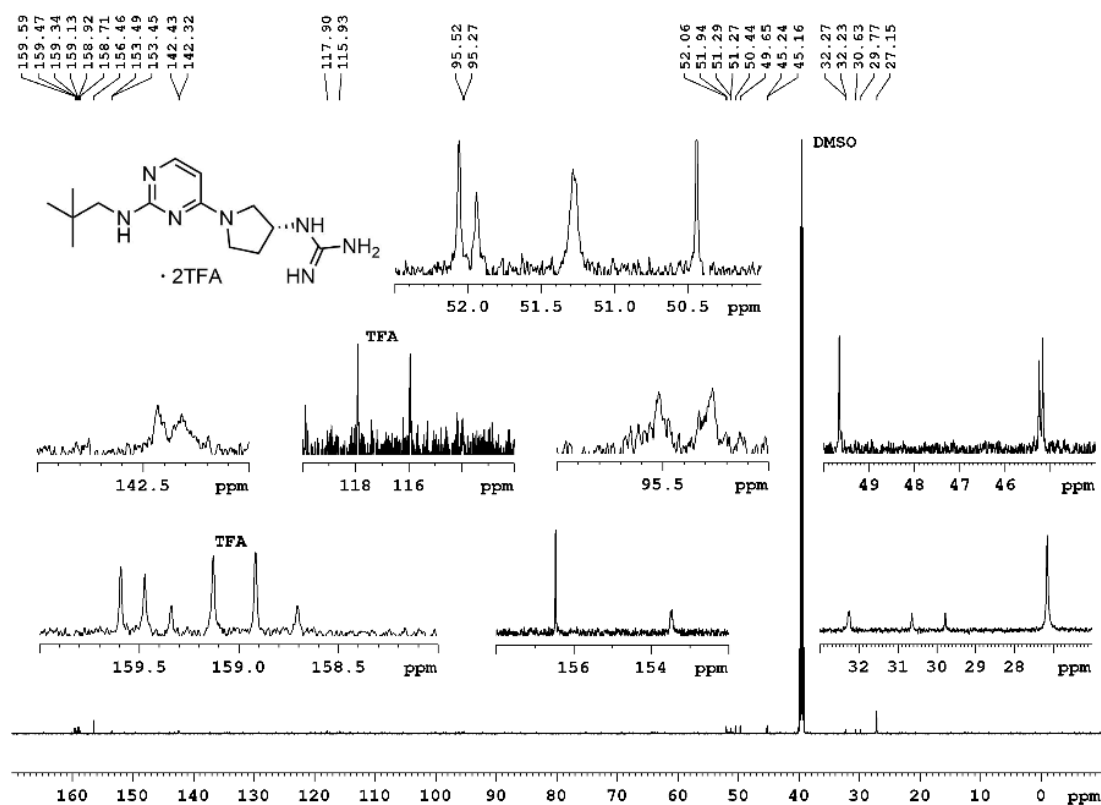
Figure A 3.22. ^{13}C-NMR spectrum (151 MHz, DMSO-d_6) of compound 3.49.

3.5.5.2 RP-HPLC chromatograms: purity control of the target compounds (3.33 – 3.52)
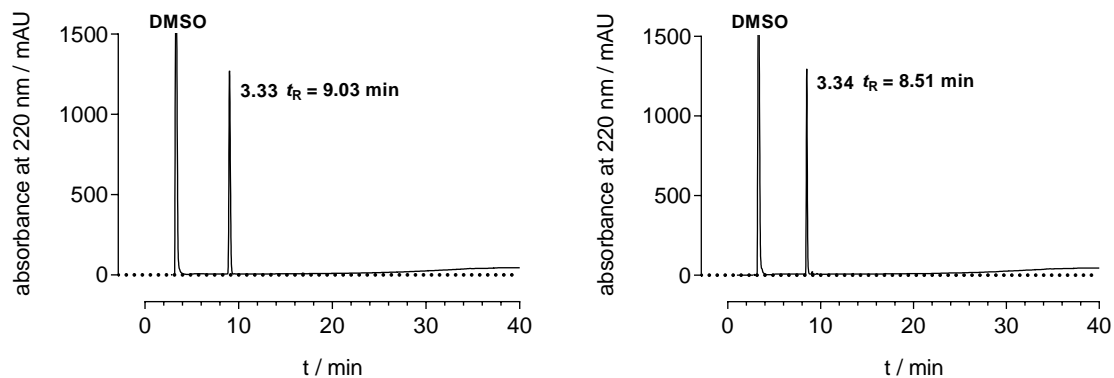
Figure A 3.23. RP-HPLC chromatograms (purity control, conditions see section 3.4.1) of 3.33 and 3.34 at 220 nm.
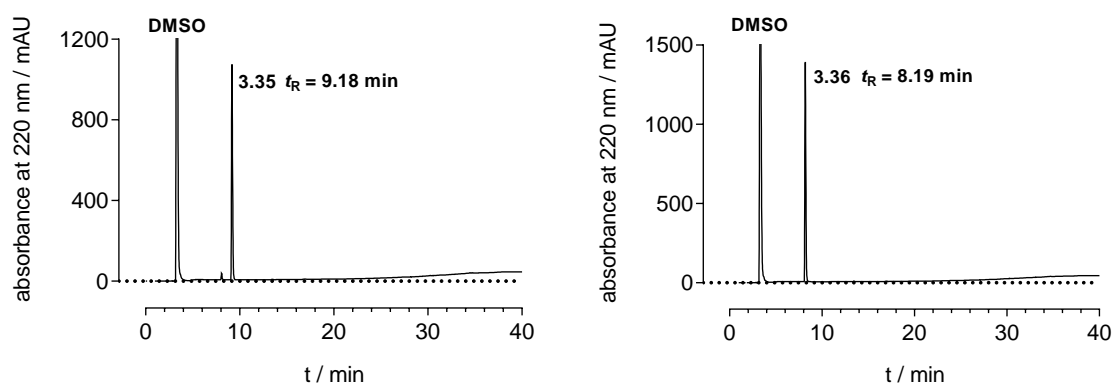
Figure A 3.24. RP-HPLC chromatograms (purity control, conditions see section 3.4.1) of 3.35 and 3.36 at 220 nm.
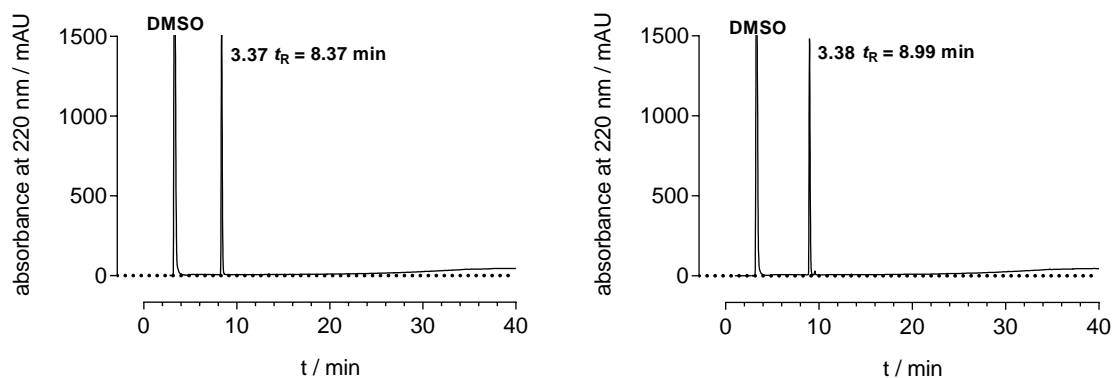
Figure A 3.25. RP-HPLC chromatograms (purity control, conditions see section 3.4.1) of 3.37 and 3.38 at 220 nm.
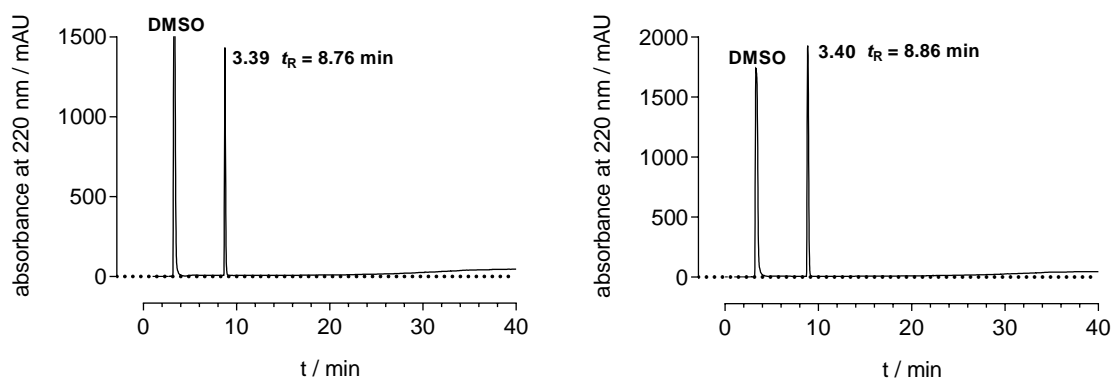
Figure A 3.26. RP-HPLC chromatograms (purity control, conditions see section 3.4.1) of 3.39 and 3.40 at 220 nm.
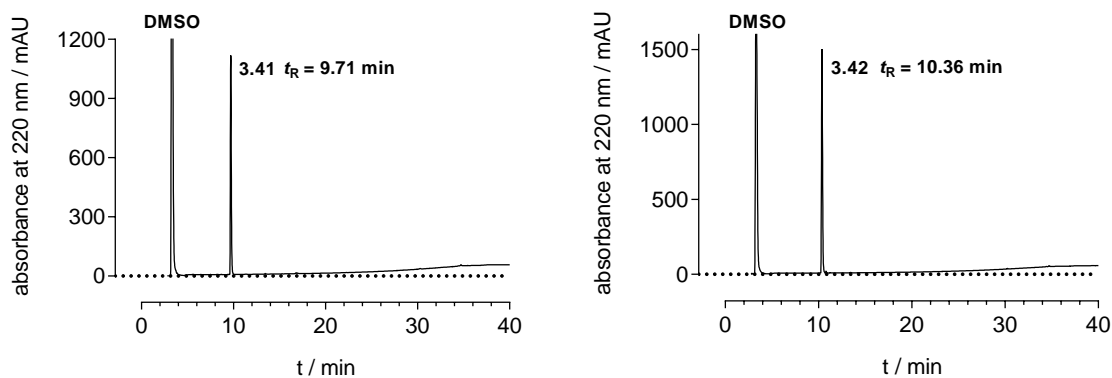
Figure A 3.27. RP-HPLC chromatograms (purity control, conditions see section 3.4.1) of 3.41 and 3.42 at 220 nm.
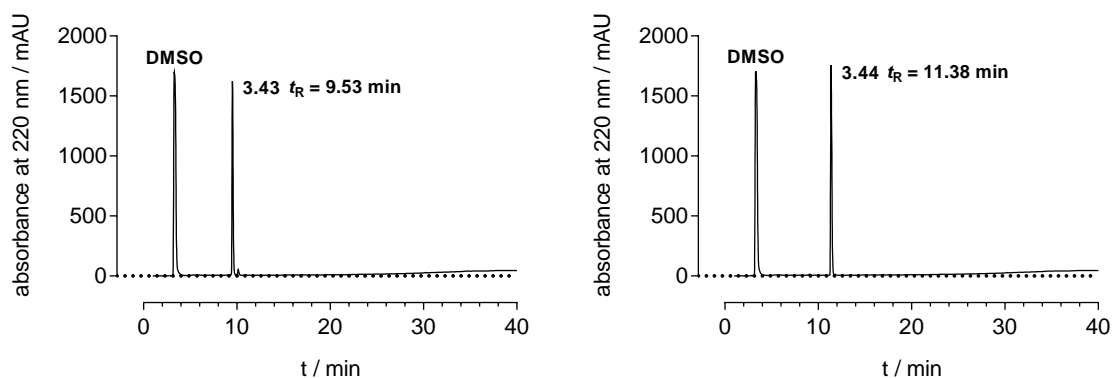
Figure A 3.28. RP-HPLC chromatograms (purity control, conditions see section 3.4.1) of 3.43 and 3.44 at 220 nm.
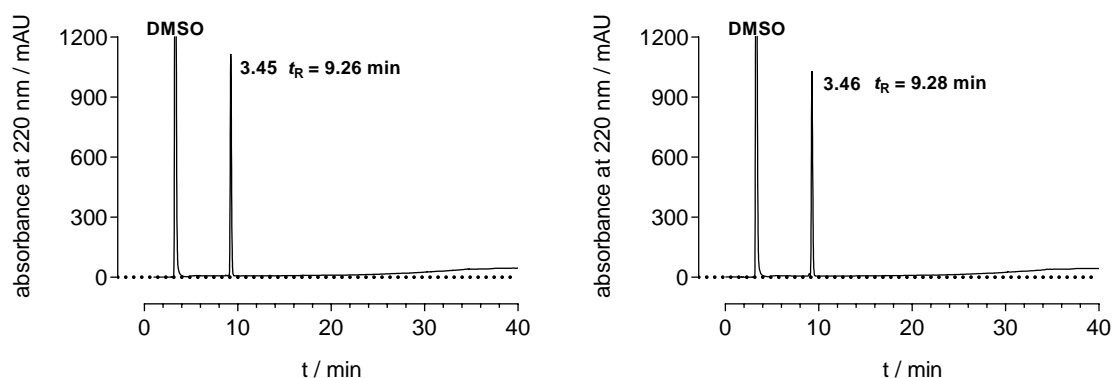
Figure A 3.29. RP-HPLC chromatograms (purity control, conditions see section 3.4.1) of 3.45 and 3.46 at 220 nm.
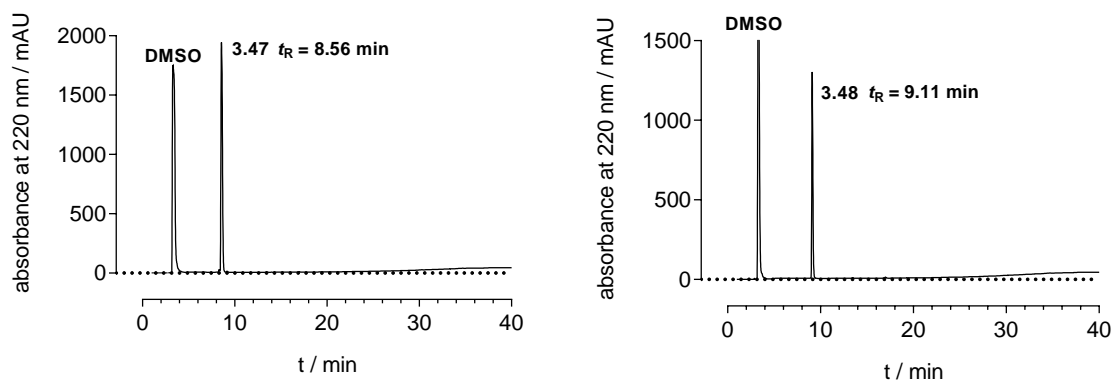
Figure A 3.30. RP-HPLC chromatograms (purity control, conditions see section 3.4.1) of 3.47 and 3.48 at 220 nm.
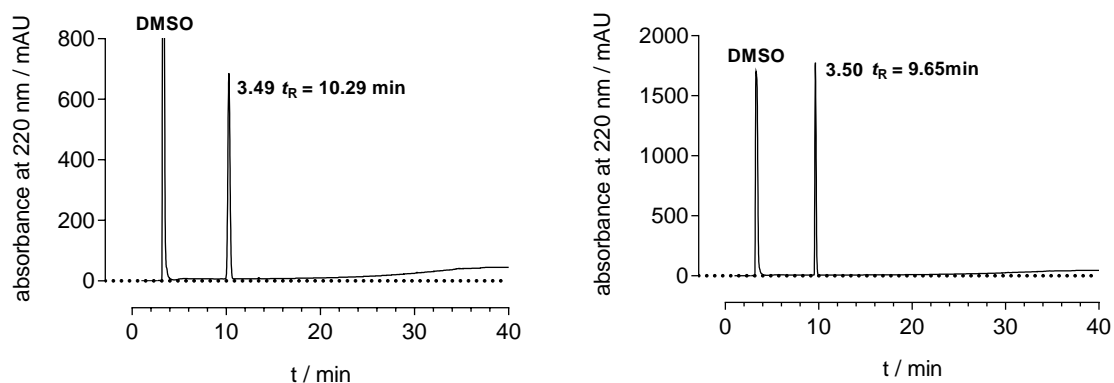
Figure A 3.31. RP-HPLC chromatograms (purity control, conditions see section 3.4.1) of 3.49 and 3.50 at 220 nm.
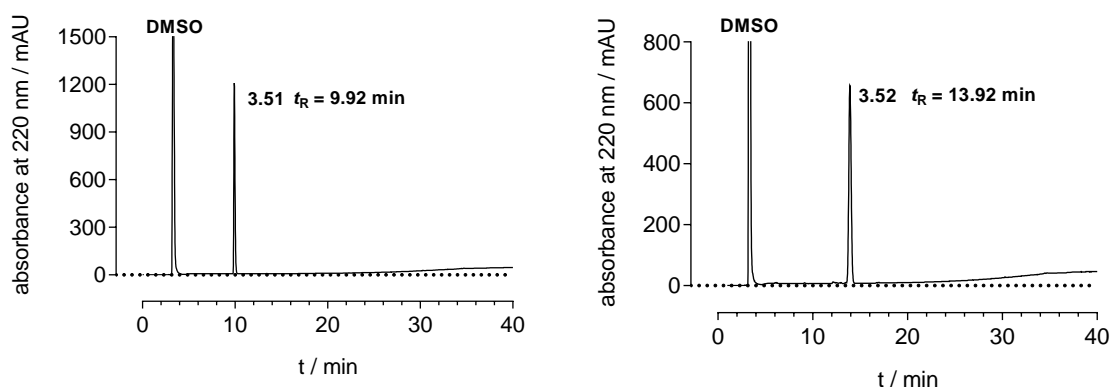
Figure A 3.32. RP-HPLC chromatograms (purity control, conditions see section 3.4.1) of 3.51 and 3.52 at 220 nm.

3.5.5.3 RP-HPLC chromatograms: chemical stability of **3.43**, **3.46**, **3.48** and **3.49**

Figure A 3.33. RP-HPLC chromatograms (chemical stability at 23° C in PBS, conditions see section 3.4.4) of 3.43 at 220 nm.

Figure A 3.34. RP-HPLC chromatograms (chemical stability at 23° C in PBS, conditions see section 3.4.4) of 3.46 at 220 nm.

Figure A 3.35. RP-HPLC chromatograms (chemical stability at 23° C in PBS, conditions see section 3.4.4) of 3.48 at 220 nm.

Figure A 3.36. RP-HPLC chromatograms (chemical stability at 23° C in PBS, conditions see section 3.4.4) of 3.49 at 220 nm.
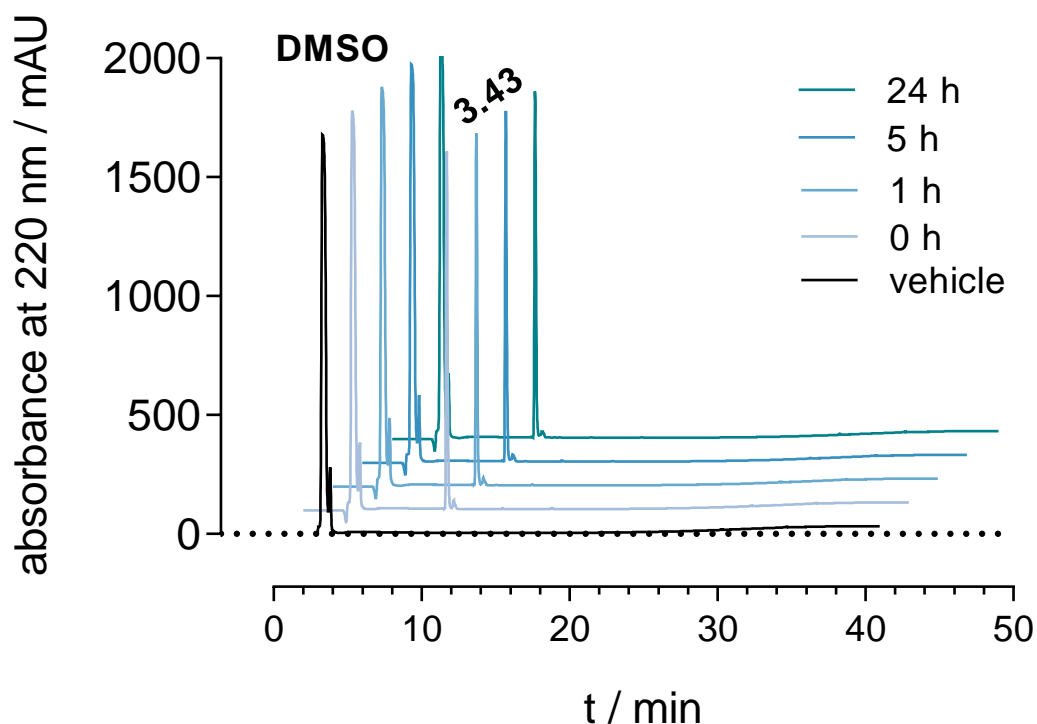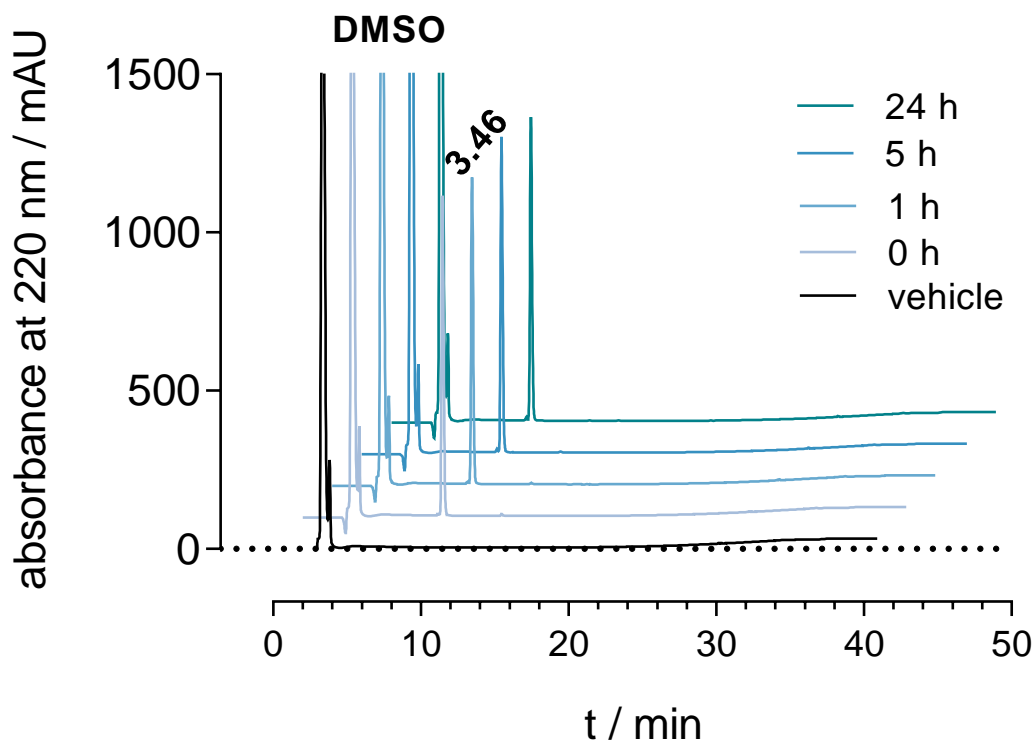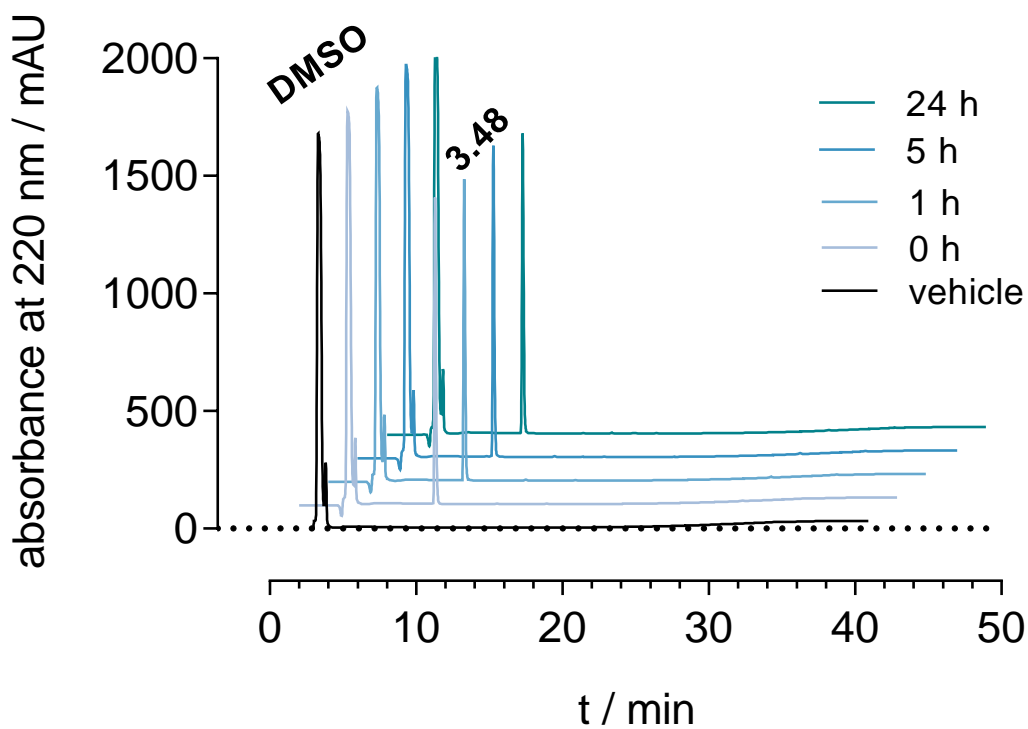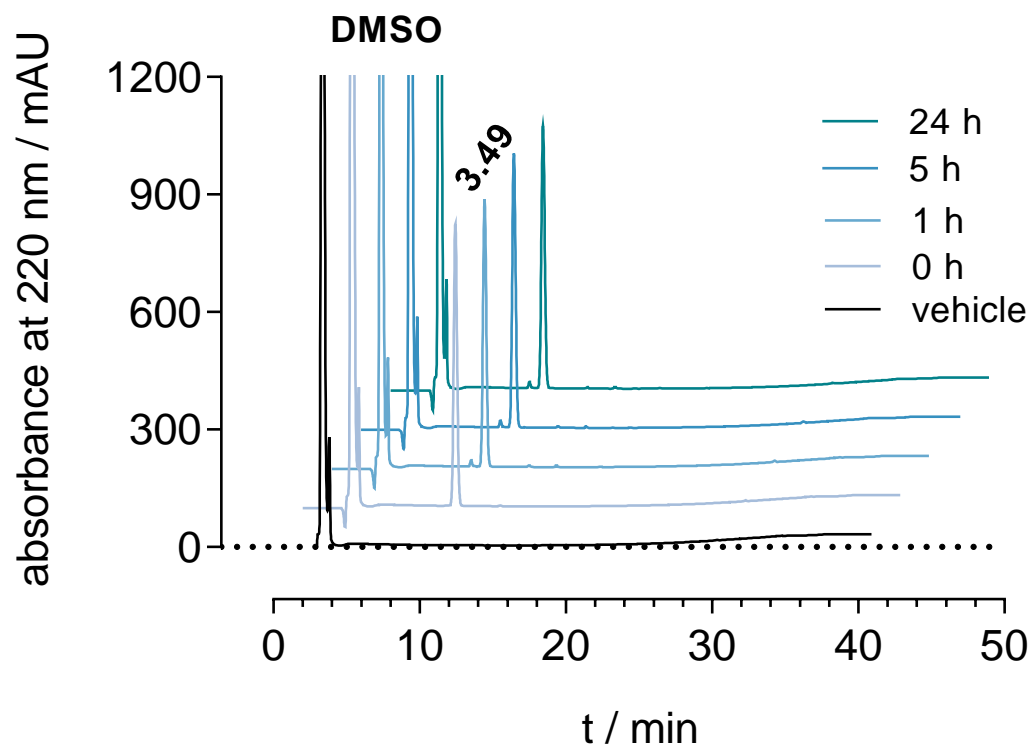
3.6 References

1. Nakamura, T.; Itadani, H.; Hidaka, Y.; Ohta, M.; Tanaka, K. Molecular cloning and characterization of a new human histamine receptor, hH$_4$R. *Biochem. Biophys. Res. Commun.* **2000**, 279, 615-620.

2. Oda, T.; Morikawa, N.; Saito, Y.; Masuho, Y.; Matsumoto, S. Molecular cloning and characterization of a novel type of histamine receptor preferentially expressed in leukocytes. *J. Biol. Chem.* **2000**, 275, 36781-36786.

3. Liu, C.; Ma, X.-J.; Jiang, X.; Wilson, S. J.; Hofstra, C. L.; Blevitt, J.; Pyati, J.; Li, X.; Chai, W.; Carruthers, N.; Lovenberg, T. W. Cloning and pharmacological characterization of a fourth histamine receptor (H$_4$) expressed in bone marrow. *Mol. Pharmacol.* **2001**, 59, 420-426.

4. Morse, K. L.; Behan, J.; Laz, T. M.; West jr., R. E.; Greenfeder, S. A.; Anthes, J. C.; Umland, S.; Wan, Y.; Hipkin, R. W.; Gonsiorek, W.; Shin, N.; Gustafson, E. L.; Qiao, X.; Wang, S.; Hedrick, J. A.; Greene, J.; Bayne, M.; Monsma jr., F. J. Cloning and characterization of a novel human histamine receptor. *J. Pharmacol. Exp. Ther.* **2001**, 296, 1058-1066.

5. Zhu, Y.; Michalovich, D.; Wu, H.-L.; Tan, K. B.; Dytko, G. M.; Mannan, I. J.; Boyce, R.; Alston, J.; Tierney, L. A.; Li, X.; Herrity, N. C.; Vawter, L.; Sarau, H. M.; Ames, R. S.; Davenport, C. M.; Hieble, J. P.; Wilson, S.; Bergsma, D. J.; Fitzgerald, L. R. Cloning, expression, and pharmacological characterization of a novel human histamine receptor. *Mol. Pharmacol.* **2001**, 59, 434-441.

6. Nguyen, D. N.; Stump, C. A.; Walsh, E. S.; Fernandes, C.; Davide, J. P.; Ellis-Hutchings, M.; Robinson, R. G.; Williams, T. M.; Lobell, R. B.; Huber, H. E.; Buser, C. A. Potent inhibitors of farnesyltransferase and geranylgeranyltransferase-I. *Bioorg. Med. Chem. Lett.* **2002**, 12, 1269-1273.

7. O'Reilly, M.; Alpert, R.; Jenkinson, S.; Gladue, R. P.; Foo, S.; Trim, S.; Peter, B.; Trevethick, M.; Fidock, M. Identification of a histamine H$_4$ receptor on human eosinophils-role in eosinophil chemotaxis. *J. Recept. Signal Transduct. Res.* **2002**, 22, 431-448.

8. Thurmond, R. L.; Venable, J.; Savall, B.; La, D.; Snook, S.; Dunford, P. J.; Edwards, J. P. Clinical development of histamine H$_4$ receptor antagonists. *Handb. Exp. Pharmacol.* **2017**, 241, 301-320.

9. Neumann, D. Role of the histamine H$_4$-receptor in bronchial asthma. *Handb. Exp. Pharmacol.* **2016**, 241, 347-359.

10. Schneider, E. H.; Seifert, R. The histamine H$_4$-receptor and the central and peripheral nervous system: a critical analysis of the literature. *Neuropharmacology* **2016**, 106, 116-128.

11. Tichenor, M. S.; Thurmond, R. L.; Venable, J. D.; Savall, B. M. Functional profiling of 2-aminopyrimidine histamine H$_4$ receptor modulators. *J. Med. Chem.* **2015**, 58, 7119-7127.

12. Igel, P.; Schnell, D.; Bernhardt, G.; Seifert, R.; Buschauer, A. Tritium-labeled N^1-[3-(1H-imidazol-4-yl)propyl]-N^2-propionylguanidine ([³H]UR-PI294), a high-affinity histamine H$_3$ and H$_4$ receptor radioligand. *ChemMedChem* **2009**, 4, 225-231.

13. Lim, H. D.; Adami, M.; Guaita, E.; Werfel, T.; Smits, R. A.; de Esch, I. J. P.; Bakker, R. A.; Gutzmer, R.; Coruzzi, G.; Leurs, R. Pharmacological characterization of the new histamine H$_4$ receptor agonist VUF 8430. *Br. J. Pharmacol.* **2009**, 157, 34-43.

14. Lim, H. D.; van Rijn, R. M.; Ling, P.; Bakker, R. A.; Thurmond, R. L.; Leurs, R. Evaluation of histamine H$_1$-, H$_2$-, and H$_3$-receptor ligands at the human histamine H$_4$ receptor: identification of 4-methylhistamine as the first potent and selective H$_4$ receptor agonist. *J. Pharmacol. Exp. Ther.* **2005**, 314, 1310-1321.

15. Jablonowski, J. A.; Grice, C. A.; Chai, W.; Dvorak, C. A.; Venable, J. D.; Kwok, A. K.; Ly, K. S.; Wei, J.; Baker, S. M.; Desai, P. J.; Jiang, W.; Wilson, S. J.; Thurmond, R. L.; Karlsson, L.; Edwards, J. P.; Lovenberg, T. W.; Carruthers, N. I. The first potent and selective non-imidazole human histamine H$_4$ receptor antagonists. *J. Med. Chem.* **2003**, 46, 3957-3960.

16. Schnell, D.; Brunskole, I.; Ladova, K.; Schneider, E. H.; Igel, P.; Dove, S.; Buschauer, A.; Seifert, R. Expression and functional properties of canine, rat, and murine histamine H$_4$ receptors in *Sf*9 insect cells. *Naunyn-Schmiedeberg's Arch. Pharmacol.* **2011**, 383, 457-470.

17. Wifling, D.; Löffel, K.; Nordemann, U.; Strasser, A.; Bernhardt, G.; Dove, S.; Seifert, R.; Buschauer, A. Molecular determinants for the high constitutive activity of the human histamine H_4 receptor: functional studies on orthologues and mutants. *Br. J. Pharmacol.* **2015**, 172, 785-798.

18. Nordemann, U.; Wifling, D.; Schnell, D.; Bernhardt, G.; Stark, H.; Seifert, R.; Buschauer, A. Luciferase reporter gene assay on human, murine and rat histamine H_4 receptor orthologs: correlations and discrepancies between distal and proximal readouts. *PLoS One* **2013**, 8, e73961.

19. Schneider, E. H.; Schnell, D.; Papa, D.; Seifert, R. High constitutive activity and a G-protein-independent high-affinity state of the human histamine H_4-receptor. *Biochemistry* **2009**, 48, 1424-1438.

20. Wifling, D.; Bernhardt, G.; Dove, S.; Buschauer, A. The extracellular loop 2 (ECL2) of the human histamine H_4 receptor substantially contributes to ligand binding and constitutive activity. *PLoS One* **2015**, 10, e0117185.

21. Liu, C.; Wilson, S. J.; Kuei, C.; Lovenberg, T. W. Comparison of human, mouse, rat, and guinea pig histamine H_4 receptors reveals substantial pharmacological species variation. *J. Pharmacol. Exp. Ther.* **2001**, 299, 121-130.

22. Lim, H. D.; de Graaf, C.; Jiang, W.; Sadek, P.; McGovern, P. M.; Istyastono, E. P.; Bakker, R. A.; de Esch, I. J. P.; Thurmond, R. L.; Leurs, R. Molecular determinants of ligand binding to H4R species variants. *Mol. Pharmacol.* **2010**, 77, 734-743.

23. Thurmond, R. L.; Desai, P. J.; Dunford, P. J.; Fung-Leung, W.-P.; Hofstra, C. L.; Jiang, W.; Nguyen, S.; Riley, J. P.; Sun, S.; Williams, K. N.; Edwards, J. P.; Karlsson, L. A potent and selective histamine H_4 receptor antagonist with anti-inflammatory properties. *J. Pharmacol. Exp. Ther.* **2004**, 309, 404-413.

24. Lim, H. D.; Jongejan, A.; Bakker, R. A.; Haaksma, E.; de Esch, I. J. P.; Leurs, R. Phenylalanine 169 in the second extracellular loop of the human histamine H_4 receptor is responsible for the difference in agonist binding between human and mouse H_4 receptors. *J. Pharmacol. Exp. Ther.* **2008**, 327, 88-96.

25. Baumeister, P. Molecular Tools for G-Protein Coupled Receptors: Synthesis, Pharmacological Characterization and [³H]-Labeling of Subtype-Selective Ligands for Histamine H_4 and NPY Y_2 Receptors. Ph. D. Dissertation, University of Regensburg, Regensburg, 2014.

26. Bernat, V.; Heinrich, M. R.; Baumeister, P.; Buschauer, A.; Tschammer, N. Synthesis and application of the first radioligand targeting the allosteric binding pocket of chemokine receptor CXCR3. *ChemMedChem* **2012**, 7, 1481-1489.

27. Baumeister, P.; Erdmann, D.; Biselli, S.; Kagermeier, N.; Elz, S.; Bernhardt, G.; Buschauer, A. [³H]UR-DE257: development of a tritium-labeled squaramide-type selective histamine H_2 receptor antagonist. *ChemMedChem* **2015**, 10, 83-93.

28. Cai, H.; Chavez, F.; Dunford, P. J.; Greenspan, A. J.; Meduna, S. P.; Quiroz, J. A.; Savall, B. M.; Tays, K. L.; Thurmond, R. L.; Wei, J.; Wolin, R. L.; Zhang, X. Diamino-Pyridine, Pyrimidine, and Pyridazine Modulators of the Histamine H_4 Receptor. WO 2009152325 A1. Chem. Abstr. 152:75050

29. Tichenor, M. S. The European Histamine Research Society 43rd Annual Meeting, May 7-10, 2014, Lyon, France. *Inflamm. Res.* **2014**, 63 Suppl 1, 1-48.

30. Nakao, A.; Suzuki, H.; Ueno, H.; Iwasaki, H.; Setsuta, T.; Kashima, A.; Sunada, S. Discovery and structural analyses of S-adenosyl-$_L$-homocysteine hydrolase inhibitors based on non-adenosine analogs. *Bioorg. Med. Chem.* **2015**, 23, 4952-4969.

31. Kraus, A.; Ghorai, P.; Birnkammer, T.; Schnell, D.; Elz, S.; Seifert, R.; Dove, S.; Bernhardt, G.; Buschauer, A. N^G-Acylated aminothiazolylpropylguanidines as potent and selective histamine H_2 receptor agonists. *ChemMedChem* **2009**, 4, 232-240.

32. Schreeb, A.; Łażewska, D.; Dove, S.; Buschauer, A.; Kieć-Kononowicz, K.; Stark, H. Histamine H_4 Receptor Ligands. In *Histamine H_4 Receptor: A Novel Drug Target in Immunoregulation and Inflammation*; Stark, Holger, Ed. Versita: London, **2013**; pp 21-62.

33. Geyer, R.; Kaske, M.; Baumeister, P.; Buschauer, A. Synthesis and functional characterization of imbutamine analogs as histamine H_3 and H_4 receptor ligands. *Arch. Pharm.* **2014**, 347, 77-88.

34. Igel, P.; Geyer, R.; Strasser, A.; Dove, S.; Seifert, R.; Buschauer, A. Synthesis and structure-activity relationships of cyanoguanidine-type and structurally related histamine H$_4$ receptor agonists. *J. Med. Chem.* **2009**, 52, 6297-6313.

35. Igel, P.; Schneider, E.; Schnell, D.; Elz, S.; Seifert, R.; Buschauer, A. N^G-Acylated imidazolylpropylguanidines as potent histamine H$_4$ receptor agonists: selectivity by variation of the N^G-substituent. *J. Med. Chem.* **2009**, 52, 2623-2627.

36. Savall, B. M.; Edwards, J. P.; Venable, J. D.; Buzard, D. J.; Thurmond, R.; Hack, M.; McGovern, P. Agonist/antagonist modulation in a series of 2-aryl benzimidazole H$_4$ receptor ligands. *Bioorg. Med. Chem. Lett.* **2010**, 20, 3367-3371.

37. van der Westhuizen, E. T.; Breton, B.; Christopoulos, A.; Bouvier, M. Quantification of ligand bias for clinically relevant β$_2$-adrenergic receptor ligands: implications for drug taxonomy. *Mol. Pharmacol.* **2014**, 85, 492-509.

38. Black, J. W.; Leff, P. Operational models of pharmacological agonism. *Proc. R. Soc. London, Ser. B* **1983**, 220, 141-162.

39. Black, J. W.; Leff, P.; Shankley, N. P.; Wood, J. An operational model of pharmacological agonism: the effect of E/[A] curve shape on agonist dissociation constant estimation. *Br. J. Pharmacol.* **1985**, 84, 561-571.

40. Evans, B. A.; Broxton, N.; Merlin, J.; Sato, M.; Hutchinson, D. S.; Christopoulos, A.; Summers, R. J. Quantification of functional selectivity at the human α$_{1A}$-adrenoceptor. *Mol. Pharmacol.* **2011**, 79, 298-307.

41. Kenakin, T.; Watson, C.; Muniz-Medina, V.; Christopoulos, A.; Novick, S. A simple method for quantifying functional selectivity and agonist bias. *ACS Chem. Neurosci.* **2012**, 3, 193-203.

42. Kenakin, T.; Christopoulos, A. Signalling bias in new drug discovery: detection, quantification and therapeutic impact. *Nat. Rev. Drug Discov.* **2013**, 12, 205-216.

43. ICRP. *Annals of the ICRP. Recommendations of the International Commission on Radiological Protection. ICRP Publication 26*. Pergamon Press: Oxford, New York, Frankfurt, 1977; Vol. 1 (3).

44. ICRP. *Annals of the ICRP. The 2007 Recommendations of the International Commission on Radiological Protection. ICRP Publication 103.* Elsevier: 2007; Vol. 37 (2-4).

45. Pegoli, A.; She, X. K.; Wifling, D.; Hübner, H.; Bernhardt, G.; Gmeiner, P.; Keller, M. Radiolabeled dibenzodiazepinone-type antagonists give evidence of dualsteric binding at the M$_2$ muscarinic acetylcholine receptor. *J. Med. Chem.* **2017**, 60, 3314-3334.

46. Pluym, N.; Baumeister, P.; Keller, M.; Bernhardt, G.; Buschauer, A. [³H]UR-PLN196: a selective nonpeptide radioligand and insurmountable antagonist for the neuropeptide Y Y$_2$ receptor. *ChemMedChem* **2013**, 8, 587-593.

47. She, X.; Pegoli, A.; Mayr, J.; Hübner, H.; Bernhardt, G.; Gmeiner, P.; Keller, M. Heterodimerization of dibenzodiazepinone-type muscarinic acetylcholine receptor ligands leads to increased M$_2$R affinity and selectivity. *ACS Omega* **2017**, 2, 6741-6754.

48. Sleight, A. J.; Stam, N. J.; Mutel, V.; Vanderheyden, P. M. Radiolabelling of the human 5-HT$_{2A}$ receptor with an agonist, a partial agonist and an antagonist: effects on apparent agonist affinities. *Biochem. Pharmacol.* **1996**, 51, 71-76.

49. Brunskole, I.; Strasser, A.; Seifert, R.; Buschauer, A. Role of the second and third extracellular loops of the histamine H$_4$ receptor in receptor activation. *Naunyn-Schmiedeberg's Arch. Pharmacol.* **2011**, 384, 301-317.

50. Yu, F.; Wolin, R. L.; Wei, J.; Desai, P. J.; McGovern, P. M.; Dunford, P. J.; Karlsson, L.; Thurmond, R. L. Pharmacological characterization of oxime agonists of the histamine H$_4$ receptor. *J. Receptor Ligand Channel Res.* **2010**, 3, 37-49.

51. Pop, N.; Igel, P.; Brennauer, A.; Cabrele, C.; Bernhardt, G. N.; Seifert, R.; Buschauer, A. Functional reconstitution of human neuropeptide Y (NPY) Y$_2$ and Y$_4$ receptors in Sf9 insect cells. *J. Recept. Signal Transduct. Res.* **2011**, 31, 271-285.

52. Hübner, H.; Haubmann, C.; Utz, W.; Gmeiner, P. Conjugated enynes as nonaromatic catechol bioisosteres: synthesis, binding experiments, and computational studies of novel dopamine receptor agonists recognizing preferentially the D₃ subtype. *J. Med. Chem.* **2000**, 43, 756-762.

53. Misawa, N.; Kafi, A. K. M.; Hattori, M.; Miura, K.; Masuda, K.; Ozawa, T. Rapid and high-sensitivity cell-based assays of protein-proteininteractions using split click beetle luciferase complementation: an approach to the study of G-protein-coupled receptors. *Anal. Chem.* **2010**, 82, 2552-2560.

54. Lieb, S.; Littmann, T.; Plank, N.; Felixberger, J.; Tanaka, M.; Schäfer, T.; Krief, S.; Elz, S.; Friedland, K.; Bernhardt, G.; Wegener, J.; Ozawa, T.; Buschauer, A. Label-free versus conventional cellular assays: functional investigations on the human histamine H₁ receptor. *Pharmacol. Res.* **2016**, 114, 13-26.

55. Kagermeier, N.; Werner, K.; Keller, M.; Baumeister, P.; Bernhardt, G.; Seifert, R.; Buschauer, A. Dimeric carbamoylguanidine-type histamine H₂ receptor ligands: a new class of potent and selective agonists. *Bioorg. Med. Chem.* **2015**, 23, 3957-3969.

56. Pockes, S.; Wifling, D.; Keller, M.; Buschauer, A.; Elz, S. Highly potent, stable, and selective dimeric hetarylpropylguanidine-type Histamine H₂ receptor agonists. *ACS Omega* **2018**, 3, 2865-2882.

57. Cheng, Y.-C.; Prusoff, W. H. Relationship between the inhibition constant (K_i) and the concentration of inhibitor which causes 50 per cent inhibition (I_{50}) of an enzymatic reaction. *Biochem. Pharmacol.* **1973**, 22, 3099-3108.

58. Durant, G. J.; Emmett, J. C.; Ganellin, C. R.; Miles, P. D.; Parsons, M. E.; Prain, H. D.; White, G. R. Cyanoguanidine-thiourea equivalence in the development of the histamine H₂-receptor antagonist, cimetidine. *J. Med. Chem.* **1977**, 20, 901-906.

59. Sellitto, G.; Faruolo, A.; de Caprariis, P.; Altamura, S.; Paonessa, G.; Ciliberto, G. Synthesis and anti-hepatitis C virus activity of novel ethyl 1*H*-indole-3-carboxylates in vitro. *Bioorg. Med. Chem.* **2010**, 18, 6143-6148.

60. Finkelstein, H. Preparation of organic iodides from the corresponding bromides and chlorides. *Ber. Dtsch. Chem. Ges.* **1910**, 43, 1528-1532.

61. Meffre, P.; Durand, P.; Le Goffic, F. Methyl (*S*)-2-phthalimido-4-oxobutanoate. *Org. Synth.* **1999**, 76, 123-132.

62. Mach, U. R.; Hackling, A. E.; Perachon, S.; Ferry, S.; Wermuth, C. G.; Schwartz, J.-C.; Sokoloff, P.; Stark, H. Development of novel 1,2,3,4-tetrahydroisoquinoline derivatives and closely related compounds as potent and selective dopamine D₃ receptor ligands. *ChemBioChem* **2004**, 5, 508-518.

63. Habermehl, G. G.; Ecsy, W. The condensation of histamine with carbonyl compounds. *Heterocycles* **1976**, 5, 127-134.

64. Sumita, K.; Koumori, M.; Ohno, S. A modified mannich reaction using 1,3-dioxolane. *Chem. Pharm. Bull.* **1994**, 42, 1676-1678.

65. Bradbury, B. J.; Baumgold, J.; Paek, R.; Kammula, U.; Zimmet, J.; Jacobson, K. A. Muscarinic receptor binding and activation of second messengers by substituted *N*-methyl-*N*-[4-(1-azacycloalkyl)-2-butynyl]acetamides. *J. Med. Chem.* **1991**, 34, 1073-1079.

66. Barker, G.; O'Brien, P.; Campos, K. R. Diamine-free lithiation-trapping of *N*-Boc heterocycles using *s*-BuLi in THF. *Org. Lett.* **2010**, 12, 4176-4179.

67. Collis, A. J.; Fox, D. N. A. Quinoline and Quinazoline Compounds useful in Therapy of Benign Prostatic Hyperplasia. US 20030045525 A1. Chem. Abstr. 130:3852

68. Jo, Y. S.; van der Vlies, A. J.; Gantz, J.; Thacher, T. N.; Antonijevic, S.; Cavadini, S.; Demurtas, D.; Stergiopulos, N.; Hubbell, J. A. Micelles for delivery of nitric oxide. *J. Am. Chem. Soc.* **2009**, 131, 14413-14418.

69. Streicher, W.; Loibner, H. Novel Aminoglycosides, their Production and Use as Anti-Microbial Agents. DE 2936120 A1, 1980. Chem. Abstr. 93:204981

70. Houssin, R.; Bernier, J.-L.; Henichart, J.-P. A convenient and general method for the preparation of *tert*-butoxycarbonylaminoalkanenitriles and their conversion to mono-*tert*-butoxycarbonylalkanediamines. *Synthesis* **1988**, 3, 259-261.

71. Amirbekyan, K.; Duchemin, N.; Benedetti, E.; Joseph, R.; Colon, A.; Markarian, S. A.; Bethge, L.; Vonhoff, S.; Klussmann, S.; Cossy, J.; Vasseur, J.-J.; Arseniyadis, S.; Smietana, M. Design, synthesis, and binding affinity evaluation of Hoechst 33258 derivatives for the development of sequence-specific DNA-based asymmetric catalysts. *ACS Catalysis* **2016**, 6, 3096-3105.

72. Mach, R. H.; Luedtke, R. R.; Unsworth, C. D.; Boundy, V. A.; Nowak, P. A.; Scripko, J. G.; Elder, S. T.; Jackson, J. R.; Hoffman, P. L.; Evora, P. H.; Rao, A. V.; Molinoff, P. B.; Childers, S. R.; Ehrenkaufer, R. L. ¹⁸F-Labeled benzamides for studying the dopamine D$_2$ receptor with positron emission tomography. *J. Med. Chem.* **1993**, 36, 3707-3720.

73. Yu, S.-W.; Lee, H.-Y.; Cho, B.-H.; An, K.-M.; Ryu, J.-S.; Lee, Y.-H.; Kang, J.-H. Synthesis and biological evaluation of *N*-formyl hydroxylamine derivatives as potent peptide deformylase inhibitors. *Bull. Korean Chem. Soc.* **2006**, 27, 1075-1078.

74. Kobayashi, S.; Komoriya, S.; Ito, M.; Nagata, T.; Mochizuki, A.; Haginoya, N.; Nagahara, T.; Horino, H. Preparation of Heterocyclic Compounds having the Sulfonyl Group as Antithrombotics. WO 9916747 A1, 1999. Chem. Abstr. 130:296694

75. Alegria, L. A.; Chong, W. K. M.; Chu, S.; Duvadie, R. K.; Li, L.; Romines, W. H., III; Yang, Y. Preparation of *N*-Heterocyclyl-substituted Aminothiozole Derivatives as Protein Kinase Inhibitors. WO 2004074283 A1, 2004. 141:243546.

76. Cook, M. C.; Gregory, G. I.; Bradshaw, J. 7*β*-[2-Etherified oximino-2-(thienyl-,furyl- or pyridylacetamido)]cephalosporins. US 4024133, 1975. Chem. Abstr. 86:139835

77. Cook, P. D.; An, H. Preparation of Compounds or Combinatorial Libraries of Compounds having a Plurality of Nitrogenous Sustituents. WO 9805961 A1. Chem. Abstr. 128:180338

78. Ghorai, P.; Kraus, A.; Keller, M.; Gotte, C.; Igel, P.; Schneider, E.; Schnell, D.; Bernhardt, G.; Dove, S.; Zabel, M.; Elz, S.; Seifert, R.; Buschauer, A. Acylguanidines as bioisosteres of guanidines: *N*$_G$-acylated imidazolylpropylguanidines, a new class of histamine H$_2$ receptor agonists. *J. Med. Chem.* **2008**, 51, 7193-7204.

79. Lee, Y.; Park, G. Y.; Lucas, H. R.; Vajda, P. L.; Kamaraj, K.; Vance, M. A.; Milligan, A. E.; Woertink, J. S.; Siegler, M. A.; Sarjeant, A. A. N.; Zakharov, L. N.; Rheingold, A. L.; Solomon, E. I.; Karlin, K. D. Copper(I)/O$_2$ chemistry with imidazole containing tripodal tetradentate ligands leading to *μ*-1,2-peroxo-dicopper(II) dpecies. *Inorg. Chem.* **2009**, 48, 11297-11309.

80. Windsor, W. T.; Weber, P. C.; Wang, J. J. S.; Strickland, C.; Njoroge, F. G.; Guzi, T. J.; Girijavallabhan, V. M.; Ferreira, J. A.; Desai, J. A.; Cooper, A. B.; Gelb, M. Treatment of Malaria with Farnesyl Protein Transferase Inhibitors. WO 2002056884 A2, 2002. Chem. Abstr. 137:125178.

81. Ghorai, P. Arpromidine-Related Acylguanidines: Synthesis and Structure-Activity Relationships of a New Class of Guanidine-Type Histamine H$_2$ Receptor Agonists with Reduced Basicity. Ph.D. Dissertation, University of Regensburg, 2006.

82. Badorc, A.; Boldron, C.; Delesque, N.; Fossey, V.; Lassalle, G.; Yvon, X. Derivatives of *N*-[(1*H*-Pyrazol-1-yl)aryl]-1*H*-indole-3-carboxamide and *N*-[(1*H*-pyrazol-1-yl)aryl]-1*H*-indazole-3-carboxamide, Their Preparation and Their Use as P2Y12 Antagonists. WO 2012146318 A1, 2012. Chem. Abstr. 157:687689.

83. Kono, M.; Matsumoto, T.; Imaeda, T.; Kawamura, T.; Fujimoto, S.; Kosugi, Y.; Odani, T.; Shimizu, Y.; Matsui, H.; Shimojo, M.; Kori, M. Design, synthesis, and biological evaluation of a series of piperazine ureas as fatty acid amide hydrolase inhibitors. *Bioorg. Med. Chem.* **2014**, 22, 1468-1478.

84. Engelhardt, H.; Schultes, S.; de Graaf, C.; Nijmeijer, S.; Vischer, H. F.; Zuiderveld, O. P.; Dobler, J.; Stachurski, K.; Mayer, M.; Arnhof, H.; Scharn, D.; Haaksma, E. E. J.; de Esch, I. J. P.; Leurs, R. Bispyrimidines as potent histamine H$_4$ receptor ligands: delineation of structure-activity relationships and detailed H$_4$ receptor binding Mode. *J. Med. Chem.* **2013**, 56, 4264-4276.

85. Tester, R.; Tan, X.; Luedtke, G. R.; Nashashibi, I.; Schinzel, K.; Liang, W.; Jung, J.; Dugar, S.; Liclican, A.; Tabora, J.; Levy, D. E.; Do, S. Amide-based inhibitors of p38αMAP kinase. Part 2: design, synthesis and SAR of sotent *N*-syrimidyl smides. *Bioorg. Med. Chem. Lett.* **2010**, 20, 2560-2563.

86. Jarusiewicz, J. A.; Jeon, J. Y.; Connelly, M. C.; Chen, Y.; Yang, L.; Baker, S. D.; Guy, R. K. Discovery of a diaminopyrimidine FLT3 inhibitor active against acute myeloid leukemia. *ACS Omega* **2017**, 2, 1985-2009.

4. UR-DEBa242: a Py-5-labeled fluorescent multipurpose probe for investigations on the histamine H₃ and H₄ receptors

Prior to the submission of this thesis, parts of this chapter were published in cooperation with partners:

Author contributions:

E.B. conceived and planned the project with input from L.G., T.L., A.B., and G.B. E.B. synthesized and characterized compounds, performed radioligand binding assays, functional assays, flow cytometric binding assays, parts of the BRET-based binding assays and UV/Vis and fluorescence spectroscopy and analyzed the data. L.G. synthesized and analytically characterized compound **4.10**, cloned the vectors NLuc-hH₃R, NLuc-hH₄R and NLuc-mH₄R, generated the respective HEK293T cell lines and performed parts of the BRET-based binding assays and bioluminescence spectroscopy and analyzed the data. E.B. and T.L. performed confocal microscopy and analyzed the data. D.W. performed molecular docking and MD simulations and processed the data. U.S. cloned the vectors pIRESneo3-SP-FLAG-hH₄R and pIRESneo3-SP-FLAG-hH₃R and generated HEK293T-SP-FLAG-hH₄R and HEK293T-SP-FLAG-hH₃R-CRE-CBR cell lines. A.B. and G.B. supervised the research. E.B., L.G., and G.B. wrote the manuscript with input from all coauthors. E.B. and L.G. contributed equally.

4.1 Introduction

The histamine H_3 and H_4 receptors (H_3R, H_4R), as well as the other histamine receptor subtypes ($H_{1,2}Rs$), belong to the superfamily of G-protein-coupled receptors (GPCRs). While the H_3R is expressed in the central nervous system and acts as a presynaptic receptor[1], the H_4R is mainly expressed in hematopoietic cells[2] and is considered a potential drug target for the treatment of disorders of the immune system[2,3] (e.g. rheumatoid arthritis, bronchial asthma, and pruritus). The expression of the H_4R in monocytes, neutrophiles and in the central and peripheral nervous system is controversially discussed in literature.[4-8] Moreover, marked species [e.g. human (h), mouse (m) and rat (r)]-dependent differences[9-11] regarding affinities, potencies and/or even the quality of action of H_4R ligands were reported.

Besides the endogenous agonist histamine **4.01**, several (inverse) agonists and antagonists, including some radiolabeled compounds, were described for the H_3R and H_4R over the years (e.g. **4.02**[12], **4.03**[13], **4.04**[14,15] and **4.05**[13], Figure 4.1). The 2,4-diaminopyrimidines **4.06** (UR-DEBa176) and **4.07** (UR-DEBa148) were recently identified as highly potent agonists at the h/m/rH_4Rs, and [^3H]**4.06** constitutes the first radioligand enabling robust binding studies at these H_4R orthologs[16] (Figure 4.1).

Over the last decades, fluorescent ligands have become more and more valuable alternatives to radioligands for investigations on ligand-receptor interactions at GPCRs, e.g. by means of fluorescence microscopy and flow cytometry.[17-19] Fluorescent ligands offer advantages over radiolabeled ligands with regard to safety, legal issues, waste disposal and costs.[19] Moreover, fluorescent probes can be used in resonance energy transfer-based assays [e.g. bioluminescent resonance energy transfer (BRET) between an N-terminally NanoLuc (NLuc)- tagged receptor and a fluorescent probe] which allow real-time detection of the receptor binding on living cells.[20,21] Over the years, several fluorescently labeled compounds for the H_1R[22,23], H_2R[24-26] and H_3R[27-29] were developed. Among the latter, bodilisant **4.08**[27](Figure 4.1) constitutes the latest described fluorescent probe for the H_3R, showing high affinity and subtype selectivity. BRET-based binding studies at the hH_3R and hH_4R were previously described by Mocking et al.[20] using the commercially available clobenpropit-BODIPY-630/650[20] and BODIPY-FL-histamine **4.09**[30] (Figure 4.1). In that study,

saturation binding experiments with **4.09** revealed only moderate affinity (K_d = 427 nM[20]) at the NLuc-hH₃R and no detectable specific binding on NLuc-hH₄R expressing cells. Therefore, **4.09** turned out inappropriate for comparable binding studies at the hH₃,₄Rs. In contrast, clobenpropit-BODIPY-630/650 displayed binding constants in the 2-digit-nM range at both receptor subtypes, which enabled competition binding experiments with several H₃,₄Rs ligands.
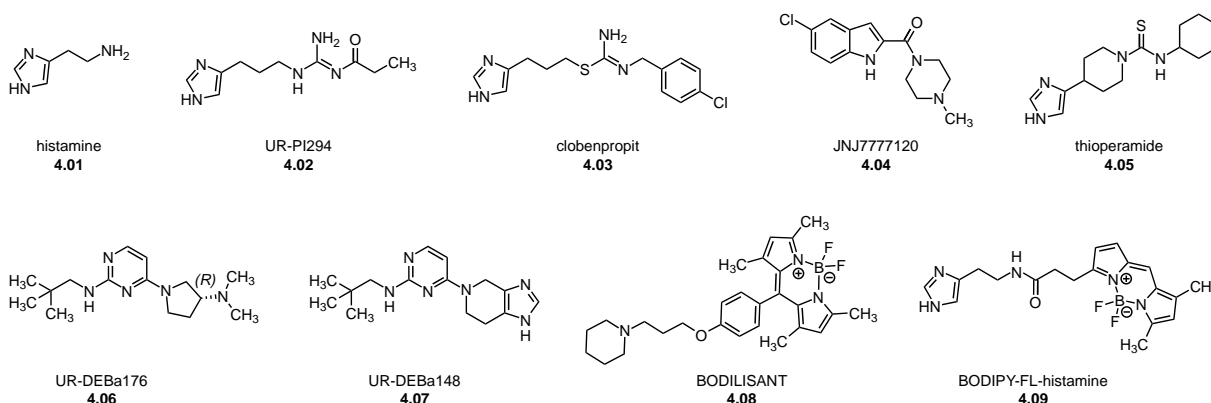
Figure 4.1. Structures of selected H₃R and H₄R (inverse) agonists and antagonists including fluorescent ligands.

However, clobenpropit-BODIPY-630/650 has some major disadvantages as it is expensive, its chemical structure is not disclosed, and analytical data (e.g. compound identity/purity and physicochemical/optical properties) are unavailable from the suppliers. To the best of our knowledge, its applicability in flow cytometry and in confocal microscopy at the hH₄R but also its affinity to rodent H₄Rs have not been reported yet. Finally, for BRET-based assays using NLuc as the bioluminescent donor, fluorophores exhibiting larger Stokes shifts (i.e. excitation using blue light, emission of red light) would be more appropriate (e.g. Figure A 4.1 in section 4.5.2).

Since a non-radioactive versatile molecular tool for investigations on the H₃R, but especially on the H₄R is highly needed, we aimed at the development of a comprehensively characterized H₃,₄Rs ligand, which is labeled with a fluorophore ideally suited for BRET-based binding assays, allowing comparable binding studies at NLuc-tagged hH₃R and h/mH₄Rs. Additionally, the fluorescent probe should be suitable for flow cytometry and allow the localization of the H₄R in live cells by confocal microscopy. In general, the development of fluorescent probes is challenging because the labeling of small molecules with relatively bulky fluorophores is often accompanied by a decrease in affinity at the target receptor.[17] Previously, different labeling

reagents [e.g. Py-5 **4.10**, Py-1 **4.11**, S0436-NHS ester **4.12** or BODIPY 650/665-X-NHS ester **4.13** (Figure 4.2A)] were used to design fluorescent probes for the H₄R.[31] Therefore, the high affinity and subtype selective 2-arylbenzimidazole-type hH₄R agonist **4.14**[32] (Figure 4.2B) was used as a template in our group: the small and polar histamine moiety was replaced by different labeling reagents (**4.10 – 4.13**) while the 2-arylbenzimidazole moiety was kept constant (Figure 4.2B). Unfortunately, markedly reduced affinities were obtained for the hH₄R ligands **4.15 – 4.18**.[31]

In this study, that approach was followed vice versa, i.e. retaining the polarity and basicity in the molecule and thereby gaining affinity at the H₃,₄Rs (Figure 4.2C). Histamine and several homologs were chosen as pharmacophores and were labeled with **4.10**, with or without the introduction of a propylene spacer. We chose the Py-5 label, as it is well-suited for an NLuc-based BRET assay (Figure A 4.1 in section 4.5.2), due to its spectral properties, its small size, and the convenient labeling procedure.

A Structures of labeling reagents
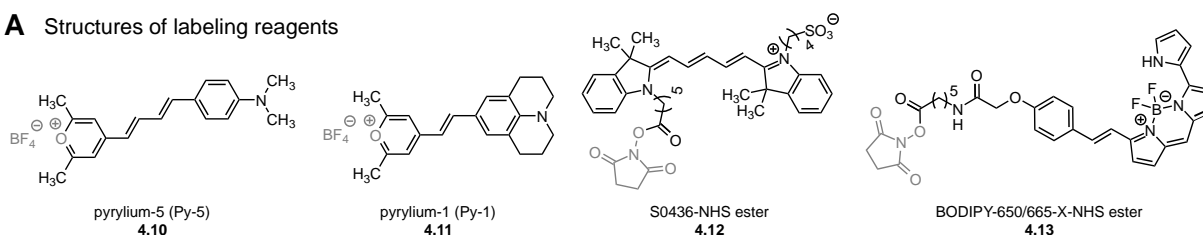
B Previous approach towards 2-arylbenzimidazole-type fluorescent ligands for the hH₄R
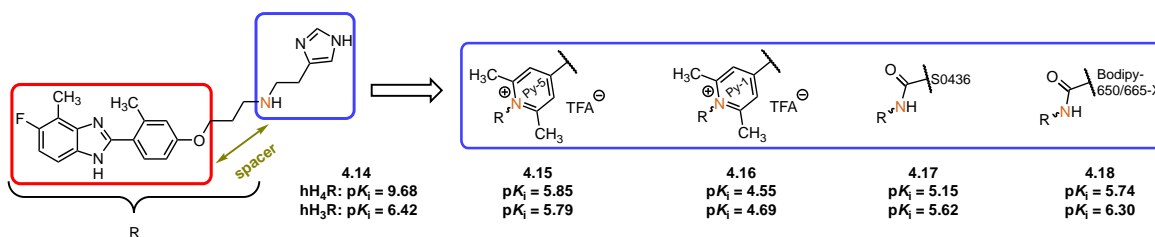
C Design strategy for the pyridinium labeled histamine derivatives applied in this study
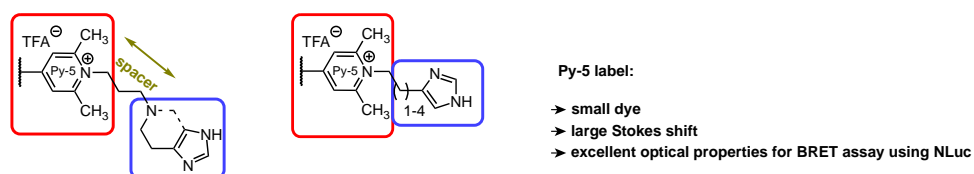
Figure 4.2. Rationale for the development of pyridinium Py-5-labeled ligands for the H₃,₄Rs. (A) Structures of labeling reagents (**4.10 – 4.13**) previously used[31] for the design of fluorescently labeled hH₄R ligands. (**B**) Structures of the 2-arylbenzimidazole-type hH₄R agonist **4.14**[32] and its previously described fluorescently labeled derivatives (**4.15 – 4.18**)[31], revealing weak to moderate affinities at the hH₃,₄Rs. (**C**) Design strategy for the herein presented Py-5-labeled histamine derivatives as fluorescent probes for H₃,₄Rs.

4.2 Results and discussion

4.2.1 Chemistry

In Scheme 4.1 the syntheses of the H$_4$R fluorescent ligands **4.24 – 4.29** are depicted. According to a previously described procedure[33], the pyrylium dye Py-5 **4.10**[34,35] (for the structure, see Figure 4.2; for the synthesis, see section 4.5.1.1) was used to label the primary amine precursors **4.01 · 2 HCl, 4.19 · 2 TFA, 4.20 · 2 TFA, 4.21 · 2 HBr, 4.22** and **4.23** (for the source or synthesis see section 4.5.1) under basic conditions (pH 8 – 9) at room temperature and in the dark to rapidly form the pyridinium-labeled compounds **4.24 – 4.29**. The transformation of the positively charged aromatic heterocycle is accompanied by a change in color (from blue to red), which makes the progress of reactions with such chameleon dyes visible.[33,34] After the conversion was complete, the reactions were quenched with trifluoroacetic acid (TFA), and the Py-5-labeled fluorescent ligands **4.24 – 4.29** were purified by preparative high performance liquid chromatography (HPLC) to obtain the respective TFA salts in high chemical purity (> 95%) (for details see in section 4.4.1).

Scheme 4.1. Synthesis of the Py-5-labeled fluorescent ligands 4.24 – 4.29.
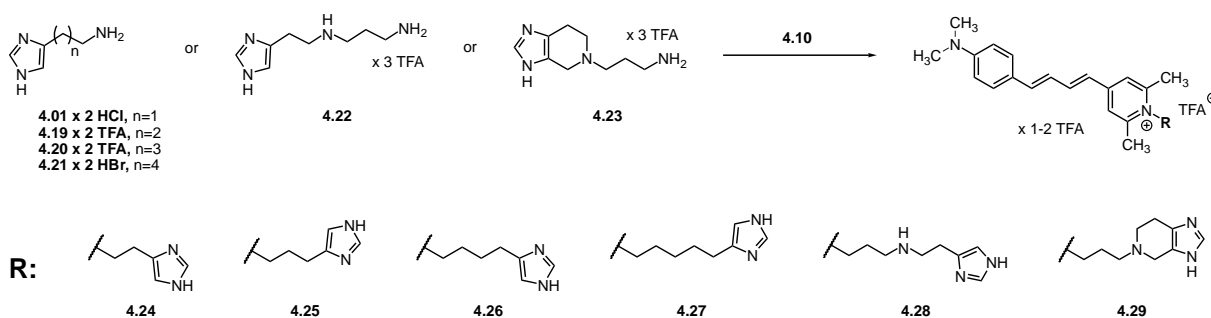
Reagents and conditions: DIPEA, DMF, rt (dark), 1.5 – 2 h, 19.4 – 70.7%.

4.2.2 Investigations on chemical stability

As a representative of the Py-5 labeled ligands, **4.26** was investigated with regard to chemical stability in phosphate-buffered saline (PBS, pH 7.4) at 23 °C, over a time period of 5 or 6 h (maximum incubation time in the applied assays) in 96-well Primaria plates (condition **A**, for radioligand binding experiments), white 96-well cell-Grade plates (condition **B**, for luciferase reporter gene-, β-arrestin2 recruitment- and BRET-based binding assays), 1.5-mL microtubes (condition **C**, for flow cytometric binding assays) and Sigmacote-treated 1.5-mL microtubes

(condition **D**). Under conditions **A** and **B** **4.26** proved stable (graphs see Figure A 4.13 and Figure A 4.14 in section 4.5.7.3). Under conditions **C** and **D** however, the analysis by reverse phase (RP)-HPLC revealed a decrease in the peak areas depending on the incubation time (≥ 1 h), while no additional peaks appeared in the chromatograms (Figure A 4.15 and Figure A 4.16 in section 4.5.7.3). Since **4.26** proved stable, the decrease in peak areas probably resulted from adsorption to the surface of the used vessels, such as under conditions **C** and **D**, i.e. differential adsorption should be considered upon storage/handling of the fluorescent probes.

4.2.3 Structure affinity, activity and subtype preference relationships of the target compounds (4.24 – 4.29) at the human histamine receptors

Radioligand competition binding experiments were performed with the fluorescent probes **4.24** – **4.29** to investigate their structure-affinity and subtype selectivity relationships at the hH$_{3,4}$Rs. For **4.26** and **4.27**, the subtype selectivity over the hH$_{1,2}$Rs was explored. Binding constants (pK_i values) at the hH$_{1-4}$Rs, stably expressed in membrane preparations of *Sf*9 insect cells, are shown in Table 4.1 and were compared to binding data of the unlabeled histamine derivatives (**4.01**, **4.19** – **4.21**).

Histamine **4.01** (hH$_{3,4}$Rs: pK_i = 7.73 and 7.90, respectively) was labeled with the Py-5 dye **4.10**, which caused a marked decline in affinities at the hH$_4$R (**4.24**: ≈ 155-fold) and the hH$_3$R (**4.24**: ≈ 46-fold), while no subtype preference was obvious. For homohistamine **4.19** (hH$_{3,4}$Rs: pK_i = 7.03 and 7.50, respectively), labeling with **4.10** reduced the affinity at the hH$_4$R (**4.25**: ≈ 19-fold) but slightly increased it at the hH$_3$R (**4.25**: ≈ 8-fold). Interestingly, **4.19** showed comparable binding constants at the hH$_{3,4}$Rs, whereas **4.25** revealed preferential binding (≈ 50-fold) at the hH$_3$R over the hH$_4$R. In comparison to **4.24**, **4.25** revealed higher affinities at the hH$_4$R (**4.25**: ≈ 3-fold) and the hH$_3$R (**4.25**: ≈ 72-fold). Apparently, the elongation of the alkyl chain by one methylene group had a beneficial impact on binding affinities for both receptor subtypes. By pursuing this approach, whereby imbutamine **4.20** and impentamine **4.21** were labeled, higher affinities were obtained for **4.26** and **4.27** at the hH$_4$Rs (**4.26**: pK_i = 7.85; **4.27**: pK_i = 7.47) and at the hH$_3$R (**4.26**: pK_i = 8.60; **4.27**: pK_i = 9.04) compared to **4.24** (hH$_{3,4}$R: pK_i = 6.07 and 5.71, respectively) and **4.25** (hH$_{3,4}$R: pK_i = 7.93 and 6.23, respectively)). Compound **4.26** was almost equi-affinic at the hH$_{3,4}$Rs, and labeling of **4.20**

only had a marginal influence on affinities and subtype preference between the two receptor subtypes. Compared to **4.21**, **4.27** revealed higher pK_i values for both receptor subtypes (**4.27**: ≈ 19-fold, hH$_4$R; **4.27**: ≈ 41-fold, hH$_3$R). Moreover, **4.27** showed a preferential binding at the hH$_3$R over the hH$_4$R (≈ 37-fold). For **4.26** and **4.27**, a distinct subtype preference over the hH$_1$R and hH$_2$R was obvious. In summary, by increasing the linker length between the Py-5 label and the imidazole moiety from an ethylene spacer to a pentylene spacer, hH$_3$R affinities increased. In the case of the hH$_4$R, the butylene spacer provided the ideal distance for the highest binding affinity (**4.26**: pK_i = 7.85). With regard to hH$_{3,4}$Rs subtype selectivity, no clear correlation with spacer length was observed.

The introduction of a propylene spacer between the pyridinium and the histamine moieties (**4.24**) yielded compound **4.28**. The elongated alkyl chain, containing a secondary amine function, was not tolerated by the hH$_4$R (Table 4.1). At the hH$_3$R, **4.28** showed higher binding affinity (≈ 63-fold compared to **4.24**) and a slight binding preference over the hH$_4$R (≈ 30-fold, compared to **4.24**). Strikingly, in contrast to **4.14** (hH$_{3,4}$R: pK_i = 6.4 and 9.7[32], respectively;[32] Figure 4.2), which contains the 2-arylbenzimidazole partial structure instead of the fluorescence label (i.e. lacking the pyridinium ion), **4.28** revealed weak affinity at the hH$_4$R (pK_i = 6.03) and a subtype preference for the hH$_3$R (≈ 69-fold). This makes **4.28** the fluorescent ligand with the highest preference for the hH$_3$R in this series.

Previously, spinaceamine, a rigid analog of histamine (**4.01**), was merged with a 2-arylbenzimidazole by Savall et al. to gain high affinity (pK_i = 8.5[32]) and subtype selectivity for the hH$_4$R (≈ 2700-fold[32]). With compound **4.29**, this concept was transferred to the series of pyridinium-labeled ligands. Unfortunately, in comparison to **4.28**, compound **4.29** revealed low pK_i values in the three-digit-nM range at both receptor subtypes.

UR-DEBa242: a Py-5-labeled fluorescent multipurpose probe for investigations on the histamine H_3 and H_4 receptors

Table 4.1. Affinities at the $hH_{1-4}Rs$ and subtype preference profile of the fluorescent probes.
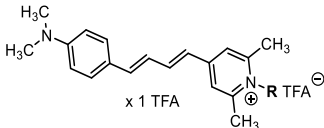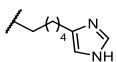
No.	R	pK_i				fold preference
		hH_4R	**hH_3R**	**hH_2R**	**hH_1R**	**H_4R/H_3R**
4.01	-	7.90[36]	7.73[36]	-	-	0.68
4.19	-	7.50[36]	7.03[36]	-	-	0.34
4.20	-	7.90[36]	8.37[36]	-	-	2.95
4.21	-	6.20[36]	7.43[36]	-	-	17.0
4.24		5.71 ± 0.08	6.07 ± 0.01	n.d.	n.d.	2.29
4.25		6.23 ± 0.01	7.93 ± 0.06	n.d.	n.d.	50.1
4.26		7.85 ± 0.03	8.60 ± 0.09	5.45 ± 0.05	< 5.32	5.62
4.27		7.47 ± 0.04	9.04 ± 0.10	5.74 ± 0.07	< 5.32	37.2
4.28		6.03 ± 0.01	7.87 ± 0.12	n.d.	n.d.	69.2
4.29		6.53 ± 0.05	6.34 ± 0.06	n.d.	n.d.	0.65

Competition binding performed on membranes of *Sf*9 insect cells expressing the $hH_4R + G\alpha_{i2} + \beta_1\gamma_2$, $hH_3R + G\alpha_{i2} + \beta_1\gamma_2$, hH_2R-$Gs_{\alpha s}$ or $hH_1R + RGS4$. Radioligands for hH_4R: [³H]**4.01** (c_{final} = 40 nM); hH_3R: [³H]**4.02**[12] (c_{final} = 2 nM); hH_2R: [³H]UR-DE257[37] (c_{final} = 20 nM); hH_1R: [³H]pyrilamine (c_{final} = 5 nM). The pK_i values represent means ± SEM. Data represent 2 (for pK_i values ≤ 6.34) or 3 (for pK_i values > 6.34) independent experiments, each performed in triplicate. Fold-preference was calculated based on the ratio of the K_i values of the respective compound at the hH_4R and hH_3R. n.d.: not determined. -: compound structure or data not shown.

Compounds **4.26** and **4.27**, which exhibited the highest affinities at the $hH_{3,4}Rs$, were functionally characterized (Table 4.2 and Figure A 4.3 – Figure A 4.4 in section 4.5.4). At the hH_3R, where the change from a butylene (**4.26**) to a pentylene spacer (**4.27**) led to a slight increase in affinity (Table 4.1), the extension of the chain length mainly affected the quality of action, turning the partial agonist **4.26** into an antagonist (**4.27**) in a reporter gene assay (Table 4.2 and Figure A 4.3 – Figure A 4.4). For the hH_4R, the opposite effect was observed: the inverse agonist **4.26** turned into a partial agonist (**4.27**), and additionally, the potency decreased (Table 4.2 and Figure A 4.3 – Figure A 4.4). This was not only true for G-protein-dependent reporter gene activity but also for β-arrestin2 recruitment (Table 4.2 and Figure A 4.3 – Figure A 4.4). Strikingly, when comparing the unlabeled compounds **4.20** and **4.21** with their fluorescently labeled derivatives (**4.26** and **4.27**, respectively) at the hH_4R, the introduction of the pyridinium label led to an inversion of the quality of action. Compound

4.20, an agonist[36] in the [^{35}S]GTPγS assay, turned into an inverse agonist (**4.26**), whereas **4.21**, an antagonist[36], became a partial agonist (**4.27**). At the hH_3R, however, Py-5 labeling of **4.20** did not alter the quality of action[36], whereas **4.21** is a partial agonist[36] and **4.27** was an antagonist. Incorporation of the pyridinium label predominantly influenced the quality of action at the hH_4R, suggesting an involvement of the fluorophore in hH_4R binding. This assumption was supported by molecular dynamics simulations with **4.26** at the hH_4R, hinting at a role of the Py-5 fluorophore in interactions with the orthosteric binding pocket (Figure A 4.5 in section 4.5.5).

Table 4.2. Functional data of 4.26 and 4.27 at the hH_3R and the h/mH_4Rs.

No.	R	pEC$_{50}$ / pIC$_{50}$ / pK_b / (α)				
		hH_3R	**hH_4R**		**mH_4R**	
		reporter gene	reporter gene	β-arr2	reporter gene	β-arr2
4.01	-	8.48 ± 0.09 (1.00)	7.77[38] (1.00)	7.47 ± 0.12 (1.00)	7.06[38] (1.00)	5.63 ± 0.07 (1.00)
4.05	-	*7.70 ± 0.09* (-0.68 ± 0.11)	6.92[38] (-0.32)	*6.31 ± 0.19* (-0.10 ± 0.03)	6.52[38] (-0.44)	**7.55 ± 0.14** (-0.02 ± 0.002)
4.26		8.77 ± 0.12 (0.61 ± 0.03)	*8.76 ± 0.18* (-0.34 ± 0.04)	*7.81 ± 0.12* (-0.09 ± 0.01)	*7.08 ± 0.06* (-0.40 ± 0.02)	**7.30 ± 0.04** (0.00 ± 0.00)
4.27		**8.71 ± 0.07** (-0.06 ± 0.03)	7.14 ± 0.10 (0.23 ± 0.02)	7.19 ± 0.01 (0.08 ± 0.01)	**< 6.64** (0.01 ± 0.01)	no potency (0.00 ± 0.00)

Data from luciferase reporter gene assays, using HEK293T-SP-FLAG-hH_3R-CRE-CBR, HEK293T-SF-hH_4R-His6-CRE-Luc or HEK293T-SF-mH_4R-His6-CRE-Luc cells and β-arrestin2 recruitment assays, using HEK293T-β-arr2-xH_4R cells (x = h, m). In agonist mode (pEC$_{50}$, pIC$_{50}$) the intrinsic activity (α) of histamine **4.01** was set to 1.00 and α values of other compounds were referred to this value: α ≥ 0.08 for agonists, α ≤ -0.09 for inverse agonists. In antagonist mode pK_b values of neutral antagonists were determined in the presence of **4.01** [for hH_3R: c_{final} = 30 nM; for mH_4R: c_{final} = 300 nM (reporter gene assay), c_{final} = 10 μM (β-arr2 recruitment assay)]. The pK_b values were calculated based on the Cheng-Prusoff equation[39]. Data (mean values ± SEM) were determined in 2 – 8 (β-arr2) or 3 – 7 (reporter gene) independent experiments, each performed in triplicate or partly in duplicate (β-arr2 assays for **4.01**, and reporter gene assay for **4.27** at the hH_3R). -: compound structure not shown.

Since **4.26** showed the highest affinity at the hH_4R in this series (Table 4.1), its applicability to confocal microscopy at HEK293T cells expressing the hH_4R was investigated. In a BRET-based binding assay employing NLuc, the fluorescent probes with the highest pK_i values at the $hH_{3,4}Rs$ (**4.26** and **4.27**) were assessed. Especially **4.26** could be a promising candidate for comparable BRET-based binding studies at the $H_{3,4}Rs$, due to its comparable high affinities at the hH_3R and hH_4R and its ideal optical properties for NLuc-based BRET (Figure A 4.1 in section 4.5.2).

4.2.4 Binding of 4.26 at the hH$_4$R determined by confocal microscopy

Since expression of the H$_4$R is still controversially discussed[4-8], we examined whether **4.26** allows fluorescent staining of hH$_4$R-expressing live cells via confocal microscopy. These experiments were performed at recombinant HEK293T-hH$_4$R (total binding of **4.26**, nonspecific binding of **4.26** in the presence of **4.05** and association of **4.26**, followed by its dissociation in the presence of **4.05**) and HEK293T-wt (wild-type) cells (total binding of **4.26**) as a negative control. Images were recorded consecutively at a frame rate of 16 s for 30 min (total/nonspecific binding of **4.26**) or 13.1 min (association/dissociation of **4.26**), from which selected frames are displayed in Figure 4.3.

In all experiments **4.26** was added during the second frame yielding a final concentration of 200 nM. In total binding/association experiments, fluorescence was immediately detected at the membrane of HEK293T-hH$_4$R cells, which is in accordance with the results of kinetic BRET experiments (Figure 4.5). After an incubation period (> 64 s), fluorescence was also detected intracellularly (Figure 4.3A, the first panel, and Figure 4.3B). This finding most likely corresponds to internalization of the ligand-receptor complex, since only marginal nonspecific internalization was observed within 20 min, when the HEK293T-hH$_4$R cells were pre-incubated with a high excess of **4.05** (Figure 4.3A, the second panel) or in the case of HEK293T-wt cells (Figure 4.3A, the third panel). In Figure 4.3B, dissociation of **4.26** from the hH$_4$R was initiated by the addition of an excess of **4.05** at 5.07 min, leading to a rapid disappearance of fluorescence from the cellular membrane within approx. 2 min, which is in accordance with the fast kinetics determined in BRET-based assays (Figure 4.5). In contrast, intracellular fluorescence remained unchanged (Figure 4.3B). Unexpectedly, **4.26**, an inverse agonist at the hH$_4$R in a β-arrestin recruitment assay (Table 4.2), was internalized in a receptor-dependent manner. This may be taken as a hint to constitutive endocytosis of the hH$_4$R by β-arrestin- or even clathrin-independent mechanisms, a process already described for various GPCRs (e.g. muscarinic acetylcholine M$_3$ receptor[40], β$_2$-adrenoceptor[40] or 5-HT$_{2A}$ serotonin receptor[41,42]). Furthermore, the observed internalization of the fluorescent probe **4.26** was in agreement with comparatively high nonspecific binding of **4.26** in flow cytometric saturation binding experiments (Figure A 4.6 in section 4.5.6.1).

Taken together, **4.26** enables time-dependent fluorescent staining of the hH$_4$R expressed in HEK293T cells, which renders it a useful molecular tool for hH$_4$R localization and trafficking studies.
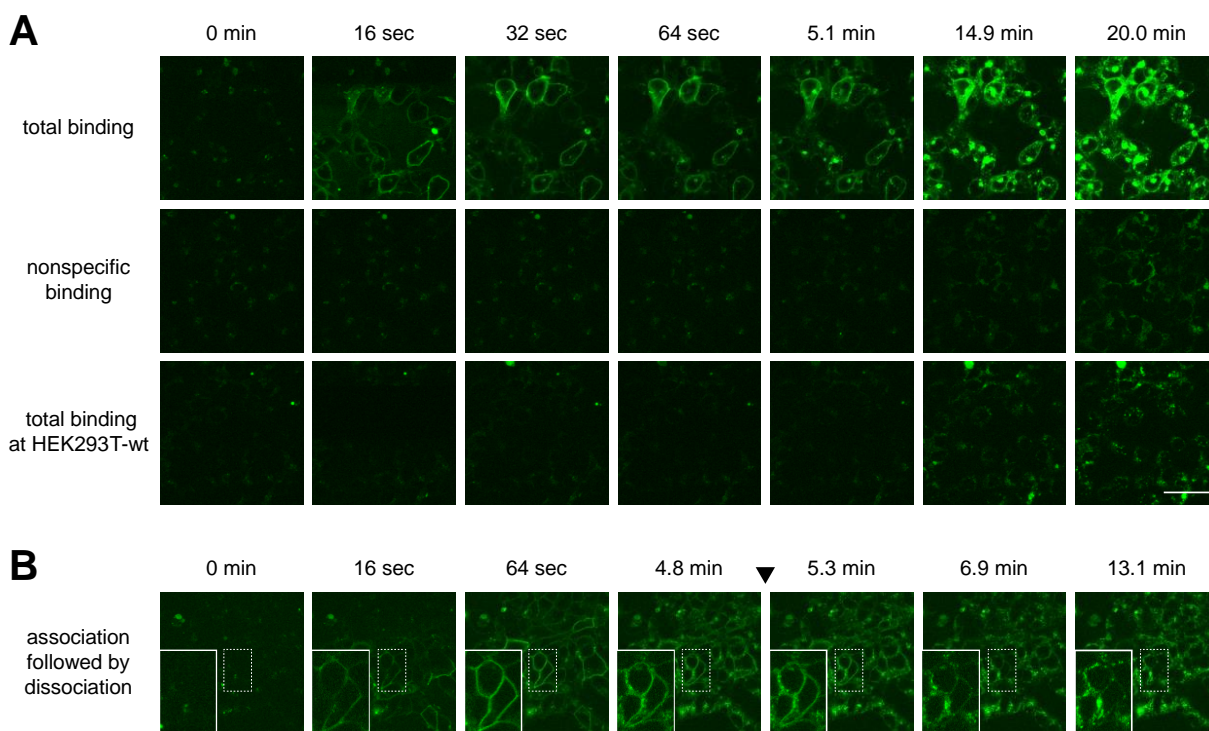
Figure 4.3. Selected frames from confocal microscopy experiments with 4.26 at HEK293T-hH$_4$R or HEK293T-wt (wild-type) cells. (**A**) Panel 1: for total binding, association was started by the addition of **4.26** (c_{final} = 200 nM) to HEK293T-hH$_4$R after recording for 16 s (frame 1). Panel 2: nonspecific binding was recorded after preincubation of HEK293T-hH$_4$R cells with **4.05** (100-fold excess compared to **4.26**) at rt for 10 min, followed by the addition of **4.26** (c_{final} = 200 nM) after recording for 16 s (frame 1). Panel 3: total binding was recorded on HEK293T-wt cells after **4.26** (c_{final} = 200 nM) was added at a 16 s (frame 1) recording time. (**B**) Association of **4.26** (c_{final} = 200 nM; addition after 16 s) to the hH$_4$R, expressed in HEK293T cells, was followed by the initiation of dissociation by adding **4.05** (100-fold excess) at a 5.07 min recording time. Scale bar (depicted in **A**, panel 3, 20 min) represents 50 µm for all frames.

4.2.5 BRET-based saturation binding at the NLuc-hH$_3$R and the NLuc-h/mH$_4$Rs

We investigated BRET-based binding with the Py-5-labeled probes **4.26** and **4.27**, which stand out due to the highest binding affinities and/or potencies at the hH$_3$R and h/mH$_4$Rs (Table 4.1 and Table 4.2). For this purpose, HEK293T cells stably expressing the hH$_3$R, the hH$_4$R or the mH$_4$R, N-terminally tagged with NLuc (NLuc-xH$_x$R), were generated. In BRET-based binding, only the fraction of receptor-bound fluorescent ligand is quantified, while nonspecifically bound ligand is only scantily detected because of the strong distance dependence of resonance energy transfer.

To get a comprehensive insight into the binding of the fluorescent ligands, especially in terms of nonspecific binding in whole cell systems, we representatively investigated **4.26** in flow cytometric saturation binding at the NLuc-hH$_4$R and NLuc-mH$_4$R (Figure A 4.6 in section 4.5.6). The obtained pK_d values from flow cytometric binding experiments (Table 4.3) were comparable to the results from radioligand binding experiments at the hH$_4$R (Table 4.1) and from functional assays at the mH$_4$R (Table 4.2). It is striking that **4.26** shows relatively high nonspecific binding in this assay at concentrations around the K_d values (Figure A 4.6 in section 4.5.6.1). This might be due to binding to intracellular proteins after internalization of the fluorescent ligand, which was also observed in confocal microscopy (Figure 4.3).

As expected, low nonspecific binding was observed in BRET-based saturation binding experiments with **4.26** and **4.27**, while retaining saturable binding to all investigated receptor constructs (NLuc-hH$_3$R, NLuc-hH$_4$R and NLuc-mH$_4$R) (Figure 4.4). The resulting binding constants (pK_d values; for **4.26**, Table 4.3; for **4.27**, H$_3$R: pK_d = 8.94 ± 0.25; hH$_4$R: pK_d = 7.11 ± 0.02; mH$_4$R: pK_d = 6.79 ± 0.03) were in good agreement with the pK_d values from flow cytometry, the pK_i values from radioligand competition binding (Table 4.1), and/or the functional data obtained in reporter gene- or β-arrestin2 recruitment assays (Table 4.2). The results confirmed that the N-terminal luciferase tag does not affect ligand binding, which is consistent with the findings of Mocking et al.[20] for the hH$_3$R and the hH$_4$R.

In summary, **4.26** and **4.27** both showed high affinities at the NLuc-hH$_3$R. At the NLuc-h/mH$_4$Rs, however, **4.26** revealed higher affinities than **4.27** in the BRET-based binding assay. To the best of our knowledge, **4.26** is the first fluorescent ligand described for the mH$_4$R. Therefore, we subjected **4.26** to an in-depth characterization by BRET-based kinetic and competition binding experiments at the NLuc-hH$_3$R and NLuc-h/mH$_4$Rs.
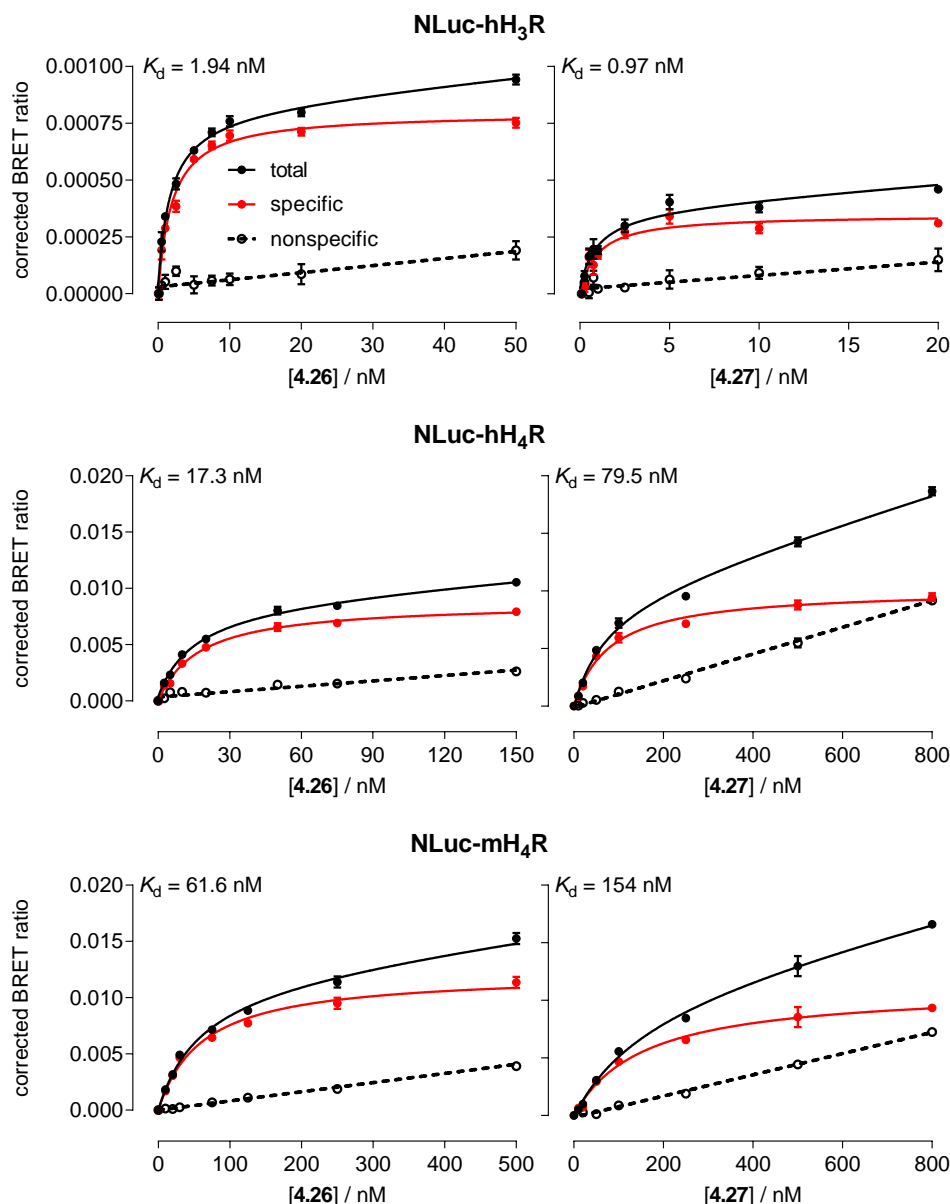
Figure 4.4. BRET-based saturation binding of 4.26 and 4.27 at the NLuc-hH₃R or NLuc-h/mH₄Rs, stably expressed in HEK293T cells. Total binding (black curves), specific binding (red curves) and nonspecific binding [dashed lines, determined in the presence of **4.05** (300-fold excess over **4.26** for NLuc-hH₃R, and 100-fold excess over **4.26** for NLuc-h/mH₄Rs)] are depicted. The results shown are representative of 3 experiments, each performed in triplicate. Data are presented as means ± error. Error bars of total and nonspecific binding represent SEMs, whereas those of specific binding are errors calculated according to the Gaussian law of error propagation.

4.2.6 BRET-based real-time kinetic binding at the NLuc-hH₃R and the NLuc-h/mH₄Rs

Besides their affinities, it is also of importance to know the binding kinetics of molecular tools, providing information on how much time is needed until an equilibrium between receptors and ligands has been established. This is especially important when performing competition

binding experiments. Therefore, we performed real-time kinetic experiments with the fluorescent ligand **4.26** using the BRET-based binding assay.

Compound **4.26** showed a rapid one-phase association to all investigated receptor constructs, stably expressed in HEK293T cells, and was fully bound after approx. 2 min (Figure 4.5, Table 4.3). After 5 min of association, dissociation was initiated by the addition of an excess of the competitive ligand **4.05**, which displaced **4.26** completely from the receptor with a half-life of 0.25 ± 0.02 min (NLuc-hH_3R), 1.15 ± 0.05 min (NLuc-hH_4R) and 0.18 ± 0.02 min (NLuc-mH_4R) (Figure 4.5, Table 4.3). For all experiments, the kinetically derived dissociation constants $[K_d \text{ (kin)} = k_{off} / k_{on}]$ were calculated and were in good agreement with the pK_d values determined by saturation binding after the equilibrium was reached (Table 4.3).
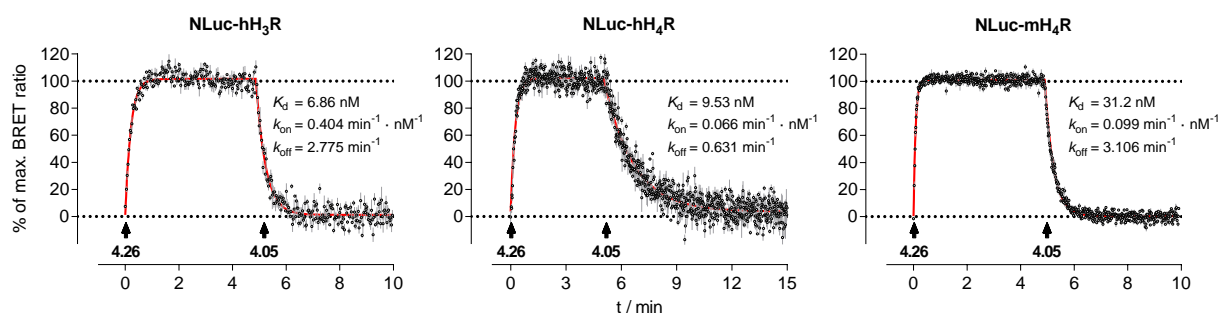
Figure 4.5. BRET-based specific binding kinetics of 4.26 at the NLuc-hH₃R or NLuc-h/mH₄Rs, stably expressed in HEK293T cells. Association was induced by the addition of **4.26**, giving a final concentration of 5 nM (NLuc-hH_3R), 50 nM (NLuc-hH_4R) or 100 nM (NLuc-mH_4R). Dissociation was initiated after 5 min by addition of **4.05** (300-fold excess over **4.26** for NLuc-hH_3R or 100-fold excess over **4.26** for NLuc-h/mH_4Rs). The results shown are representative of 3 independent experiments, each performed in triplicate. Data are presented as means ± errors. Errors were calculated according to the Gaussian law of error propagation.

Table 4.3. Comparison of thermodynamic and kinetic binding constants of 4.26 at the NLuc-hH₃R and the NLuc-h/mH₄Rs.

NLuc-	Flow cytometry		BRET-based binding					
	K_d (sat)[a] / nM	pK_d (sat)[a]	K_d (sat)[b] / nM	pK_d (sat)[b]	K_d (kin)[c] / nM	pK_d (kin)[c]	k_{on}[d] / $min^{-1} \cdot nM^{-1}$	k_{off}[e] / min^{-1} $t_{1/2}$[e] / min
hH₃R	n.d.	n.d.	1.71; 1.94; 1.35	8.78 ± 0.05	5.84; 6.86; 2.54	8.33 ± 0.13	0.635 ± 0.165	2.794 ± 0.216 0.25 ± 0.02
hH₄R	38.8; 44.5	7.38 ± 0.03	19.7; 16.5; 17.3	7.75 ± 0.02	14.4; 9.53; 9.16	7.97 ± 0.06	0.057 ± 0.007	0.605 ± 0.028 1.15 ± 0.05
mH₄R	76.3; 52.2	7.20 ± 0.08	74.7; 60.9; 61.6	7.18 ± 0.03	75.4; 31.2; 42.1	7.33 ± 0.11	0.084 ± 0.010	3.871 ± 0.493 0.18 ± 0.02

[a]Equilibrium dissociation constants (K_d values) from single experiments determined by flow cytometric saturation binding at the NLuc-hH₄R or NLuc-mH₄R, stably expressed in HEK293T cells. K_d values were transformed into pK_d values for each experiment and indicated pK_d values are means ± SEM from 2 independent experiments, each performed in duplicate; n.d.: not determined. [b]Equilibrium dissociation constants (K_d values) from single experiments determined in BRET-based binding assays at the NLuc-hH₃R, NLuc-hH₄R or NLuc-mH₄R, stably expressed in HEK293T cells. K_d values were transformed into pK_d values for each experiment and indicated pK_d values represent means ± SEM from 3 independent experiments each performed in triplicate. [c]Kinetically derived dissociation constant determined by BRET-based binding assays at the NLuc-hH₃R, NLuc-hH₄R or NLuc-mH₄R, stably expressed in HEK293T cells. pK_d values were calculated for each experiment and indicated pK_d values represent means ± SEM from 3 independent experiments. [d]Association rate constant (means ± SEM), [e]Dissociation rate constant (means ± SEM) and derived half-life (means ± propagated error) from 3 independent experiments, each performed in triplicate.

4.2.7 BRET-based competition binding at the NLuc-H$_{3,4}$Rs

BRET-based competition binding experiments at the NLuc-hH₃R and NLuc-h/mH₄Rs were performed to evaluate the potential of **4.26** as a molecular tool, allowing the identification and characterization of new unlabeled H₃R and H₄R ligands. Several well-characterized H$_{3,4}$Rs ligands were investigated using the HEK293T cells described above. The live cells were incubated with a distinct concentration of **4.26** (NLuc-hH₃R: c_{final} = 5 nM; NLuc-hH₄R: c_{final} = 30 nM; NLuc-mH₄R: c_{final} = 100 nM) and serial dilutions of the respective unlabeled ligands **4.01**, **4.03 – 4.07** that should be investigated.

All ligands displaced **4.26** completely from the respective receptor (Figure 4.6). For the NLuc-hH₃R and NLuc-hH₄R, all investigated ligands showed similar affinities (pK_i values) in our assay setup, compared to published BRET-based binding data obtained with BODIPY 630/650-labeled clobenpropit[20] as a BRET acceptor (Table 4.4). However, in case of agonists we determined lower affinities at both receptors in our BRET experiments compared to published results from radioligand binding experiments performed at wild-type receptors (Table 4.4). Possible explanations for this observation were discussed by Mocking et al.[20]. For instance, the authors adduced the use of live cells instead of membrane preparations as receptor source, the nature of the assay, an allosteric effect of sodium ions, and the influence of the quality of action of molecular tools. Receptor-dependent and receptor-independent internalization of the fluorescent ligand, as observed for **4.26** at the hH₄R by confocal microscopy (Figure 4.3), may play a role in the aforementioned discrepancies as well.

To the best of our knowledge, no BRET-based binding assay for the NLuc-mH₄R is described in the literature. Therefore, no reference data for this assay is available, but for compounds **4.01**, **4.03** and **4.05**, the determined binding constants were in good agreement with results from radioligand competition binding experiments on homogenates of HEK293T-SF-His6-CRE-Luc cells expressing the mH₄R, and functional data from luciferase reporter gene- and β-arrestin2 recruitment assays for ligands **4.04**, **4.06** and **4.07** (Table 4.4). Taken together, the BRET-based binding assay utilizing **4.26** offers a robust test system for the characterization of putative new ligands for the hH₃R and the h/mH₄Rs.
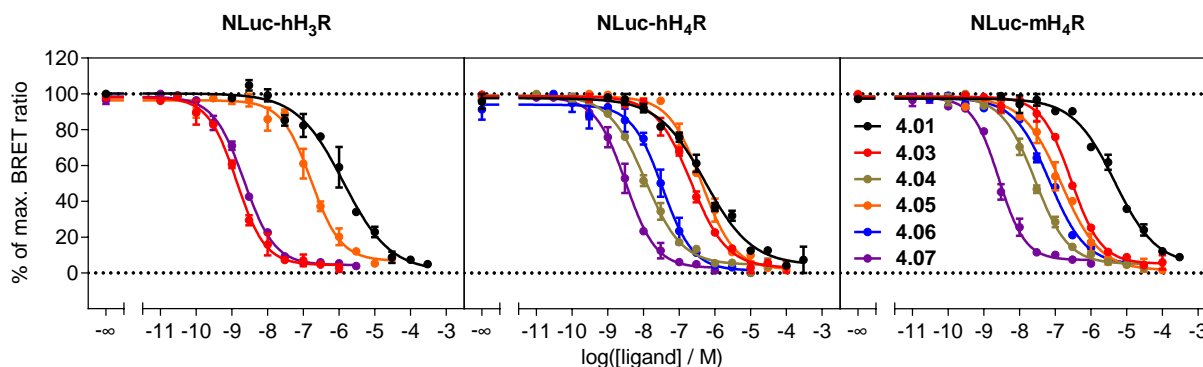
Figure 4.6. Displacement curves of 4.01 and 4.03 – 4.07 at the NLuc-hH₃R [c_{final} (4.26) = 5 nM], NLuc-hH₄R [c_{final} (4.26) = 30 nM] or NLuc-mH₄R [c_{final} (4.26) = 100 nM], stably expressed in HEK293T cells, from BRET-based competition binding with 4.26 as BRET acceptor. Data represent means ± SEM of 4 independent experiments, each performed in triplicate.

Table 4.4. Comparison of the BRET-based binding data (pK_i) of H₃,₄R ligands, using 4.26 as a BRET acceptor at the NLuc-hH₃R and the NLuc-h/mH₄Rs, with reference data.

No.	pK_i / **pEC₅₀** or pK_b / (α)					
	hH₃R		**hH₄R**		**mH₄R**	
	4.26[a]	reference	**4.26**[a]	reference	**4.26**[a]	reference
4.01	6.50 ± 0.09	6.3[b] 8.0[c[1]]; 8.0[c[9]]	6.66 ± 0.05	6.8[b] 7.2 − 8.2[c[1, 3-7]]	5.67 ± 0.06	6.3[c[7]]
4.03	9.47 ± 0.04	9.6[b] 9.3[c[1]]; 8.6[c[9]]	7.11 ± 0.06	7.4[b] 7.3 − 8.3[c[1, 4-7]]	6.91 ± 0.01	6.8[c[7]]
4.04	n.d.	-	8.38 ± 0.05	7.9[b] 7.2 − 8.4[c[1-7]]	7.93 ± 0.05	6.9[c[7]] *7.6* (-0.23)[d]
4.05	7.36 ± 0.06	7.3[b] 7.4[c[1]]; 7.3[c[9]]	6.81 ± 0.08	7.2[b] 6.3 − 7.6[c[1-7]]	7.18 ± 0.07	7.1[c[7]]
4.06	n.d.	-	7.92 ± 0.08	7.9[c[3]]	7.51 ± 0.05	**9.0** (0.93)[d] **7.3** (0.74)[e]
4.07	9.27 ± 0.02	8.5[c[8]]	8.93 ± 0.07	8.3[c[3]]	8.91 ± 0.05	**9.6** (0.77)[d] **7.9** (0.58)[e]

[a]Data from BRET-based competition binding experiments (pK_i) with **4.26** for H₃,₄R ligands, determined at the NLuc-hH₃R, NLuc-hH₄R or NLuc-mH₄R, stably expressed in intact HEK293T cells. The pK_i values represent means ± SEM and were determined in 4 – 5 independent experiments, each performed in triplicate. [b]Data taken from Mocking et al., determined by BRET-based competition binding experiments with clobenpropit-BODIPY-630/650 at the NLuc-hH₃R or NLuc-hH₄R, transiently expressed in intact HEK293T cells[20]. [c]Data from radioligand competition binding experiments with [1] [³H]**4.02**, [2-6] [³H]**4.01**, [7] [³H]**4.06**, or [8,9] [³H]Nα-methylhistamine performed on: [1] membrane preparations of *Sf*9 insect cells, stably expressing the hH₃R + Gα$_{i2}$ + Gβ₁γ₂ + RGS4 or the hH₄R-RGS19 fusion protein + Gα$_{i2}$ + Gβ₁γ₂[12], [2] membrane preparations of *Sf*9 insect cells, stably expressing the hH₄R-RGS19 fusion protein + Gα$_{i2}$ + Gβ₁γ₂[10], [3] membrane preparations of *Sf*9 insect cells, stably expressing the hH₄R + Gα$_{i2}$ + Gβ₁γ₂[11,16,36,43], [4] homogenates of SK-N-MC-cells, stably expressing the hH₄R[13], [5] membranes from SK-N-MC cells, stably expressing the hH₄R[15,44,45] , [6] homogenates of HEK293T cells expressing the hH₄R[46], [7] homogenates of HEK293T-SF-His6-CRE-Luc cells, stably expressing the hH₄R or mH₄R[16], [8] membrane preparations of *Sf*9 insect cells, stably expressing the hH₃R + Gα$_{i2}$ + β₁γ₂[16], or [9] homogenates of SK-N-MC-cells, stably expressing the hH₃R[13]. [d]Data from luciferase reporter gene assays, using HEK293T-SF-mH₄R-His6-CRE-Luc cells[16,38]. [e]Data from β-arrestin2 recruitment assays, using HEK293T-β-arr2-mH₄R cells[16].

4.3 Conclusion

Here we report on the discovery and the comprehensive characterization of a set of Py-5 labeled histamine derivatives as fluorescent probes for the hH₃R and the h/mH₄Rs. Radioligand binding studies revealed high affinities in the sub- to the two-digit-nM range at the hH₃,₄Rs, especially for UR-DEBa242 (**4.26**) and **4.27**. Additionally, in luciferase reporter gene and β-arrestin recruitment assays, potencies or antagonistic activities in the one- to the three-digit-nM range for UR-DEBa242 (**4.26**, hH₃R-partial agonist; hH₄R-inverse agonist; mH₄R-inverse agonist/antagonist) and **4.27** (hH₃R-antagonist; hH₄R-partial agonist; mH₄R-antagonist) were obtained. Molecular dynamics simulations with **4.26** at the hH₄R suggested interactions of the pyridinium moiety with the orthosteric binding pocket. Since **4.26** showed the highest affinity to the hH₄R in this series, confocal microscopy experiments were performed and proved it a suitable probe for staining the hH₄R in live cells. Comprising ideal optical properties as a BRET acceptor for NLuc, **4.26** enables robust and comparative BRET-based binding studies at the NLuc-hH₃R and NLuc-h/mH₄Rs [pK_d = 8.78, 7.75, 7.18, respectively; fast association/dissociation kinetics (approx. 2 min)]. By applying **4.26** to flow cytometry, binding constants in the two-digit-nM range at the NLuc-h/mH₄Rs could be confirmed. With **4.26**, we present an easy-to-synthesize, comprehensively characterized and multipurpose fluorescent probe for the H₃,₄Rs. Compound **4.26** constitutes a useful molecular tool for hH₄R localization and trafficking studies using confocal microscopy and can therefore contribute to investigations with regard to the expression of the H₄R in distinct cells or potentially even in tissue, which is currently highly controversially discussed in the scientific community. Additionally, allowing investigations on ligand-receptor interactions and the characterization of novel molecular tools or potential drug candidates in BRET-based binding assays at the H₃,₄Rs, **4.26** represents a valuable complementary tool to radioligands. Moreover, as the first fluorescent probe described for the mH₄R, **4.26** enables pharmacological investigations on the H₄R with regard to translational animal models.

4.4 Experimental section

4.4.1 General experimental conditions

Chemicals and solvents were purchased from Acros Organics B.V.B.A (Geel, Belgium), Alfa Aesar & Co. KG (Karlsruhe, Germany), Merck KGaA (Darmstadt, Germany), Sigma-Aldrich Chemie GmbH (Taufkirchen, Germany), TCI Deutschland GmbH (Eschborn, Germany) and Tocris Bioscience (Bristol, UK) and were used without further purification. All solvents were purchased in analytical grade or were distilled prior to use and stored over molecular sieves (4 Å). Acetonitrile for HPLC (gradient grade) was obtained from Merck KGaA (Darmstadt, Germany). Millipore water was used for the preparation of HPLC eluents. Deuterated solvents for nuclear magnetic resonance (NMR) spectroscopy were obtained from Deutero GmbH (Kastellaun, Germany). For column chromatography, Merck silica gel 60 (0.040 – 0.063 mm) was used. Flash chromatography was performed on an Intelli Flash-310 Flash-Chromatography Workstation from Varian Deutschland GmbH (Darmstadt, Germany). Reaction controls were performed using thin-layer chromatography (TLC) on Merck silica gel 60 F_{254} TLC aluminum sheets and the visualization was realized by UV radiation (λ = 254 or 310 nm) and staining with ninhydrine or vanillin solutions. For microwave driven reactions, a Biotage Initiator microwave synthesizer (Biotage AB, Uppsala, Sweden) was used. NMR spectra were recorded on a Bruker Avance 300 (7.05 T, ^{1}H 300 MHz), Bruker Avance III HD 400 (9.40 T, ^{1}H 400 MHz; ^{13}C 101 MHz) or Bruker Avance III HD 600 equipped with a cryogenic probe (14.1 T, ^{1}H 600 MHz) (Bruker BioSpin GmbH, Karlsruhe, Germany) with tetramethylsilane (TMS) as an external standard. Multiplicities are specified with the following abbreviations: s (singlet), d (doublet), t (triplet), q (quartet), qui (quintet) m (multiplet), br (broad signal), quat. (quaternary carbon atom). The coupling constants (J values) are given in hertz (Hz). High-resolution mass spectrometry (HRMS) analysis was performed on an Agilent 6540 UHD Accurate-Mass Q-TOF LC/MS system (Agilent Technologies, Santa Clara, CA, USA) using an ESI source. Melting points (mp) were determined (if applicable) on a Büchi B-540 (Büchi GmbH, Essen, Germany) and were uncorrected. Preparative HPLC was performed on a Knauer device (Berlin, Germany) equipped with two K-1800 pumps and a K-2001 detector. A Phenomenex Kinetex 5u XB-C18 (250 × 21.2 mm) with a flow rate of 15 or 20 mL/min was used as a stationary phase. Mixtures of 0.1% TFA (B) and MeCN (A) were used as the mobile phase.

The detection wavelength was set to 220 nm. The solvent of the collected fractions was removed by lyophilization using an Alpha 2-4 LD apparatus (Martin Christ GmbH, Osterode am Harz, Germany) equipped with an RZ 6 rotary vane vacuum pump (Vacuubrand GmbH & Co KG, Wertheim, Germany). For all target compounds, 5 mM stock solutions were prepared in dimethyl sulfoxide (DMSO) and stored in aliquots (10 µl) in thin-walled tubes with a flat cap (0.2 mL, PEQL 82-0620-A, VWR Life Science Competence Center, Erlangen, Germany) at -80 °C. Analytical HPLC analysis was performed with a system from Agilent Technologies (Series 1100) composed of a binary pump equipped with a degasser (G1312A), an autosampler (ALS, G1329A), a thermostated column compartment (COLCOM, G1316A) and a diode array detector (DAD, G1315B). A Phenomenex Kinetex-XB C18 (2.6 µm, 100 mm × 3 mm) was used as the stationary phase at a flow rate of 0.8 mL/min. Mixtures of 0.5% TFA (A) and MeCN + 0.5% TFA (B) served as the mobile phase. The following linear gradient was applied throughout: A/B (*v/v*) 0 – 30 min, 90/10 – 10/90; 30 – 33 min, 10/90 – 5/95; 33 – 40 min, 5/95. For all analytical runs, the oven temperature was set to 30 °C, and the detection was performed at 220 nm. The injection volume was 60 µL of a 100 µM solution (5 mM stock solution diluted with starting eluent, A/B 90/10). The retention (capacity) factor (k) was calculated based on the determined retention time (t_R) according to $k = (t_R - t_0)/t_0$ (t_0 = dead time = 3.21 min).

4.4.2 Compound characterization

All synthesized compounds were characterized by HRMS and melting points (if applicable). Additionally, the intermediates **4.19**, **4.20**, **4.22**, **4.23**, **4.35** – **4.39**, **4.41**, **4.42**, **4.44** and **4.46** were characterized by ^{1}H- and ^{13}C-NMR spectroscopy. The pyrylium dye **4.10** and, as representatives of the target fluorescent probes, **4.26** and **4.29** were characterized by ^{1}H-NMR spectroscopy (for ^{1}H-NMR spectra of **4.26** and **4.29,** see Figure A 4.7 and Figure A 4.8 in section 4.5.7.1). The purity of the fluorescent probes (**4.24 – 4.29**) was > 95% throughout, determined by RP-HPLC (220 nm) (chromatograms see Figure A 4.9 – Figure A 4.12 in section 4.5.7.2). For **4.26**, as representative of the herein presented fluorescent probes, the excitation/emission maxima, the absorption coefficients, and the quantum yields were determined in PBS and in PBS + bovine serum albumin (BSA, 1%) at 22 °C (Table A 4.1 in section 4.5.2.2).

4.4.3 Synthesis of the target compounds (4.24 – 4.29)

<u>General procedure</u>

The respective amine precursors (1 equiv) and *N,N*-diisopropylethylamine (DIPEA, 15 – 20 equiv) were dissolved in dimethylformamide (DMF, dry). The pyrylium dye **4.10** (0.75 – 2 equiv) was dissolved in DMF (dry) (600 μL) and added gradually (3 × 200 μL, every 15 min) to the reaction. The reaction in the dark was stopped by the addition of TFA after stirring at rt for 1.5 – 2 h. The reaction mixture was diluted with MeCN/0.1% TFA 5/95 (*v/v*) and the product was purified by preparative HPLC.

1-[2-(1*H*-Imidazol-4-yl)ethyl]-4-{(1*E*,3*E*)-4-[4-(dimethylamino)phenyl]buta-1,3-dienyl}-2,6-dimethylpyridinium hydrotrifluoroacetate trifluoroacetate (4.24). 4.01 · 2 HCl (5.0 mg, 27 μmol), DIPEA (72.0 μL, 413 μmol), **4.10** (20.0 mg, 54.5 μmol), DMF (0.4 mL), TFA (0.4 mL), MeCN/0.1% TFA 5/95 (5 mL). Yield: 70.7% (11.46 mg); preparative HPLC [gradient: 0 – 30 min: A/B (*v/v*) 10/90 – 43/57, flow 20 mL/min, t_R = 15 min]. RP-HPLC (220 nm): 98.3% (k = 2.52). HRMS (ESI): *m/z* [*M*]⁺ calcd for [$C_{24}H_{29}N_4$]⁺ 373.2387, found 373.2390. $C_{24}H_{29}N_4^+ \cdot C_4HF_6O_4^-$ (373.52 + 227.04).

1-[3-(1*H*-Imidazol-4-yl)propyl]-4-{(1*E*,3*E*)-4-[4-(dimethylamino)phenyl]buta-1,3-dienyl}-2,6-dimethylpyridinium hydrotrifluoroacetate trifluoroacetate (4.25). 4.19 · 2 TFA (3.0 mg, 8.5 μmol), DIPEA (30.0 μL, 172 μmol), **4.10** (6.2 mg, 17 μmol), DMF (0.2 mL), TFA (0.2 mL), MeCN/0.1% TFA 5/95 (3 mL). Yield: 62.0% (3.24 mg); preparative HPLC [gradient: 0 – 30 min: A/B (*v/v*) 10/90 – 43/57, flow 20 mL/min, t_R = 15 min]. RP-HPLC (220 nm): 99.1% (k = 2.63). HRMS (ESI): *m/z* [*M*]⁺ calcd for [$C_{25}H_{31}N_4$]⁺ 387.2543, found 387.2546. $C_{25}H_{31}N_4^+ \cdot C_4HF_6O_4^-$ (387.55 + 227.04).

1-[4-(1*H*-Imidazol-4-yl)butyl]-4-{(1*E*,3*E*)-4-[4-(dimethylamino)phenyl]buta-1,3-dienyl}-2,6-dimethylpyridinium hydrotrifluoroacetate trifluoroacetate (4.26). 4.20 · 2 TFA (18.0 mg, 49.0 μmol), DIPEA (171 μL, 982 μmol), **4.10** (22.0 mg, 59.9 μmol), DMF (0.8 mL), TFA (0.6 mL), MeCN/0.1% TFA 5/95 (6 mL). Yield: 22.8% (7.01 mg); preparative HPLC [gradient: 0 – 30 min: A/B (*v/v*) 10/90 – 43/57, flow 20 mL/min, t_R = 16.5 min]. RP-HPLC (220 nm): 96.4% (k = 2.83). ¹H-NMR (600 MHz, DMSO-*d₆*): δ (ppm) 14.24 (br, 2H), 8.96 (s, 1H), 7.85 (s, 2H), 7.69 (m, 1H),

7.45 (m, 3H), 7.00 (m, 2H), 6.71 (d, J = 8.9 Hz, 2H), 6.57 (d, J = 15.2 Hz, 1H), 4.34 (t, J = 7.4 Hz, 2H), 2.97 (s, 6H), 2.75 (s, 6H), 2.72 (m, 2H), 1.78 (m, 4H). HRMS (ESI): m/z [M]$^+$ calcd for [$C_{26}H_{33}N_4$]$^+$ 401.2700, found 401.2701. $C_{26}H_{33}N_4^+ \cdot C_4HF_6O_4^-$ (401.58 + 227.04).

1-[5-(1H-Imidazol-4-yl)pentyl]-4-{(1E,3E)-4-[4-(dimethylamino)phenyl]buta-1,3-dienyl}-2,6-dimethylpyridinium hydrotrifluoroacetate trifluoroacetate (4.27). 4.21 · 2 HBr (10.0 mg, 31.7 µmol), DIPEA (85.0 µL, 488 µmol), **4.10** (11.7 mg, 31.9 µmol), DMF (0.2 mL), TFA (0.2 mL), MeCN/0.1% TFA 5/95 (3 mL). Yield: 19.4% (3.96 mg); preparative HPLC [gradient: 0 − 30 min: A/B (v/v) 10/90 − 48/52, flow 20 mL/min, t_R = 17 min]. RP-HPLC (220 nm): 95.7% (k = 3.05). HRMS (ESI): m/z [M]$^+$ calcd for [$C_{27}H_{35}N_4$]$^+$ 415.2856, found 415.2862. $C_{27}H_{35}N_4^+ \cdot C_4HF_6O_4^-$ (415.60 + 227.04).

1-(3-{[2-(1H-Imidazol-4-yl)ethyl]amino}propyl)-4-{(1E,3E)-4-[4-(dimethylamino)phenyl]buta-1,3-dienyl}-2,6-dimethylpyridinium bis(hydrotrifluoroacetate) trifluoroacetate (4.28). 4.22 (5.0 mg, 9.8 µmol), DIPEA (34.0 µL, 195 µmol), **4.10** (2.9 mg, 7.9 µmol), DMF (0.2 mL), TFA (0.2 mL), MeCN/0.1% TFA 5/95 (3 mL). Yield: 27.6% (1.68 mg); preparative HPLC [gradient: 0 − 30 min: A/B (v/v) 10/90 − 34/66, flow 20 mL/min, t_R = 16 min]. RP-HPLC (220 nm): 95.1% (k = 2.29). HRMS (ESI): m/z [M]$^+$ calcd for [$C_{27}H_{36}N_5$]$^+$ 430.2965, found 430.2969. $C_{27}H_{36}N_5^+ \cdot C_6H_2F_9O_6^-$ (430.62 + 341.06).

1-{3-(3,4,6,7-Tetrahydro-5H-imidazo[4,5-c]pyridin-5-yl)propyl}-4-{(1E,3E)-4-[4-(dimethylamino)phenyl]buta-1,3-dienyl}-2,6-dimethylpyridinium bis(hydrotrifluoroacetate) trifluoroacetate (4.29). 4.23 (5.0 mg, 9.6 µmol), DIPEA (34.0 µL, 195 µmol), **4.10** (7.1 mg, 19 µmol), DMF (0.2 mL), TFA (0.2 mL), MeCN/0.1% TFA 5/95 (3 mL). Yield: 39.6% (2.98 mg); preparative HPLC [gradient: 0 − 30 min: A/B (v/v) 10/90-43/57, flow 20 mL/min, t_R = 13.5 min]. RP-HPLC (220 nm): 98.9% (k = 2.27). ^{1}H-NMR (600 MHz, DMSO-d_6): δ (ppm) 8.62 (br, 1H), 7.86 (s, 2H), 7.71 (m, 1H), 7.46 (d, J = 8.9 Hz, 2H), 6.99 (m, 2H), 6.72 (d, J = 9.0 Hz, 2H), 6.59 (d, J = 15.3 Hz, 1H), 4.39 (t, J = 8.2 Hz, 2H), 4.03 (br, 2H), 3.99 − 3.33 (3 protons superimposed by H₂O peak), 3.20 (br, 4H), 2.97 (s, 6H), 2.85 (m, 2H), 2.77 (s, 6H), 2.15 (m, 2H). HRMS (ESI): m/z [M]+ calcd for [$C_{28}H_{36}N_5$]$^+$ 442.2965, found 442.2970. $C_{28}H_{36}N_5^+ \cdot C_6H_2F_9O_6^-$ (442.63 + 341.06).

4.4.4 Chemical stability

The chemical stability of **4.26** was investigated in PBS (pH 7.4) at 23 °C over 5 or 6 h (maximum incubation time in the applied assays). For this purpose, dilutions of **4.26** (200 µM) in PBS (stock solution of **4.26**: 5 mM in DMSO) were prepared and incubated in flat bottomed 96-well plates [(**A**) Primaria™, REF 353872, surface modified polystyrene, Corning Inc., NY, USA and (**B**) cellGrade™, REF 781965, surface modified polystyrene, Brand GmbH & Co. KG, Wertheim, Germany], 1.5-mL microtubes [(**C**) SafeSeal, REF 72.690.001, polypropylene, Sarstedt AG & Co. KG, Nümbrecht, Germany] and 1.5-mL microtubes [(**D**) SafeSeal microtubes] treated with Sigmacote® (SL2, Sigma-Aldrich Chemie GmbH, Taufkirchen, Germany) according to the supplier suggested protocol. After 0, 1, 3 and 5 or 6 h, 100 µL of this solution was added to 100 µL of MeCN/0.5% TFA 10/90 (*v/v*). This solution was analyzed by RP-HPLC (injection volume: 90 µL; for conditions for analytical HPLC, see section 4.4.1; for graphs see Figure A 4.13 – Figure A 4.16 in section 4.5.7.3).

4.4.5 Radioligand competition binding

Radioligand competition binding experiments on membrane preparations of *Sf*9 insect cells, expressing the $hH_1R + RGS4$, $hH_2R\text{-}Gs_{\alpha s}$, $hH_3R + G\alpha_{i2} + \beta_1\gamma_2$ or $hH_4R + G\alpha_{i2} + \beta_1\gamma_2$, were essentially performed as described in chapter 3[16] (section 3.4.7), with the following modifications: the experiments were performed in Primaria™ plates (Corning Inc., NY, USA) in a total volume of 100 µL, containing 5 µg (hH_4R), 11 µg (hH_3R), 15 µg (hH_2R) and 28 µg (hH_1R) of soluble membrane protein and 0.2% BSA (bovine serum albumin). The used radioligands are as follows:

H_1R: [³H]pyrilamine (c_{final} = 5 nM, specific activity 20.0 Ci/mmol, K_d = 4.5 nM[47], Hartmann Analytics GmbH, Braunschweig, Germany).

hH_2R: [³H]UR-DE257[37] [resynthesized by Dr. Sabrina Biselli (data not published): c_{final} = 20 nM, specific activity 33.0 Ci/mmol, K_d = 12.1 nM].

hH_3R: [³H]UR-PI294[12] ([³H]**4.02**) (c_{final} = 2 nM, specific activity 93.3 Ci/mmol, K_d = 1.1 ± 0.2 nM).

hH_4R: [³H]histamine ([³H]**4.01**) (c_{final} = 40 nM, specific activity 25.0 Ci/mmol, K_d = 45 nM, Biotrend Chemikalien GmbH, Köln, Germany).

For data analysis, total binding [in disintegrations per minute (dpm)] was plotted versus log(concentration competitor) and normalized [1.0 = bound radioligand (dpm) in the absence of competitor, 0.0 = nonspecifically bound radioligand (dpm) in the presence of **4.01** (c$_{final}$ = 10 µM, hH$_{3,4}$Rs), diphenhydramine (c$_{final}$ = 10 µM, hH$_1$R) or famotidine (c$_{final}$ = 1 mM, hH$_2$R)]. Applying a four-parameter logistic equation [log(inhibitor) versus response-variable slope] (GraphPad Prism Software 8.1, GraphPad Software Inc., San Diego, CA, USA), pIC$_{50}$ values were obtained. The pK_i values were calculated based on the Cheng-Prusoff equation[39].

4.4.6 Luciferase reporter gene assay

Luciferase reporter gene assays at the hH$_3$R or mH$_4$R were performed using a cell lysis-based technique, such as described in chapter 3[16] (section 3.4.8). For the hH$_4$R, the procedure was modified due to weak adherence of the cells and was performed on live cells to avoid handling issues. The generation and cultivation of HEK293T-SF-hH$_4$R-His6-CRE-Luc or HEK293T-SF-mH$_4$R-His6-CRE-Luc cells were described in chapter 3[16] (section 3.4.6). A pronounced signal depletion was observed in the presence of high concentrations (> 1 µM) of the fluorescent ligands during the bioluminescence readout in the case of the hH$_4$R or the mH$_4$R (Figure A 4.2 in section 4.5.3), which made correctional calculations necessary (Figure A 4.3 and Figure A 4.4 in section 4.5.4). To avoid such an interference at the hH$_3$R, the firefly luciferase (Luc, λ$_{max}$ = 560 nm[48]), previously used as a reporter, was replaced by a red light-emitting luciferase from the click beetle *Pyrophorus plagiophthalamus* (CBR, λ$_{max}$ = 613 nm[49]). This led to a better separation of the emission spectrum of the luciferase from the excitation spectrum of the fluorophore. These cells were generated as follows: the pIRESneo3-SP-FLAG-hH$_3$R construct was prepared by replacing the hH$_4$R sequence in the pIRESneo3-SP-FLAG-hH$_4$R vector (see section 4.4.8) by the sequence of the hH$_3$R (cDNA Resource Center, Rolla, MO, USA) using the PCR protocol for Q5® Hot Start High-Fidelity DNA Polymerase and the NEBuilder HiFi DNA Assembly Reaction Protocol (New England Biolabs GmbH, Frankfurt/Main, Germany). The quality of the vector was controlled by sequencing (Eurofins Genomics GmbH, Ebersberg, Germany). As described for the HEK293T-SP-FLAG-hH$_4$R (see section 4.4.8), a stable HEK293T-SP-FLAG-hH$_3$R cell line was generated. The best clone in terms of receptor expression (HEK293T-SP-FLAG-hH$_3$R K16) was selected and cells were stably co-transfected with the pGL4.29 vector encoding the cAMP response element (CRE) and CBR according to the

procedure described for the generation of HEK293T-SP-FLAG-hH₄R (see section 4.4.8). The selection occurred in the presence of 600 µg/mL hygromycin B (MoBiTec GmbH, Göttingen, Germany) until stable growth was observed. These cells were further used as a polyclonal HEK293T-SP-FLAG-hH₃R-CRE-CBR cell line.

The luciferase reporter gene assay was carried out as follows: cells were seeded [1.8×10^5 (hH₃R), 0.8×10^5 (hH₄R) and 1.6×10^5 (mH₄R) cells per well (160 µL)] into white 96-well cell-Grade™ plates (Brand & Co. KG, Wertheim, Germany), using Dulbecco's modified eagle's medium (DMEM, Sigma-Aldrich Chemie GmbH, Taufkirchen, Germany) without phenol red supplemented with 5% (*v/v*) fetal calf serum FCS (Biochrom GmbH, Berlin, Germany). Forskolin was used in a final concentration of 1 µM (hH₃R, mH₄R) or 0.5 µM (hH₄R). After the incubation for 5 h [humidified atmosphere (95% air, 5% CO₂, 37 °C)], for the hH₃R and mH₄R[16] the lysis-based technique was followed. Bioluminescence was measured for 1 s per well using the GENios Pro microplate reader, the TECAN InfiniteLumi plate reader (Tecan GmbH, Grödig/Salzburg, Austria) or the EnSpire multimode reader (Perkin Elmer, Rodgau, Germany).

For the hH₄R, after incubation for 5 h [humidified atmosphere (95% air, 5% CO₂, 37 °C)], 20 µL of a solution of D-luciferin monopotassium salt (Fisher Scientific GmbH, Schwerte, Germany) in DMEM (5% FCS) (c_{final} = 1 mM) were added to each well (total volume: 220 µL per well). Live cells were incubated for an additional 30 min in a humidified atmosphere (95% air, 5% CO₂, 37 °C), before bioluminescence was measured at 37 °C for 1 s per well with a TECAN InfiniteLumi plate reader (Tecan Austria GmbH, Grödig/Salzburg, Austria).

Data from agonist mode were processed as described in chapter 3[16] (section 3.4.8). For (inverse) agonists, the normalized data were analyzed by applying four-parameter logistic equations [log(x) versus response – variable slope, x = agonist or inhibitor] (GraphPad Prism 8.1) to obtain pEC_{50} or pIC_{50} values.

For the antagonist mode, cells were pre-incubated with solutions containing different concentrations of the respective antagonist for 15 min, before forskolin (c_{final} = 1 µM for hH₃R or mH₄R), supplemented with histamine **4.01** (c_{final} = 30 nM for hH₃R, 300 nM for mH₄R), was added. Data from antagonist mode were processed by plotting the relative light units (RLUs) vs log (concentration antagonist) followed by normalization (0.0 = induced change in forskolin-stimulated luciferase activity caused by 30 nM or 300 nM of **4.01**;

1.0 = forskolin-stimulated luciferase activity) and transformation steps (standard function: Y = 1.0 − Y). Data analysis was performed applying a four-parameter logistic equation [log(antagonist) versus response − variable slope, GraphPad Prism 8.1] to obtain pIC_{50} values. The pK_b values were calculated based on the Cheng-Prusoff equation[39].

4.4.7 β-Arrestin2 recruitment assay

The recruitment of β-arrestin2 was measured via split-luciferase complementation as described in chapter 3[16] (section 3.4.9) in white 96-well cell-Grade™ plates (Brand & Co. KG, Wertheim, Germany). Data from agonist mode were processed as described[16]. In the antagonist mode, cells were incubated with the solutions containing the antagonist for 15 min, before a solution of histamine (**4.01**) in H_2O (c_{final} = 10 µM for mH₄R) was added. Data from antagonist mode were processed by plotting the RLUs vs log(concentration antagonist) followed by a normalization step (1.0 = β-arrestin2 recruitment caused by 10 µM of **4.01**, 0.0 = basal activity). The normalized data were analyzed by applying a four-parameter logistic equation [log(inhibitor) versus response − variable slope] (GraphPad Prism 8.1) to obtain pIC_{50} values. The pK_b values were calculated according to the Cheng-Prusoff equation[39]. Due to the emission spectrum of the emerald luciferase (ELuc) employed in this assay, which has its maximum at 538 nm[50], an interference of the pyridinium fluorophore was observed during readout for this assay as well. Effects were observed for > 1 µM concentrations of the fluorescent ligands (Figure A 4.2 in section 4.5.3), assessed and subsequently corrected (Figure A 4.3 and Figure A 4.4 in section 4.5.4).

4.4.8 Confocal microscopy

For the generation of the HEK293T-SP-FLAG-hH₄R cells, the pIRESneo3-SP-FLAG-hH₄R vector had to be constructed first. The pcDNA3.1 vector encoding the human H₄R sequence (hH₄R) was from the cDNA Resource Center (Rolla, MO, USA). The pIRESneo3 vector was a gift from Prof. G. Meister (Institute of Biochemistry, Genetics and Microbiology, University of Regensburg, Germany). The hH₄R was N-terminally fused to the membrane signal peptide (SP) of the murine 5-HT₃ₐ receptor and tagged with codon-optimized FLAG-tag using the PCR Protocol for Phusion® Hot Start Flex DNA Polymerase (New England Biolabs GmbH, Frankfurt/Main, Germany) and cloned into pcDNA3.1 according to the NEBuilder HiFi DNA

Assembly Reaction Protocol (New England Biolabs GmbH). Afterward, the SP-FLAG-hH₄R construct was subcloned into the pIRESneo3 vector via a standard restriction endonuclease reaction using NheI-HF and NotI-HF restriction enzymes (New England Biolabs GmbH) yielding the pIRESneo3-SP-FLAG-hH₄R vector. The quality of the vector was controlled by sequencing (Eurofins Genomics GmbH, Ebersberg, Germany).

The stable HEK293T-SP-FLAG-hH₄R cells were generated as follows: the day before transfection HEK293T-wt (wild-type) cells were seeded into a 6-well plate (Sarstedt AG & Co. KG, Nümbrecht, Germany) at a density of 7.5×10^5 cells/well. The cells were transfected with the respective vector using XtremeGENE™ HP (Roche Diagnostics GmbH, Mannheim, Germany) according to the manufacturer's instructions. Two days after transfection, the cells were detached by trypsinization and seeded into a 150 mm-culture dish (Thermo Fisher Scientific, Dreieich, Germany) in DMEM containing 10% FCS. The cells were allowed to attach for 1 day, before geneticin (G418, Biochrom GmbH, Berlin, Germany) was added at a final concentration of 1 mg/mL. The medium was changed regularly, until cell colonies became visible. Subsequently, the colonies were isolated individually into a 12-well plate (Sarstedt AG & Co. KG, Nümbrecht, Germany) and cultured in growth medium containing 600 µg/mL G418, until each clone was screened for the best signal in a DMR assay as described previously[51] with minor modifications: After seeding the cells into the label-free 384-well plate, the incubation period was extended to 48 h until the cell layer reached a confluency of approx. 90%. The assay temperature was set to 28 °C (instead of 37 °C) and the response to **4.01** (c_{final} = 100 µM) was recorded for 60 min. The best clone in terms of receptor expression (HEK-SP-FLAG-hH₄R K3) was selected for further experiments.

Two days prior to the confocal microscopy experiment, a sterile ibiTreat 15 µ-slide chamber with 8 wells (Ibidi GmbH, Martinsried, Germany) was coated with Poly-D-Lysin hydrobromide (Sigma-Aldrich Chemie GmbH, Taufkirchen, Germany) according to the supplier's protocol. After washing once with sterile-filtered PBS (300 µL), the chamber was allowed to dry at rt for 60 min. The HEK293T-wt or HEK293T-SP-FLAG-hH₄R cells were detached from a 75-cm² flask by treatment with trypsin/ethylenediaminetetraacetic acid (EDTA) (0.05%/0.02%), centrifuged ($500 \times g$, 5 min) and resuspended in Leibovitz' L-15 + 5% FCS + 10 mM 2-[4-(2-hydroxyethyl)piperazin-1-yl]ethanesulfonic acid (HEPES) and adjusted to

2.66×10^5 cells/mL. In the ibiTreat chamber, 8.0×10^4 cells/well (300 µL) were seeded and incubated for 2 days in a humidified atmosphere (37° C, no CO_2). On the day of the experiment, confluency of the cells was 50 – 70%. Then, 100 µL of the medium was removed from each well.

The working solutions (A – D) of **4.26** and/or **4.05** were prepared from the respective stock solutions (see section 4.4.1) immediately before conducting experiments:

Solution A: **4.26** (600 nM) in L-15 + 5% FCS + 10 mM HEPES

Solution B: **4.26** (800 nM) in **4.05** (20 µM, L-15 + 5% FCS + 10 mM HEPES

Solution C: **4.05** (60 µM) in L-15 + 5% FCS + 10 mM HEPES

Solution D: **4.05** (80 µM) in **4.26** (200 nM, in L-15 + 5% FCS + 10 mM HEPES)

A total of 100 µL of the working solutions (A – D) were added per well of the ibiTreat chamber to reach final volumes of 300 or 400 µL. For total binding/association, **4.26** (c_{final} = 200 nM, working solution A) was added to HEK293T-SP-FLAG-hH₄R cells after recording for 16 s. For nonspecific binding, **4.26** was either added to HEK293T-SP-FLAG-hH₄R cells (**4.26**: c_{final} = 200 nM, working solution B), preincubated with **4.05** (c_{final} = 20 µM, working solution C) for 10 min, or to HEK293T-wt cells (**4.26**: c_{final} = 200 nM, working solution A) after recording for 16 s. For dissociation of **4.26** from the hH₄R, **4.05** (c_{final} = 20 µM, working solution D) was added to HEK293T-SP-FLAG-hH₄R cells after recording association of **4.26** (c_{final} = 200 nM, working solution A) for 5.07 min. Movies were acquired with a Zeiss Axiovert 200 M microscope, equipped with an LSM 510 laser scanner (Carl Zeiss Microscopy GmbH, Oberkochen, Germany), in the dark at rt with an oil immersion objective (Plan-Apochromat, 63 ×, NA 1.4). The following settings were used for the detection of **4.26**: excitation, 488 nm (10% laser transmissivity); emission, > 560 nm, long pass filter; pinhole, 170 µm; frame rate, 3.75 (16 s per image). Data from confocal microscopy were processed with the Carl Zeiss Zen 2.1 and the ImageJ 1.52i[52] software.

4.4.9 BRET-based binding assay

For the cloning of the plasmids, the cDNAs encoding the hH₃R or hH₄Rs were purchased from the Missouri cDNA resource center (Rolla, MO, USA). The plasmid pcDNA3.1 SF-mH₄R-His₆[38] was used as a template for the cDNA encoding the mH₄R. The H₄ receptor sequences were

amplified using standard PCR techniques, introducing a *Bam*HI restriction site at their 5'- and an *Apa*I restriction site at their 3'-ends, and cloned into the pcDNA3.1/myc-HIS (B) vector backbone. The plasmid encoding NLuc was provided by Promega GmbH (Mannheim, Germany) and used as a template to generate the following sequence: *Hind*III (5') and *Bam*HI (3') restriction sites as well as the membrane signal peptide of the murine 5HT$_{3A}$ receptor upstream from the luciferase gene were added to the ends of NLuc by PCR. This sequence was cloned into the vector backbone described above generating NLuc-hH$_4$R and NLuc-mH$_4$R constructs. The NLuc-hH$_3$R construct was generated by replacing the sequence encoding the h/mH$_4$Rs using NEBuilder® HiFi DNA Assembly Master Mix (New England Biolabs GmbH, Frankfurt/Main, Germany) after linearization of the vector, amplification of the hH$_3$R by PCR and restriction digest with *Dpn*I. All sequences were verified by sequencing (Eurofins Genomics GmbH, Ebersberg, Germany).

HEK293T-wt cells were cultivated in DMEM + 10% FCS in a water-saturated atmosphere containing 5% CO$_2$ at 37 °C and were regularly monitored for mycoplasma infection. For transfection, cells were seeded at a density of 3×10^5 cells/mL in a 6-well plate (Sarstedt AG & Co. KG, Nümbrecht, Germany). The following day, cells were transfected with 2 μg of cDNA using the XtremeGene HP transfection reagent (Roche Diagnostics GmbH, Mannheim, Germany). After 2 days of incubation in a humidified atmosphere (95% air, 5% CO$_2$, 37 °C), transfected cells were transferred to a 15 cm cell culture dish (Sarstedt AG & Co. KG, Nümbrecht, Germany) in DMEM + 10% FCS. Geneticin (G418, Biochrom GmbH, Berlin, Germany) was added at a final concentration of 1 mg/mL for selection. The medium was regularly exchanged until colonial growth could be observed. For maintaining the selected cells, the concentration of geneticin in the cell culture medium was reduced to 600 μg/mL.

For BRET-based binding assays, HEK293T cells, stably expressing the NLuc-GPCR fusion constructs, were grown to 80 – 90% confluency and detached from the respective flasks by treatment with trypsin/EDTA (0.05%/0.02%) for 5 min at 37 °C 1 day prior to the experiment. After centrifugation ($600 \times g$, 5 min), the cell pellet was resuspended in Leibovitz' L-15, + 5% FCS + 10 mM HEPES, and 1.0×10^5 cells/well were seeded in 70 μL (saturation and competition binding) or 80 μL (kinetic experiments) of the assay medium into white 96-well cell-Grade™ plates (Brand GmbH & Co. KG, Wertheim, Germany). The plates were then

incubated at 37 °C in a humidified atmosphere (no CO_2) overnight. For saturation binding experiments, serial dilutions (10-fold concentrated with regard to final concentrations) of the fluorescent probe (**4.26** or **4.27**) and **4.05** (300-fold excess over **4.26** or **4.27** for hH_3R, 100-fold excess over **4.26** or **4.27** for h/mH_4Rs, nonspecific binding) were prepared in L-15 + 2% BSA + 10 mM HEPES. Ten µL of diluted **4.26** or **4.27** and 10 µL of L-15 (total binding) or **4.05** (nonspecific binding) were added to the cells. After 30 min of incubation at 27 °C, 10 µL of the pre-diluted substrate furimazine (Promega GmbH, Mannheim, Germany) was added and measurement was started immediately. For competition binding experiments, increasing concentrations of the competitor (**4.01**, **4.03** – **4.07**) and one fixed concentration of **4.26** [c_{final} (hH_3R) = 5 nM, c_{final} (hH_4R) = 30 nM, c_{final} (mH_4R) = 100 nM] were added to the cells as described above. After incubation at 27 °C for 30 min and the addition of the substrate (see above), measurements were started. For kinetic measurements, 10 µL of L-15 (total binding) or **4.05** (300-fold excess over **4.26** for hH_3R or 100-fold excess over **4.26** for h/mH_4R, nonspecific binding) were added to the cells prior to the experiment. After the addition of the substrate (see above), the cells were incubated in the dark at 27 °C for 5 min before the measurement was started in well-mode. After one repeat, 50 µL of a 3-fold concentrated solution of **4.26** was added using the injector module of the plate reader and the association was measured for 5 min. Then, 50 µL of a 4-fold concentrated solution of **4.05** (300-fold excess over **4.26** for hH_3R or 100-fold excess over **4.26** for h/mH_4R) were added with the injector module to start dissociation and the measurement was continued for additional 5 min (hH_3R, mH_4R) or 10 min (hH_4R) respectively. All measurements were performed on a TECAN InfiniteLumi plate reader (Tecan Austria GmbH, Grödig/Salzburg, Austria) at 27 °C using a 460 ± 35 nm band-pass and > 610 nm long-pass filter with an integration time of 100 ms per data point for both channels. For the kinetic experiments with **4.26** at the hH_4R, integration times for both channels were increased to 200 ms per data point. For all experiments at the NLuc-hH_3R, integration time for the red channel was increased to 1000 ms per data point due to a markedly lower signal amplitude in comparison with the NLuc-hH_4R, keeping integration time for the blue channel at 100 ms per data point. BRET ratios were calculated by dividing the acceptor emission (red long-pass filter) by the donor luminescence (blue band-pass filter). For all experiments, specific binding was calculated by subtraction of nonspecific binding from total binding.

For saturation binding experiments, all values were baseline-corrected by subtracting a buffer control yielding the "corrected BRET ratio". Total and nonspecific binding data were fitted by the model "One site-total and nonspecific binding" (GraphPad Prism 8.1) using a hyperbolic curve fit for total binding and linear regression for nonspecific binding. Specific binding was fitted to the model "One site-specific binding". For each experiment, K_d values obtained from the specific binding were transformed into pK_d. Means and SEMs were calculated for the respective pK_d values.

For competition binding experiments, data were normalized to buffer control (0%) and a 100%-control only containing fluorescent ligand **4.26** (NLuc-hH₃R: c_{final} = 5 nM; NLuc-hH₄R: c_{final} = 50 nM; NLuc-mH₄R: c_{final} = 100 nM) in the absence of competitor. Normalized data was fitted applying a four-parameter logistic fit [log(inhibitor) vs response-variable slope] yielding pIC_{50} values. These were transformed into pK_i values using the Cheng-Prusoff equation[39].

For kinetic experiments, data were normalized to start values (0%) and the BRET ratio after reaching the plateau (100%) and a combined "association then dissociation" model was applied yielding estimates for association rate (k_{on}) and dissociation rate (k_{off}) constants. Kinetic dissociation constants K_d (kin) were calculated by dividing k_{off} by k_{on} and transformed into pK_d (kin) for every single experiment. The dissociation half-life of the fluorescent ligand **4.26** ($t_{1/2}$) was calculated for each experiment applying the equation $t_{1/2} = \ln(2)/k_{off}$. For pK_d (kin) and $t_{1/2}$, means were calculated, and errors were propagated using the Gaussian law of error propagation.

4.5 Appendix

4.5.1 Source or preparation of the intermediate compounds

The quatromethine pyrylium dye Py-5 (**4.10**) was synthesized in accordance to a previously described procedure[35] by a one-step reaction from **4.30** and **4.31** (commercially available) in MeOH (Scheme A 4.1).

Scheme A 4.1. Synthesis of 4.10
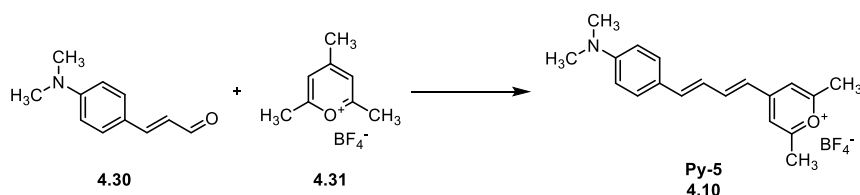
Reagents and conditions: MeOH, reflux, 10 min, 84.6%.

To obtain the Py-5 labeled target structures **4.24 – 4.29**, the amine precursors **4.19 · 2 TFA**, **4.20 · 2 TFA, 4.22** and **4.23** had to be prepared. Compounds **4.01 · 2 HCl** and **4.21 · 2 HBr** were purchased from TCI Tokyo and Tocris, respectively. Compound **4.32**[53] (Scheme A 4.2) was kindly provided by Dr. Patrick Igel.

Scheme A 4.2. Synthesis of 4.19 · 2 TFA
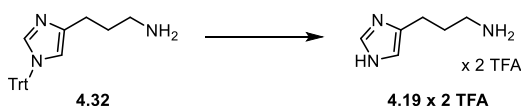
Reagents and conditions: TFA, DCM, rt, overnight, 72.6%.

The cleavage of the trityl group in **4.32** with TFA is depicted in Scheme A 4.2. Compound **4.19 · 2 TFA** was purified by preparative HPLC prior use in the labeling reaction with **4.10**.

Scheme A 4.3. Synthesis of 4.20 · 2 TFA

Reactions and conditions: (I) K$_2$CO$_3$, KI, DMF, 100 °C, 18 h, 73.2%; (II) urea, Br$_2$, MeOH, rt, 5 h, 43.1%; (III) formamide, 160 °C, 5 h, 41.3%; (IV) trityl chloride, TEA, MeCN, rt, overnight, 81.6%; (V) hydrazinium hydroxide, n-BuOH, rt, overnight, 100.8%; (VI) TFA, DCM, rt, 6 h, 58.6%.
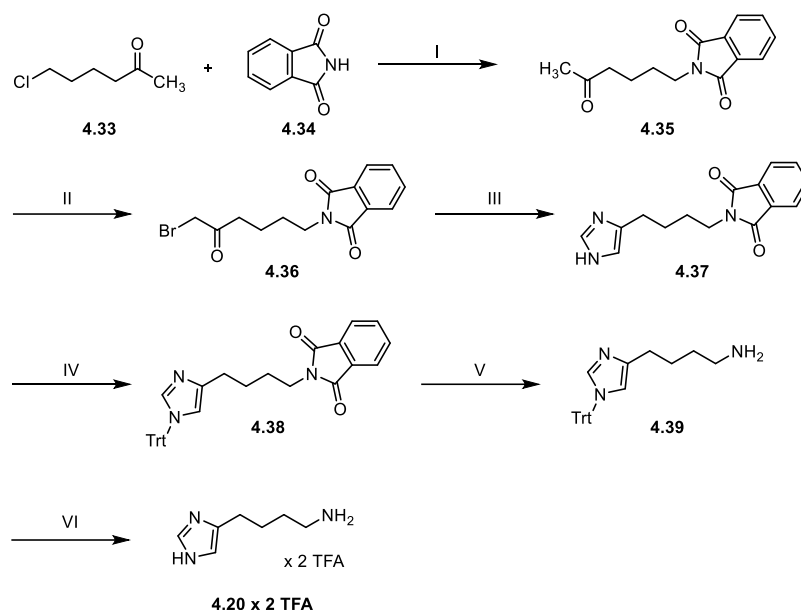
In Scheme A 4.3 the preparation of **4.20 · 2 TFA** is depicted. The synthesis started from a reaction of the commercially available 6-chlorohexan-2-one (**4.33**) and phthalimide (**4.34**) to obtain **4.35**.[53] The subsequent regioselective bromination of **4.35** afforded **4.36** by performing the reaction in MeOH and in the presence of urea.[53] In contrast to the published procedure[53], the formation of the imidazole in **4.37** was realized by using formamide instead of formamidine to react with the α-bromoketone **4.36** in a *Bredereck* synthesis (Scheme A 4.3). To afford the trityl- and phtaloyl-protected imbutamine **4.38**, the introduction of the trityl group in **4.37** was performed as reported for the histamine derivative in chapter 3[16] (section 3.5.1). Compound **4.38** was primarily synthesized for the use in different projects. The liberation of the primary amine in **4.38** was performed via *Ing-Manske* hydrazinolysis as a variation of the Gabriel synthesis, essentially as previously described[36] for histamine and imbutamine analogs. (Scheme A 4.3) After the cleavage of the trityl group in **4.39**, the imbutamine **4.20 · 2 TFA** was purified by preparative HPLC prior use in the labeling reaction with **4.10** (Scheme A 4.3).

Scheme A 4.4. Synthesis of 4.41 and 4.42
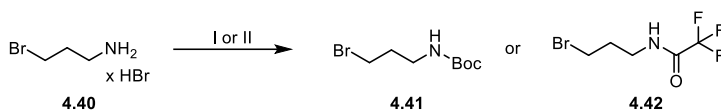
Reagents and conditions: (I) Boc anhydride, DIPEA, DCM, 0 → rt, 20 h, 88.8% (**4.41**); (II) trifluoroacetic anhydride, TEA, DCM, 0 → rt, overnight, 91.0% (**4.42**).

The synthesis of the amine precursors **4.22** and **4.23** (Scheme A 4.5) started with the commercially available **4.40**, which was protected with boc anhydride[54] or trifluoroacetic anhydride[55] to give **4.41** and **4.42**, respectively (Scheme A 4.4). The subsequent alkylation reaction towards the histamine derivative (**4.44**) was performed in a microwave reactor under basic conditions, using **4.41** and an excess of **4.43** [synthesis and analytical characterization see in chapter 3[16] (section 3.5.1.2)] (Scheme A 4.5). In terms of improving the yield, the spinaceamine derivative **4.46** was prepared by a similar approach, using 0.9 equivalent of **4.45** [synthesis and analytical characterization see in chapter 3[16] (section 3.5.1.3)] and the TFA-protected alkyl bromide **4.42**, instead of the Boc-protected alkyl bromide **4.41** (Scheme A 4.5). Cleavage of the protecting groups in **4.44** and **4.46** using trifluoroacetic acid (Boc- and Trityl group) and K$_2$CO$_3$ (TFA group) afforded the desired amine precursors **4.22** and **4.23** (Scheme A 4.5). Additionally, **4.22** and **4.23** were purified by preparative HPLC prior use in the labeling reaction with **4.10**.

Scheme A 4.5. Synthesis of 4.22 and 4.23
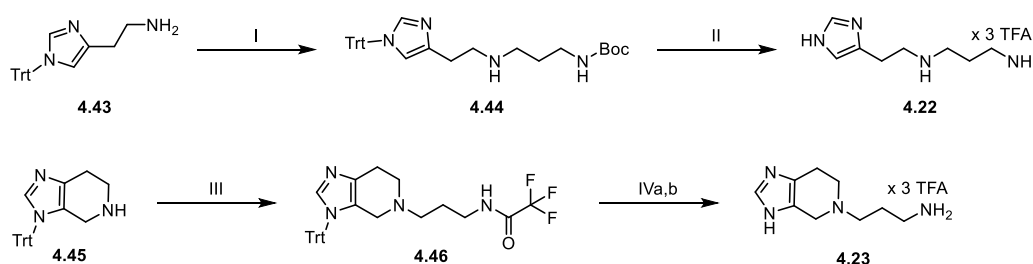
Reagents and conditions: (I) **4.41**, TEA, MeCN, 70 °C (microwave), 20 min, 56.0% (**4.44**); (II) TFA, DCM, rt, overnight, 61.2%; (III) **4.42**, TEA, MeCN, 110 °C (microwave), 50 min, 43.8%; (IVa) K$_2$CO$_3$, MeOH/H$_2$O 12/1 (*v/v*), rt, overnight; EtOAc, rt, 2 h, (IVb) TFA, DCM, rt, overnight, 59.5%.

4.5.1.1 Synthesis of **4.10**

4-{(1E,3E)-4-[4-(Dimethylamino)phenyl]buta-1,3-dienyl}-2,6-dimethylpyrylium tetrafluoroborate (4.10)[34,35]. 4.30 (400 mg, 2.28 mmol) (TCI) and **4.31** (630 mg, 3.00 mmol) (Alfa Aesar) were dissolved in MeOH (5 mL) and stirred at reflux conditions for 10 min to obtain a blue solution. The solvent was removed under reduced pressure and the crude dye was purified via column chromatography [isocratic, $CHCl_3$/MeOH 90/10 (*v/v*), SiO_2] to give **4.10** as blue crystals (708 mg, 84.6%). R_f = 0.5 ($CHCl_3$/MeOH 90/10). ¹H-NMR (300 MHz, MeOH-*d₄*): δ (ppm) 8.17 (m, 1H), 7.59 (d, *J* = 9.0 Hz, 2H), 7.51 (s, 2H), 7.43 (d, *J* = 14.7 Hz, 1H), 7.15 (m, 1H), 6.80 (d, *J* = 9.1 Hz, 2H), 6.58 (d, *J* = 14.5 Hz, 1H), 3.12 (s, 6H), 2.63 (s, 6H). HRMS (ESI): m/z [M]⁺ calcd for $[C_{19}H_{22}NO]^+$ 280.1696, found 280.1695. $C_{19}H_{22}BF_4NO$ (367.19).

4.5.1.2 Synthesis of **4.19 · 2 TFA**

3-(1*H*-Imidazol-4-yl)propan-1-amine bis(2,2,2-trifluoroacetate) (4.19 · 2 TFA)[56] (· 2 HCl[53]). 4.32 (100 mg, 0.272 mmol) was dissolved in dichloromethane (DCM, 1 mL) and TFA (0.5 mL). The reaction mixture was stirred at rt overnight. After removing the solvent under reduced pressure the residue was purified by preparative HPLC [gradient: 0 – 30 min: A/B (*v/v*) 10/90 – 15/85, flow 15 mL/min, t_R = 4.5 min] to give **4.19 · 2 TFA** as pale yellow oil (69.8 mg, 72.6%). R_f = 0.01 (DCM/MeOH 90/10). ¹H-NMR (400 MHz, MeOH-*d₄*, COSY): δ (ppm) 8.78 (m, 1H), 7.36 (s, 1H), 3.00 (t, *J* = 7.7 Hz, 2H), 2.85 (t, *J* = 7.7 Hz, 2H), 2.05 (qui, *J* = 7.7 Hz, 2H). ¹³C-NMR (101 MHz, MeOH-*d₄*, HSQC): δ (ppm) 163.21 (q, *J* = 35.0 Hz, TFA), 134.97, 133.96 (quat. 1C), 118.21 (q, *J* = 294.5 Hz, TFA), 117.11, 39.71, 27.37, 22.33. HRMS (ESI): m/z [M + H]⁺ calcd for $[C_6H_{12}N_3]^+$ 126.1026, found 126.1028. $C_6H_{11}N_3 \cdot C_4H_2F_6O_4$ (125.18 + 228.05).

4.5.1.3 Synthesis of **4.20 · 2 TFA**

2-(5-Oxohexyl)isoindoline-1,3-dione (4.35)[53,57]. 4.33 (10.0 g, 74.3 mmol), K_2CO_3 (20.5 g, 148 mmol), **4.34** (10.9 g, 74.1 mmol) and a catalytic amount of potassium iodide (100 mg, 0.602 mmol) was suspended in DMF (90 mL). The reaction mixture was stirred at 100 °C for 18 h. After ice cold H_2O (400 mL) was added, the product was extracted by DCM (3 × 200 mL). The organic phases were combined, washed with saturated $NaHCO_{3\,(aq)}$ (150 mL), 2% HCl $_{(aq)}$ (200 mL) and brine (200 mL). After drying over $MgSO_4$, the solvent was removed under reduced pressure. The product was purified by automated flash chromatography

[gradient 0 – 30 min: petroleum ether (PE)/EtOAc 100/0 – 70/30 (*v/v*), SF 25-40g] to give **4.35** as white crystals (13.3 g, 73.2%), mp 58.8 – 60.2 °C (lit 63 °C)[53]. R_f = 0.25 (PE/EtOAc 75/25). ^{1}H-NMR (400 MHz, CDCl₃, COSY): δ (ppm) 7.75 (m, 4H), 3.67 (t, *J* = 6.9 Hz, 2H), 2.47 (t, *J* = 7.1 Hz, 2H), 2.11 (s, 3H), 1.60 (m, 4H). ^{13}C-NMR (100 MHz, CDCl₃, HSQC, HMBC): δ (ppm) 208.43 (quat., 1C), 168.48 (quat., 2C), 134.02 (2C), 132.19 (quat., 2C), 123.30 (2C), 42.95, 37.57, 30.04, 28.02, 20.87. HRMS (ESI): m/z [M + H]$^+$ calcd for [C₁₄H₁₆NO₃]$^+$ 246.1125, found 246.1130. C₁₄H₁₅NO₃ (245.28).

2-(6-Bromo-5-oxohexyl)isoindoline-1,3-dione (4.36)[53]. **4.35** (13.0 g, 53.0 mmol) and urea (3.20 g, 53.3 mmol) were suspended in MeOH (40 mL). Bromine (8.50 g, 53.2 mmol) was added. The reaction mixture turned from a red solution to a pale yellow suspension at rt over 5 h. The precipitated product was filtered and washed with MeOH (10 mL). The residual solvent was removed under reduced pressure and the pale red product was crystallized from DCM/hexane to give **4.36** as white solid (7.4 g, 43.1%), mp 114.3 – 115.7 (lit 112 – 113 °C)[53]. ^{1}H-NMR (400 MHz, CDCl₃, COSY): δ (ppm) 7.76 (m, 4H), 3.87 (s, 2H), 3.69 (t, *J* = 6.7 Hz, 2H), 2.71 (t, *J* = 6.9 Hz, 2H), 1.67 (m, 4H). ^{13}C-NMR (101 MHz, CDCl₃, HSQC, HMBC): δ (ppm) 201.63 (quat., 1C), 168.49 (quat., 2C), 134.07 (2C), 132.16 (quat., 2C), 123.34 (2C), 39.04, 37.42, 34.30, 27.86, 20.95. HRMS (ESI): m/z [M + H]$^+$ calcd for [C₁₄H₁₅BrNO₃]$^+$ 324.0230, found 324.0236. C₁₄H₁₄BrNO₃ (324.17).

2-[4-(1*H*-Imidazol-4-yl)butyl]isoindoline-1,3-dione (4.37)[53]. **4.36** (7.00 g, 21.6 mmol) was suspended in formamide (50 mL). The reaction mixture was stirred at 160 °C for 5 h. After saturated NaHCO₃ (aq) (100 mL) was added, the product was extracted by DCM (4 × 200 mL). The organic phases were combined, washed with 3% HCl (aq) (2 × 100 mL) and brine (200 mL). After drying over MgSO₄, the solvent was removed under reduced pressure and the product was purified by automated flash chromatography in two fractions [gradient 0 – 30 min: DCM/MeOH 100/0 – 90/10 (*v/v*), SF 15-12 g] to give **4.37** as brown oil (2.4 g, 41.3%). R_f = 0.25 (DCM/MeOH 90/10). ^{1}H-NMR (400 MHz, MeOH-*d*₄, COSY): δ (ppm) 7.97 (s, 1H), 7.78 (m, 4H), 6.95 (s, 1H), 3.68 (t, *J* = 6.6 Hz, 2H), 2.68 (t, *J* = 6.9 Hz, 2H), 1.69 (m, 4H). ^{13}C-NMR (101 MHz, MeOH-*d*₄, HSQC, HMBC): δ (ppm) 169.81 (quat., 2C), 136.81 (quat., 1C), 135.38 (2C), 135.33, 133.32 (quat., 2C), 124.05 (2C), 117.66, 38.38, 28.90, 27.45, 26.12. HRMS (ESI): m/z [M + H]$^+$ calcd for [C₁₅H₁₆N₃O₂]$^+$ 270.1237, found 270.1238. C₁₅H₁₅N₃O₂ (269.30).

2-[4-(1-Trityl-1*H*-imidazol-4-yl)butyl]isoindoline-1,3-dione **(4.38)**[58,59]. **4.37** (2.00 g, 7.43 mmol), trityl chloride (3.10 g, 11.1 mmol) and triethylamine (TEA, 1.50 mL, 10.8 mmol) were dissolved in MeCN (200ml). The reaction mixture was stirred at rt overnight. The solvent was removed under reduced pressure. The product was purified by automated flash chromatography in two fractions [gradient $0 - 30$ min: PE/EtOAc $90/10 - 40/60$ (*v/v*), SF 15-20 g] to give **4.38** as pale yellow powder (3.1 g, 81.6%), mp $164.4 - 166.4$ °C. $R_f = 0.2$ (PE/EtOAc 50/50). ^{1}H-NMR (400 MHz, CDCl₃, COSY): δ (ppm) 7.74 (m, 4H), 7.20 (m, 16 H), 6.51 (s, 1H), 3.67 (t, $J = 6.7$ Hz, 2H), 2.56 (t, $J = 6.6$ Hz, 2H), 1.68 (m, 4H). ^{13}C-NMR (101 MHz, CDCl₃, HSQC, HMBC): δ (ppm) 168.43 (quat., 2C), 142.69 (quat., 3C), 141.39 (quat., 1C), 138.42, 133.87 (2C), 132.30 (quat., 2C), 129.87 (6C), 128.05 (6C), 127.98 (3C), 123.19 (2C), 118.02, 75.10, 37.94, 28.26, 28.05, 26.74. HRMS (ESI): m/z [M + H]$^+$ calcd for [C₃₄H₃₀N₃O₂]$^+$ 512.2333, found 512.2337. C₃₄H₂₉N₃O₂ (511.63).

4-(1-Trityl-1*H*-imidazol-4-yl)butan-1-amine **(4.39)**[59,60]. **4.38** (1.00 g, 1.95 mmol) and hydrazinium hydroxide (475 μL, 9.76 mmol) were dissolved in n-BuOH (20 mL). The reaction was stirred at rt overnight. The precipitated white solid was filtered off. The filtrate was concentrated under reduced pressure to give crude **4.39** as yellow sticky oil (750 mg, 101%). ^{1}H-NMR (400 MHz, CDCl₃, COSY): δ (ppm) $7.30 - 7.23$ (m, 10H), $7.10 - 7.01$ (m, 6H), 6.45 (s, 1H), 3.16 (br, 2H), 2.66 (t, $J = 7.0$ Hz, 2H), 2.47 (t, $J = 7.4$ Hz, 2H), 1.52 (m, 4H). ^{13}C-NMR (101 MHz, CDCl₃, HSQC, HMBC): δ (ppm) 142.67 (quat., 3C), 141.74 (quat., 1C), 138.36, 129.88 (6C), 128.09 (6C), 128.06 (3C), 117.86, 75.18 (quat., 1C), 41.65, 32.74, 28.22, 26.66. HRMS (ESI): m/z [M + H]$^+$ calcd for [C₂₆H₂₈N₃]$^+$ 382.2278, found 382.2280. C₂₆H₂₇N₃ (381.52).

4-(1*H*-Imidazol-4-yl)butan-1-amine bis(2,2,2-trifluoroacetate) (4.20 · 2 TFA) (HBr salt[53]). **4.39** (50 mg, 0.13 mmol) was dissolved in DCM (1 mL). TFA (0.7 mL) was added and the reaction mixture was stirred at rt for 6 h. After removing the solvent under reduced pressure the residue was purified by preparative HPLC [gradient: $0 - 30$ min: A/B (*v/v*) $10/90 - 15/85$, flow 15 mL/min, $t_R = 4.5$ min] to give **4.20 · 2 TFA** as pale yellow oil (28 mg, 58.6%). $R_f = 0.01$ (DCM/MeOH 90/10). ^{1}H-NMR (400 MHz, MeOH-d_4, COSY): δ (ppm) 8.78 (s, 1H), 7.32 (s, 1H), 2.97 (t, $J = 7.7$ Hz, 2H), 2.79 (t, $J = 7.2$ Hz, 2H), 1.74 (m, 4H). ^{13}C-NMR (101 MHz, MeOH-d_4, HSQC): δ (ppm) 163.14 (TFA), 134.93, 134.75 (quat., 1C), 116.87, 40.21, 27.77, 36.36, 24.73.

HRMS (ESI): m/z [M + H]$^+$ calcd for [C$_7$H$_{14}$N$_3$]$^+$ 140.1182, found 140.1184. C$_7$H$_{13}$N$_3$ · C$_4$H$_2$F$_6$O$_4$ (139.20 + 228.05).

4.5.1.4 Synthesis of **4.41** and **4.42**

***tert*-Butyl (3-bromopropyl)carbamate (4.41)**[54,61,62]. **4.40** (8.70 g, 39.7 mmol) and DIPEA (16.7 mL, 95.9 mmol) were dissolved in DCM (80 mL). The reaction mixture was cooled to 0 °C. A solution of boc anhydride (10.5 g, 48.1 mmol) in DCM (30 mL) was slowly added. The reaction could warm to rt for 20 h and H$_2$O (50 mL) was added. The mixture was acidified to pH 5 with 2 M HCl $_{(aq)}$. The organic phase was washed with H$_2$O (50 mL) and brine (50 mL). After drying over MgSO$_4$, the solvent was removed under reduced pressure. The product was purified by automated flash chromatography (isocratic, DCM 100%, SF 25-40 g) to give **4.41** as white solid (8.4 g, 88.8%), mp 36 °C (lit 36 − 38 °C)[62]. R$_f$ = 0.4 (DCM). ^{1}H-NMR (400 MHz, CDCl$_3$): δ (ppm) 4.67 (br, 1H), 3.43 (t, *J* = 6.5 Hz, 2H), 3.26 (t, *J* = 6.5 Hz, 2H), 2.04 (qui, *J* = 6.5 Hz, 2H), 1.43 (s, 9H). ^{13}C-NMR (101 MHz, CDCl$_3$): δ (ppm) 156.07 (quat., 1C), 79.57 (quat., 1C), 39.12, 32.83, 30.88, 28.50 (3C). HRMS (ESI): m/z [M + H]$^+$ calcd for [C$_8$H$_{17}$BrNO$_2$]$^+$ 238.0437, found 238.0438. C$_8$H$_{16}$BrNO$_2$ (238.13).

***N*-(3-Bromopropyl)-2,2,2-trifluoroacetamide (4.42)**[55,63]. **4.40** (1.0 g, 4.6 mmol) and TEA (1.4 mL, 10 mmol) were dissolved in dry DCM (20 mL). The reaction mixture was cooled to 0 °C. Trifluoroacetic anhydride (650 μL, 4.61 mmol) was added slowly and the reaction mixture could warm to rt overnight. DCM (200 mL) was added and the organic phase was washed with H$_2$O (2 × 100 mL) and brine (100 mL). After drying over MgSO$_4$, the solvent was removed under reduced pressure to give **4.42** as pale yellow oil (980 mg, 91.0%). R$_f$ = 0.4 (PE/EtOAc 73/17). ^{1}H-NMR (400 MHz, DMSO-d_6, COSY): δ (ppm) 9.48 (br, 1H), 3.53 (t, *J* = 6.5 Hz, 2H), 3.31 (m, 2H), 2.03 (qui, *J* = 6.7 Hz, 2H). ^{13}C-NMR (101 MHz, DMSO-d_6, HSQC, HMBC): δ (ppm) 156.38 (q, *J* = 36.1 Hz, quat., 1C), 115.89 (q, *J* = 288.2 Hz, quat., 1C), 37.87, 31.75, 31.31. HRMS (ESI): m/z [M + H]$^+$ calcd for [C$_5$H$_8$BrF$_3$NO]$^+$ 233.9736, found 233.9736. C$_5$H$_7$BrF$_3$NO (234.02).

4.5.1.5 Synthesis of **4.22**

***tert*-Butyl (3-{[2-(1-trityl-1*H*-imidazol-4-yl)ethyl]amino}propyl)carbamate (4.44)**. **4.43** (370 mg, 1.05 mmol), **4.41** (100 mg, 0.420 mmol) and TEA (180 μL, 1.29 mmol) were dissolved in MeCN (15 mL). The reaction mixture was stirred in the microwave reactor (1 − 2 bar) at

70 °C for 20 min. The solvent was removed under reduced pressure and the residue was purified by automated flash chromatography [gradient 0 – 20 min: DCM/MeOH 100/0 – 90/10 (*v/v*), SF 10-4 g] to give **4.44** as pale yellow oil (120 mg, 56.0%). R_f = 0.2 (DCM/MeOH 90/10). ^{1}H-NMR (400 MHz, CDCl₃, COSY): δ (ppm) 7.33 (m, 10H), 7.09 (m, 6H), 6.65 (s, 1H), 5.41 (br, 1H), 3.17 (m, 8H), 2.07 (m, 2H), 1.37 (s, 9H). ^{13}C-NMR (101 MHz, CDCl₃, HSQC, HMBC): δ (ppm) 156.76 (quat., 1C), 142.06 (quat., 3C), 138.44, 136.94 (quat., 1C), 129.78 (6C), 128.34 (6C), 128.28 (3C), 118.91, 79.70 (quat., 1C), 75.71 (quat., 1C), 48.25, 44.78, 37.04, 28.46 (3C), 26.98, 23.06. HRMS (ESI): m/z [M + H]$^+$ calcd for [$C_{32}H_{39}N_4O_2$]$^+$ 511.3068, found 511.3073. $C_{32}H_{38}N_4O_2$ (510.68).

N^1-[2-(1*H*-Imidazol-4-yl)ethyl]propane-1,3-diamine tris(2,2,2-trifluoroacetate) (4.22) (free base: [CAS 1524210-30-7]). **4.44** (80 mg, 0.16 mmol) was dissolved in DCM (1 mL). TFA (0.4 mL) was added and the reaction mixture was stirred at rt overnight. After removing the solvent under reduced pressure the residue was purified by preparative HPLC [gradient: 0 – 30 min: A/B (*v/v*) 10/90 – 15/85, flow 15 mL/min, t_R = 4.5 min] to give **4.22** as pale yellow oil (50 mg, 61.2%). R_f = 0.01 (DCM/MeOH 90/10). ^{1}H-NMR (400 MHz, MeOH-d_4, COSY): δ (ppm) 8.83 (s, 1H), 7.46 (s, 1H), 3.40 (t, *J* = 7.4 Hz, 2H), 3.21 (m, 4H), 3.06 (t, *J* = 7.6 Hz, 2H), 2.11 (qui, *J* = 7.7 Hz, 2H). ^{13}C-NMR (101 MHz, MeOH-d_4, HSQC): δ (ppm) 163.53 (TFA), 135.60, 130.33 (quat., 1C), 118.45, 118.27 (TFA), 47.23, 46.00, 37.79, 25.27, 22.56. HRMS (ESI): m/z [M + H]$^+$ calcd for [$C_8H_{17}N_4$]$^+$ 169.1448, found 169.1450. $C_8H_{16}N_4$ · $C_6H_3F_9O_6$ (168.24 + 342.07).

4.5.1.6 Synthesis of **4.23**

2,2,2-Trifluoro-*N*-{3-(3-trityl-3,4,6,7-tetrahydro-5*H*-imidazo[4,5-c]pyridin-5-yl)propyl}acetamide (4.46). **4.45** (290 mg, 0.793 mmol), **4.42** (210 mg, 0.897 mmol) and TEA (250 µL, 1.79 mmol) were suspended in MeCN (15 mL). The reaction mixture was stirred in the microwave reactor (1 – 2 bar) at 110 °C for 50 min. The solvent was removed under reduced pressure and the residue was purified by chromatography [DCM/MeOH 100/0 – 95/5 (*v/v*), SiO₂ 47 g, height 14.5 cm] to give **4.46** as pale yellow hygroscopic foam (180 mg, 43.8%). R*f* = 0.4 (DCM/MeOH 90/10). ^{1}H-NMR (400 MHz, CDCl₃, COSY): δ (ppm) 9.46 (br, 1H), 7.33 (m, 10H), 7.12 (m, 6H), 3.63 (m, 2H), 3.45 (m, 2H), 2.70 (t, *J* = 5.4 Hz, 2H), 2.51 (m, 2H), 1.75 (m, 2H), 1.67 (t, *J* = 5.3 Hz, 2H). ^{13}C-NMR (101 MHz, CDCl₃, HSQC, HMBC): δ (ppm) 157.06 (q,

J = 36.4 Hz, quat., 1C), 141.69 (quat., 3C), 138.04, 135.54 (quat., 1C), 130.08 (6C), 128.19(6C), 128.14 (3C), 125.99 (quat., 1C), 116.14 (q, J = 288.1 Hz, quat., 1C), 74.95 (quat., 1C), 57.88, 52.14, 51.14, 41.13, 24.31, 23.39. HRMS (ESI): m/z [M + H]⁺ calcd for [$C_{30}H_{30}F_3N_4O$]⁺ 519.2366, found 519.2369. $C_{30}H_{29}F_3N_4O$ (518.58).

3-(3,4,6,7-Tetrahydro-5*H*-imidazo[4,5-c]pyridin-5-yl)propan-1-amine   tris(2,2,2-trifluoroacetate) (4.23). 4.46 (100 mg, 0.193 mmol) was dissolved in a mixture of MeOH/H_2O 12/1 (*v/v*) (3ml). K_2CO_3 (160 mg, 1.16 mmol) was added and the reaction mixture was stirred at rt overnight. The solvent was removed under reduced pressure and EtOAc (2 mL) was added. The mixture was stirred at rt for 2 h. The white precipitate was filtered off and the filtrate was concentrated under reduced pressure. The obtained crude hygroscopic foam (100 mg, 0.237 mmol) was dissolved in DCM (2 mL). TFA (1 mL) was added and the reaction mixture was stirred at rt overnight. After removing the solvent under reduced pressure the residue was purified by preparative HPLC [gradient: 0 – 30 min: A/B (*v/v*) 10/90 – 15/85, flow 15 mL/min, t_R = 4.5 min] to give **4.23** as pale yellow oil (60 mg, 59.5%). R_f = 0.01 (DCM/MeOH 90/10). ¹H-NMR (400 MHz, MeOH-*d₄*, COSY): δ (ppm) 8.80 (s, 1H), 4.48 (s, 2H), 3.67 (t, J = 6.0 Hz, 2H), 3.41 (t, J = 7.8 Hz, 2H), 3.10 (m, 4H), 2.22 (qui, J = 7.7 Hz, 2H). ¹³C-NMR (101 MHz, MeOH-*d₄*, HSQC): δ (ppm) 163.11 (q, J = 35.4 Hz, TFA), 136.04, 126.32 (quat., 1C), 122.88 (quat., 1C), 118.13 (q, J = 291.7 Hz, TFA), 54.18, 50.82, 48.22, 38.01, 23.90, 19.71. HRMS (ESI): m/z [M + H]⁺ calcd for [$C_9H_{17}N_4$]⁺ 181.1448, found 181.1450. $C_9H_{16}N_4$ · $C_6H_3F_9O_6$ (180.26 + 342.07).

4.5.2 Optical characterization of 4.26 and NLuc

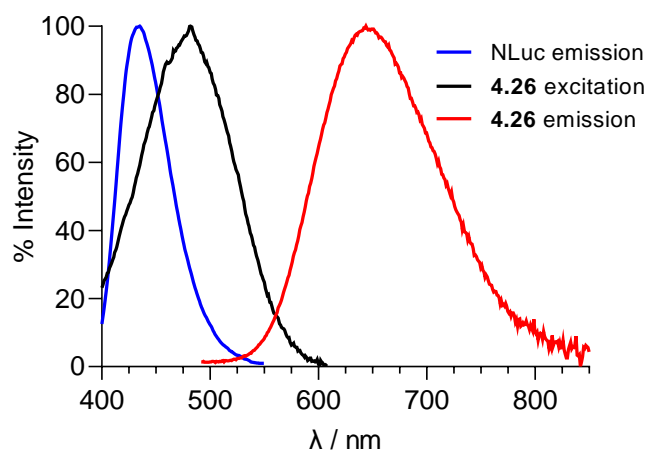### 4.5.2.1 Excitation/emission spectra of **4.26** and bioluminescence spectrum of the NLuc

Figure A 4.1. Excitation (black line) and corrected emission spectra (red line) of the Py-5-labeled fluorescent probe 4.26 (c = 4 µM) in PBS supplemented with 1% BSA recorded with a Cary Eclipse spectrofluorimeter at 22°C and with the slit combinations (ex./em. slit) 5/10 nm for excitation and 10/5 nm for emission. Bioluminescence spectrum of the NLuc (blue line) recorded with a LS50 B luminescence spectrophotometer using a suspension of NLuc-hH₄R expressing HEK293T cells in Leibovitz' L-15 + 10% FCS + 10 mM HEPES.

4.5.2.2 Excitation/emission maxima, absorption coefficients and quantum yields of **4.26**

Table A 4.1. Excitation/emission maxima, absorption coefficients ε and quantum yields Φ of 4.26, determined in PBS and PBS + BSA 1% at 22 °C with cresyl violet perchlorate as reference.

Buffer	$\lambda_{exc,max}/\lambda_{em,max}$ / nm	ε / $M^{-1} \cdot cm^{-1}$	Φ / %
PBS, pH 7.42	448/707	30667	2.53
PBS, pH 7.42 + BSA 1%	481/646	33000	17.22

4.5.2.3 Methods: fluorescence spectroscopy and determination of quantum yields

According to a previously described procedure[33], the quantum yields of **4.26** were determined in PBS (pH 7.4) and PBS + 1% BSA with cresyl violet perchlorate (Acros Organics B.V.B.A, Geel, Belgium) as a red fluorescent standard with slight modifications: Measurements were performed with a Cary Eclipse spectrofluorimeter (Varian Inc., Mulgrave, Victoria, Australia) and a PerkinElmer Lambda650 UV/Vis spectrophotometer (Perkin Elmer GmbH, Rodgau,

Germany). The spectra were recorded in polymethyl methacrylate cuvettes (12 × 12 × 45 mm, 4 CLEAR SIDE, ART 01961-00, Kartell S. p. A., Noviglio, Italy) and polystyrene cuvettes (10 × 4 ×45 mm, REF 67.742, Sarstedt AG & Co. KG, Nümbrecht, Germany).

With UV/Vis spectroscopy, the absorption spectra were recorded (350 nm – 800 nm, scan rate: 300 nm/min, slits: fixed 2.00 nm) for concentrations of 2 μM (cresyl violet in EtOH, $\lambda_{abs,max}$ = 575 nm), 6 μM (**4.26** in PBS, $\lambda_{abs,max}$ = 436 nm) or 4 μM (**4.26** in PBS + 1% BSA, $\lambda_{abs,max}$ = 458 nm) to reach absorbances between 0.1 and 0.2 at the respective absorption maximum. The solutions were freshly prepared from a 2 mM (cresyl violet) or 5 mM (**4.26**) stock solution in DMSO. All prepared solutions were immediately protected from light. Emission spectra were recorded at three different slit adjustments (ex./em.): 5/5 nm, 10/5 nm and 10/10 nm. The emission starting point was 15 nm above $\lambda_{abs,max}$ (excitation wavelength), the endpoint was 850 nm. Excitation spectra were recorded at two different slit adjustments (ex./em.): 5/10 nm and 10/10 nm. The excitation starting point was 400 nm, the endpoint was 10 nm below $\lambda_{em,max}$ (uncorrected). The reference spectra were determined with pure solvent. For the determination of quantum yields every emission spectrum was corrected (subtraction of reference spectrum followed by multiplication with the lamp correction spectrum), followed by an integration step. Additionally, the absorbances (cresyl violet in EtOH: A = 0.137; **4.26** in PBS: A = 0.184; **4.26** in PBS + 1% BSA: A = 0.132) were determined by recording the absorption spectra immediately after the recording of emission spectra (~ 20 min after the solutions were prepared). The absorbances were obtained from the net absorption spectra. The quantum yields were calculated[33] for every slit combination (emission) and were averaged (Table A 4.1). Representative excitation and emission spectra of **4.26** are depicted in Figure A 4.1. Excitation/emission maxima and absorption coefficients are presented in Table A 4.1.

4.5.2.4 Methods: bioluminescence spectroscopy

The bioluminescence spectrum of the NLuc (Figure A 4.1) was determined using a suspension of HEK293T cells expressing the NLuc-hH₄R (see section 4.4.9) in Leibovitz' L-15 + 5% FCS + 10 mM HEPES. The cells were detached from a 25 cm² flask by treatment with trypsin/EDTA (0.05%/0.02%) for 5 min at 37 °C, centrifuged (500 × g, 5 min) and resuspended in 5 mL of medium (see above). 1.5 mL of the cell suspension were transferred to an acrylic cuvette (10 x 10 x 45 mm, REF 67.755, Sarstedt AG & Co. KG, Nümbrecht, Germany), the

substrate furimazine (Promega GmbH, Mannheim, Germany) was added and the spectrum was recorded under constant stirring to prevent sedimentation of the cells. The spectrum was recorded using a LS50 B luminescence spectrophotometer (Perkin Elmer GmbH, Rodgau, Germany) from 300 to 700 nm (bioluminescence mode with the following settings: emission slit: 10 nm, integration time: 1 s).

4.5.3 Signal reduction in functional assays caused by 4.26

In the luciferase reporter gene- and β-arrestin2 recruitment assay for the h/mH₄Rs the readout is based on the bioluminescence of the firefly (Luc, American firefly *Photinus pyralis*) and the emerald (ELuc, Brazilian click beetle *Pyrearinus termitilluminans*) luciferase with D-Luciferin as their substrate. Due to their green/yellow light-emission (Luc: λ_{max} = 560 nm[48]; ELuc: λ_{max} = 538 nm[50]), the readouts were influenced when determining Py-5 fluorescent probes by an overlap of the excitation spectrum of Py-5 ligands (e.g. **4.26**, Figure A 4.1) and the emission spectra of the used luciferases.

The concentration-dependent influence of **4.26** on the bioluminescence-based readout in luciferase reporter gene- and β-arrestin2 recruitment assays was assessed using HEK293T-CRE-Luc cells[38] and HEK293T cells, stably expressing NPY Y₄R-ELucC/ELucN-β-arrestin2[64], to preclude pharmacological effects of the analyzed ligands as good as possible. The luciferase reporter gene assay was performed by applying 1 µM, 5 µM and 10 µM of **4.26** in the presence of 1 µM of forskolin. The β-arrestin2 recruitment assay was performed as described previously[64], while distinct concentrations of **4.26** (1 µM, 5 µM and 10 µM) were investigated in the presence of 1 µM of human pancreatic polypeptide (hPP). Results obtained in the presence of the different concentrations of the fluorescent ligand were compared to the respective control in which only forskolin or hPP was added (Figure A 4.2) using a one-way ANOVA and a Dunnett's post-hoc test (GraphPad Prism 8.2). Significant differences ($p < 0.0001$) were observed for concentrations > 1 µM. Therefore, the raw values obtained for the 5 µM concentrations of **4.26** and **4.27** were corrected by increasing the measured values by 8.9% (reporter gene) or 13.7% (β-arrestin2), followed by data processing as stated in the section 4.4.6 and 4.4.7 for the respective functional assay. The (corrected) concentration-response curves of **4.26** and **4.27** (agonist and/or antagonist mode) are depicted in Figure A 4.3 and Figure A 4.4.
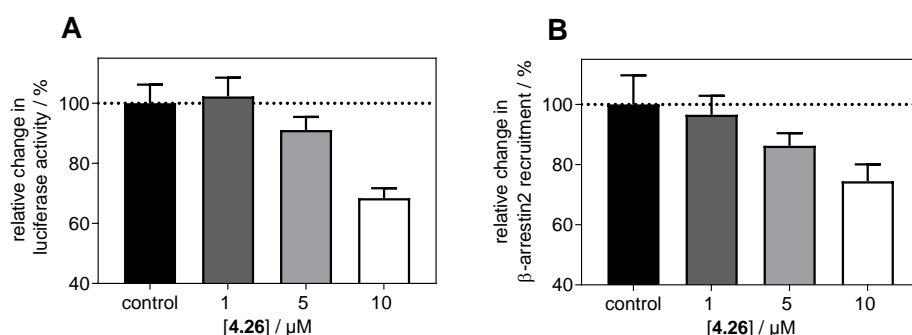
Figure A 4.2. Analysis of the concentration-dependent influence of 4.26 on the bioluminescent-based readout in luciferase reporter gene- (A) and β-arrestin2 recruitment (B) assays, using HEK293T-CRE-Luc cells or HEK293T cells, stably expressing NPY Y₄R-ELucC/ELucN-β-arrestin2. The data was normalized to control [1 µM of forskolin (**A**) or 1 µM of hPP (**B**)], maximal stimulation of which was defined as 100%. The Y-axes are adapted to improve visibility. Data are presented as means ± SD from n = 21 – 24 experiments. A one-way ANOVA and a Dunnett's post-hoc test (GraphPad Prism 8.2) were applied. Significant differences (p < 0.0001) were observed for concentrations 5 µM and 10 µM.

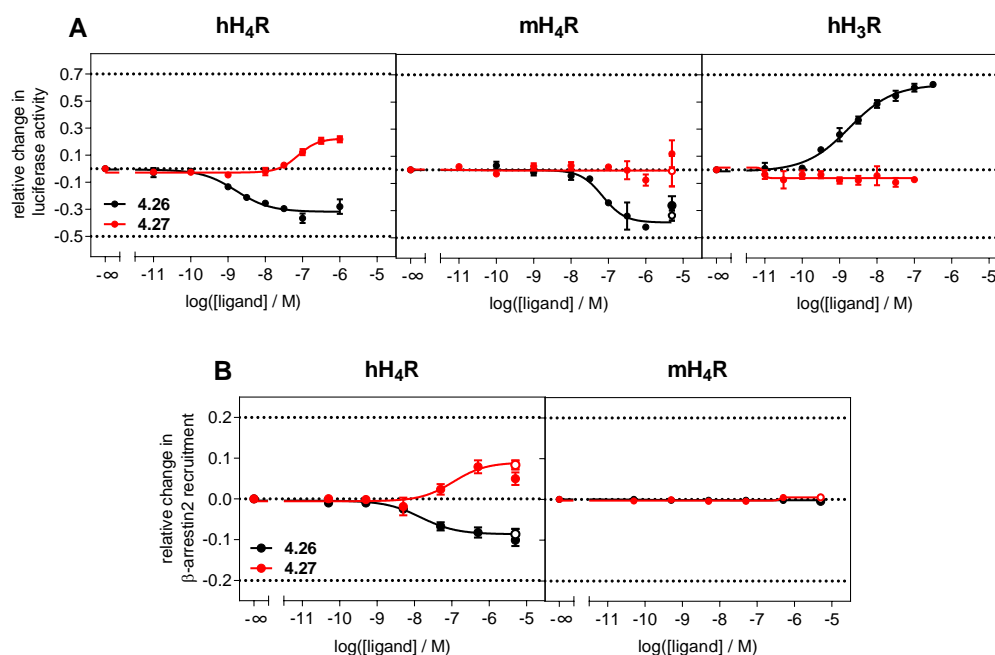## 4.5.4 Functional characterization of 4.26 and 4.27 at the hH₃R and h/mH₄Rs

Figure A 4.3. Functional characterization of 4.26 and 4.27 in agonist mode at the hH₃R and the h/mH₄Rs in (A) luciferase reporter gene assays, using HEK293T-SP-FLAG-hH₃R-CRE-CBR, HEK293-SF-hH₄R-His6-CRE-Luc or HEK293T-SF-mH₄R-His6-CRE-Luc cells and/or (B) β-arrestin2 recruitment assays, using HEK293T-β-arr2-xH₄R cells (x = h, m). Colored dots represent uncorrected values; hollow dots represent the corrected values by 8.9% (reporter gene) or 13.7% (β-arrestin2) (Figure A 4.2). Data was normalized to histamine **4.01** for each receptor, maximal stimulation of which was defined as α = 1.0. The Y-axes are adapted to improve visibility. Data are presented as means ± SEM from at least two (β-arrestin2) or three (reporter gene) independent experiments, each performed in duplicates or triplicates. The pEC₅₀, *pIC₅₀* and the intrinsic activity (α) values of **4.26** or **4.27** are presented in Table 4.2 in section 4.2.3.
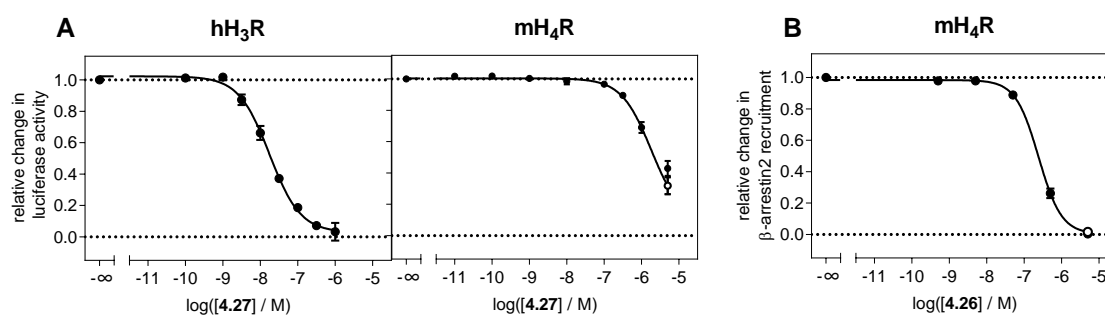
Figure A 4.4. Functional characterization of 4.26 and 4.27 in antagonist mode at the hH₃R and/or the mH₄R in (A) luciferase reporter gene assays, using HEK293T-SP-FLAG-hH₃R-CRE-CBR or HEK293T-SF-mH₄R-His6-CRE-Luc cells and/or in (B) β-arrestin2 recruitment assays, using HEK293T-β-arr2-mH₄R cells. Colored dots represent uncorrected values; hollow dots represent the corrected values by 8.9% (reporter gene) or 13.7% (β-arrestin2) (Figure A 4.2). Data was normalized to histamine **4.01** [reporter gene: c_{final} = 30 nM (hH₃R), c_{final} = 300 nM (mH₄R); β-arrestin2: c_{final} = 10 µM (mH₄R)], which was defined as α = 1.0. Data are presented as means ± SEM from three independent experiments, each performed in duplicates or triplicates. The pK_b values of **4.26** or **4.27** are presented in Table 4.2 in section 4.2.3.

4.5.5 Molecular dynamics simulations of 4.26 at the hH₄R

4.5.5.1 Results

A potential influence of the pyridinium label in hH₄R binding was investigated by induced-fit docking and molecular dynamics (MD) simulation (1 µs) using Py-5 labeled imbutamine **4.26** (Figure A 4.5). During the MD simulation, the pyridinium label of **4.26** rapidly changed its conformation, while the part of **4.26** corresponding to imbutamine was less mobile (Figure A 4.5A). In the cluster 1 binding pose, the imidazole ring of **4.26** formed a hydrogen-assisted salt bridge with D94$^{3.32}$ (imidazole N$^\pi$-H) as well as hydrophobic and π-π contacts with F344$^{7.39}$ (Figure A 4.5B). By contrast, the part of **4.26** corresponding to the fluorophore exhibited a π-π contact with Y95$^{3.33}$ and hydrophobic contacts with Y95$^{3.33}$, W157^{ECL2}, F168^{ECL2} and F169^{ECL2}. Therefore, the Py-5 fluorophore is suggested to play a fundamental role in the receptor interactions within the orthosteric binding pocket.
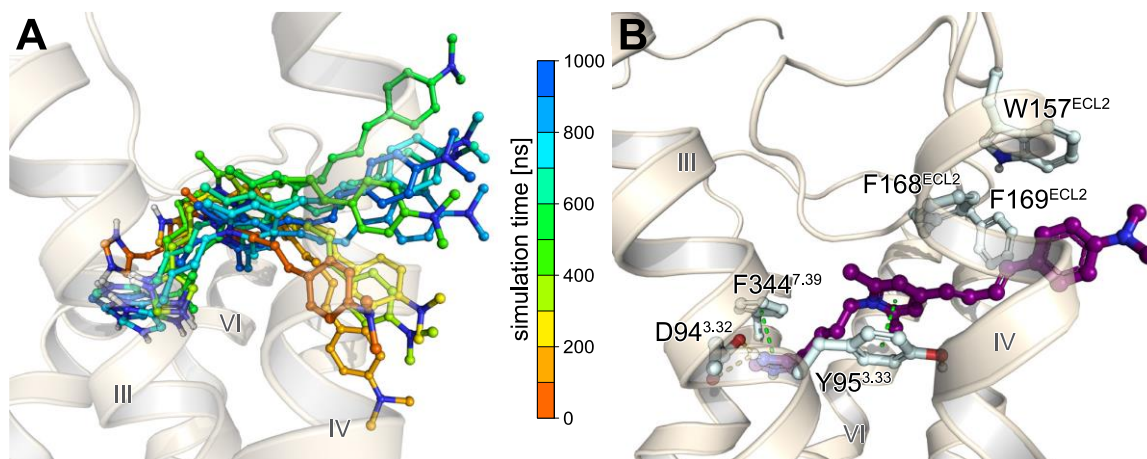
Figure A 4.5. MD simulations (1 μs) of the hH₄R (homology model based on the inactive state hH₁R, PDB ID: 3RZE[65]) bound to 4.26. A) Time course of the 1 μs MD simulation of the hH₄R bound to **4.26** showing superimposed snap shots collected every 100 ns. **B**) Cluster 1 binding pose of **4.26**, obtained from analysis of the MD simulation trajectories. Amino acids, involved in H-bonding, salt bridges (indicated as yellow dashed lines) or π-π interactions (green dashed lines) with **4.26** are labeled: D94$^{3.32}$ (HB, SB), Y95$^{3.33}$ (π-π), F344$^{7.39}$ (π-π) (**B**). In addition, the Py-5 fluorophore formed hydrophobic contacts with Y95$^{3.33}$, W157^{ECL2}, F168^{ECL2} and F169^{ECL2}, and the imidazole ring with F344$^{7.39}$ (**B**).

4.5.5.2 Methods

To study ligand-receptor interactions of **4.26** at the hH₄R, a previously described[11,66,67] hH₄R homology model was used. This model is based on the crystal structure of the inactive state hH₁R bound to the antagonist doxepin (PDB ID: 3RZE[65]). Protein preparation (Schrödinger LLC, Portland, OR, USA) and the assignment of ionization states were performed as described by Pegoli et al.[68,69]. Disulfide bonds were maintained.

Induced-fit docking (Schrödinger LLC) of **4.26** to the hH₄R was performed to find the initial ligand binding pose for subsequent MD simulations. Ligand (**4.26**) geometries were energetically optimized using the LigPrep module (Schrödinger LLC). The pyridinium nitrogen of **4.26** was singly protonated, and the imidazole ring was considered in both deprotonated (τ-H or π-H) and protonated (τ-H and π-H) states. Structure **4.26** was docked within a box of 46 × 46 × 46 Å^3 around the center of mass of the amino acids D94$^{3.32}$, E182$^{5.46}$ and Q347$^{7.42}$ using the standard protocol. Redocking was performed in the extended precision mode. Based on MM-GBSA scores (Schrödinger LLC) and reasonability of the resulting ligand binding poses, one pose was selected as input structure for subsequent MD simulation.

MD simulation of **4.26** bound to the hH₄R was essentially performed as described for muscarinic receptors by Pegoli et al.[69] with the following modifications: The selected ligand-receptor complex was aligned to the crystal structure entry of the hH₁R (PDB ID: 3RZE[65])

in the orientations of proteins in membranes (OPM) database.[70] The system comprising ligand, receptor, membrane [1-palmitoyl-2-oleoyl phosphatidylcholine (POPC)], water molecules and ions contained about 73.000 atoms and the initial box size was approximately $82 \times 82 \times 120$ Å³. Productive-level MD simulation over 1 µs was performed using the CUDA version of OpenMM[71] 7.2. A time step of 2 fs was used because hydrogen mass repartitioning (HMR) was not applied.

Data were collected every 100 ps and analyzed by means of cpptraj (Amber18, University of California, San Francisco, CA, USA) every ns. For cluster analysis, the average linkage algorithm[72] was applied, setting a cluster size of 5. Ligand-receptor interactions were analyzed using PLIP 1.4.2.[73]. For time course illustrations, frames were collected every 100 ns (10 frames). Illustrations, showing the molecular structure of the hH₄R in complex with **4.26** (Figure A 4.5), were generated with PyMOL Molecular Graphics system, version 2.2.0 (Schrödinger LLC).

4.5.6 Flow cytometric saturation binding with 4.26 at the NLuc-h/mH₄Rs

4.5.6.1 Results
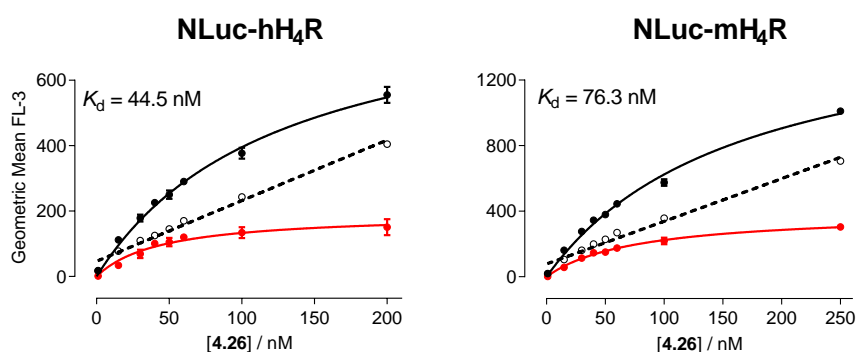
Figure A 4.6. Representative flow cytometric saturation binding experiments with fluorescent ligand 4.26 at the human or mouse NLuc-H₄Rs, expressed in HEK293T cells. Total binding (black curve), specific binding (red curve) and nonspecific binding [dashed line, determined in the presence of **4.05** (100-fold excess to final concentrations of **4.26**)] are depicted. The experiments were performed in duplicates. Errors of specific binding were calculated according to the Gaussian law of error propagation. Error bars of total and nonspecific binding represent the SEM. The K_d and pK_d values of **4.26** are presented in Table 4.3 in section 4.2.6.

4.5.6.2 Methods

The flow cytometric saturation binding experiments were performed at HEK293T cells expressing the NLuc-hH₄R or NLuc-mH₄R (see section 4.4.9). A FACSCalibur™ flow cytometer

(Becton Dickinson GmbH, Heidelberg, Germany), equipped with an argon laser (488 nm) was used by loosely following a previously described procedure[33].

The cells were detached from a 75 cm^2 flask by scraping, centrifuged (500 × g, 5 min) and resuspended in Leibovitz' L-15 + 5%FCS + 10 mM HEPES and adjusted to 1 × 10^6 cells/mL. To 490 μL of the cell suspension, **4.26** [5 μL, 100-fold serial dilutions: 5 mM stock diluted with 30% DMSO (L-15 + 5% FCS + 10 mM HEPES)] and L-15 + 5% FCS + 10 mM HEPES (5 μL) were added into 1.5-mL micro tubes (Sarstedt AG & Co. KG, Nümbrecht, Germany). Nonspecific binding was determined in the presence of **4.05** [100-fold excess with regard to each dilution of **4.26** (see above)]. The final concentration of DMSO was approx. 0.3%. After incubation in the dark for 45 min at rt, the samples were measured by flow cytometry using an excitation wavelength of 488 nm with the following instrumental settings: FSC: E-1, SSC: 280 V, Fl-3: 600 V, 670 LP. Data acquisition was stopped after counting 10 000 gated events. The raw data were processed with the FlowJo™ V10 software (FlowJo LLC, Becton Dickinson, Ashland, OR, USA). Specific binding data (geometrical mean value) were plotted against the concentration of **4.26** in nM and analyzed by a three-parameter equation describing hyperbolic binding ("one site-specific binding", GraphPad Prism 8.1) to obtain K_d values. For each experiment, K_d values (Table 4.3 in section 4.2.6) obtained from the specific binding were transformed into pK_d. Means and SEMs were calculated for the respective pK_d values (Table 4.3 in section 4.2.6). Nonspecific binding data were fitted by linear regression. Representative flow cytometric saturation binding curves are depicted in Figure A 4.6.

4.5.7 ¹H-NMR spectra and RP-HPLC chromatograms

4.5.7.1 ¹H-NMR spectra of the target compounds **4.26** and **4.29**
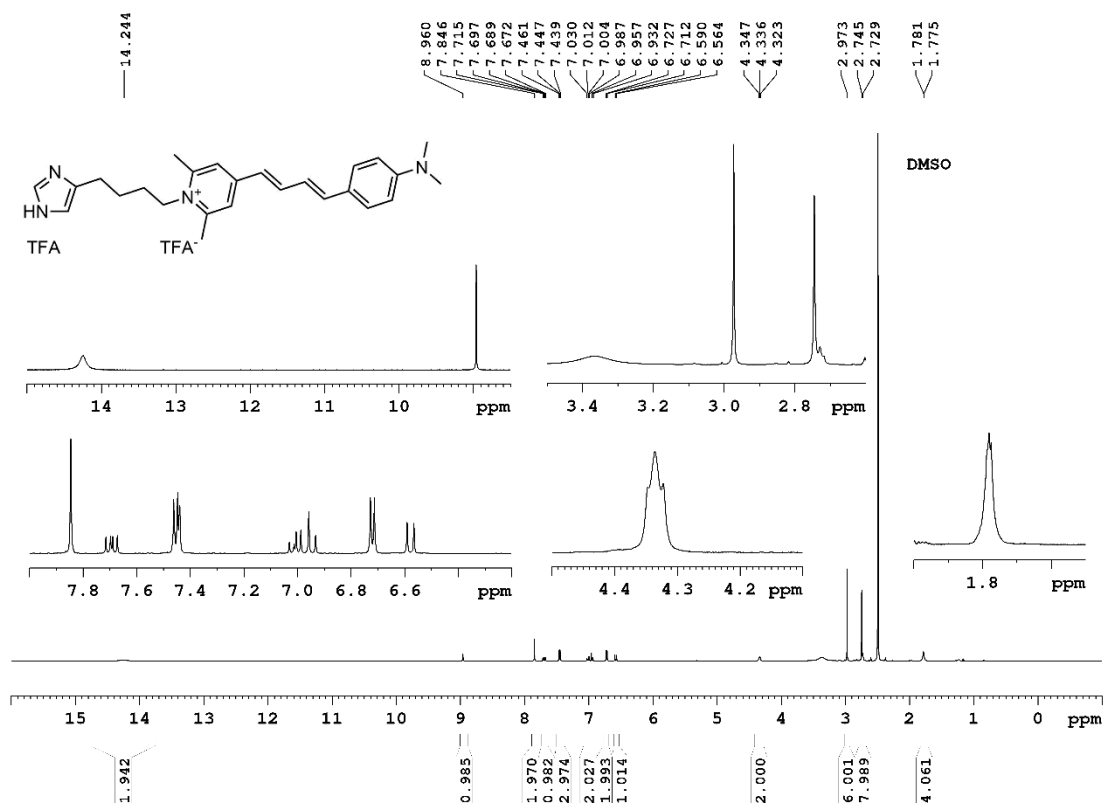
Figure A 4.7. ¹H-NMR spectrum (600 MHz, DMSO-*d₆*) of compound 4.26.

Figure A 4.8. ¹H-NMR spectrum (600 MHz, DMSO-*d₆*) of compound 4.29.
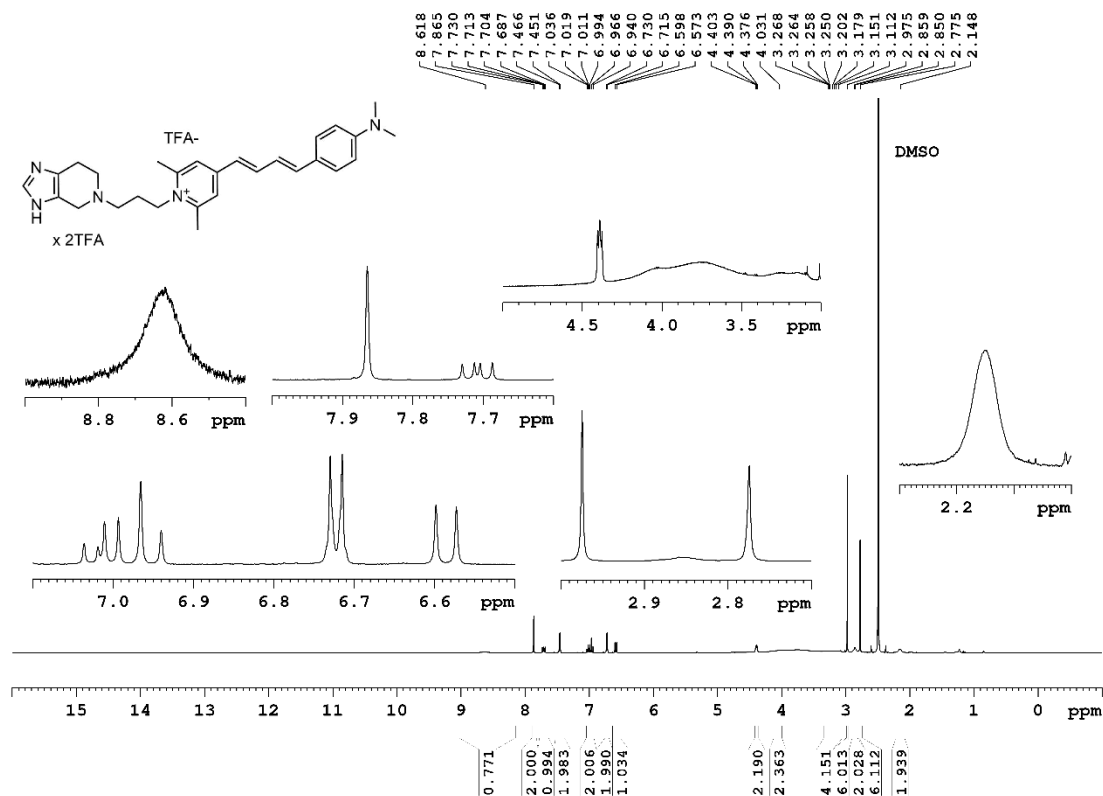
4.5.7.2 RP-HPLC chromatograms: purity control of the target compounds (4.24 – 4.29)
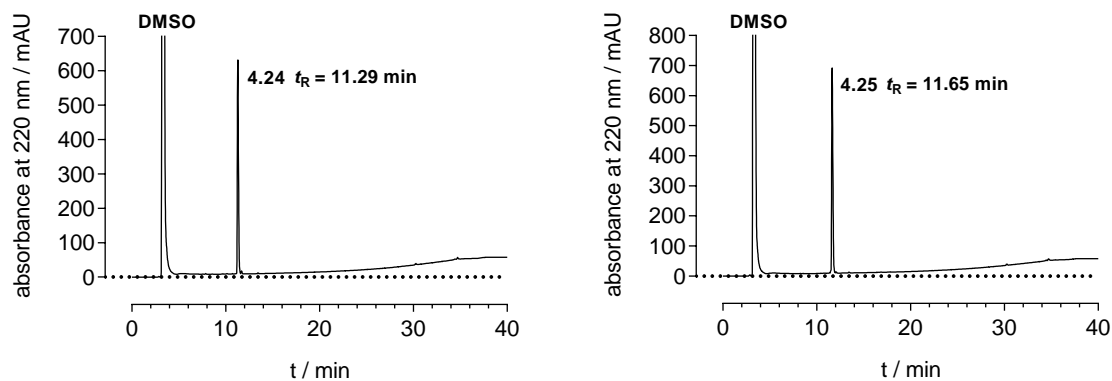
Figure A 4.9. RP-HPLC chromatograms (purity control) of 4.24 and 4.25 at 220 nm, for conditions see section 4.4.1.
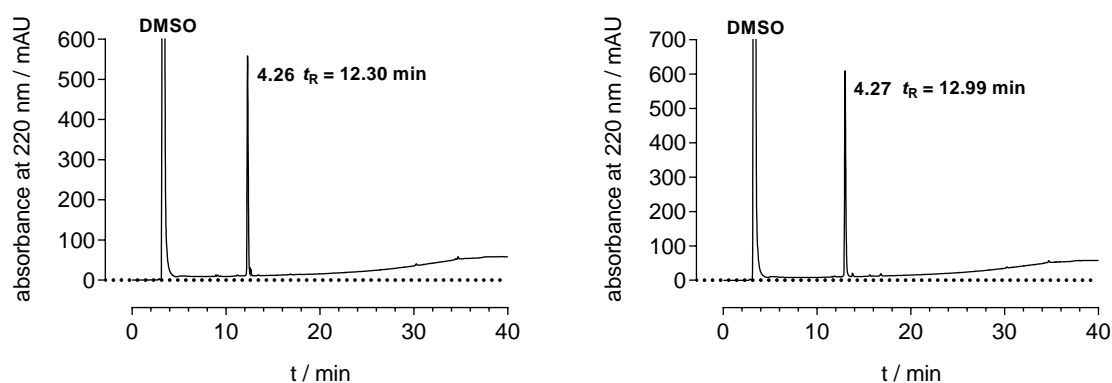
Figure A 4.10. RP-HPLC chromatograms (purity control) of 4.26 and 4.27 at 220 nm, for conditions see section 4.4.1.
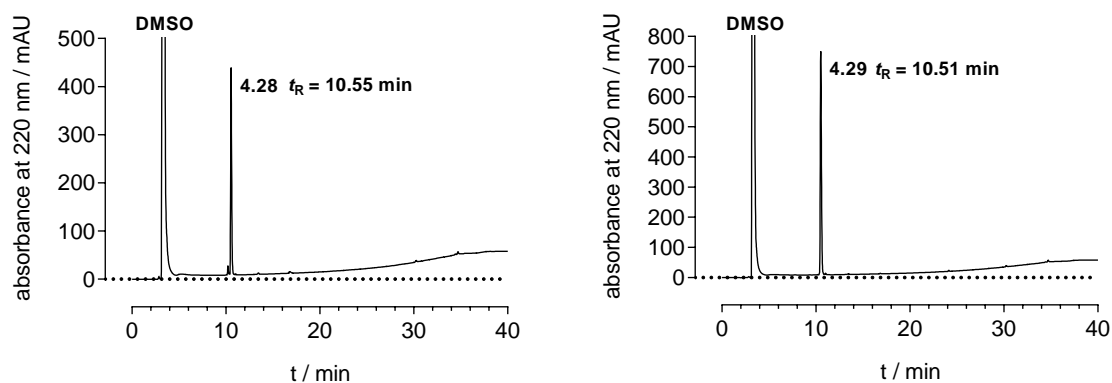
Figure A 4.11. RP-HPLC chromatograms (purity control) of 4.28 and 4.29 at 220 nm, for conditions see section 4.4.1.
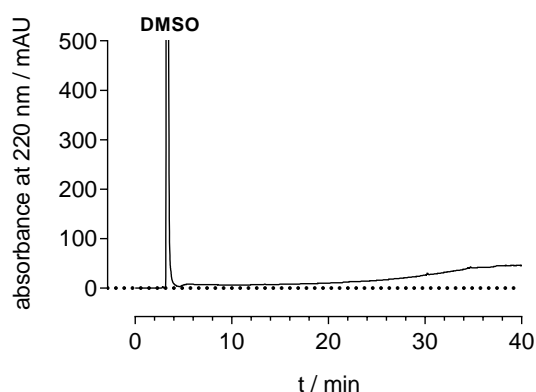
Figure A 4.12. RP-HPLC chromatograms (purity control) of blank at 220 nm, for conditions see section 4.4.1.

4.5.7.3 RP-HPLC chromatograms: chemical stability of 4.26
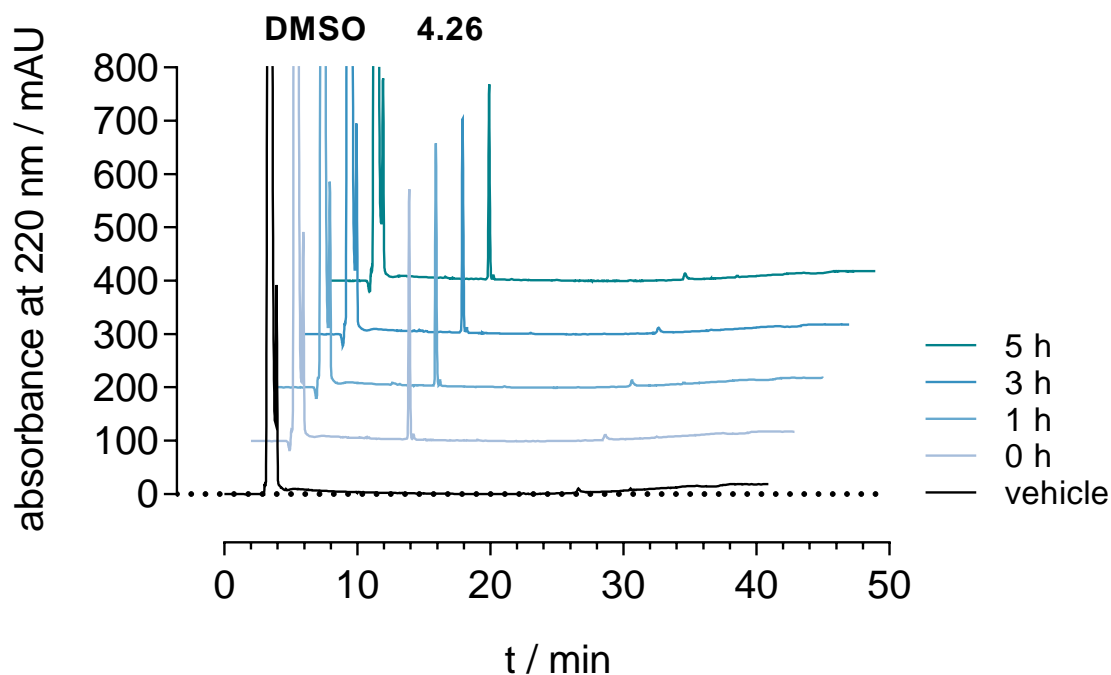
Figure A 4.13. RP-HPLC chromatograms (chemical stability, condition A: Primaria^TM plates, 23 °C in PBS) of 4.26 at 220 nm, see section 4.4.4.
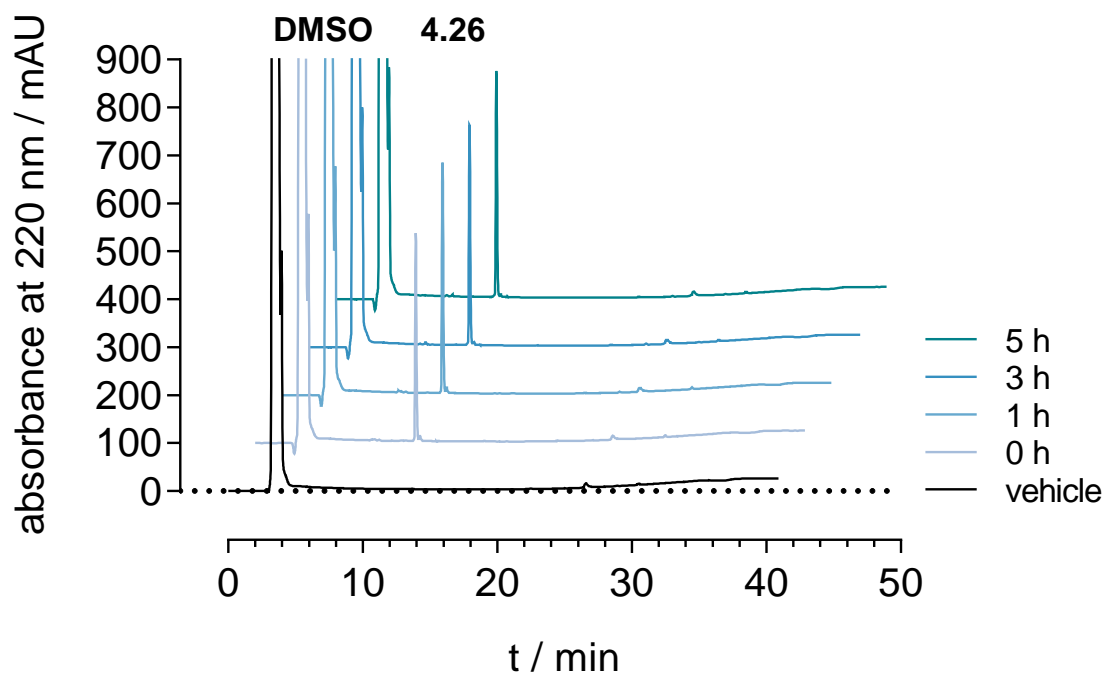
Figure A 4.14. RP-HPLC chromatograms (chemical stability, condition B: cellGrade™ plates, 23 °C in PBS) of 4.26 at 220 nm, see section 4.4.4.
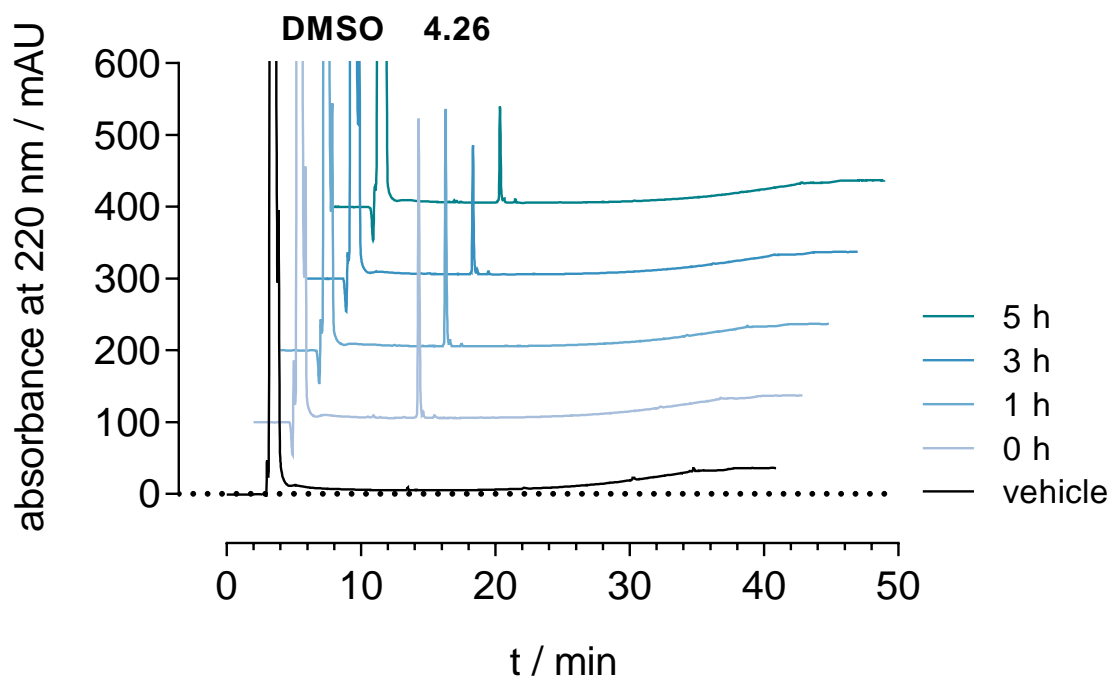
Figure A 4.15. RP-HPLC chromatograms (chemical stability, condition C: 1.5 mL microtubes, 23 °C in PBS) of 4.26 at 220 nm, see section 4.4.4.
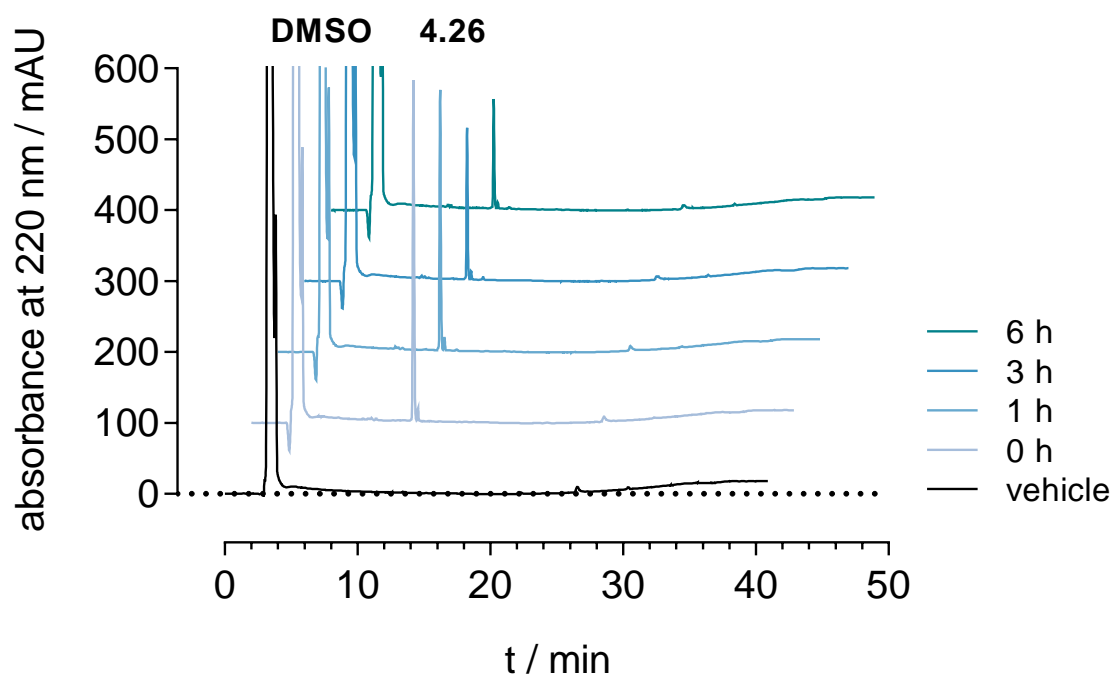
Figure A 4.16. RP-HPLC chromatograms (chemical stability, condition D: siliconized 1.5 mL microtubes, 23 °C in PBS) of 4.26 at 220 nm, see section 4.4.4.

4.6 References

1. Leurs, R.; Bakker, R. A.; Timmerman, H.; de Esch, I. J. P. The histamine H_3 receptor: from gene cloning to H_3 receptor drugs. *Nat. Rev. Drug Discovery* **2005**, 4, 107-120.

2. Neumann, D. Role of the histamine H_4-receptor in bronchial asthma. *Handb. Exp. Pharmacol.* **2016**, 241, 347-359.

3. Thurmond, R. L.; Venable, J.; Savall, B.; La, D.; Snook, S.; Dunford, P. J.; Edwards, J. P. Clinical development of histamine H_4 receptor antagonists. *Handb. Exp. Pharmacol.* **2017**, 241, 301-320.

4. Capelo, R.; Lehmann, C.; Ahmad, K.; Snodgrass, R.; Diehl, O.; Ringleb, J.; Flamand, N.; Weigert, A.; Stark, H.; Steinhilber, D.; Kahnt, A. S. Cellular analysis of the histamine H_4 receptor in human myeloid cells. *Biochem. Pharmacol.* **2016**, 103, 74-84.

5. Popiolek-Barczyk, K.; Lazewska, D.; Latacz, G.; Olejarz, A.; Makuch, W.; Stark, H.; Kiec-Kononowicz, K.; Mika, J. Antinociceptive effects of novel histamine H_3 and H_4 receptor antagonists and their influence on morphine analgesia of neuropathic pain in the mouse. *Br. J. Pharmacol.* **2018**, 175, 2897-2910.

6. Sanna, M. D.; Ghelardini, C.; Thurmond, R. L.; Masini, E.; Galeotti, N. Behavioural phenotype of histamine H_4 receptor knockout mice: focus on central neuronal functions. *Neuropharmacology* **2017**, 114, 48-57.

7. Schneider, E. H.; Neumann, D.; Seifert, R. Histamine H_4-receptor expression in the brain? *Naunyn-Schmiedeberg's Arch. Pharmacol.* **2015**, 388, 5-9.

8. Schneider, E. H.; Seifert, R. The histamine H_4-receptor and the central and peripheral nervous system: a critical analysis of the literature. *Neuropharmacology* **2016**, 106, 116-128.

9. Liu, C.; Wilson, S. J.; Kuei, C.; Lovenberg, T. W. Comparison of human, mouse, rat, and guinea pig histamine H_4 receptors reveals substantial pharmacological species variation. *J. Pharmacol. Exp. Ther.* **2001**, 299, 121-130.

10. Schnell, D.; Brunskole, I.; Ladova, K.; Schneider, E. H.; Igel, P.; Dove, S.; Buschauer, A.; Seifert, R. Expression and functional properties of canine, rat, and murine histamine H_4 receptors in *Sf*9 insect cells. *Naunyn-Schmiedeberg's Arch. Pharmacol.* **2011**, 383, 457-470.

11. Wifling, D.; Bernhardt, G.; Dove, S.; Buschauer, A. The extracellular loop 2 (ECL2) of the human histamine H_4 receptor substantially contributes to ligand binding and constitutive activity. *PLoS One* **2015**, 10, e0117185.

12. Igel, P.; Schnell, D.; Bernhardt, G.; Seifert, R.; Buschauer, A. Tritium-labeled N^1-[3-(1*H*-imidazol-4-yl)propyl]-N^2-propionylguanidine ([^{3}H]UR-PI294), a high-affinity histamine H_3 and H_4 receptor radioligand. *ChemMedChem* **2009**, 4, 225-231.

13. Lim, H. D.; van Rijn, R. M.; Ling, P.; Bakker, R. A.; Thurmond, R. L.; Leurs, R. Evaluation of histamine H_1-, H_2-, and H_3-receptor ligands at the human histamine H_4 receptor: identification of 4-methylhistamine as the first potent and selective H_4 receptor agonist. *J. Pharmacol. Exp. Ther.* **2005**, 314, 1310-1321.

14. Jablonowski, J. A.; Grice, C. A.; Chai, W.; Dvorak, C. A.; Venable, J. D.; Kwok, A. K.; Ly, K. S.; Wei, J.; Baker, S. M.; Desai, P. J.; Jiang, W.; Wilson, S. J.; Thurmond, R. L.; Karlsson, L.; Edwards, J. P.; Lovenberg, T. W.; Carruthers, N. I. The first potent and selective non-imidazole human histamine H_4 receptor antagonists. *J. Med. Chem.* **2003**, 46, 3957-3960.

15. Thurmond, R. L.; Desai, P. J.; Dunford, P. J.; Fung-Leung, W.-P.; Hofstra, C. L.; Jiang, W.; Nguyen, S.; Riley, J. P.; Sun, S.; Williams, K. N.; Edwards, J. P.; Karlsson, L. A potent and selective histamine H_4 receptor antagonist with anti-inflammatory properties. *J. Pharmacol. Exp. Ther.* **2004**, 309, 404-413.

16. Bartole, E.; Littmann, T.; Tanaka, M.; Ozawa, T.; Buschauer, A.; Bernhardt, G. [^{3}H]UR-DEBa176: a 2,4-diaminopyrimidine-type radioligand enabling binding studies at the human, mouse, and rat histamine H_4 receptors. *J. Med. Chem.* **2019**, 62, 8338-8356.

17. Iliopoulos-Tsoutsouvas, C.; Kulkarni, R. N.; Makriyannis, A.; Nikas, S. P. Fluorescent probes for G-protein-coupled receptor drug discovery. *Expert Opin. Drug Discovery* **2018**, 13, 933-947.

18. Kuder, K. J.; Kiec-Kononowicz, K. Fluorescent GPCR ligands as new tools in pharmacology-update, years 2008-early 2014. *Curr. Med. Chem.* **2014**, 21, 3962-3975.

19. Vernall, A. J.; Hill, S. J.; Kellam, B. The evolving small-molecule fluorescent-conjugate toolbox for class A GPCRs. *Br. J. Pharmacol.* **2014**, 171, 1073-1084.

20. Mocking, T. A. M.; Verweij, E. W. E.; Vischer, H. F.; Leurs, R. Homogeneous, real-time NanoBRET binding assays for the histamine H$_3$ and H$_4$ receptors on living cells. *Mol. Pharmacol.* **2018**, 94, 1371-1381.

21. Stoddart, L. A.; Johnstone, E. K. M.; Wheal, A. J.; Goulding, J.; Robers, M. B.; Machleidt, T.; Wood, K. V.; Hill, S. J.; Pfleger, K. D. G. Application of BRET to monitor ligand binding to GPCRs. *Nat. Methods* **2015**, 12, 661-663.

22. Rose, R. H.; Briddon, S. J.; Hill, S. J. A novel fluorescent histamine H$_1$ receptor antagonist demonstrates the advantage of using fluorescence correlation spectroscopy to study the binding of lipophilic ligands. *Br. J. Pharmacol.* **2012**, 165, 1789-1800.

23. Li, L.; Kracht, J.; Peng, S.; Bernhardt, G.; Buschauer, A. Synthesis and pharmacological activity of fluorescent histamine H$_1$ receptor antagonists related to mepyramine. *Bioorg. Med. Chem. Lett.* **2003**, 13, 1245-1248.

24. Erdmann, D. Histamine H$_2$- and H$_3$-Receptor Antagonists: Synthesis and Characterization of Radiolabelled and Fluorescent Pharmacological Tools. Ph.D. Dissertation, University of Regensburg, Regensburg, 2011.

25. Malan, S. F.; van Marle, A.; Menge, W. M.; Zuliani, V.; Hoffman, M.; Timmerman, H.; Leurs, R. Fluorescent ligands for the histamine H$_2$ receptor: synthesis and preliminary characterization. *Bioorg. Med. Chem.* **2004**, 12, 6495-6503.

26. Li, L.; Kracht, J.; Peng, S.; Bernhardt, G.; Elz, S.; Buschauer, A. Synthesis and pharmacological activity of fluorescent histamine H$_2$ receptor antagonists related to potentidine. *Bioorg. Med. Chem. Lett.* **2003**, 13, 1717-1720.

27. Tomasch, M.; Schwed, J. S.; Paulke, A.; Stark, H. Bodilisant - a novel fluorescent, highly affine histamine H$_3$ receptor ligand. *ACS Med. Chem. Lett.* **2013**, 4, 269-273.

28. Tomasch, M.; Schwed, J. S.; Weizel, L.; Stark, H. Novel chalcone-based fluorescent human histamine H$_3$ receptor ligands as pharmacological tools. *Front. Syst. Neurosci.* **2012**, 6, 14.

29. Amon, M.; Ligneau, X.; Camelin, J. C.; Berrebi-Bertrand, I.; Schwartz, J.-C.; Stark, H. Highly potent fluorescence-tagged nonimidazole histamine H$_3$ receptor ligands. *ChemMedChem* **2007**, 2, 708-716.

30. Mirzahosseini, A.; Kovacs, M.; Kanai, K.; Csutora, P.; Dalmadi, B. BODIPY® FL histamine as a new modality for quantitative detection of histamine receptor upregulation upon IgE sensitization in murine bone marrow-derived mast cells. *Cytometry Part A* **2015**, 87A, 23-31.

31. Geyer, R. Hetarylalkyl(aryl)cyanoguanidines as Histamine H$_4$ Receptor Ligands: Synthesis, Chiral Separation, Pharmacological Characterization, Structure-Activity and -Selectivity Relationships. Ph.D. Dissertation, University of Regensburg, Regensburg, 2011.

32. Savall, B. M.; Edwards, J. P.; Venable, J. D.; Buzard, D. J.; Thurmond, R.; Hack, M.; McGovern, P. Agonist/antagonist modulation in a series of 2-aryl benzimidazole H$_4$ receptor ligands. *Bioorg. Med. Chem. Lett.* **2010**, 20, 3367-3371.

33. Keller, M.; Erdmann, D.; Pop, N.; Pluym, N.; Teng, S. J.; Bernhardt, G.; Buschauer, A. Red-fluorescent argininamide-type NPY Y$_1$ receptor antagonists as pharmacological tools. *Bioorg. Med. Chem.* **2011**, 19, 2859-2878.

34. Wetzl, B. K.; Yarmoluk, S. M.; Craig, D. B.; Wolfbeis, O. S. Chameleon labels for staining and quantifying proteins. *Angew. Chem. Int. Ed.* **2004**, 43, 5400-5402.

35. Höfelschweiger, B. K. The Pyrylium Dyes: A New Class of Biolabels. Synthesis, Spectroscopy, and Application as Labels and in General Protein Assay. Ph. D. Dissertation, University of Regensburg, Regensburg, 2005.

36. Geyer, R.; Kaske, M.; Baumeister, P.; Buschauer, A. Synthesis and functional characterization of imbutamine analogs as histamine H$_3$ and H$_4$ receptor ligands. *Arch. Pharm.* **2014**, 347, 77-88.

37. Baumeister, P.; Erdmann, D.; Biselli, S.; Kagermeier, N.; Elz, S.; Bernhardt, G.; Buschauer, A. [^{3}H]UR-DE257: development of a tritium-labeled squaramide-type selective histamine H_2 receptor antagonist. *ChemMedChem* **2015**, 10, 83-93.

38. Nordemann, U.; Wifling, D.; Schnell, D.; Bernhardt, G.; Stark, H.; Seifert, R.; Buschauer, A. Luciferase reporter gene assay on human, murine and rat histamine H_4 receptor orthologs: correlations and discrepancies between distal and proximal readouts. *PLoS One* **2013**, 8, e73961.

39. Cheng, Y.-C.; Prusoff, W. H. Relationship between the inhibition constant (K_i) and the concentration of inhibitor which causes 50 per cent inhibition (I_{50}) of an enzymatic reaction. *Biochem. Pharmacol.* **1973**, 22, 3099-3108.

40. Scarselli, M.; Donaldson, J. G. Constitutive internalization of G protein-coupled receptors and G proteins via clathrin-independent endocytosis. *J. Biol. Chem.* **2009**, 284, 3577-3585.

41. Hendrik Schmidt, J.; Perslev, M.; Bukowski, L.; Stoklund, M.; Herborg, F.; Herlo, R.; Lindegaard Madsen, K. Constitutive internalization across therapeutically targeted GPCRs correlates with constitutive activity. *Basic Clin. Pharmacol. Toxicol.* **2019**, 00, 1-6.

42. Wolfe, B. L.; Trejo, J. Clathrin-dependent mechanisms of G protein-coupled receptor endocytosis. *Traffic* **2007**, 8, 462-470.

43. Brunskole, I.; Strasser, A.; Seifert, R.; Buschauer, A. Role of the second and third extracellular loops of the histamine H_4 receptor in receptor activation. *Naunyn-Schmiedeberg's Arch. Pharmacol.* **2011**, 384, 301-317.

44. Liu, C.; Ma, X.-J.; Jiang, X.; Wilson, S. J.; Hofstra, C. L.; Blevitt, J.; Pyati, J.; Li, X.; Chai, W.; Carruthers, N.; Lovenberg, T. W. Cloning and pharmacological characterization of a fourth histamine receptor (H_4) expressed in bone marrow. *Mol. Pharmacol.* **2001**, 59, 420-426.

45. Yu, F.; Wolin, R. L.; Wei, J.; Desai, P. J.; McGovern, P. M.; Dunford, P. J.; Karlsson, L.; Thurmond, R. L. Pharmacological characterization of oxime agonists of the histamine H_4 receptor. *J. Receptor Ligand Channel Res.* **2010**, 3, 37-49.

46. Lim, H. D.; de Graaf, C.; Jiang, W.; Sadek, P.; McGovern, P. M.; Istyastono, E. P.; Bakker, R. A.; de Esch, I. J. P.; Thurmond, R. L.; Leurs, R. Molecular determinants of ligand binding to H_4R species variants. *Mol. Pharmacol.* **2010**, 77, 734-743.

47. Kagermeier, N.; Werner, K.; Keller, M.; Baumeister, P.; Bernhardt, G.; Seifert, R.; Buschauer, A. Dimeric carbamoylguanidine-type histamine H_2 receptor ligands: a new class of potent and selective agonists. *Bioorg. Med. Chem.* **2015**, 23, 3957-3969.

48. Shinde, R.; Perkins, J.; Contag, C. H. Luciferin derivatives for enhanced in vitro and in vivo bioluminescence assays. *Biochemistry* **2006**, 45, 11103-11112.

49. Littmann, T.; Ozawa, T.; Hoffmann, C.; Buschauer, A.; Bernhardt, G. A split luciferase-based probe for quantitative proximal determination of $G\alpha_q$ signalling in live cells. *Sci. Rep.* **2018**, 8, 17179.

50. Nishiguchi, T.; Yamada, T.; Nasu, Y.; Ito, M.; Yoshimura, H.; Ozawa, T. Development of red-shifted mutants derived from luciferase of brazilian click beetle pyrearinus termitilluminans. *J. Biomed. Opt.* **2015**, 20, 101205.

51. Lieb, S.; Littmann, T.; Plank, N.; Felixberger, J.; Tanaka, M.; Schäfer, T.; Krief, S.; Elz, S.; Friedland, K.; Bernhardt, G.; Wegener, J.; Ozawa, T.; Buschauer, A. Label-free versus conventional cellular assays: functional investigations on the human histamine H_1 receptor. *Pharmacol. Res.* **2016**, 114, 13-26.

52. Rueden, C. T.; Schindelin, J.; Hiner, M. C.; DeZonia, B. E.; Walter, A. E.; Arena, E. T.; Eliceiri, K. W. ImageJ2: ImageJ for the next generation of scientific image data. *BMC Bioinf.* **2017**, 18, No. 529.

53. Igel, P.; Geyer, R.; Strasser, A.; Dove, S.; Seifert, R.; Buschauer, A. Synthesis and structure-activity relationships of cyanoguanidine-type and structurally related histamine H_4 receptor agonists. *J. Med. Chem.* **2009**, 52, 6297-6313.

54. Georgiades, S. N.; Clardy, J. Total synthesis of psammaplysenes A and B, naturally occurring inhibitors of FOXO1a nuclear export. *Org. Lett.* **2005**, 7, 4091-4094.

55. Wolff, J. A.; Hagstrom, J. E.; Budker, V. G.; Trubetskoy, V. S.; Slattum, P. M.; Hanson, L. J. Method for Making a Compound for Delivery to Cells by Forming a Polymer in the Presence of a Template Drug, Especially Nucleic Acid. WO 9829541 A1, 1998. Chem. Abstr. 129:118754.

56. Bouix-Peter, C.; Carlavan, I.; Soulet, C.; Parnet, V.; Voegel, J. Melanocortin Receptor Antagonist Compounds, Process for Preparing Them and Use Thereof in Human Medicine and Cosmetics. US 20110281913 A1, 2011. Chem. Abstr. 167:380098.

57. Chapman, J. M., Jr.; Cocolas, G. H.; Hall, I. H. Hypolipidemic activity of phthalimide derivatives. 1. N-Substituted phthalimide derivatives. *J. Med. Chem.* **1979**, 22, 1399-1402.

58. Lee, B. Y.; Kim, J. G.; Hwang, S. H.; Yi, W. H.; Jung, Y. H.; Shim, J. Y.; Park, Y. H.; Shim, W. J. Preparation of Pyrazolyl-Containing Thiourea and Isothiourea Derivatives, Method of Preparation and Inhibition of RAS-Transformed Cell Growth. WO 2001009128 A1, 2001. Chem. Abstr: 134:147604.

59. Baumeister, P. Molecular Tools for G-Protein Coupled Receptors: Synthesis, Pharmacological Characterization and [³H]-Labeling of Subtype-Selective Ligands for Histamine H₄ and NPY Y₂ Receptors. Ph. D. Dissertation, University of Regensburg, Regensburg, 2014.

60. Wolin, R.; Connolly, M.; Afonso, A.; Hey, J. A.; She, H.; Rivelli, M. A.; Willams, S. M.; West, R. E., Jr. Novel H₃ receptor antagonists. Sulfonamide homologs of histamine. *Bioorg. Med. Chem. Lett.* **1998**, 8, 2157-2162.

61. Lee, B. H.; Miller, M. J. Natural ferric ionophores: total synthesis of schizokinen, schizokinen A, and arthrobactin. *J. Org. Chem.* **1983**, 48, 24-31.

62. Vernekar, S. K. V.; Hallaq, H. Y.; Clarkson, G.; Thompson, A. J.; Silvestri, L.; Lummis, S. C. R.; Lochner, M. Toward biophysical probes for the 5-HT₃ receptor: structure-activity relationship study of granisetron derivatives. *J. Med. Chem.* **2010**, 53, 2324-2328.

63. Stromgaard, K.; Brierley, M. J.; Andersen, K.; Slok, F. A.; Mellor, I. R.; Usherwood, P. N. R.; Krogsgaard-Larsen, P.; Jaroszewski, J. W. Analogues of neuroactive polyamine wasp toxins that lack inner basic sites exhibit enhanced antagonism toward a muscle-type mammalian nicotinic acetylcholine receptor. *J. Med. Chem.* **1999**, 42, 5224-5234.

64. Kuhn, K. K.; Littmann, T.; Dukorn, S.; Tanaka, M.; Keller, M.; Ozawa, T.; Bernhardt, G.; Buschauer, A. In search of NPY Y₄R antagonists: incorporation of carbamoylated arginine, aza-amino acids, or D-amino acids into oligopeptides derived from the C-termini of the endogenous agonists. *ACS Omega* **2017**, 2, 3616-3631.

65. Shimamura, T.; Shiroishi, M.; Weyand, S.; Tsujimoto, H.; Winter, G.; Katritch, V.; Abagyan, R.; Cherezov, V.; Liu, W.; Han, G. W.; Kobayashi, T.; Stevens, R. C.; Iwata, S. Structure of the human histamine H₁ receptor complex with doxepin. *Nature* **2011**, 475, 65-70.

66. Wifling, D.; Löffel, K.; Nordemann, U.; Strasser, A.; Bernhardt, G.; Dove, S.; Seifert, R.; Buschauer, A. Molecular determinants for the high constitutive activity of the human histamine H₄ receptor: functional studies on orthologues and mutants. *Br. J. Pharmacol.* **2015**, 172, 785-798.

67. Wifling, D.; Pfleger, C.; Kaindl, J.; Ibrahim, P.; Kling, R. C.; Buschauer, A.; Gohlke, H.; Clark, T. Basal histamine H₄ receptor activation: agonist mimicry by the diphenylalanine motif. *Chem. Eur. J.* **2019**, 25, 14613-14624.

68. Pegoli, A.; She, X. K.; Wifling, D.; Hübner, H.; Bernhardt, G.; Gmeiner, P.; Keller, M. Radiolabeled dibenzodiazepinone-type antagonists give evidence of dualsteric binding at the M₂ muscarinic acetylcholine receptor. *J. Med. Chem.* **2017**, 60, 3314-3334.

69. Pegoli, A.; Wifling, D.; Gruber, C. G.; She, X.; Hübner, H.; Bernhardt, G.; Gmeiner, P.; Keller, M. Conjugation of short peptides to dibenzodiazepinone-type muscarinic acetylcholine receptor ligands determines M₂R selectivity. *J. Med. Chem.* **2019**, 62, 5358-5369.

70. Lomize, M. A.; Lomize, A. L.; Pogozheva, I. D.; Mosberg, H. I. OPM: orientations of proteins in membranes database. *Bioinformatics* **2006**, 22, 623-625.

71. Eastman, P.; Swails, J.; Chodera, J. D.; McGibbon, R. T.; Zhao, Y.; Beauchamp, K. A.; Wang, L. P.; Simmonett, A. C.; Harrigan, M. P.; Stern, C. D.; Wiewiora, R. P.; Brooks, B. R.; Pande, V. S. OpenMM 7: rapid development of high performance algorithms for molecular dynamics. *PLoS Comp. Biol.* **2017**, 13, e1005659.

72. Sokal, R. R.; Michener, C. D. A statistical method for evaluating systematic relationships. *Univ. Kans. Sci. Bull.* **1958**, 38, 1409-1438.

73. Salentin, S.; Schreiber, S.; Haupt, V. J.; Adasme, M. F.; Schroeder, M. PLIP: fully automated protein-ligand interaction profiler. *Nucleic Acids Res.* **2015**, 43, W443-W447.

5. Summary

Over the years, the histamine H_3 and H_4 receptors have emerged as promising therapeutic targets. By contrast to the H_3R, the number of drug candidates for the H_4R is highly limited. Possible reasons are the not fully elucidated expression pattern of the H_4R and the marked species [human (h), mouse (m), rat (r)]-dependent differences, regarding affinities, potencies and/or the quality of action of several H_4R ligands. Consequently, the translational value of rodent animal models is compromised.

Radio- and fluorescent ligands with a balanced affinity-/functional profile at the H_4R species orthologs can be valuable molecular tools to gain a deeper understanding of the H_4R by means of rodent animal models. However, no radioligand is known to be eligible for comparative and robust binding studies at the h/m/rH_4Rs. Furthermore, highly affinic fluorescent ligands are strongly needed to contribute to investigations on the expression of the H_4R. In addition to their application in imaging, e.g. confocal microscopy, these molecular tools could be applied in bioluminescence resonance energy transfer (BRET)-based binding studies as well. Advantages of such studies include e.g. a medium to high-throughput performance and a high temporal resolution. For the hH_3R, only two commercially available fluorescent probes were previously applied in BRET-based binding assays, but both are poorly characterized and show less than ideal spectral properties.

Therefore, this thesis aimed at the development of two complementary molecular tools: on one hand, a high affinity radioligand that can be used for comparative binding studies at the h/m/rH_4Rs. On the other hand, an extensively characterized fluorescent ligand, which enables localization studies of the hH_4R in live cells and comparative BRET-based binding studies at the NanoLuc (NLuc)-tagged h/mH_4Rs and hH_3R.

To achieve the first goal, a library of 2,4-diaminopyrimidines was prepared, based on the structure of the equipotent h/m/rH_4Rs agonist (*R*)-4-(3-aminopyrrolidin-1-yl)-*N*-neopentylpyrimidin-2-amine (**3.33**). The parent compound was modified in position 4 by introducing (cyclic) aliphatic amines (partly methylated, propionylated or guanidinylated) and histamine (homologs). After an initial characterization of the prepared compounds in radioligand competition binding assays, the 2,4-diaminopyrimidines with pK_i values > 7.0 at the hH_4R were investigated in luciferase reporter gene- and β-arrestin2 recruitment assays at the h/m/rH_4Rs to guide the selection of target structures for radiolabeling.

On one hand, UR-DEBa148 (**3.43**) was found to exhibit sub-nM potencies at the h/m/rH$_4$Rs in reporter gene assays and was slightly G protein biased. On the other hand, the (partial) agonist UR-DEBa176 (**3.46**), with comparably high potencies at the h/m/rH$_4$Rs in both functional assays [e.g. pEC$_{50}$ (reporter gene assays): 8.7, 9.0, 9.2, respectively], was found to constitute the "cold" form of a potential radioligand. By employing [^{3}H]methyl nosylate, [^{3}H]UR-DEBa176 was obtained (radiochemical purity: 99%; specific activity: 43.1 Ci/mmol) and proved to have a high radiochemical stability over a storage period of 11 month (EtOH/H$_2$O 70/30; −20 °C). In radioligand saturation binding experiments at the h/m/rH$_4$Rs, [^{3}H]UR-DEBa176 revealed comparable binding constants (pK_d: 7.4, 7.8, 7.7, respectively), accompanied by a low nonspecific binding (11–17% of total binding, ≈K_d). Likewise, the association and dissociation kinetics, studied at the h/m/rH$_4$Rs, were comparable (establishment of thermodynamic equilibria ≈ 25–30 min). In competition binding experiments, [^{3}H]UR-DEBa176 appeared as useful molecular tool to determine h/m/rH$_4$Rs binding affinities of H$_4$R ligands.

To meet the second aim, a set of histamine (homologs) were labeled with the pyrylium-5 (Py-5) fluorophore (**4.10**), with or without the introduction of a propylene spacer. Py-5 was chosen, as it is well suited for NLuc-based BRET assays, due to its spectral properties, its small size and the convenient synthesis. Radioligand competition binding studies revealed high affinities in the sub- to the two-digit-nM range at the hH$_{3,4}$Rs, especially for the imbutamine UR-DEBa242 (**4.26**) and the impentamine **4.27**. UR-DEBa242 was found to be the most notable compound in this series: in functional assays (reporter gene-, β-arrestin2 recruitment), potencies or antagonistic activities in the one- to the two-digit-nM range were obtained at the hH$_3$R (partial agonist), the hH$_4$R (inverse agonist) and the mH$_4$R (inverse agonist/antagonist). Since UR-DEBa242 revealed the highest affinity at the hH$_4$R among the synthesized compounds, confocal microscopy was performed and proved it a suitable probe for staining the hH$_4$R in live HEK293T cells. Comprising ideal optical properties (well-matching excitation maximum and large Stokes shift) as a BRET acceptor for NLuc, UR-DEBa242 enabled BRET-based saturation binding experiments at the NLuc-hH$_3$R and the NLuc-h/mH$_4$Rs with binding constants [pK_d: 8.8, 7.8, 7.2, respectively] in good agreement to pK_i and/or pEC$_{50}$/pIC$_{50}$/pK_b values from canonical assays. Worth mentioning, in flow cytometric saturation experiments, binding constants in the two-digit-nM range at the NLuc-h/mH$_4$Rs could be confirmed. BRET-based real-time association and dissociation kinetics with

UR-DEBa242 at the NLuc-hH$_3$R and the NLuc-h/mH$_4$Rs were comparable (establishment of thermodynamic equilibria ≈ 2 min). Competition binding experiments proved UR-DEBa242 suitable to determine NLuc-hH$_3$R and NLuc-h/mH$_4$Rs binding affinities of H$_{3,4}$R ligands.

In summary, [^{3}H]UR-DEBa176 and UR-DEBa242 constitute the first described highly affinic radio- and fluorescent ligands, enabling comparative and robust binding studies at the H$_4$R species orthologs. As molecular tools, they can support pharmacological investigations on the H$_4$R with respect to translational rodent animal models (e.g. early stage characterization of novel molecular tools or potential drug candidates in radioligand binding or BRET-based binding assays). Moreover, UR-DEBa242 can contribute to investigations on the expression of the H$_4$R by enabling the localization of the hH$_4$R in live cells. Finally, as being easy-to-synthesize, comprehensively characterized and, most importantly, ideally suited for NLuc-based BRET, UR-DEBa242 represents a superior alternative to the commercially available fluorescent ligands, which were previously used in BRET-based binding assays at the NLuc-hH$_{3,4}$Rs.

6. Appendix

6.1 List of abbreviations

(aq)	aqueous
[RL]	concentration of radioligand
$\Delta\Delta\log(\tau/K_A)$	bias factor
A	absorbance
abs.	absolute
AC	adenylyl cyclase
ADP	adenosine diphosphate
approx.	approximately
ATP	adenosine triphosphate
AU	absorbance unit
$B_{(eq)}$	maximum of specifically bound radioligand
$B_{(plateau)}$	bottom of specifically bound radioligand
$B_{(t)}$	specifically bound radioligand
B_{max}	maximal number of binding sides
Boc	*tert*-butoxycarbonyl
Bq	Becquerel
br	broad signal (NMR)
BRET	bioluminescence resonance energy transfer
BSA	bovine serum albumin
calcd	calculated
cAMP	cyclic adenosine monophosphate
CAS	chemical abstract service registry number
CBR	red click beetle luciferase from *Pyrophorus plagiophthalamus* (Germar, 1841)
Cbz	benzyloxycarbonyl
$CDCl_3$	deuterated chloroform
c_{final}	final concentration in the assay
Ci	Curie
CNS	central nervous system

COSY	correlation spectroscopy
cpm	counts per minute
CRE	cAMP response element
d	doublet (NMR)
DAG	diacylglycerol
DCM	dichloromethane
dec	decomposition
DIPEA	*N,N*-diisopropylethylamine
DMEM	Dulbecco's modified eagle's medium
DMF	*N,N*-dimethylformamide
DMR	dynamic mass redistribution
DMSO	dimethyl sulfoxide
DMSO-*d₆*	deuterated DMSO
dpm	disintegrations per minute
EDTA	ethylenediaminetetraacetic acid
eGFP	enhanced green-fluorescent protein
EI	electron ionization
ELuc	beetle luciferase from *Pyrearinus termitilluminans* (Costa, 1982)
em.	emission
equiv	equivalents
ESI	electrospray ionization
EtOAc	ethyl acetate
EtOH	ethanol
ex.	excitation
FCS	fetal calf serum
FRET	Förster resonance energy transfer
FSC	forward scatter
G418	geneticin sulfate
GC	gas chromatography
GDP	guanosine diphosphate
GPCR	G-protein-coupled receptor

GRK	G-protein-coupled receptor kinase
$Gs_{\alpha s}$	G-alpha subunit s, short isoform
GTP	guanosine triphosphate
GTPase	hydrolase enzyme that can bind and hydrolyse GTP
GTPγS	guanosine-5'-thiotriphosphate
$G\alpha_{i2}$	G-alpha subunit i2
$G\alpha_x$	G-alpha subunits s, i, q/11 or 12/13
Gαβγ	heterotrimeric G-protein
Gβγ	G-beta/gamma subunit
h	hour(s) or human
$H_{1-4}Rs$	the histamine receptor family
HB	hydrogen bond
HEK293T	human embryonic kidney 293T cells
HEPES	2-[4-(2-hydroxyethyl)piperazin-1-yl]ethanesulfonic acid
HMBC	heteronuclear multiple bond correlation
HMR	hydrogen mass repartitioning
HPLC	high performance liquid chromatography
hPP	human pancreatic polypeptide
HRMS	high resolution mass spectrometry
HSQC	heteronuclear single quantum correlation
IP_3	inositol-1,4,5-triphosphate
i-PrOH	isopropyl alcohol
J	coupling constants in hertz (Hz)
k	retention (capacity) factor
K_d (kin)	kinetically derived dissociation constant
K_d	dissociation constant (saturation binding experiment)
k_{obs}	observed association rate constant
k_{off}	dissociation rate constant
k_{on}	association rate constant
L-15	Leibovitz' L-15 medium
lit.	value, found in literature

LP	long-pass
Luc	firefly luciferase from *Photinus pyralis* (Linnaeus, 1767)
m	mouse, milli or multiplet (NMR)
m/z	mass-to-charge ratio
MAPK	mitogen-activated protein kinase
MD	molecular dynamics
MeCN	acetonitrile
MeOH	methanol
MeOH-*d$_4$*	deuterated methanol
min	minute(s)
mp	melting point
MTBE	methyl *tert*-butyl ether
n-BuOH	n-butanol
NHS	*N*-hydroxysuccinimide
NLuc	NanoLuc luciferase
NMR	nuclear magnetic resonance
OPM	orientations of proteins in membranes
PBS	phosphate-buffered saline
Pd/C	palladium on activated carbon
PDB ID	protein database identification number
PE	petroleum ether
pEC$_{50}$	negative logarithm of the half-maximum activity concentration
PET	positron emission tomography
P$_i$	inorganic phosphate
pIC$_{50}$	negative logarithm of the half-maximum inhibitory concentration
pK_b	negative logarithm of the dissociation constant of the antagonist-receptor complex, according to Cheng et al., *Biochem. Pharmacol.* **1973**, 22, 3099-3108.
pK_d (kin)	negative logarithm of the K_d (kin)
pK_d	negative logarithm of the K_d

pK_i	negative logarithm of the dissociation constant of the ligand-receptor complex, according to Cheng et al., *Biochem. Pharmacol.* **1973**, 22, 3099-3108.
PLC	phospholipase C
POPC	1-palmitoyl-2-oleoyl phosphatidylcholine
ppm	parts per million
PTFE	polytetrafluoroethylene
q	quartet (NMR)
quat.	quaternary carbon atom (NMR)
qui	quintet (NMR)
QY	quantum yield
r	rat
reporter gene	luciferase reporter gene assay
R$_f$	retardation factor
RGS19	regulator of G-protein signaling 19
RGS4	regulator of G-protein signaling 4
RLUs	relative light units
RP	reversed phase
rpm	revolutions per minute
rt	room temperature
s	second(s) or singlet (NMR)
SB	salt bridge
SD	standard deviation
SEM	standard error of the mean
SF	SuperFlash
*Sf*9	insect cell line from *Spodoptera frugiperda* (Smith, 1797)
SK-N-MC	human neuroblastoma cell line
SSC	sideward scatter
t	time or triplet (NMR)
t_0	dead time
$t_{1/2}$	dissociation half-life

TEA	triethylamine
TFA	trifluoroacetic acid
THF	tetrahydrofuran
TLC	thin layer chromatography
TM	transmembrane
TMS	tetramethylsilane
t_R	retention time
Tris-HCl	tris(hydroxymethyl)aminomethane hydrochloride
Trt, trityl	triphenylmethyl
UV	ultraviolet
Vis	visible
wt	wild-type
α	maximum intrinsic activity relative to reference agonist (e.g. histamine)
$\beta_1\gamma_2$	fusion of beta1 subunit and gamma2 subunit
β-arr2	β-arrestin2 recruitment assay
ε	molar absorption coefficient
λ	wavelength
$\lambda_{abs,max}$	absorption maximum
$\lambda_{em,max}$	emission maximum
$\lambda_{exc,max}$	excitation maximum
Φ	quantum yield

6.2 Declaration

Ich erkläre hiermit an Eides statt, dass ich die vorliegende Arbeit ohne unzulässige Hilfe Dritter und ohne Benutzung anderer als der angegebenen Hilfsmittel angefertigt habe; die aus anderen Quellen direkt oder indirekt übernommenen Daten und Konzepte sind unter Angabe des Literaturzitats gekennzeichnet.

Einige der experimentellen Arbeiten wurden in Zusammenarbeit mit anderen Institutionen und Personen durchgeführt. Vermerke zu den Beiträgen der betreffenden Personen finden sich in den jeweiligen Kapiteln (Kapitel 3 und 4). Eine Auflistung aller Kooperationen enthält zudem der Abschnitt „Acknowledgements".

Weitere Personen waren an der inhaltlich-materiellen Herstellung der vorliegenden Arbeit nicht beteiligt. Insbesondere habe ich hierfür nicht die entgeltliche Hilfe eines Promotionsberaters oder anderer Personen in Anspruch genommen. Niemand hat von mir, weder unmittelbar noch mittelbar, geldwerte Leistungen für Arbeiten erhalten, die im Zusammenhang mit dem Inhalt der vorgelegten Dissertation stehen.

Die Arbeit wurde bisher weder im In- noch im Ausland in gleicher oder ähnlicher Form einer anderen Prüfungsbehörde vorgelegt.

Regensburg, _____   _____

Edith Bartole